Materials Advances

ROYAL SOCIETY OF CHEMISTRY

REVIEW

View Article Online
View Journal | View Issue

Cite this: *Mater. Adv.*, 2024, 5, 7891

Engineering strategies in the rational design of Cu-based catalysts for electrochemical CO_2 reduction: from doping of elements to defect creation

Sheraz Yousaf,[a] Iqbal Ahmad,*[b] Muhammad Farooq Warsi[a] and Asad Ali*[c]

Copper (Cu)-based catalyst design for electrochemical CO_2 reduction (e-CO_2R) has attracted much interest. This is because it could help climate change by converting CO_2 into useful chemical products. This study considers a range of techniques used to optimize Cu-based catalysts, from element doping to defect engineering. Each technique has its advantages as well as its own unique problems. Doping Cu with noble metals such as silver (Ag) can result in very high catalytic activity and selectivity, but it also has disadvantages in terms of cost and long-term stability. In contrast, defect engineering which uses Cu as a material is both economically viable and sustainable. Maintaining stability and reliability is a demanding task that requires precise control. In addition, the single-atom approach has been a breakthrough method. It can efficiently and cheaply accommodate multiple carbon materials from CO_2, and other than this it is quite stable and steady. It is possible for us to gain control over the active sites at an atomic level, even if we have inefficiency and selectivity problems that remain to be resolved. Due to this method, the chemical toolbox for Cu-based catalyst design has been expanded with many other tricks in addition. As they are flexible and can be tailored to specific applications or requirements, new types of Cu-based catalysts will be able to help in e-CO_2R. When technologies mature, their sustainable deployment and global impact will depend on rigorous environmental impact assessments. It is important to emphasize the importance of Cu-based catalysts in the fight against climate change. In this crucial undertaking the paper also highlights the need for further research, innovations, and collaboration between nations.

Received 27th March 2024,
Accepted 1st July 2024

DOI: 10.1039/d4ma00321g

rsc.li/materials-advances

[a] *Institute of Chemistry, The Islamia University of Bahawalpur, Baghdad-ul-Jadeed Campus, Bahawalpur-63100, Pakistan*
[b] *Department of Chemistry, Allama Iqbal Open University, 44000 Islamabad, Pakistan. E-mail: iqbal.ahmad@aiou.edu.pk, iqbalahmadchem@gmail.com*
[c] *Energy Engineering, Division of Energy Science, Luleå University of Technology, 97187 Luleå, Sweden. E-mail: asad.ali@associated.ltu.se*

Sheraz Yousaf

Dr Sheraz Yousaf completed his doctorate under the supervision of Prof. Dr M. Farooq Warsi at The Islamia University of Bahawalpur, Pakistan. Dr Yousaf is specialized in the field of electrocatalysis, with a focus on the development of various electrocatalysts for energy conversion and storage applications. He has made significant contributions to advancing the understanding and performance of electrocatalysts through experimental approaches. Dr Yousaf's work is widely recognized, and he has published numerous articles in prestigious journals. For more information about his research and publications, please visit his Google Scholar profile (Sheraz Yousaf – Google Scholar), ORCID profile, and Scopus profile.

Iqbal Ahmad

Dr Iqbal Ahmad is an Assistant Professor at the Department of Chemistry, Allama Iqbal Open University. He completed his PhD in Chemistry from Quaid-i-Azam University, Islamabad, Pakistan, in 2017. He then secured a post-doctoral fellowship at the School of Chemical Engineering and Technology, Xian Jiaotong University, China, in 2019, and received the prestigious International Post-doctoral Exchange Fellowship from the Chinese government. Dr Ahmad has published over 70 research articles, and his research expertise includes electrocatalysis, particularly oxygen evolution reaction (OER), hydrogen evolution reaction (HER), and CO_2 reduction reaction (CO_2RR), as well as supercapacitors.

1. Introduction

As global carbon dioxide (CO_2) levels rise and climate change becomes more entrenched the world faces an ongoing dilemma of how to cope with environmental problems. Very recently, there has been considerable consultation on sustainable technologies.[1] Copper plays a crucial role in enabling sustainable technologies and copper-containing catalysts are totally unique as they convert CO_2 into feedstocks for chemical production. Here's a new way of thinking: where CO_2 is considered as a resource, not a pollutant. This novel approach to carbon economy has the potential of being both sustainable and circular.[2] This review focuses on Cu-containing catalysts and their use in e-CO_2R. It explores the engineering skills required for the rational design and synthesis of these catalysts. Engineering strategies include techniques such as selectively adding elements through doping, inducing defects within crystal lattices and using the single-atom approach to control overactive sites for innovation in precision. Conversion of CO_2 to beneficial compounds through reactions is the focus of e-CO_2R. This entire area of research has the urgency to find some solution as the emissions are becoming an issue for global warming today. This is done through capturing CO_2 from sources such as power plants, industrial processes and the atmosphere. The captured CO_2 is converted into products that have various uses. Different methods could be used to collect CO_2 which are post-combustion capture, pre-combustion capture, and direct air capture.[3]

The capture and storage of carbon is an essential step in limiting CO_2 emissions. CO_2 can be employed in the production of goods in transformation processes. The output depends on which products one wants to create as well as what resources are available. Common types of CO_2 conversion include electrochemical, photocatalytic and biological reduction, using different reaction agents, such as metal coatings at the nanoscale.[4] Catalysts such as copper and silver metal catalysts for electrochemical reduction are very important.[5,6] And semiconductor materials are important in these strategies. It is essential to supply energy to drive these conversion reactions, which can be sourced from diverse renewable sources like geothermal, wind, or residual energy from industrial processes. Energy sources that prioritize both efficiency and sustainability not only promote CO_2 emission reduction but also contribute to lowering the overall carbon footprint.

Carbon dioxide reduction can produce various valuable products such as fuels, chemicals, and materials. Typical outputs comprise of methane, methanol, formic acid, carbon monoxide, and diverse hydrocarbons. Product selection is influenced by market demand, feasibility of application, and environmental factors. It has the potential to mitigate climate change by reducing greenhouse gas emissions.[7] The environmental impact of CO_2 conversion processes must be assessed, taking into account resource availability, energy efficiency, and waste management. This review centers on the investigation of engineering approaches in the logical design of Cu-based catalysts for e-CO_2R. This review seeks to clarify the complex world of catalyst optimization with a wide range of techniques covered, from element doping to defect engineering.

Muhammad Farooq Warsi

Dr Muhammad Farooq Warsi, after completing MPhil degree in Physical Chemistry from Quaid-i-Azam University (Islamabad-Pakistan), joined the physical-organic research laboratory of Professor Dr Victor Chechik as a PhD fellow, at the Department of Chemistry, The University of York, United Kingdom. He completed the PhD degree in 2010 in the research area of gold nanoparticle based MRI contrast agents. Immediately after PhD award, in January 2011, he joined as Assistant Professor of Physical Chemistry, at the Islamia University of Bahawalpur-Pakistan. Dr Warsi established the electrochemistry and nanocatalysts research laboratory, which is one of the state-of-the-art research laboratories, at Southern Punjab universities in Pakistan. He has published more than 250 research articles since he joined the Islamia University of Bahawalpur (Pakistan). His research interest includes electrocatalysts, supercapacitors, photocatalysis and electrochemical sensors. Currently, Dr Warsi is working as Professor of Physical Chemistry, in the Institute of Chemistry at The Islamia University of Bahawalpur-Pakistan.

Asad Ali

Dr Asad Ali received his PhD degree in chemical engineering and technology from Guangxi University, China, in 2022. He is a postdoctoral researcher in the Division of Energy Engineering at Luleå University of Technology, Sweden. He has authored over 50 high-quality reviews and research articles published in journals such as Electrochemical Energy Reviews, Advanced Energy Materials, Chemical Engineering Journal, Journal of Materials Chemistry A, Nano Research, etc. His research focuses on preparing nanomaterials and their applications for hydrogen production and biomass (lignin) conversion to valuable products.

By exploring the underlying theories and mechanisms of e-CO_2R, it establishes the foundation for a sophisticated comprehension of the various approaches used in catalyst design. The aim of this endeavor is to create a comprehensive resource for researchers, engineers, and policymakers to guide future advancements in the field by consolidating and synthesizing the wealth of knowledge accumulated across various research domains.

2. Fundamentals and mechanisms involved in electrochemical CO_2 reduction

To assess the performance of a system and to determine the effectiveness of an electrocatalyst, several fundamental parameters could be considered for evaluation of the e-CO_2R process. Their assessments are done using some common key parameters employed in evaluating the reaction. Faradaic efficiency gives the ratio of electrons employed in generating the desired CO_2R products with respect to the total number of electrons that flow through the system and therefore can be used as an indication of selectivity for specific products.[8] The rate at which electrons are transferred by electron transfer processes occurring over a particular unit surface area is reported as current density and is given in mA cm^{-2}. Higher current densities would indicate faster kinetics for CO_2R and higher catalytic activity.[9,10]

Further, the energy efficiency assesses the energy consumption of the electrochemical CO_2 reduction process. It quantifies the amount of electrical energy required to produce a certain amount of desired products. Higher energy efficiency indicates a more sustainable and economically viable process.[11,12] The TOF represents the number of CO_2 molecules converted into the desired product per active site on the catalyst per unit time.[13] It provides information about the intrinsic catalytic activity of the electrocatalyst, independent of the electrode size or current density.[14] Further, its dependence on geometrical activity, specific activity and mass activity is schematically shown in Fig. 1.

Product selectivity refers to the distribution of different carbonaceous products obtained during CO_2 reduction. It evaluates the electrocatalyst's ability to favor specific target products over others. Selectivity can be determined through product analysis using techniques such as gas chromatography, mass spectrometry, or NMR spectroscopy. Fig. 2 shows the schematic representation of production of various organic products during an electrocatalysis based experiment.[15,16]

The electrocatalyst's stability and durability are important for long-term operation. Evaluating the catalyst's performance over time and under different operating conditions helps to determine its durability and potential for practical use.[17] The catalyst loading is the amount of material used on an electrode. Optimizing the catalyst loading improves the electrode's efficiency and the usage of the catalyst. Learning about the kinetics of CO_2R can give us important information about the mechanisms and rate-limiting steps.[18] We can use cyclic voltammetry and electrochemical impedance spectroscopy to analyse reaction kinetics. A comparative study can help to give an idea of how well an electrocatalyst is performing according to different catalyst materials and electrode configurations as well as working modes. Evaluation procedures vary according to study objectives and desired CO_2R products and also the choice of evaluation parameters should suit

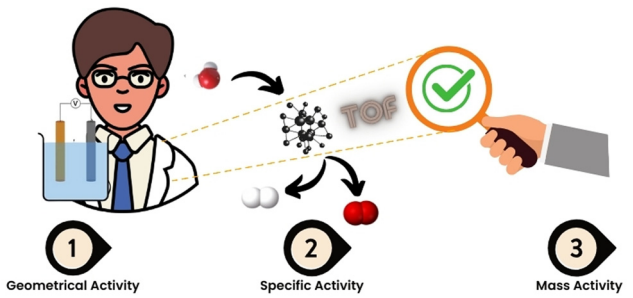

Fig. 1 Dependence of TOF on geometrical activity, specific activity and mass activity.

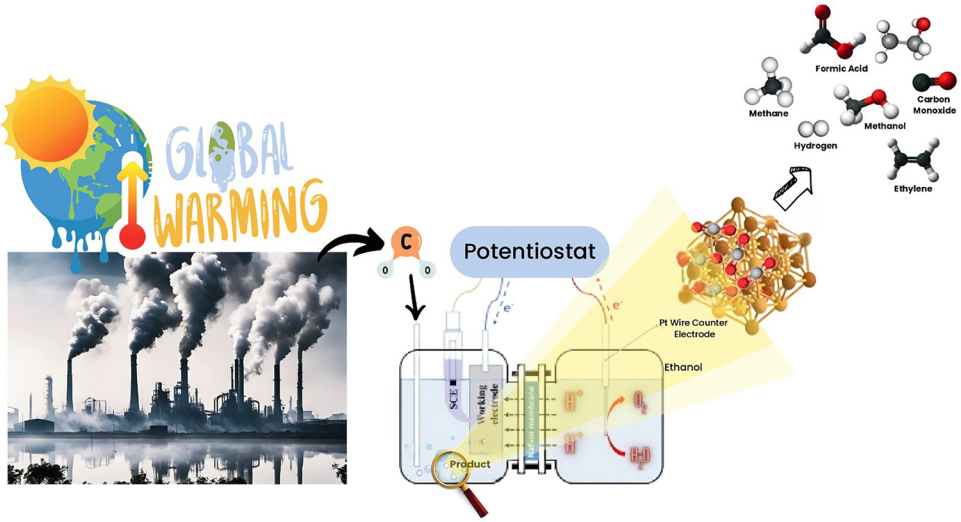

Fig. 2 Schematic illustration of production of different gaseous and liquid products over the surface of electrocatalyst's active sites.

the study objectives and the products of CO_2R that are wanted. The performance, selectivity and potential of e-CO_2R technology can be evaluated by analysing these parameters.

A multitude of intermediate products and steps lie in the reduction of CO_2 on the electrocatalyst's surface. Catalyst material and experimental conditions affect the catalytic mechanism. Generally, certain key steps are taken to be necessary. First, CO_2 molecules come to rest on the electrocatalyst's surface. Adsorption happens due to weak interactions, such as van der Waals forces, or chemisorption, in which CO_2 forms chemical bonds on the surface of the catalyst. The adsorbed carbon dioxide is activated upon breaking of its C═O bond, allowing subsequent reduction. To carry out this process, energy must be provided, and both the potential applied and the electronic properties of the catalyst can affect it.[19]

Activated CO_2 can undergo intermediate formation steps, resulting in the production of various reaction intermediates. Frequently encountered intermediates comprise carbon monoxide (*CO), formate (*HCOO),[20] formyl (*CHO),[21] and carboxyl (*COOH) species.[5] Electrons from the cathode electrode are transferred to the adsorbed reaction intermediates. The electron transfer is facilitated by the potential difference applied to the electrochemical cell. Protons from aqueous electrolytes can participate in the reaction. Protons react with adsorbed intermediates to produce reduced carbon compounds. The electrochemical reduction of CO_2 generates reduced carbon compounds that subsequently desorb from the catalyst surface. This step facilitates the collection of products for subsequent utilization or analysis.

Electrochemical CO_2 conversion involves a range of mechanistic pathways leading to the formation of various products. Here are different mechanisms for the electrochemical CO_2 conversion to different products. CO_2 reduction to CO typically involves a 2-electron transfer process. Mechanistically, CO_2 is first adsorbed onto the catalyst surface, followed by the electrochemical reduction of CO_2 to the carboxyl intermediate. The carboxyl intermediate further undergoes protonation and electron transfer steps to form CO and water.

This mechanism is preferred at low overpotentials and in the absence of other competing reduction pathways. It occurs most often on Cu-based catalysts.

$$CO_2 \rightarrow CO_2^*$$

$$CO_2 + * \rightarrow COOH + O$$

$$CO_2 + * \rightarrow COOH + O$$

$$CO^* \rightarrow CO$$

$$CO_2 + 2H^+ + 2e^- \rightarrow CO + H_2O \quad E^\circ = -0.52\ \text{V } \textit{vs.}\ \text{SHE}$$

The conversion of CO_2 to formic acid (HCOOH) *via* reduction usually involves a 4 electron transfer process. First, CO_2 is reduced to CO, which then undergoes further reduction, being protonated and losing an electron to produce CHO. The formyl intermediate is then further protonated and accepts an electron, forming acid and water. High overpotentials and an acidic environment favor the formation of formic acid. At the same time, some catalysts such as Ag, Au, and Pd exhibit a higher selectivity for formic acid.

$$CO_2 \rightarrow CO_2^*$$

$$CO_2 + * \rightarrow CO + O$$

$$*CO + H^+ + e^- \rightarrow *HCOO$$

$$HCOO + H^+ + e^- \rightarrow HCOOH + O$$

$$CO_2 + 2H^+ + 2e^- \rightarrow HCOOH \quad E^\circ = -0.61\ \text{V } \textit{vs.}\ \text{SHE}$$

Usually, conversion of $CO_2$to methanol (CH_3OH) is a complex process. The typical course of conversion of CO_2 is as follows: first, $CO_2$is reduced to CO in a two-step reaction sequence, and then goes into the formation of HCOO. The HCOO intermediate then undergoes additional reductions with protonation and electron transfer, leading to formaldehyde. Formaldehyde, in turn, undergoes a series of hydrogenation reactions which consist of multiple protonation and electron transfer steps, and finally forms methanol. In the generation of methanol, higher the overpotential and the more reducing the environment the more likely is product formation. Quite a number of Cu-based catalysts have shown high methanol selectivity, especially those with alloying elements.

$$CO_2 \rightarrow CO_2^*$$

$$CO_2 \rightarrow CO_2^*$$

$$*CO + H^+ + e^- \rightarrow *HCOO$$

$$*HCOO + H^+ + e^- \rightarrow CHO + O$$

$$*CHO + 3H^+ + 3e^- \rightarrow CH_3OH + H_2O$$

$$CO_2 + 6H^+ + 6e^- \rightarrow CH_3OH + H_2O \quad E^\circ = -0.38\ \text{V } \textit{vs.}\ \text{SHE}$$

Turning CO_2 into hydrocarbons such as ethylene (C_2H_4) through electrochemical reduction typically involves multiple steps. CO_2 is first reduced to CO, and this species can then undergo hydrogenation as well as C–C coupling reactions. CO can transform by a series of protonation, electron transfer, and bond formation steps to $*C_2H_x$ (ethylene precursor). Further hydrogenation reactions produce ethylene. At high cathodic potentials, alkaline conditions in general favor the formation of ethylene. Transition metals like Cu assist in C–C coupling and catalyze CO_2 activation; these enhance ethylene production.

$$CO_2 \rightarrow CO_2^*$$

$$CO_2 + * \rightarrow CO + O$$

$$*CO + 2H^+ + 2e^- \rightarrow *CH_2O + H_2O$$

$$*CH_2O + *CH_2O \rightarrow *C_2H_4O + H_2O$$

$$*C_2H_4O + 2H^+ + 2e^- \rightarrow C_2H_4 + H_2O$$

$$CO_2 + 8H^+ + 8e^- \rightarrow C_2H_4 + 2H_2O \quad E^\circ = -0.04\ \text{V } \textit{vs.}\ \text{SHE}$$

The formation of methane (CH_4) by the reduction of CO_2 is typically accomplished through a complex series of reactions. In the beginning, CO_2 is turned into CO, which is then hydrogenated to produce CHO (formyl intermediate). The *CHO intermediate can be further reduced to $*CH_3$ (methyl intermediate) through protonation and electron transfer steps. Subsequent hydrogenation reactions lead to the formation of methane. Methane formation is favored at high cathodic potentials and under reducing conditions. Catalysts like Ni, Cu, or bimetallic systems often exhibit higher methane selectivity. All mechanisms for e-CO_2R to C_1 and C_2 products are schematically shown in Fig. 3.

$$CO_2 \rightarrow CO_2^*$$

$$CO_2 + * \rightarrow CO + O$$

$$*CO + 4H^+ + 4e^- \rightarrow *CH_3OH + H_2O$$

$$*CH_3OH + H^+ + e^- \rightarrow *CH_3 + H_2O$$

$$*CH_3 + 3H^+ + 3e^- \rightarrow CH_4 + H_2O$$

$$CO_2 + 8H^+ + 8e^- \rightarrow CH_4 + 2H_2O \quad E^\circ = -0.24\ \text{V vs. SHE}$$

The electrocatalyst selectivity and activity have a significant impact on the reaction pathway and the resulting product distribution. The catalyst material, composition, and surface structure significantly impact the CO_2 reduction efficiency and selectivity. The reaction mechanism can be complex, with multiple competing pathways occurring simultaneously. The catalyst's surface morphology and defects, as well as reaction

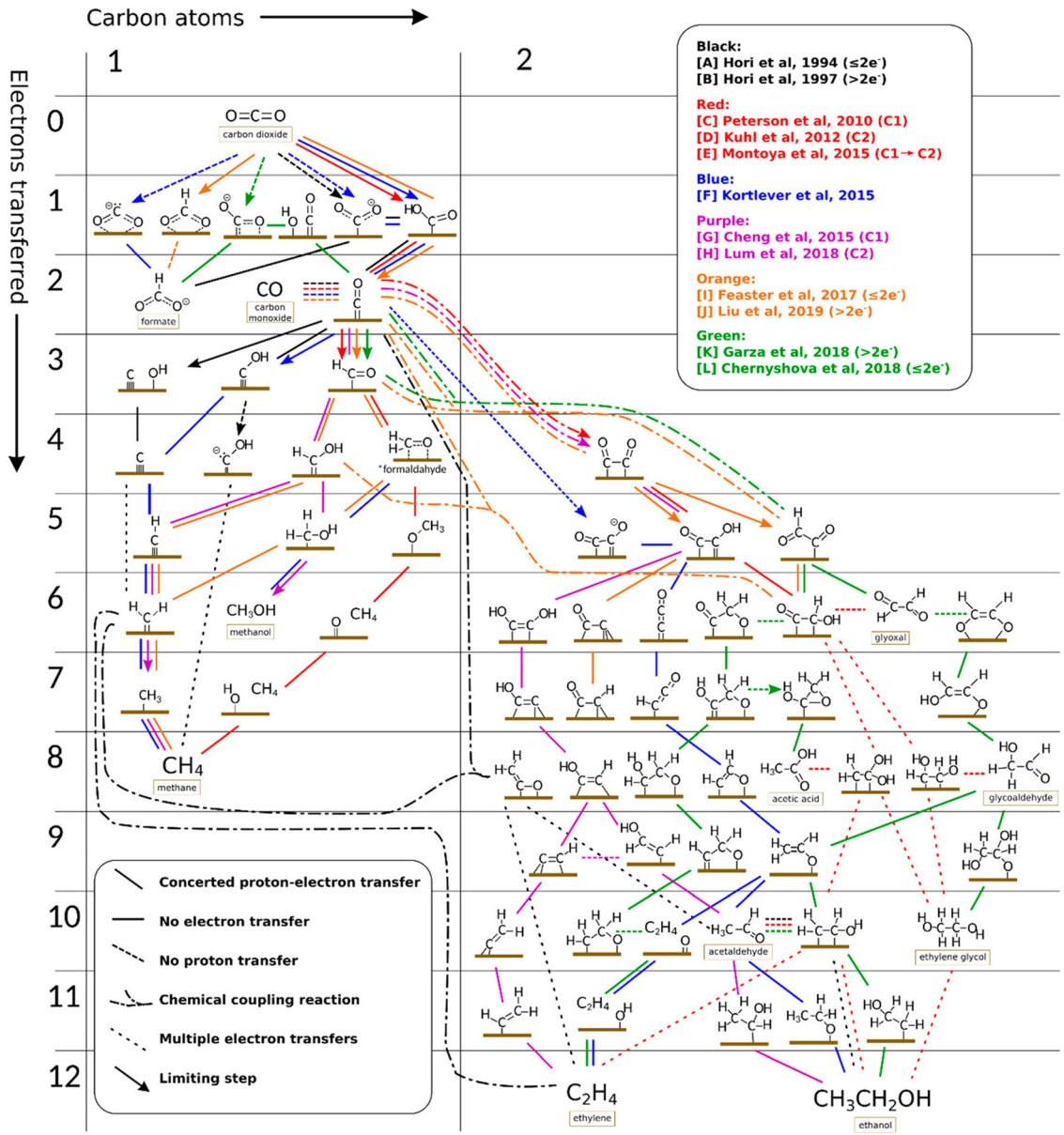

Fig. 3 Possible different routes for the production of C_1 and C_2 products over the surface of polycrystalline copper upon e-CO_2R. Reproduced with permission from ref. 11. Copyright 2023, American Chemical Society.

conditions such as temperature, pressure, and pH, can affect the reaction mechanism and product distribution.[22]

Modern electrocatalysis research aims to enhance comprehension of these mechanisms and create efficient catalysts that can boost CO_2 reduction selectivity and activity. This will facilitate the development of sustainable and economically possible carbon capture and utilization technologies.

3. Importance of Cu-based catalysts in e-CO_2R

Cu-based catalysts have gained significant importance in electrochemical CO_2 reduction for several reasons like their high selectivity for C–C bond formation. Copper-based electrocatalysts show a great deal of selectivity in the formation of C–C bonds during the reduction of CO_2.[23] Due to this, it is possible to synthesize valuable hydrocarbon compounds such as ethylene (C_2H_4) and methane (CH_4), highly varied in industrial applications as fuels or for use in chemical feedstocks. Natural limit defects of these Cu nanosheets (2–14 nm) were designed to produce ethylene with a high ethylene faradaic efficiency of 83.2% from carbon dioxide. These defects enhance the formation of ethylene by promoting C–C coupling through reaction intermediates and hydroxyl ions.[24] In the same way, CuO nanoparticles were made and deposited on conductive carbon materials, resulting in a higher faradaic efficiency (FE) of over 70% for ethylene but only 30% for hydrogen.

The catalyst exhibited durability and selectivity for ethylene production, due to its active domains and high local pH.[25] The Cu–polyamine hybrid catalyst significantly improved ethylene production selectivity by 87% at −0.47 V. Additionally, the full-cell energetic efficiency reached 50%. Raman measurements indicated that incorporating polyamine in a Cu electrode enhances surface pH, CO content, and intermediate stabilization. This demonstrates the positive effect of polymer incorporation on product selectivity.[26] The tw-Cu foil electrocatalyst has dense twin boundaries and shows a faradaic efficiency of $86.1 \pm 5.3\%$ for CH_4. It also reduces the barrier for reduction and has high selectivity for CH_4.[27] Moreover, copper-based catalysts have shown favorable kinetics for CO_2 reduction reactions.[28] They possess lower overpotential, resulting in a reduced energy requirement for driving the desired electrochemical reactions. This characteristic is responsible for an increase in the energy efficiency of the process.

Copper-based catalysts can have different oxidation states and undergo structural changes during electrochemical processes.[29,30] The versatility of Cu catalysts makes them able to form and react with a greater variety of intermediates, leading to different products from the same source. Copper, widely available and plentiful, is an inexpensive choice for massive carbon dioxide reduction. Copper catalysts have low cost and can be used widely. Cu-based electrocatalysts are preferred because of their adjustable catalytic properties. It is possible to change the catalytic properties of Cu-based catalysts by controlling particle size, morphology, and surface composition. Researchers can optimize the catalyst performance and customize selectivity for specific CO_2 reduction products. Copper catalysts are stable and durable for electrochemical CO_2 reduction. They resist deactivation and degradation, allowing them to operate efficiently for a long time. Cu-based catalysts are important in electrochemical CO_2 reduction because they can efficiently produce valuable carbon-based compounds with high selectivity. Their abundance, cost-effectiveness, tunable properties, and stability make them ideal for scaling up CO_2 reduction technologies and using carbon dioxide sustainably in various industrial processes.[31,32]

Although Cu-based electrocatalysts show promise for CO_2 conversion, there are still some challenges and current issues that need to be addressed. The key issues associated with Cu-based electrocatalysts for CO_2 conversion include their low faradaic efficiency. Cu catalysts often exhibit low faradaic efficiency for specific CO_2 reduction products like C_2 products.[33–35] Undesired side reactions, such as hydrogen evolution and competitive reduction pathways, can limit the selectivity towards desired products like ethylene or methane.[36] Enhancing the faradaic efficiency and selectivity for these materials remains a major challenge. Cu based electrocatalysts can suffer from stability issues during prolonged CO_2 conversion reactions.[37,38] A hydrophobic coating of long-chain alkanethiols on Cu dendrites enhances CO_2 reduction selectivity by creating a plastron effect. This creates a gas layer on the electrode, which increases the concentration of CO_2 in that area. The current electrode has drawbacks. Future work should focus on promoting stable hydrophobicity on high-surface-area microporous electrodes. This supports the idea that gas diffusion electrodes can produce stable C_2 products, which may explain the low long-term stability of electrocatalytic surfaces.[39] Surface restructuring, agglomeration, or dissolution of Cu nanoparticles may occur, leading to decreased catalytic activity and selectivity over time.[40] Improving the stability of Cu-based catalysts under harsh reaction conditions is critical for their practical applications. Additionally, the reduction of CO_2 on Cu surfaces often requires a high overpotential, meaning a higher energy input is needed to drive the electrochemical reactions efficiently. Reducing the overpotential would enhance the energy efficiency of the process and make it more economically viable.[41] Diffusion of CO_2 to the catalyst surface can be a limiting factor, especially in dense electrode structures or in the case of thick catalyst layers. Insufficient CO_2 transport to the catalyst surface can lower the reaction rate and efficiency. Efficient CO_2 mass transport is important for catalyst designs and electrode architectures.[42]

Cu-based electrocatalysts are susceptible to poisoning or deactivation by adsorbed species or impurities in the reaction environment.[43,44] Oxygen- or sulfur-containing species that are adsorbed can block active sites or alter the electronic properties of the catalyst, leading to reduced activity and selectivity.[45] Mitigating catalyst poisoning effects is crucial for ensuring long-term performance. Despite the abundance and cost-effectiveness of copper (Cu), scaling up copper-based catalysts for large-scale CO_2 conversion processes is still challenging.

Innovative synthesis approaches are important for addressing challenges in CO_2 conversion with Cu-based electrocatalysts. Various synthesis techniques can precisely control catalyst composition, morphology, and structure. These approaches improve the selectivity and activity of Cu-based catalysts by giving them specific properties. Metals can be added through alloying or surface modification. Bimetallic or composite catalysts can exhibit improved catalytic performance and selectivity by leveraging the synergistic effects between Cu and other metals. Bottom-up assembly methods can be used to develop nanostructured Cu catalysts, providing control over particle size, shape, and surface properties. This leads to improvements, in both the efficiency and stability of reactions. Researchers have the opportunity to employ synthesis techniques in order to design electrocatalysts based on copper that exhibit improved performance, selectivity, stability and scalability for efficient conversion of CO_2.

4. Mechanistic insights from spectroscopic techniques

Recent discoveries and developments from spectroscopic techniques such as XAS, Raman and IR spectroscopy have provided mechanistic knowledge of CO_2 reduction on Cu-based electrode catalysts. XAS, especially XANES and EXAFS, demonstrates the change of the Cu oxidation state and the ability of local geometry around Cu, which represents the transition from Cu(II), Cu(I) to active Cu(0) during the catalytic process. Raman spectroscopy identifies surface species such as CO and CHO which play important roles in the reaction route map while IR spectroscopy is useful in gaining information on the adsorbed species and reaction intermediates. Each of these spectroscopic strategies combined provides a detailed description of the dynamic processes occurring at the catalyst surface and with CO_2, which is profitable for the development of enhanced and selective electrocatalysts. EC-RSoXS was employed to study the real-time and real-space particle interactions as well as the chemical surroundings of Cu nanocatalysts in e-CO_2R. The changes of Cu nanoparticle properties depending on the particle size and interaction with soft X-ray beams were analyzed. The 7-nanometer nanoparticles were primarily oxidized to CuO, whereas the larger 18-nanometer particles showed more resistance to damage. EC-RSoXS combines soft XAS (X-ray absorption spectroscopy) and SAXS (small-angle X-ray scattering) methods to give a complete picture of how chemical and physical states affect the interparticle dynamics of nanocatalysts.[46] Furthermore, another research study has showcased that the utilization of Ce–Cu_2O, a catalyst characterized by a unique orbital coupling between high-order Ce^{4+} 4f and O 2p, brings about significant improvements in e-CO_2RR (Fig. 4). Throughout a 7-hour operational run, the as-synthesized $CeCu_2O$ sample consistently generated C_2H_4 and demonstrated a C_2H_4/CO ratio 1.69 times higher than that of the Cu_2O catalyst. The Ce–Cu_2O catalyst maintained stable Cu^+ species during the entire CO_2RR process.[47]

In another facet of this research, pure Cu, a metal known for catalyzing the conversion of CO_2 to hydrocarbons with high FE, was utilized for e-CO_2RR. Researchers closely monitored the structural dynamics of Cu during the electrochemical process using techniques such as electrochemical scanning tunneling microscopy and Raman spectroscopy. Through control of polarization potential and *in situ* synthesis time, it was discovered that polycrystalline Cu surfaces could give rise to Cu nanocuboids. Additionally, a graphene monolayer was grown on the Cu surface to create smaller features with enhanced catalytic activity.[48]

Furthermore, the study employed *in situ* HERFD XAS to investigate the potential dependency of a single Cu layer, revealing significant differences compared to bulk Cu electrodes. Unlike thick Cu electrodes, which exhibit two redox transitions, only one redox transition was observed for 1 ML Cu/Au(111) and 1 ML Cu/Pt. This single Cu layer exhibited an anodic shift at the onset of Cu oxidation. The considerable tensile strain experienced by a single Cu monolayer when deposited on Au, Pt, and platinum-group metals was found to influence the redox behavior and interaction with e-CO_2R intermediates. This tensile strain allowed for tunability of the ratio of methane to ethylene formed.[49] Moreover, the research demonstrated that the incorporation of s-ZnO into s-CuO during the fabrication of a series of sputtering electrocatalysts significantly altered the product profile of the CO_2RR. Specifically, the efficiency of CH_4 generation increased, while the production of C_{2+} products decreased under ideal conditions. *In situ* XAS analysis revealed that the coordination number of Cu sites played a crucial role in CH_4 formation, which was influenced by the presence of Zn sites and led to a reversal of Ostwald ripening during the CO_2RR.[50]

Furthermore, in another research study, the scientists employed the carbon nanoparticle moderator method, wherein a copper-complex catalyst was confined in a membrane electrode assembly. Real-time XAS experiments demonstrated that increased carbon nanoparticle loadings reduced the coordination number of metallic copper. The system operated continuously for over 110 hours, achieving a CO_2-to-methane selectivity of 62%, a methane partial current density of 136 mA cm^{-2}, and a copper coordination number of 4.2.[51] Lei *et al.* have designed nanocrystals of $Cu_2(OH)_2CO_3$, $Cu(OH)_2$, and CuO for e-CO_2R. *In situ* XRD and Raman spectroscopy confirmed the complete reduction of precursors to Cu(0), and Cu(0) was identified as the active species responsible for the improved selectivity. Initially, the strong C_{2+} selectivity was attributed to the small grain size of the resulting Cu. Interestingly, Cu nanocrystals synthesized from $Cu(OH)_2$ and $Cu_2(OH)_2CO_3$ were found to possess substantial tensile stresses, as indicated by *in situ* XRD. These stresses play a crucial role in promoting hydrogenation of *CO and C–C coupling, ultimately enhancing the overall e-CO_2RR selectivity while reducing HER rates.[52]

5. Theoretical calculations and computational studies

Theoretical calculations and computational studies, particularly those involving density functional theory (DFT), play a

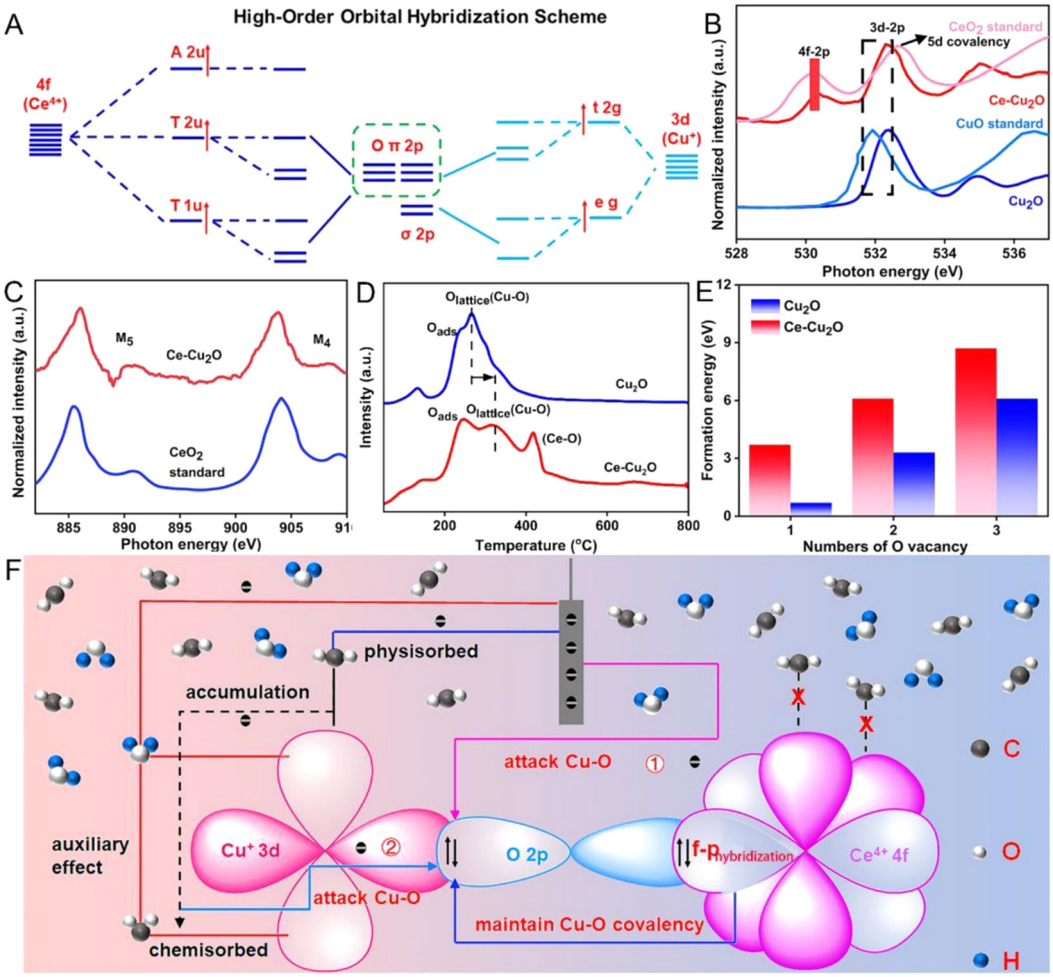

Fig. 4 Molecular orbital representation of Ce^{4+} 4f O 2p Cu^{+} 3d coupling (A). *Ex situ* sXAS measurements of the O-K edge in $CeCu_2O$ and Cu_2O catalysts (B). *Ex situ* sXAS at the Ce-M4,5 edge in Ce–Cu_2O (C). Ce–Cu_2O and Cu_2O O_2-TPD spectra (D). Formulation Energy requirenments for OVs in Ce–Cu_2O and Cu_2O, is presented in (E). (F) A schematic showing how the connection between the high-order orbitals 4f and 2p in Ce–Cu_2O prevents CuO deactivation and shields the Cu^{+} site from electron attack during the CO_2RR. Reproduced with permission from ref. 47. Copyright 2023, American Chemical Society.

crucial role in the design and optimization of catalysts for CO_2 reduction. These approaches allow researchers to model and predict the electronic structure, potential energy surfaces, and reaction pathways of catalyst materials at an atomic level. A DFT study found that Cu–M bimetallic catalysts have notable effects on the reaction barrier of CO_2RR and HER and display catalytic activity. The Cu–Pd catalyst is better for CO_2RR than for HER. This information can help in designing effective electrocatalysts and syngas production applications.[53] By simulating interactions between CO_2 and catalyst surfaces, computational studies can identify active sites, determine the most favorable reaction intermediates, and predict product selectivity. This theoretical insight complements experimental findings, guiding the rational design of catalysts with enhanced activity and selectivity. For instance, DFT calculations have helped in optimizing the composition and structure of Cu-based catalysts to improve their performance, ensuring a more efficient conversion of CO_2 to valuable chemicals.

The self-supporting and through-hole structure of CuSAs/TCNFs facilitated an increase in the number of useful Cu atoms while simultaneously reducing the number of incorporated metal atoms in the material. These individual Cu atoms played a pivotal role in the e-CO_2RR. Notably, the process yielded stable C_1 products with a current density of -93 mA cm^{-2}, maintaining stability in water for over 50 hours. DFT simulations suggested relatively high binding energy for the *CO intermediate in isolated Cu atoms. These findings suggest the potential for CO conversion into other valuable products, such as methanol, contributing to the reduction of CO levels.[54] Besides, ethanol synthesis emerged as one focal point: copper nitrogen-doped carbon materials with porphyrin-like Cu graphene structures played a critical role. The reversible transformation of porphyrin-like Cu sites to metallic copper nanoclusters complicates understanding their specific activities. A computational method was used to model the structure of the Cu–N–C material. Employing DFT calculations, the main focus of the work was on e-CO_2R for ethanol and ethylene production. In both CO reduction and ethanol production, Cu nanoclusters are significantly better than single sites. This all-encompassing piece of

research helps to further our knowledge of Cu-based catalysts for many different CO_2 conversion processes.[55]

Further expanding the investigation, the research delved into the CO_2RR process catalyzed by a material housing a single Cu site within an N-doped carbon surface. Utilizing periodic DFT computations, distinct surface models were developed for the first CuN_4 site and a secondary Cu cluster at negative potentials. While the feasibility of the single-site surface was found to be thermodynamically challenging, the mechanistic study highlighted the significant activity of the $Cu_{13}N_4$ nanocluster surface in driving CO_2R. Notably, the catalytic activity of the Cu, N-doped carbon with a single site heavily depended on the presence of $Cu_{13}N_4$ nanoclusters on its surface, owing to their unique capability to facilitate the crucial C–C coupling reactions required for C_2 product formation.[55]

DFT simulations were also employed to investigate the binding energies of CO_2R intermediates. Surface slab models for Cu(111), Sn(200), and Cu_3Sn(002) were constructed based on XRD data. The binding energy of H* on Cu_3Sn(002) was similar to that on Cu(111), while CO* binding energy on Cu_3Sn(002) was lower. This difference, along with the energetically preferable CO desorption process over CO* reduction, contributed to improved CO selectivity compared to Cu(111). The presence of surface Sn dramatically impacted HCOOH formation selectivity, allowing for control over two-electron reduction product selectivity through Cu–Sn alloying.[56] In the same study, DFT calculations were employed to examine the adsorption properties of CO_2 on clusters of Cu_{55}, $Cu_{54}Ni_1$, and $Cu_{42}Ni_{13}$, featuring highly symmetric cub-octahedral, decahedral, and icosahedral structures. The composition of these clusters was found to influence the energy required for CO_2 adsorption, with the icosahedral $Cu_{42}Ni_{13}$ cluster demonstrating the highest CO_2 adsorption capacity.[57]

Further, using DFT calculations, the impact of Zr doping on CO_2 hydrogenation to CHO in icosahedral Cu NPs was investigated. The findings indicated that Zr doping of Cu NPs improved CO_2 adsorption and hydrogen dissociation. Zr atoms played a crucial role in stabilizing chemical intermediates by lowering energy barriers.[58] Additionally, the structure, activity, and selectivity of the B-doped copper (B@Cu(111)) catalyst were probed with DFT simulations. It was revealed that CO adsorption and activation occurred at the B site, with CO favoring coupling to $*C_2O_2$. B played a crucial role in the conversion of carbon dioxide to ethanol and in capturing CO. The electronic structure and Bader charge analysis demonstrated that B stabilized C_2 intermediates by providing both empty and occupied orbitals for CO adsorption and activation.[59] In another study, the DFT simulations were employed to study e-CO_2R using Cu–X catalysts. Thermodynamic studies linked the O affinity of dopant atom sites and the Cu site's selectivity towards C_2 hydrocarbons and alcohols. Doping Cu–X catalysts with strong O affinity atoms, such as boron, favored the ethylene route. Non-metal doping on Cu surfaces often improved ethane selectivity while suppressing ethanol selectivity. The effect of electrical characteristics on intermediate adsorption and inherent selectivity was also addressed.[60]

In a related study, Chang and coworkers employed DFT calculations to investigate the highly selective formation of C_2 during CO_2RR on different copper surfaces, with a particular focus on Cu(711). The Cu(711) surface presents a unique challenge due to the presence of a high dipole–dipole repulsive force, which excludes the formation of an OC–CO intermediate *via* the CO–CO route. Instead, adsorbed CO undergoes protonation, leading to the creation of CHO or COH intermediates. Lowering the activation energy for C–C bond formation with adsorbed CO is achievable through the production of COH or CHO. In contrast, Cu(100) and Cu(111) surfaces are thermodynamically unfavorable for these reactions. Given the increased likelihood of COH participation in the C–C coupling processes of CO_2RR, its stabilization on the Cu(711) surface is more probable.[61] Additionally, the benefits of Cu cluster-doped C_3N_4 as a CO_2 reducer were investigated utilizing DFT calculations. Cu clusters were identified as ideal active sites for CO_2 adsorption and activation due to their structure and electrical properties, facilitating the separation and transport of photo-generated electrons and holes. The study revealed that C–O carbon atoms in gas-phase molecules could link with C–N_4 carbon atoms in the substrate, reducing the adsorption energy. Furthermore, it evaluated how the energy requirements for producing CO through the CO_2R process compare to those of the rival HER reaction. The reaction barrier for C_2 production on Cu_4–C_3N_4 was found to be larger than the HER reaction barrier due to the dimerization of *CO.[62]

In addition, Xue *et al.* developed efficient and selective electrocatalysts for the e-CO_2RR. Twenty-one MOF supported flexible, self-adaptive dual-metal-site pairs (DMSPs) were screened using DFT calculations. For e-CO_2R to C_2H_6 and C_2H_5OH, the computed limiting potential is −0.87 V, while MOF-808-EDTA-FePt shows even better activity at −0.35 V for CO_2R to C_1 products.[63] Furthermore, DFT was employed to investigate the adsorption, structural changes, energy profiles, and reaction processes caused by CO coverage on the active sites of the Cu_2O(111) surface. Due to the presence of unsaturated Cu atoms, the coordinatively unsaturated Cu site (Cu_{CUS}) on the Cu_2O(111) surface is shown to be highly reactive towards CO adsorption and subsequent reactions. C–C coupling is favored because the energy barrier of $*CH_2$ dimerization is lowered at higher CO coverage, specifically between 0.13 and 0.25. The maximum barrier energy occurs in the *CHO route, making the C–C coupling the rate-determining step.[64]

Moreover, Das *et al.* modeled the $CuAl_2O_4$(111) surface for CO_2 conversion to DME using DFT calculations, elucidating the importance of dopants (Ga and Zn) in modifying the catalyst's active center. They also revealed Ga's role in changing the acidic site of the $CuAl_2O_4$(111) surface, enabling methanol conversion to DME.[65] Furthermore, twenty bimetallic M–Cu–BTCs were subjected to DFT calculations to examine their CO_2 adsorption and activation properties. Linear adsorption emerged as a more effective means of interaction between CO_2 molecules and most bimetallic MOFs, except for Pt–Cu–BTC and Pd–Cu–BTC. CO_2 activation was observed on W–, Mo–, Re–, and Os–Cu–BTC complexes. While CO_2 adsorption was stronger on Os–Cu and Re–Cu nodes, W–Cu–BTC and Mo–Cu–BTC showed promise for

investigating the underlying mechanisms due to their higher H_2 adsorption capacities. The study also explored both the carboxyl (COOH*) and formate (HCOO*) routes of CO_2 hydrogenation with H_2 molecules on W–Cu and Mo–Cu complexes. While the energy barrier for W–Cu–BTC was 1.27 eV, it was only 1.10 eV for Mo–Cu–BTC.[66]

6. Engineering strategies in the rational design of Cu-based catalysts for electrochemical CO_2 reduction

There are various synthesis techniques utilized to manipulate the composition, structure, and morphology of copper-based catalysts to reduce CO_2. The choice of synthesis methods plays a part in determining performance and selectivity. Some strategies for synthesizing copper-based catalysts are introduced here.

6.1. Single crystal approach

The single crystal approach includes the use of single-crystal surfaces with well-defined atomic arrangements to design electrocatalysts for e-CO_2RR. In this context, the key to developing and making electrocatalysts is creating catalysts with specific surfaces of the single crystal. Adjusting the crystallographic orientation and atomic arrangements can provide more information about the catalytic mechanism and develop highly effective and selective catalysts. A number of different ways can be used with this technology to create materials with the desired properties. Epitaxial growth, surface etching, atomically accurate deposition, selective growth, template-based growth, and tip-based scanning tunnelling microscopy (STM) manipulation are all examples of this kind of technique. That is one important advantage of being able to design active sites consisting of single atoms. In this field, researchers have become interested in making electrocatalysts that can convert CO_2 to CH_3OH using single-atom Cu. It can be seen from first-principles calculations that the Co@Cu SA catalyst has potential to catalyze CO_2 reactions. The d-band of the catalyst becomes narrowed and its center shifts up, making it more stable for CO_2. As a result, energy barriers of the reaction are significantly reduced. This phenomenon enables us to selectively and efficiently produce CH_3OH, which has a profound effect on the entire procedure. The reaction pathway, $CO_2 \rightarrow COOH^* \rightarrow CO^* \rightarrow COH^* \rightarrow CHOH^* \rightarrow CH_2OH^* \rightarrow CH_3OH$, is guided by the modified catalyst. It is significant that the SA has a small lattice mismatch, so that it is stable against surface reconstruction. The catalyst's superiority is further highlighted by the difference in activation energy for the reduction of COOH* compared to Cu. Specifically, the activation energy required is 0.54 eV, which is 0.22 eV lower than the 0.76 eV required on Cu and reaction is exothermic. In another aspect, the narrow cobalt d-band plays a vital role in the performance of this catalyst by preventing the buildup of unwanted byproducts. This feature results in a higher yield of CH_3OH, further enhancing the overall sustainability and efficiency of the synthesis process. Collectively, the utilization of single-atom catalysts and the precise manipulation of crystallographic orientations hold promise for advancing the field of electrocatalysis and enabling more sustainable energy production through the selective and efficient conversion of CO_2 to valuable chemicals like methanol.[67]

The pursuit of high-rate e-CO_2RR activity, selectivity, and stability led Sassenburg *et al.* to investigate five distinct transition metal catalysts (Ag, Au, Pd, Sn, and Cu). Notably, Au and Pd exhibited CO-limiting current densities of 72 and 50 mA cm^{-2}, respectively, emerging as standout contenders among the 88 diverse catalysts examined. The study showcased the convergence of product selectivity for Cu catalysts across both neutral and alkaline environments. Additionally, the investigation highlighted Sn's susceptibility to instability under highly alkaline conditions (Fig. 5). The research encompassed an assessment of catalytic selectivity at 10 and 200 mA cm^{-2}, as well as a fundamental comparison of reaction rates.[68]

Furthermore, the evolution of a nanotwinned copper electrocatalyst specifically for e-CO_2RR aimed at methane production. At a potential of -1.2 ± 0.02 V *vs.* RHE, the catalyst exhibited impressive selectivity in generating methane, achieving a FE of $86.1 \pm 5.3\%$. The pivotal role of twin boundaries on Cu(111) facets in reducing the barrier for CO hydrogenation underscores their significance in the creation of CH_4. Notably, the presence of these twin boundaries on Cu(111) renders the surface more predisposed to CH_4 selectivity than a planar copper surface (Fig. 6). This multifaceted investigation and the nuanced understanding of catalyst behavior contribute to the advancement of electrocatalytic strategies for sustainable energy conversion.[27]

In contrast, the work by Lyu *et al.* explored the impact of trace copper loading within N-doped graphene quantum dots (NGQDs) on both e-CORR and e-CO_2RR. Interestingly, a rise in Cu loading within NGQDs exhibited the capacity to alter the selectivity of catalytic methane oxidation, shifting from primarily C_1 products to C_2 products. A notable outcome was achieved by introducing copper with an increased atomic size of 2.5 mg cm^{-2}, resulting in an increased selectivity of up to 52% for C_2 products, accompanied by a reduced selectivity of 62% for CH_4. Elevating the Cu loading further to 3.8 mg cm^{-2} led to the peak of C_2 product production efficiency at 78%. This observation is particularly significant considering the low partial pressure of CO during e-CO_2RR. The heightened copper loading becomes imperative to enhance selectivity toward C_2 products, thus illustrating the intricate interplay between catalyst composition and product selectivity in the context of sustainable energy conversion strategies.[69] With a shift of focus, Qai *et al.* carried out research experiments to probe the multifaceted role of crystalline structure and valency in oxide-derived copper (OD-Cu) catalysis as well as the mechanism and characteristics of e-CO_2R. The experiment also used single crystal Cu(111) foils, enabling regulatory analysis of their intrinsic variation in morphology and crystallography. It was interesting that the overall efficiency of OD-Cu in reducing CO_2, and particularly in achieving C_2H_4 selectivity, was shown to be significantly correlated with the initial oxidation degree of the Cu(111) foil. There is no significant effect on the catalytic activity of catalyst due to grain boundaries and polycrystallinity. These findings highlight a complex web of connections among

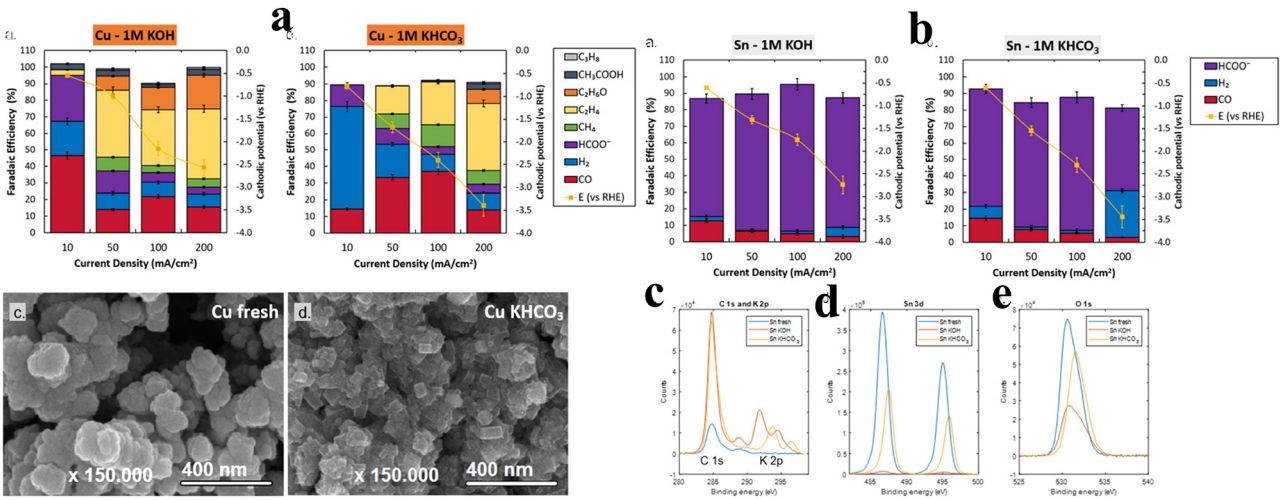

Fig. 5 (a) Analysis of electrodes with copper coating: the FE, in relation to activity, is explored across varying cathodic potentials in 1 M KOH and 1 M $KHCO_3$ solutions. Noteworthily, the error bars in both the panels illustrate the findings from distinct experimental runs. Employing HR-SEM, the visual depiction of fresh copper and its state after 1 hour of $KHCO_3$ electrolysis underscores the emergence of the distinct cubic faceting pattern on catalyst's surface. (b) Exploring Sn-coated electrodes: the characterization involves the assessment of faradaic efficiency concerning activity across cathodic potentials in 1 M KOH and 1 M $KHCO_3$ solutions. The error bars in both the panels depict the data variations from distinct experimental iterations. Further insights are gained through X-ray photoelectron spectroscopy (XPS) analyses, specifically examining C 1s and K 2p (c), Sn 3d (d), and O 1s (e) scans before and after subjecting the system to a 200 mA cm^{-2} experiment in both electrolytes. Reproduced from ref. 68. Open access article, American Chemical Society.

the structural features, oxidation states, and performance levels of OD-Cu, and therefore make important contributions to the understanding of environmentally friendly energy conversion processes.[70]

The study examined the catalytic activity of copper in the e-CO_2RR and how it varies according to the crystal phase. This was done by depositing ultra-pure Cu, which remained in the 4H and 4H/fcc phases. The study found that non-traditional crystal structures had better overall activity and selectivity in e-CO_2RR than the standard fcc-Cu structure towards ethylene. DFT calculations reveal that the 4H phase and 4H/fcc interface of Cu promote the C_2H_4 formation pathway more efficiently than fcc Cu, resulting in a crystal phase-dependent selectivity towards C_2H_4. This meant that different crystal phases had different C_2H_4 selectivity.[71] In an effort to research further, a widespread plan was drawn up by researchers. The goal was to effectively use copper-decorated through-hole carbon nanofibers (CuSAs/TCNFs) in e-CO_2R for the transformation of CO_2 to methanol. The fabricated CuSAs/TCNFs membrane achieved an impressive FE value of 44% for methanol.

6.2. Single atom approach

The single atom approach in the design of electrocatalysts for e-CO_2RR involves the dispersion of individual metal atoms on a suitable support material, often carbon-based. This method maximizes the utilization of metal atoms, ensuring that each atom acts as an active site, thereby significantly enhancing catalytic efficiency. By isolating metal atoms, this approach also allows for precise tuning of electronic properties and coordination environments, which can lead to superior selectivity and activity for specific CO_2RR pathways. The unique atomic configuration of single atom catalysts (SACs) can facilitate the stabilization of key intermediates and lower energy barriers, contributing to higher overall performance in CO_2RR. Chen *et al.* aimed to increase the efficiency of converting CO_2 to methane by designing a Cu-based catalyst that is augmented with a Lewis acid support. For example, metal oxides like Al_2O_3 and Cr_2O_3 can do it in this way. They can modulate the electronic structure of Cu atoms according to the requirements of intermediate adsorption. The specific study explored the potential of an ultrathin porous Al_2O_3 that was highlighted by its numerous Lewis acid sites, to bind Cu atoms at the single atom level. Remarkably, it yielded a notable increase in FE for CH_4 synthesis, reaching 62%, operating at a potential of −1.2 V and a current density of 153 mA cm^{-2}. This precise manipulation of individual copper atoms demonstrated a remarkable efficacy in the conversion of carbon dioxide to methane, offering a significant step towards efficient and sustainable energy conversion processes.[72] Zhao and his colleagues switched gears in their work, pursuing methanol production through electrolysis of CO_2. They developed a method in which copper-monitoring MXene was made with much success. The fourth MAX phases underwent selective etching. Only aluminum and copper from the hybrid A layers were specifically targeted for removal. It makes use of the saturated vapor pressure differences between aluminum and copper products. As a result, installing a Cu single-atom catalyst attains an impressive FE of 59.1% in making CH_3OH. The catalyst not only showed promise for electrocatalytic stability but also the potential for e-CO_2R because of its unsaturated electronic structure at the copper atom. Because of its unique properties, the e-CO_2RR has a low-energy barrier in the rate-determining step. In fact, copper-immobilized MXene plays a key role in promoting the development of sustainable energy solutions.[73]

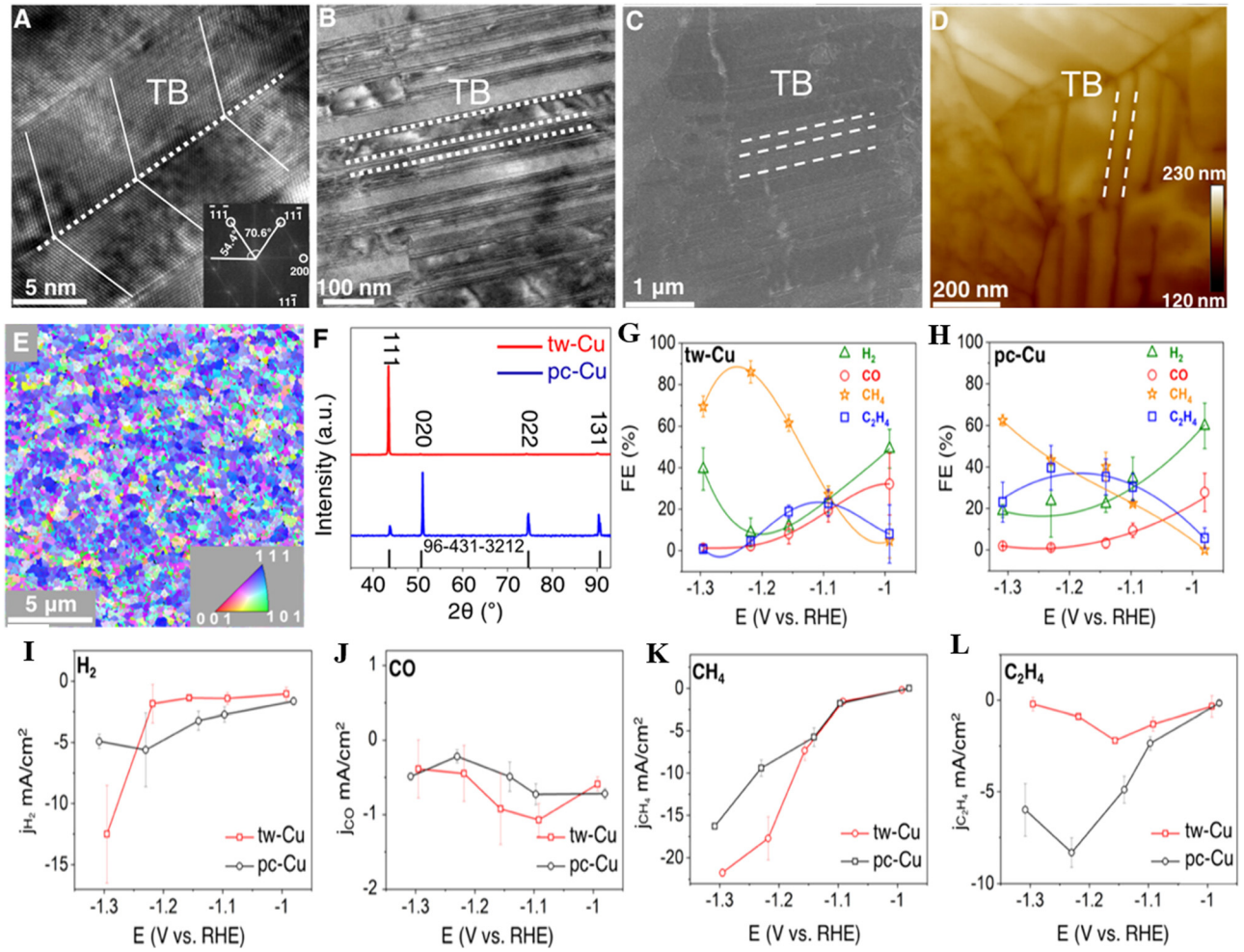

Fig. 6 Structural characterization of twin-bound and polycrystalline copper catalysts: (A) the intricate structure of tw-Cu captured through HRTEM. The cross-sectional image reveals the assembly of twin boundaries (TB). Inset: FFT of the corresponding Cu TEM, which indicates the ⟨110⟩ axial direction and expression of the {111} planes. (B) Offering a broader perspective, a low-magnification TEM image showcases tw-Cu, where dashed white lines delineate the characteristic twin boundaries. (C) This structural insight is further corroborated by a SEM image of tw-Cu, with white dashed lines again indicating the presence of twin boundaries. (D) A detailed AFM image of tw-Cu discloses a surface roughness of 2.7 nm. (E) The crystallographic texture of the tw-Cu surface is illuminated through EBSD orientation maps. The inset highlights color-coded crystallographic vectors, vividly suggesting a robust (111) texture. (F) XRD patterns of both tw-Cu and pc-Cu reveal the strikingly high orientation toward (111) planes in tw-Cu, in sharp contrast to pc-Cu. This distinction is emphasized through a comparison with the reference sample represented by the black line with PDF number 96-431-3212. e-CO_2RR: FEs of (G) tw-Cu and (H) pc-Cu. The data points corresponding to H_2, CO, CH_4, and C_2H_4 are color-coded as green, red, orange, and blue, respectively. Visualization of the partial current densities of (I) H_2, (J) CO, (K) CH_4, and (L) C_2H_4, where red lines signify tw-Cu and black lines represent pc-Cu. Each error bar emanates from three distinct measurements, while all potentials underwent *iR*-correction. Reproduced from ref. 27. Open access article, American Chemical Society.

Researchers considered the e-CO_2RR using a carbon substrate featuring coordinated copper atoms within a unique CuN_4 structure. This material showed impressive rates of conversion. It converted 55% of ambient CO_2 with distilled water as its source into ethanol; more impressively, 80% of dissolved CO was converted to C_2-products such as ethanol or ethylene. After all, the high faradaic yield in both cases proved this. Metal copper sites are responsible for catalytic action. Furthermore, the starting material was entirely recoverable.[74] Turning attention to another interesting study, Bao *et al.* illuminated the realm of e-CO_2R, employing single copper atoms on MXene nanosheets. The researchers achieved a remarkable selectivity of 98% for multi-carbon products and an impressive FE of 71% for ethylene synthesis at a potential of −0.7 V *vs.* RHE. The process involved the combination of carbon monoxide molecules to form the *CO–CHO species, effectively reducing the free energy barrier of the potential-determining step. This catalyst had something special about it as it continued being active all the way through the 68 hours of the electrolysis process, thereby proving that single copper atoms could produce useful compounds made up of many carbon atoms in a substantial way.[75]

In a separate project, the effort to achieve e-CO_2R led to the fabrication of atomically dispersed Cu catalysts on defective Ag nanowires. This innovative approach hinged upon a site-specific underpotential deposition method and an electrochemical conditioning treatment strategy, resulting in the dispersion of the

Cu/Ag(S) catalyst. The integration of Cu single-atom catalysts remarkably elevated the selectivity and activity of the catalyst in CO_2 reduction. The alteration of the d-band structure and the facilitated interaction between Cu single-atom catalysts and the conditioned surface's defects played a pivotal role. This augmentation led to an enhanced adsorption of e-CO_2RR intermediates, subsequently boosting the efficiency of the process. Impressively, at an e-CO_2RR current density of 2.9 mA cm^{-2}, the Cu/Ag(S) catalyst exhibited an outstanding FE of 93.0%, surpassing the performance of the Ag(S) catalyst lacking Cu single-atom catalysts. The presence of Cu SACs in proximity to faulty silver surfaces induced increased microstrain and a downward shift in the center of the d-band, effectively reducing the activation energy required for *CO generation by approximately 0.5 eV. This synergistic interplay resulted in heightened efficiency and specificity in CO_2 reduction, particularly in the production of CO and C_2 products, underscoring the catalytic competence of the Cu/Ag(S) catalyst.[76]

In a distinct exploration by Zheng *et al.*, a catalyst consisting of a single lead atom with copper was employed to successfully convert CO_2 into formic acid. The catalyst's remarkable 96% FE in formate generation underscores its exceptional performance. The active copper sites regulated the first protonation step extremely accurately so that the reaction went towards formate synthesis without the formation of other products. The authors supported the use of this method for producing valuable liquid fuels with high purity.[77] Moreover, Song *et al.* delved into the catalytic performance of two Cu SACs with asymmetric surfaces in e-CO_2RR. The CuN_3O/C catalyst exhibited outstanding selectivity for e-CO_2RR, boasting a CO FE of over 90% across a potential range of −0.5 to −0.9 V *vs.* RHE. With a potential of −0.8 V, the selectivity for CO production reached an impressive 96%. In complete contrast, the $CuCo_3$/C catalyst showed terrible CO selectivity even at −0.5 V *vs.* RHE, only 20.0% CO FE was observed. In particular, the CuN_3O/C catalyst displayed a TOF of 2782.6 h^{-1} at −0.9 V *vs.* RHE, greatly in excess of the highest TOF recorded for $CuCo_3$, 4.8 h^{-1}.[78]

Furthermore, the e-CO_2R rate can be improved by using Cu single-atom catalysts with adjustable concentrations in addition to nitrogen attachment. In addition to facilitating water dissociation, CH_4 synthesis in the presence of nitrogen involves the metal assisting in the binding of hydrogen to make COOH intermediates. At a potential of −1.8 V *vs.* RHE, CH_4 yield for Cu catalysts was as high as 68.2% along with an impressive CH_4 j of 493.1 mA cm^{-2}.[79]

So as to convert CO_2 into acetate and syngas more efficiently, a new tandem catalyst had to be developed. A cost-effective catalyst has copper nanoparticles that integrate nickel single atoms selectively. These single Ni atoms make CO coverage bigger, and the C–C bond tends to cause an expanded interaction with adjacent Cu nanoparticles to facilitate acetate synthesis. It is worth noting that when flexibility with respect to production of syngas (H_2/CO) is desired, the tandem catalyst varies from 0.06 : 1 to 19.5 : 1. The intention of this method is to supply liquid fuels more effectively by following CO_2RR for the production of syngas and helping to achieve a higher selectivity. The target is single C_2 molecules. This is the first critical step from production in the laboratory to implementing it in industry on a large scale.[80] Table 1 lists the different kinds of electrocatalysts developed and designed for e-CO_2R to different products based on the single crystal and single atom approach.

6.3. Oxidation state engineering

One technique to develop materials for CO_2 conversion involves manipulating the oxidation states of elements. Materials scientists can modify the oxidation states of elements to regulate both activity and selectivity. This way, we learn that oxidation states can change material structure, surface chemistry, and reactivity. Through the control of oxidation states, CO_2 absorption and charge transfer are made possible, affecting reaction pathways. Numerous methods exist for engineering oxidation states. Through controlled changes made to a material's surface, for example the addition of groups or the creation of defects, the oxidation state of the surface oxide atom can be altered. To adjust oxidation states and improve the catalytic activity of a material, controlled doping involves introducing atoms into the lattice structure. Advanced *in situ* techniques, as potential modulation tools, allow oxidation states to be manipulated in real time during catalysis and enable dynamic control over reaction pathways. Owing to these techniques, researchers have a wide range of tools that can manipulate oxidation states. They can create materials that efficiently convert CO_2 into useful products. According to this idea, one groundbreaking study found that Cu_xO-decorated graphene oxide (G-Cu_xO-T) has the potential to be used as an electrocatalyst that is capable of controlling e-Co_2R. It was found that the function of the electrocatalyst G-Cu_xO-2h (x = 1–3) can be controlled by the valency of Cu. Key to this control is the multivalence of Cu. It is Cu(I) above all that has been chosen to improve the adsorption of CO_2 and enable the facile desorption of $HCOO^-$, so the catalysis process can be optimized. However, Cu(II) was important in maintaining durability, and thus in enhancing the overall stability.[82]

In a parallel avenue of investigation, another study's focus shifted to the impact of the substrate (Cu_2O) on the catalytic selectivity of the deposited Sn catalyst. Notably, the presence of Sn played a significant role in formate formation, with the potential to limit the HER requiring a deposition time of less than 120 seconds. Surface analysis revealed the presence of Cu^+ either on or beneath the surface, attributed to kinetic constraints during cathodic Sn deposition and e-CO_2R. Positioned between Sn^{2+} and Sn^{4+} in terms of electronegativity, Cu^+ occupied a midrange position. The Sn-deposited electrode exhibited enhanced catalytic selectivity when the deposition time was under 120 seconds, attributed to the stabilizing influence of residual Cu^+ species on the surface of Sn, maintaining it at a positive oxidation state between +2 and +4.[83] Concurrently, a separate avenue of inquiry was pursued, leading to the discovery that a Cu/ZnO catalyst could serve as a catalyst for converting CO_2 into alcohols, specifically ethanol and methanol. This was achieved through the oxidation of Cu nanoparticles at a low temperature, followed by their amalgamation with ZnO crystalline powder. Through a liquid-phase setup, the study scrutinized

Table 1 Based on the single crystal/atom catalyst approach, a number of electrocatalysts have been specifically crafted for CO_2R. A review of the work reveals the selective as well as the energetic considerations that must be taken into account in good catalyst design in order to achieve efficiency

				≈FE%									
No.	Material	Electrolyte	V *vs.* RHE	H_2	CO	CH_4	C_2H_4	$HCOO^-$	$C_2H_5^+$	CH_3OH	C_2H_5OH	$C_2H_3O_2^-$	Ref.
1	Tw-Cu	0.1 M $KHCO_3$	−1.31	39.3	1.1	69.5	0.74	0.01	0.04	—	—	—	27
2	Pc-Cu			18.7	1.86	62.5	23.02	0.01	0.04	—	—	—	
3	Cu@GDE	1 M KOH	−2.6	7	18	6	39	4	—	—	21	—	68
4	Cu@GDE	1 M $KHCO_3$	−3.4	10	17	3	46	3	—	—	8	—	
5	Cu(111)-LO@GDE	1 M KOH	−1.8	40	6	8	8	—	—	—	—	—	70
6	Cu(111)-MO@GDE			32	4.8	12	20	—	—	—	—	—	
7	Cu(111)-HO@GDE			38	2.9	2.3	27.4	—	—	—	—	—	
8	p-Al_2O_3	1 M KOH	−1.4	68	4	—	—	8	—	—	—	4	72
9	Cu/p-Al_2O_3 SAC			10	10	49	1	9	—	—	1	9	
10	Poisoned Cu/p-Al_2O_3 SAC			19	21	14	2	—	—	—	—	9	
11	Cu NPs/*p*-Al_2O_3			10	10	39	2.5	2	—	—	12.5	13	
12	SA–Cu–MXene	0.1 M $KHCO_3$	−1.8	75.5	—	—	—	—	—	17.5	5	—	73
13	Cu-particles–MXene			—	—	—	—	—	—	4	—	—	
14	$Cu_{0.5}NC$	0.1 M $CsHCO_3$	−1.3	45	22	—	—	—	—	—	28	—	74
15	4H Au@Cu	0.1 M $KHCO_3$	−1.13	22.5	17.5	2	45	8	—	—	—	—	71
16	4H/fcc Au@Cu			29	9	3	39	20	—	—	—	—	
17	Cu SAs/TCNFs	0.1 M $KHCO_3$	−1.2	33	45	—	—	—	—	25	—	—	54
18	Cu SAs/CNFs			45	33	—	—	—	—	22	—	—	
19	Cu–SA/$Ti_3C_2T_x$	1 M KOH	−0.9	18	—	—	55	—	—	—	25	—	75
20	Cu-NP/$Ti_3C_2T_x$			80	—	—	8	—	—	—	10	2	
21	BNC–Cu	0.5 M $KHCO_3$ 1 M KOH	−1.46	25	1	72	2	—	—	—	2	—	81
22	Ag	0.1 M $KHCO_3$	−1.4		22			2					76
23	Ag(S)				25			5					
24	Cu/Ag(S)			—	52	4	1	6	—	—	13	—	
25	Pb_1Cu SAAs	0.5 M $KHCO_3$	−1.62 (Ag/AgCl)	12.4	0.7	—	—	78.4	—	—	—	—	77
26	CuN_3O/C	$KHCO_3$	−0.9	—	96	—	—	—	—	—	—	—	78
	$CuCO_3/C$			—	5	—	—	—	—	—	—	—	
27	Cu SAs-0.1	KOH	−1.4	32	12	54	—	—	—	—	—	—	79
28	Ni SACs–Cu NPs	1 M KOH	−1.0	25	33	5	10	13	—	—	8	—	80

ZnO's influence on the restructuring of the Cu-based catalyst and its electrocatalytic efficiency in alcohol production under varying applied potentials. Enhanced carbon–carbon coupling and ethanol generation were attributed to ZnO inducing higher CO productivity on the Cu/ZnO-based electrode compared to the Cu-only counterpart. The production of ethanol within this tandem catalyst, as a precursor to further CO reduction into C_{2+} alcohols, was directly linked to the abundance of Cu^{1+} and Cu^0 combinations on the CZ catalytic surface.[84]

Moreover, the research revealed the catalytic role of the original copper electrodes in influencing their future activity and stability. More specifically, it was found that Cu(I) oxide would dissolve because of its low conductivity when dispersing in electrolyte for e-CO_2R, but Cu(II) oxide would just as easily be converted into metallic copper. That is to say, when these materials were used as electrodes and maintained at above room temperature they behaved more like liquid crystals than crystalline solids. However, the high activity and selectivity reported in the literature for OD-Cu electrodes could potentially be attributed to the fact that Cu(II) dissolution, which is more prevalent in bulk electrodes like foils or single crystals, exposes the metallic surface beneath the porous Cu(II) oxide structure. The outcomes of this study demonstrated that metallic copper is an excellent electrocatalyst for e-CO_2R and that the metal's intrinsic activity can be modified without compromising its conductivity. In order to maintain the stability of the metallic copper matrix phase, moderate doping levels must be used, which might influence activity and selectivity.[85] In another study, Cu-MOF/NP catalysts were made from MOF templates. More specifically, the Cu-MOF20/300 nanoparticles proved to be potent electrocatalysts for electrochemical CO generation because of their Cu/Cu_2O heterogeneous structure and vast active surface area. Impressively, the Cu-MOF20/300 catalyst demonstrated a high faradaic efficiency (FE_{CO}) of 43.8% for CO generation. Furthermore, the electrochemical reaction performance of the flow MEA reactor displayed significant enhancements compared to the conventional H-type setup. The reactor's compact design allowed it to reach current densities in excess of 230 mA cm^{-2} at a low applied potential, effectively lowering both ohmic and charge transfer resistances. The incorporation of a fillable gas–liquid separation component made it much more sensitive to changes, thereby facilitating detection and estimation.[86]

To gain deeper insights, the study explored the complex relationship between torsion and porous Cu electrode oxidation state. It turned out that substrates with high tortuosity have lower CO_2 content especially in deeper layers. Amazingly high tortuosity in the network resulted in bubbles of CO traveling farther, increasing the chance of CO going back to surface catalytic surfaces. The generation of C_{2+} products was favored by this phenomenon. The generation of CO, HCOOH, CH_4 and C_{2+} products were elucidated in this study, showing that their production was influenced by CO_2 and CO availability and an intricate interplay between them. The Cu oxidation state was used as a means of extracting insight into selectivity from

research on yield/efficiency of carbon dioxide reduction. This detailed analysis showed that metallic copper had more favorable C_{2+} alcohol pathways than copper derived from Cu^{2+} or Cu^{+} particles.[87] In another facet of their research, scientists also succeeded in regenerating the Cu catalyst *in situ* for the sustainable reduction of CO_2 into various carbon products. Using an AC intermittent working mode, the catalysts went through periodic invigoration by the oxidizing Cu surface. When operated in this effective manner, at a constant current density of 150 mA cm^{-2} the Cu catalyst remained active for an impressive 120 hours and maintained 40% selectivity throughout.[88]

The authors demonstrated that, for better efficiency, optimizing the placement of the semiconductor sensitizer and CuO_x co-catalyst was better. In addition, the research also explores the role played by thin Cu_2O. The findings showed that CO_2 reduction was affected by the distribution of the Cu surface's oxidation states. Because of CO_{atop} intermediate species and C_1 hydrocarbon-product production, electrodeposited Cu electrodes had higher Cu(I) in them. Conversely, the presence of Cu(0) in the initially prepared electrodes hindered hydrocarbon product development. Moreover, the coexistence of Cu(I) and Cu(0) in the CO_2-reduction products yields not only CO_{bridge} but also CO_{atop}, leading to the high selectivity for the C_2 product.[89] When using HQ-Cu or AN-Cu, both of which are electrodes comprised of mixed oxidation states, a greater selectivity for C_{2+} products was noted. The distribution and historical development of different Cu species were characterized using FIB-TEM/EELS. Notably, during the steady state of CO_2RR, the HQ-Cu electrode underwent complete reduction to metallic Cu, indicating that the observed high C_{2+} selectivity did not rely on specific Cu oxidation states. To ensure complete reduction to Cu^0 prior to CO_2RR, the electrodes underwent electro-reduction pretreatment. Further bolstering the pivotal catalytic role of Cu^0 and the minimal impact of the initial oxidation state of oxidized Cu, the pretreated electrodes exhibited slightly enhanced selectivity toward C_{2+} products. Notably, an oxidation–reduction cycle led to crystal fragmentation, observed when oxide crystals in HQ-Cu and AN-Cu were reduced and fragmented into small irregular Cu grains under the negative potential of electro-reduction pretreatment or CO_2RR.[90]

In the pursuit of exceptional CO_2RR performance, a 1D composite SnCu-CNS was resourcefully developed, boasting a hierarchical structure of nanotubes and loaded nanorods. This composite showcased a remarkable trait, achieving a partial current density of 205.1 mA cm^{-2} for formate at 1.0 V *vs.* RHE cathode potential, and reaching an impressive peak FE of 95.1% within an H-type cell.[91] Another study's findings unveiled a synergistic connection between the structural evolution of Cu_2O and the surface—interface CO_2 reaction. During the cathodic scanning phase of CV, CO* derived from CO_2R assumed the role of a stabilizer, effectively preventing the oxidation of metallic Cu. This stabilization process expedited the shift from inert Cu_2O to the more dynamic Cu/Cu_2O under regular operational conditions. Importantly, the incorporation of Cu/Cu_2O led to a substantial increase in FE for ethanol, elevating it from 5.15% to an impressive 56.56%, and significantly fostered the generation of C_2 products.[92]

To ensure the stability of Cu^+ sites during the CO_2RR, the researchers designed $PdCu_3N$, a catalyst built upon the anti-perovskite type Cu_3N. Remarkably, the incorporation of negative-valence Pd into the catalyst significantly augmented the synthesis of C_2 products, resulting in a substantial increase in the FE of C_2 (78.2%) compared to the Cu_3N catalyst with only single Cu^+ sites (5.6%).[93] Concurrently, another study delved into the utilization of Cu nanosheets decorated with small Cu_2S nanocrystals as catalysts for the e-CO_2R into C_2H_5OH (Fig. 7). The investigation showcased that in an H-cell containing 0.1 M $KHCO_3$, the total current density reached 45 mA cm^{-2}, accompanied by a substantial $J_{C_2H_5OH}$ of approximately 20.7 mA cm^{-2}. The advantageous attributes of decorating Cu nanosheets with nanocrystals encompassed a non-flat, stepped surface, a high localized positive charge of Cu^+, and well-established interfaces between Cu^+ and Cu^0. These attributes collectively enhanced CO_2 adsorption, facilitated charge transfer for CO_2RR kinetics, facilitated the dissociation of the *COOH intermediate into *CO, heightened the affinity of *CO on the catalyst, reduced the energy barrier of CC coupling, created favorable spatial conditions for C_2H_5OH production, and facilitated the spontaneous hydrogenation of $*CH_2CHO$ to $*CH_3CHO$.[94]

In a related investigation, the selective production of CH_4 and C_2H_4 in the CO_2RR process on CuO_x catalysts with varying oxidation states and reductant agents was investigated. The study identified the optimal oxidation state of the copper catalyst, leading to the highest selectivity for C_2H_4 (FE = 53%). The study explored several potential reaction pathways, including CC coupling, hydrogenation of CO to produce CHO, direct dimerization of CO to produce C_2H_4, and hydrogenation of CO to yield CHO or COH.[95] Table 2 presents an overview of different electrocatalysts designed by following the oxidation state engineering approach for e-CO_2R to a number of fuels.

6.4. Alloying approach

The use of alloying is a versatile strategy in designing electrocatalysts for CO_2R. By combining metals catalysts with customized properties can be created to enhance efficiency and selectivity in converting CO_2 into products. This approach plays a role in tackling challenges related to clean energy conversion. Researchers can carefully mix metals to optimize the binding strength for CO_2 and its byproducts, minimize overpotentials and improve catalytic performance. Importantly alloying can result in effects where the resulting alloy's properties surpass those of metals, making it an invaluable tool in the pursuit of sustainable CO_2R.

There are two primary types of alloying approaches used in electrocatalysis: pure metallic alloys and compound alloys. In pure metallic alloys, metals are blended to create alloys with enhanced catalytic activity and selectivity. Metals are selected based on their characteristics and desired catalytic outcomes. On the other hand, in compound alloys, a metal is combined with a metal element or a compound. This approach introduces active sites and modifies the electronic structure of the alloy leading to improved performance in CO_2R.

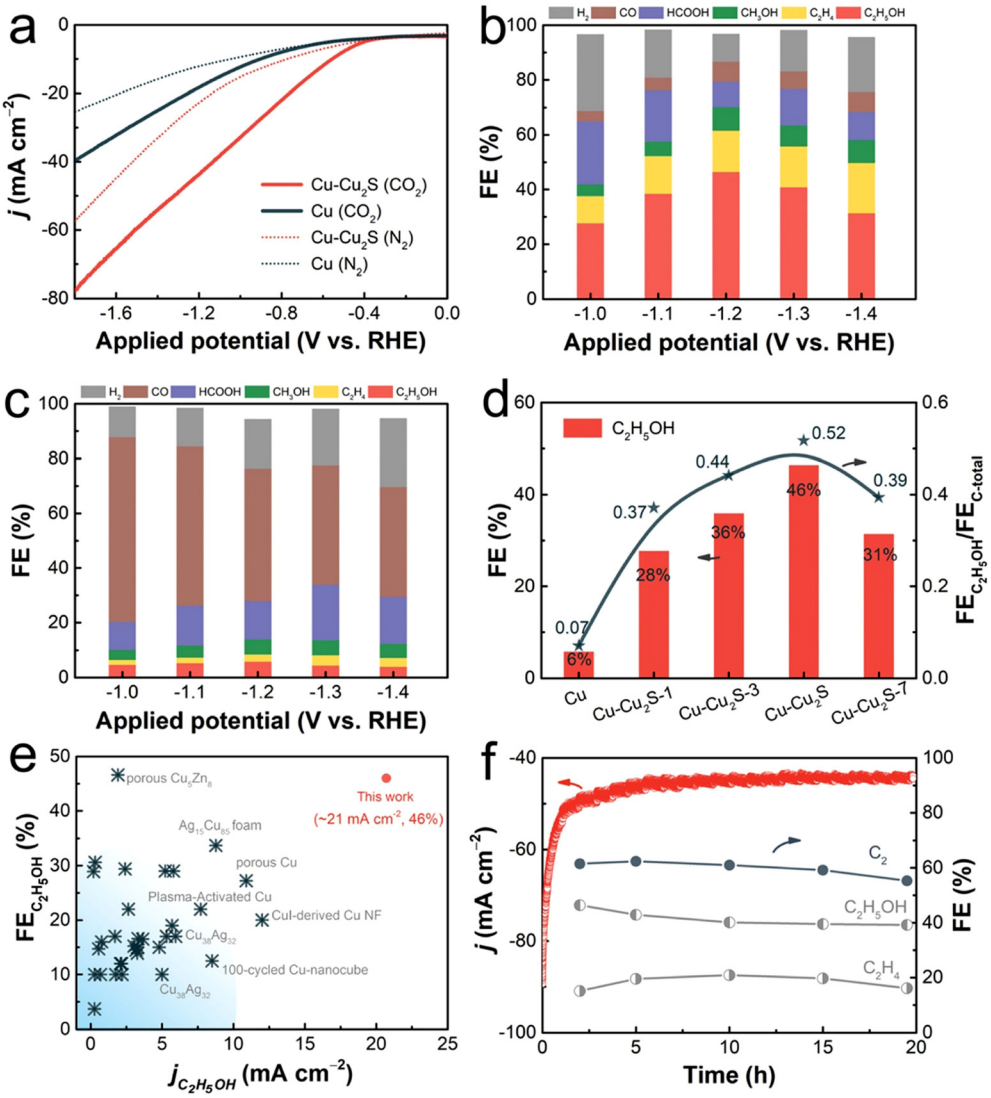

Fig. 7 Electrochemical activity of the manufactured catalysts for CO_2R. In a N_2- and CO_2-saturated 0.1 M $KHCO_3$ aqueous electrolyte (a), the LSV curves of pure Cu and $CuCu_2S$ are shown. Distributions of the products of the catalyzed CO_2RR for (b) $CuCu_2S$ nanosheets and (c) pure Cu nanosheets at various applied potentials. At 1.2 V (against RHE), $FE_{C_2H_5OH}$ and $FE_{C_2H_4OH/FEC}$ products for $CuCu_2S$, pure Cu, and $CuCu_2S$-1,3,7 in an H-cell containing 0.1 M $KHCO_3$ solution (d). The comparison of partial current density for C_2H_5OH and the $FE_{C_2H_5OH}$ of $CuCu_2S$ with those of previously reported catalysts. Some examples of these catalysts are copper nanocubes, copper nanofibrils, nanofibrils generated from copper ions, copper alloys, copper activated in plasma, copper foam, and porous copper (e). 20 hours of stability at 1.2 V (against RHE) in terms of geometrical current density and field strength for carbonaceous compounds catalyzed by Cu and Cu_2S (f). Reproduced with permission from ref. 94. Copyright 2023, American Chemical Society.

6.4.1. Pure metallic alloys. The use of metal alloys as a strategy for designing e-CO_2R shows potential in the field of sustainable energy conversion. This approach involves creating catalysts by combining metals to take advantage of their unique electronic and structural properties resulting in synergistic effects. Pure metal alloys are valuable because they can enhance activity, selectivity and stability for CO_2RR. Researchers can carefully combine metals to create catalysts with customized behaviors enabling conversion of CO_2 into valuable chemicals and fuels. The significance of this strategy lies in its ability to promote the use of materials found on Earth reducing reliance on precious metals like platinum and palladium. There are different methods used to obtain metal alloys for e-CO_2R. One common approach is controlled electrodeposition, where different metal precursors are deposited together onto a conductive surface, under specific electrochemical conditions. Alloying can also be achieved through treatment by mixing metal precursors and heating them to encourage solid state diffusion and alloy formation. The resulting alloys exhibit effects that improve the binding of CO_2 intermediates and facilitate their conversion into desired products. Pure metallic alloys, in essence, provide an eco-friendly approach to creating electrocatalysts. This significantly contributes to the progress of energy technologies and helps curb the release of greenhouse gases.

Gunji *et al.* have explored the electrocatalytic selectivity of Pd-based bimetallic nanoparticles for CO_2 reduction. PdZn

Table 2 By investigating materials synthesized through oxidation state engineering this table explores the landscape in CO_2R. Specifically tailored catalysts show promise in energy production through their performance in CO_2RR, which involves generating hydrogen, carbon monoxide, methane and other compounds

				≈FE%									
No.	Material	Electrolyte	V *vs.* RHE	H_2	CO	CH_4	C_2H_4	$HCOO^-$	$C_2H_5^+$	CH_3OH	C_2H_5OH	$C_2H_3O_2^-$	Ref.
1	G-Cu_xOT	0.5 M $KHCO_3$	−0.8	64	—	—	—	9	—	2	—	—	82
2	Cu foil	0.5 M $KHCO_3$	−1.2	25	22	—	—	20	—	—	—	—	83
3	Soaked Cu 0 s			24	31	—	—	37	—	—	—	—	
4	Sn foi			30	7	—	—	68	—	—	—	—	
5	S Sn			22	8	—	—	73	—	—	—	—	
6	Cu calc		−1.4	68	3	2	—	9	—	—	5	—	84
7	CZ calc			78	5	1	—	4	—	1	7	—	
8	PVD Cu films @ 25 °C	100 mM $KHCO_3$	−1.8 Ag/AgCl	76	2	9	9	3	—	—	1	—	85
9	PVD Cu films @ 150 °C			67	1	13	12	1	—	—	6	—	
10	Cu/MOF 20/300	0.5 M $KHCO_3$	−0.66	62	35	—	—	—	—	—	—	—	86
11	OD-Cu-16	0.1 M $KHCO_3$	−1.0	—	22	2	15	23	—	—	—	—	87
12	OD-Cu-32			—	23	3	21	21	—	—	—	—	
13	OD-Cu-45			—	5	4	31	14	—	—	—	—	
14	OD-Cu-70			—	3	6	28	17	—	—	—	—	
15	Cu/PTFE 200 nm	1 M $KHCO_3$	100 mA cm^{-2}	17	4	16	38	4	—	—	10	—	88
16	Cu/PTFE 700 nm			19	7	1	42	8	—	—	17	—	
17	Cu/PTFE 1000 nm			18	9	1	42	10	—	—	37	—	
18	Electrodeposited Cu	0.1 M $KHCO_3$	−1.0	53	—	32	—	9	—	—	—	—	89
19	As-prepared Cu			49	3	—	—	14	—	—	—	—	
20	CV-treated Cu			10	5	38	42	8	—	—	—	—	
21	Electropolished Cu	0.1 M $KHCO_3$	−1.0	70	11	2	15	—	—	—	—	—	90
22	HQ-Cu			30	2	5	27	—	—	—	—	—	
23	AN-Cu			29	3	3	23	—	—	—	—	—	
24	SnCu-CNS	0.1 M $KHCO_3$	−1.0	9	28	—	—	63	—	—	—	—	91
25	*o*-Cu_2O	0.1 M $KHCO_3$	−1.06	30	22	—	13	12	—	—	5	—	92
26	Cu/Cu_2O-CV			9	8	—	9	14	—	5	58	5	
27	Ce–Cu_2O	0.5 M $KHCO_3$	−1.1	—	8	—	11	—	—	—	—	—	47
28	Cu_2O			—	4	—	8	—	—	—	—	—	
29	Cu_3N	1 M KOH	−1.1	19	43	—	2	36	—	—	—	—	93
30	$Pd^{\delta-}$–Cu_3N			9	10	—	39	4	—	—	32	—	
31	$Pd_{0.1}$			—	90	1	—	—	—	9	—	—	96
32	Cu			—	89	—	—	—	—	11	—	—	
33	$CuPd_{0.05}$			—	65	—	—	—	—	35	—	—	
34	$CuPd_{0.1}$			—	93	—	—	—	—	7	—	—	
35	$CuPd_{0.5}$			—	87	—	—	—	—	13	—	—	
36	$CuPd_2$			—	89	1	—	—	—	10	—	—	
37	$CuPd_{5.7}$			—	91	1	—	—	—	8	—	—	
38	Cu–Cu_2S	0.1 M $KHCO_3$	−1.1	18	3	—	14	19	—	6	38	—	94
39	Pristine Cu nanosheets			15	57	—	3	15	—	3	5	—	
40	CuO_{x-1}	0.1 M $KHCO_3$	−1.5	—	—	40	20	—	—	—	—	—	95

NPs/CB and PdCu NPs/CB exhibited selectivity for $HCOO^-$ production, while PdSn NPs/CB and $PdAg_3$ NPs/CB favored CO generation. Notably, PdZn NPs/CB displayed a higher selectivity for $HCOO^-$, achieving approximately 100% faradaic efficiency for $HCOO^-$ generation at −0.1 V. The presence of PdSn NPs and $PdAg_3$ NPs/CB suppressed $HCOO^-$ production, leading to CO selectivity. The underlying mechanism driving this selectivity is currently undergoing further theoretical investigation.[97] Additionally, CuZn catalysts with varying Zn contents were developed to enhance CO_2R into various products, particularly HCOOH. These catalysts were used as cathodes in PEC reactions and electrodes in electrochemical CO_2 reduction. The CuZn-0.5 catalyst exhibited significantly higher current density compared to Cu-foil, with a FE of 60%. The synergistic interaction between Cu and Zn sites played a crucial role in increasing the selectivity for HCOOH during CO_2R.[98]

In comparison to an electrodeposited Cu electrode, the $Cu_{76}Sn_{24}$ alloy, composed of Cu_3Sn, demonstrated reduced H_2 and hydrocarbon formation during CO_2R. The alloy exhibited selectivity for CO generation across all applied potentials, with an increase in HCOOH production as the potential was increased. Furthermore, another study, by analyzing the structure of the active site, highlights that Cu–Sn binary catalysts have shown improved selectivity. To mitigate hydrogen generation in electrochemical operations, Sn single atoms should replace nearby terrace Cu atoms. The active Cu edge atoms are responsible for this mechanism. These structures maintain thermodynamic stability under reducing conditions. It is advisable to avoid creating competing structures during material preparation. Substituting Sn prevents the HER process by disrupting the local 3-fold symmetry required for efficient H adsorption at Cu edges. By facilitating CO formation from CO_2 through charge transfer from the Sn atom to the Cu edge atoms, increased selectivity for CO is achieved.[99] Similarly, Yoo *et al.* have fabricated 3D-h CuSn in order to examine the impact of composition and geometry on CO_2R. Remarkably, the

FE_{CO} was significantly increased to 98.6% at −0.45 V *vs.* RHE when tiny Sn NPs partially covered the Cu surface. Effective CO production was demonstrated at this low Cu/Sn ratio. This change in the FE landscape for the CO_2R is attributed to the hierarchical nanoscale architecture, which generates a strong localized electric field, resulting in K^+ accumulation near the catalyst surfaces.[100]

Using a co-reduction strategy, Tang *et al.* have developed a Cu-decorated Cu_2O catalyst with tunable activity by adjusting the amount of Ag. The modified CuAg-0.75% catalyst displayed enhanced catalytic performance in producing liquid multi-carbon compounds, particularly ethanol. It achieved a maximum $J_{\text{liquid }C_{2+}}$ of 288 mA cm^{-2} and a j_{ethanol} of 214 mA cm^{-2} at a low overpotential. DFT simulations suggested that the CC coupling process might benefit from the overflow of CO from sites with strong CO adsorption on Cu sites.[101] In another experiment, a CuNiZn alloy was used as the electrocatalyst for the e-CO_2R and e-COR. The primary hydrocarbons produced were alkenes, while formate, carbon monoxide, and methane were byproducts of the initial CO_2R.[102] Another study highlighted the ability to manipulate bimetallic Cu–Pd nanoalloys to achieve specific morphologies and compositions. Spherical Cu–Pd nanoalloys with a Cu/Pd molar ratio of 1/0.3 exhibited the highest FE for CO conversion, while dendritic Cu–Pd nanoalloys were efficient for H_2 synthesis *via* HER (65.2% at a polarized potential of −0.87 V).[103]

In addition, Liu *et al.* investigated the electrical and nano/mesostructural effects of uniformly produced Au–Cu bimetallic films, with an emphasis on their utilization in e-CO_2R. The introduction of Au drastically altered the d-band electronic structure, leading to a reduction in the binding strength of CO. The binding energy in the d-band could be tuned by varying the composition of the alloy. Increasing the Au content was found to enhance e-CO_2R activity and selectivity, demonstrating that the electronic effect alone was not sufficient to overcome the linear scaling relationship. Interestingly, copper oxide/hydroxide species on Au–Cu surfaces were less stable compared to those on pure copper, despite the presence of gold. Alloying Cu with Au could prevent the formation of $HCOO^-$ by reducing the adsorption energy of *OCHO. The generation of $HCOO^-$ was profoundly affected by the electrical effect and d-band structure, although the activity did not scale linearly with changes in composition.[104]

Again, for e-CO_2R, Cu–Co bimetallic nanoparticles were synthesized on porous carbon using a similar process as adapted by Guo *et al.* These catalysts achieved current densities as high as 62.1 mA cm^{-2} in an electrolyte containing 0.5 M $[Bmim]PF_6$ in MeCN, resulting in a FE_{CO} of 97.4%. Catalytic activity was increased due to the interaction between Cu and Co, which increased the electrochemical surface area and CO_2 adsorption capacity.[105] However, Velasco-Vélez *et al.* have discovered that adding Zn heteroatoms to a copper metal lattice did not significantly boost the creation of profitable multi-carbon species during the e-CO_2RR. The presence of Cu^+ species in the reaction pathway had little effect on these species.[106] Further, the impact of metal content and particle size of CuCo nanoparticles generated *via* inverse micellar encapsulation on e-CO_2RR activity was investigated. The results demonstrated that initially both metals were oxidized, and even a small amount of Co significantly enhanced the activity of CuCo nanoparticles. As particle size increased, e-CO_2RR outperformed HER.[107]

Furthermore, pulsed laser ablation in liquids (PLALs) was used to produce noble metal-free multi-principal element alloy nanoparticles (MPEA-NPs) for the e-CO_2R. The electrochemical testing confirmed the unique activity of MPEA-NPs stabilized with poly-(diallyldimethylammonium chloride) (PDADMAC) for CO_2R. It was discovered that $Al_8Cr_{17}Co_{17}Cu_8Fe_{17}Ni_{33}$ MPEA-NPs exhibited highly efficient catalysis for CO_2R, potentially replacing costly noble metal electrocatalysts.[108] Okatenko *et al.* had shown that the stability of Cu nanoparticles under CO_2RR had been significantly enhanced by the addition of Ga. Ga-Added nanoparticles had remained stable for up to 20 hours, whereas the parent Cu nanoparticles had decayed quickly (Fig. 8). Employing various experimental and theoretical methods based on the known reconstruction mechanism of Cu nanoparticles under CO_2RR, the researchers had provided an explanation for this observation. They had hoped that their findings would lay the foundation for the development of alloyed Cu-based nano-catalysts that could withstand CO_2RR and other reducing reaction conditions. Similar mechanisms to prevent Cu reconstruction and produce more stable nanoparticles had been found in the study for metals with higher oxophilicity and strong M–Cu bonding energies.[109]

Foucher *et al.* have presented a strategy for the synthesis of Cu–Pt nanocrystals of varying sizes and crystal shapes. A Cu-rich core had been found to be enclosed in a Pt-rich layer, as determined by a thorough STEM-EDS study. Cu–Pt particles had been stable as catalysts because, after being annealed at 800 °C, they had become intermetallic CuPt particles. Non-intermetallic CuPt had been found to be stable at 400 °C in H_2 or O_2 using *in situ* STEM analysis. The production of a Cu oxide layer, which would cover and render Pt inactive, had been prevented by the intermetallic CuPt phase. They had shown that copper alloys didn't always oxidize and decay as quickly as feared, and that nanoscale CuPt structures could help conserve otherwise costly Pt. CuPt particle stability had been of significant interest and may be useful in a number of different chemical processes.[110] In a related context, another study delved into bimetallic CuAg electrodes. These electrodes had bulk compositions closely matching their surface compositions, primarily consisting of Cu and Ag crystallites. During CO_2RR, the presence of CO adsorbates induced the segregation of initially dissolved Cu in the Ag phase, resulting in Cu surface enrichment on the Ag-rich bimetallic electrodes. CO formation primarily occurred on the surface of the Ag domains, while CO reduction was exclusive to the Cu domains. The distribution of products changes when they are produced on a stable CuAg electrode. Changing from pure Cu electrodes significantly decreases hydrogen generation and favors carbonyl compounds.[111]

The study proposed an alternate route using the chemical named DAT to co-electrodeposit high-surface-area CuAg alloys. Instead of nucleus formation the way this method worked merely prevents nucleation, producing more evenly distributed

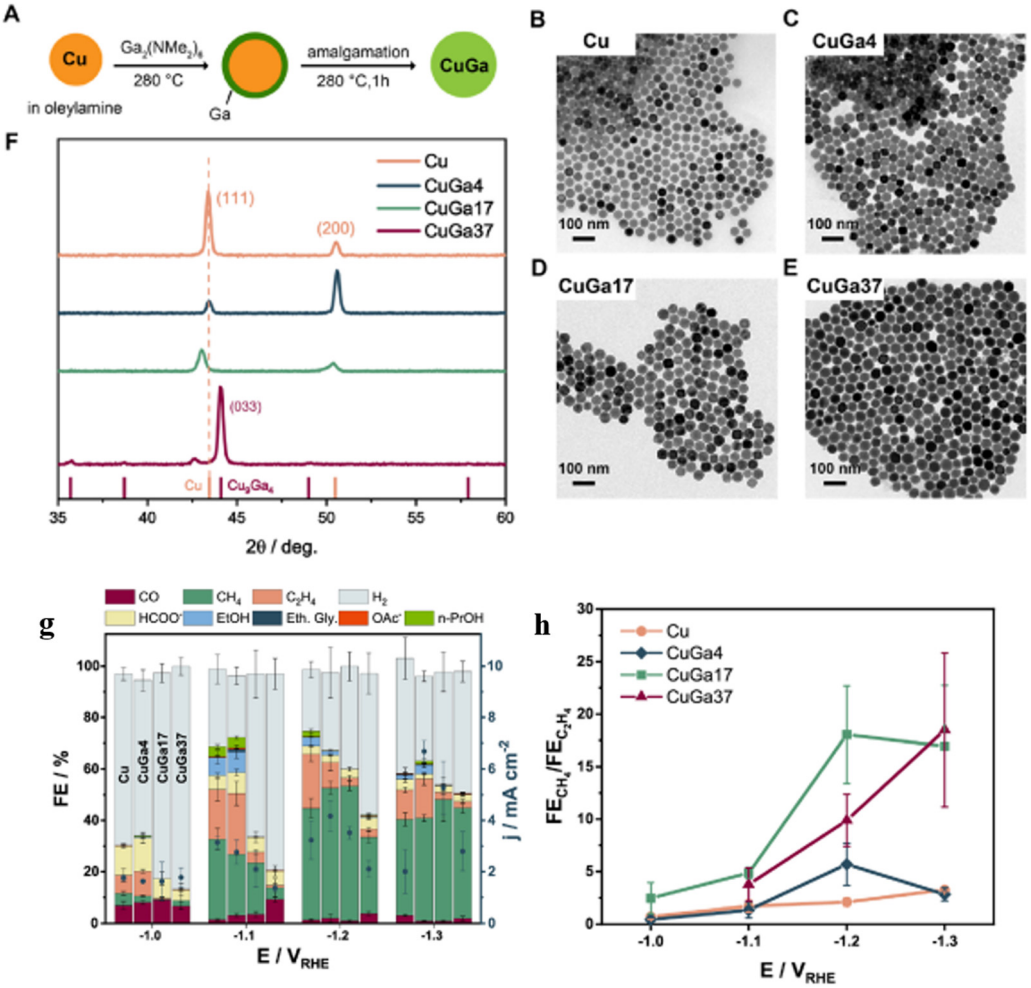

Fig. 8 CuGa NPs were synthesized and characterized. (A) A streamlined approach to synthesis. Bright field TEM images of Cu, $CuGa_4$, $CuGa_{17}$, and $CuGa_{37}$ NPs (B)–(E) and their matching XRD patterns (F). These results point to the synthesis of CuGa NPs with a consistent shape, extremely similar diameters, and varying Ga concentrations. How well the CuGa NPs electrocatalyze CO_2RR. (g) Mean FE (left axis) and geometric current density (right axis) for Cu, $CuGa_4$, $CuGa_{17}$, and $CuGa_{37}$ NPs at various applied potentials (NP loading was held constant at 15 g on glassy carbon with a geometric area of 1.33 cm^2) during 45 min CO_2RR in CO_2-saturated 0.1 M $KHCO_3$. The advancement in CH_4 production using CuGa NPs is indicated by the ratio of the FE for CH_4 and C_2H_4 across the same potential range (h). Reproduced with permission from ref. 109. Copyright 2023, American Chemical Society.

samples of Cu and Ag atoms in the CuAg-wire. Using a flow electrolyzer, we found that CuAg-wire samples were more active and coherent in terms of selectivity compared to CuAg-poly and Cu-wire in the e-CO_2R. Products such as C_2H_4 and C_2H_5OH were detected.[112] Seeking a different avenue of study, Pd@Au nanoparticles were developed by impregnating Au nanoparticles with specified amounts of Pd. Intriguingly, it was shown that at varying Pd loadings the catalytic activity for CO_2R was non-linear. In addition, the bimetallic Pd–Au surfaces with isolated Pd presented lower energy barriers for CO_2 activation and were less prone to poisoning by strongly binding *CO intermediates.[113]

Moreover, the research delved into the impact of the starting Cu/Zn ratio and the extent of alloying between Cu and Zn components on the product selectivity of CuZn nanoparticles. Under CO_2R conditions, CH_4 was predominantly generated near the metallic Cu in proximity to ZnO, while the exclusive production of CO and H_2 resulted from the reduction of ZnO species and the enhanced Cu–Zn contact.[114] Additionally, Li *et al.* have attained FE exceeding 95% in industrial-scale CO_2 reduction to CO, by using a novel antimony–copper single-atom alloy catalyst (Sb_1Cu). This catalyst offered improved selectivity and throughput due to the atomic-level SbCu interface, which facilitated CO_2 adsorption while reducing CO* binding (Fig. 9).[9]

In a different facet of the research, bimetallic $Au_{0.5}Cu_{0.5}$ NPs with a narrow size distribution were synthesized using inverse micelle encapsulation. Smaller NPs exhibited higher current density during e-CO_2R due to their larger population of low-coordinated sites, as confirmed by X-ray spectroscopy. While faradaic selectivity showed less size dependence, with H_2 being the predominant product at approximately 80% selectivity, larger NPs yielded a 7% increase in CO output and a 7% decrease in H_2 production.[115] Table 3 provides a comprehensive overview of different designed electrocatalysts for e-CO_2RR following the pure metallic alloy approach on Cu-based materials.

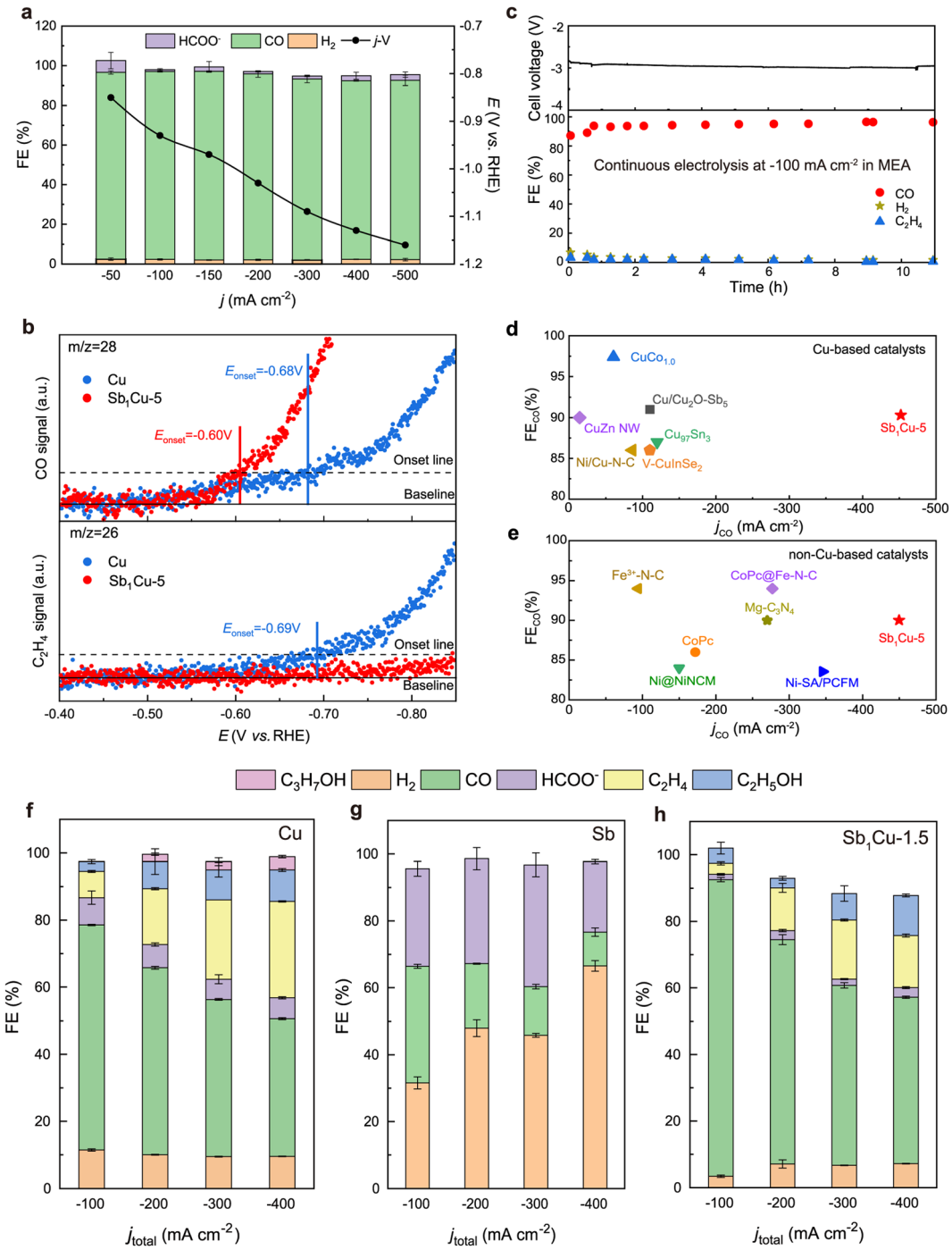

Fig. 9 CO_2RR performance over Sb_1Cu catalysts and Cu. FEs of all CO_2RR products at different current densities and the associated j–V curve for Sb_1Cu-5 (a). *In situ* DEMS measurement of the production of (up) CO and (down) C_2H_4 during CO_2RR on Cu and Sb_1Cu-5 catalysts (b). Stability test at 100 mA cm^{-2} current density in MEA for more than 10 hours. GC analysis shows an average FE_{CO} of about 95% (c). Different reported electrocatalysts for CO_2RR-to-CO (d) Cu-based and (e) non-Cu-based catalysts' performance measures. Product FEs on (f) Cu, (g) Sb, and (h) Sb_1Cu-1.5 compared. The error bars show the average difference between three different readings. Reproduced from ref. 9. Open access article, Nature.

6.4.2. Compound alloys. The strategy of combining elements to create alloys plays a role in designing electrocatalysts for e-CO_2R. This approach has the potential to enhance the catalytic performance and selectivity of these materials. When two or more elements with different properties are combined their synergy can result in catalytic activity. By selecting elements with different electronegativity, electronic structures and atomic sizes, researchers can customize the surface properties and reactivity of the alloy, which in turn affects its ability to convert CO_2. Compound alloying is crucial because it allows for optimization of the binding energies between CO_2 and reaction intermediates. This optimization promotes selective conversion of

Table 3 Delving into the realm of the pure metallic alloy approach, this comprehensive table evaluates electrocatalyst materials designed for CO_2R. It sheds light on the behavior of these materials and highlights how metallic alloys significantly influence product selectivity under different reaction conditions

				≈FE%									
No.	Material	Electrolyte	V *vs.* RHE	H_2	CO	CH_4	C_2H_4	$HCOO^-$	$C_2H_5^+$	CH_3OH	C_2H_5OH	$C_2H_3O_2^-$	Ref.
1	Pd NPs/CB	0.1 M $KHCO_3$	−1.0	63	38	—	—	3	—	—	—	—	97
2	Ag NPs/C			43	63	—	—	3	—	—	—	—	
3	PdZn NPs/CB			44	17	—	—	42	—	—	—	—	
4	PdCu NPs/CB			53	57	—	—	1	—	—	—	—	
5	PdSn NPs/CB			62	15	—	—	1	—	—	—	—	
6	$PdAg_3$ NPs/CB			18	84	—	—	1	—	—	—	—	
7	Cu	0.1 M $KHCO_3$	−1.09	18	5	—	—	10	—	—	—	—	56
8	Cu_3Sn ($Cu_{76}Sn_{24}$)			5	38	—	—	43	—	—	—	—	
9	Sn			5	3	—	—	89	—	—	—	—	
10	Cu	0.1 M $KHCO_3$	−1.1	45	4	—	—	19	—	—	—	—	98
11	CuZn-0.1			40	5	—	—	33	—	—	—	—	
12	CuZn-0.5			26	7	—	—	60	—	—	—	—	
13	CuZn-1			28	10	—	16	31	—	—	—	—	
14	Zn			20	55	—	—	15	—	—	—	—	
15	Flat Cu–Sn	0.1 M $KHCO_3$	−1.0	—	77	—	—	—	—	—	—	—	100
16	3D-h-Cu–Sn		−0.4	—	91	—	—	—	—	—	—	—	
17	Cu_2O		−0.75	20	22	7	28	4	—	—	13	—	101
18	CuAg-0.25%			19	18	8	34	1	—	—	16	—	
19	CuAg-0.75%			16	19	5	37	1	—	—	17	—	
20	CuAg-2%			14	19	2	45	1	—	—	15	—	
21	CuNiZn	0.1 M $KHCO_3$	−1.2	68	4	2	2	38	—	—	—	—	102
22	Cu–Pd-D	0.5 M $KHCO_3$	−0.87	65	30	—	—	—	—	—	—	—	103
23	Cu–Pd-0.8			9	86	—	—	—	—	—	—	—	
24	Cu–Pd-C			71	48	—	—	—	—	—	—	—	
25	Cu–Pd-0.3			5	92	—	—	—	—	—	—	—	
26	Cu–Pd-S			25	55	—	—	—	—	—	—	—	
27	Cu–Pd-0.1			40	53	—	—	—	—	—	—	—	
28	Pd/C			68	37	—	—	—	—	—	—	—	
29	Au	0.1 M $KHCO_3$	−0.8	22	78	—	—	1	—	—	—	—	104
30	$Au_{75}Cu_{25}$			42	66	—	—	2	—	—	—	—	
31	$Au_{50}Cu_{50}$			58	49	—	—	3	—	—	—	—	
32	$Au_{25}Cu_{75}$			63	29	—	—	4	—	—	—	—	
33	Cu			59	12	—	—	13	—	—	—	—	
34	Cu	0.5 M [Bmim]PF_6	−2.1	77	23	—	—	—	—	—	—	—	105
35	$CuCo_{0.4}$			50	50	—	—	—	—	—	—	—	
36	$CuCo_{0.6}$			12	88	—	—	—	—	—	—	—	
37	$CuCo_{1.0}$			2	99	—	—	—	—	—	—	—	
38	$CuCo_{1.9}$			22	79	—	—	—	—	—	—	—	
39	Co			66	22	—	—	—	—	—	—	—	
40	Cu : Zn 100 : 0	100 mM $KHCO_3$	−1.8 Ag/AgCl	38	2	3	30	—	—	—	—	—	106
41	Cu : Zn 91 : 9			32	5	7	31	—	—	—	—	—	
42	Cu : Zn 83 : 17			30	8	5	35	—	—	—	—	—	
43	Cu : Zn 50 : 50			23	10	17	28	—	—	—	—	—	
44	Cu : Zn 9 : 91			67	20	18	4	—	—	—	—	—	
45	Cu : Zn 0 : 100			70	25	28	1	—	—	—	—	—	
46	Co	0.1 M $KHCO_3$	−1.1 V	98	1	—	—	1	—	—	—	—	107
47	$Cu_{30}Co_{70}$			93	2	—	—	6	—	—	—	—	
48	$Cu_{50}Co_{50}$			92	3	—	—	5	—	—	—	—	
49	$Cu_{70}Co_{30}$			92	4	—	—	5	—	—	—	—	
50	$Cu_{90}Co_{10}$			82	5	—	—	13	—	—	—	—	
51	Cu			87	8	—	—	8	—	—	—	—	
52	Cu	0.1 M $KHCO_3$	−1.0	67	7	6	7	11	—	—	—	—	109
53	$CuGa_4$			58	8	3	9	14	—	—	—	—	
54	$CuGa_{17}$			80	6	2	1	3	—	—	—	—	
55	$CuGa_{37}$			85	6	2		3	—	—	—	—	
56	Cu wire	0.1 M $KHCO_3$	−0.8	—	15	—	35	—	—	—	28	—	112
57	Cu–Ag poly				8	—	27	—	—	—	16	—	
58	Cu–Ag wire				7	—	55	—	—	—	26	—	
59	Cu	0.1 M $KHCO_3$	−0.8		58	—	—	—	—	—	—	—	113
60	Pd_2@Cu_{98}				48	—	—	—	—	—	—	—	
61	Pd_5@Cu_{95}			30	58	—	—	7	—	—	—	—	
62	Pd_{10}@Cu_{90}				41	—	—	10	—	—	—	—	
63	Pd_{20}@Cu_{80}				40	—	—	22	—	—	—	—	
64	Pd				9	—	—	38	—	—	—	—	
65	Cu	0.1 M $KHCO_3$	−1.35	52	1	40	3	2	—	—	—	—	114
66	$Cu_{90}Zn_{10}$			32	2	62	1	2	—	—	—	—	

Table 3 (*continued*)

No.	Material	Electrolyte	V *vs.* RHE	≈FE%									Ref.
				H_2	CO	CH_4	C_2H_4	$HCOO^-$	$C_2H_5^+$	CH_3OH	C_2H_5OH	$C_2H_3O_2^-$	
67	$Cu_{70}Zn_{30}$			25	4	70	2	3	—	—	—	—	
68	$Cu_{50}Zn_{50}$			50	5	68	2	4	—	—	—	—	
69	$Cu_{30}Zn_{70}$			51	38	9	1	5	—	—	—	—	
70	$Cu_{10}Zn_{90}$			52	42	2	1	1	—	—	—	—	
71	Zn_{10}			53	43	1	1	1	—	—	—	—	
72	Ni–N–C	0.5 M $KHCO_3$	−1.0	—	70	—	—	—	—	—	—	—	116
73	Cu–Ni–C			—	12	—	—	—	—	—	—	—	
74	Ni/Cu–N–C			—	92	—	—	—	—	—	—	—	
75	Cu	0.5 M $KHCO_3$	−100	11	68	—	7	9	—	—	3	—	9
76	Sn			31	34	—		30	—	—	—	—	
77	Sb_1–Cu-1.5			3	80	—	3	2	—	—	4	—	
78	Sb_1–Cu-5			2	96	—	—	1	—	—	—	—	
79	AuCu-5 nm	0.1 M $KHCO_3$	−1.2	83	13	3	—	—	—	—	—	—	115
80	$Cu_{100}Bi$		50 mA cm^{-2}	50	8	—	—	—	—	—	—	—	117
81	$Cu_{50}Bi$			70	14	3	2	—	—	—	—	—	
82	$Cu_{10}Bi$			20	44	—	—	—	—	—	—	—	
83	Cu_5Bi			19	31	—	—	42	—	—	—	—	

CO_2. Additionally alloying helps to address issues such as catalyst deactivation and unwanted byproduct formation, thus contributing to the development of economically viable technologies for CO_2 conversion. There are methods to achieve compound alloying, including wet chemistry synthesis, electrodeposition and physical vapor deposition. Each method offers control over the composition and structure of the alloy. Through these techniques researchers can explore a range of combinations to discover new electrocatalysts with exceptional performance. This research brings us closer to achieving CO_2 conversion and advancing energy production.

Lai *et al.* have reported that the inclusion of the organic additive 1-Br_2 can enhance CO_2R activity and selectivity in Cu alloys containing Co, In, Mn, and Zn. This covered the way for the development of hybrid electrocatalysts with improved performance in CO_2R to higher-order products. It was noteworthy that these compounds displayed strong correlations with CH_4 and C_{2+}, underscoring a fundamental limitation in selectivity tuning through alloying. The hybrid organic–inorganic catalysts demonstrated the potential to exert control over branching ratios within the CO_2R reaction network.[118] Further, a novel activation approach by Nafion on $Cu(OH)_2$-derived Cu was applied for transforming this material into an effective e-CO_2RR catalyst for flow cell applications (Fig. 10). Notably, under optimized conditions, a $FE_{C_2H_4}$ of 44% and a total CO_2 reduction FE of 83% were achieved at 300 mA cm^{-2}, showcasing exceptional performance. This activation strategy showcased its efficacy by promoting C_2H_4 production and simultaneously mitigating the occurrence of hydrogen evolution reactions.[119]

Further, Chang *et al.* investigated the structural changes, CO_2RR activity, and selectivity of the Ag@Cu core–shell system. Employing a straightforward polyol reduction strategy, researchers manipulated the compositions and structures of nanoparticles (NPs). The study underscored the significance of synergistic interactions between Ag and Cu, which led to elevated CO or hydrocarbon production within specific NP configurations, such as Ag@Cu-5 or Ag@Cu-20.[120] Additionally, the synthesis of granular particles featuring a Cu-based nanostructure and approximately 10 nm nanopores was undertaken using a Na-melt technique (Fig. 11). The process involved the electrochemical extraction of calcium from Cu_5Ca, facilitating the further evolution of these nanostructures. The application of a large negative voltage to the Cu_5Ca particles resulted in the generation of platelet Cu particles with comparable nanopores.[121]

Remarkable findings emerged from the study of bimetallic Cu–Sn catalysts, unveiling spontaneous surface transformations driven by local galvanic corrosion during CO_2RR. The distinct oxidation potential gap between Cu and Sn induced accelerated corrosion of the thin Sn layer on Cu foil, prompting the emergence of finer Sn patterns and outward Sn migration. This intriguing redox interplay fostered thinner Sn patterns and showcased the novel Cu/*p*-Sn 3-nm catalysts, boasting an exceptional catalytic selectivity of 58.1% at −1.0 V_{RHE}.[122] Further, in the pursuit of effective ethylene synthesis *via* CO_2RR, a groundbreaking CeO_2/CuO electrocatalyst was synthesized. This catalyst, with innovatively integrated CeO_2 quantum dots, harnessed heterointerfaces to enhance CO_2 and CO adsorption, while stabilizing Cu^+ for CO_2RR, remarkably surpassing both CuO and CuO–CeO_2 hybrid counterparts.[123]

Moreover, the electrochemical process unraveled the potential of $CuWO_4$ to shine as an exceptional electrocatalyst for CO_2R, surpassing conventional CuO.[124] Further, the synthesis of a new composite by combining Cu–BTC with GrO yielded a transformative breakthrough, showcasing augmented adsorption capabilities. With the infusion of GrO, the composite's BET surface area and pore volume were elevated compared to its Cu–BTC precursor. This composite displayed a significantly elevated capacity for CO_2 adsorption, while the CH_4 adsorption remained essentially unaltered.[125] Embracing innovative methodologies, Huang *et al.* harnessed a unique seeded-growth colloidal technique to synthesize AgCu NDs, unraveling intricate interplays between varying Cu domain sizes. This approach, indicates dimer systems such as CuRu, CuRh, and CuIr, presented a gateway to synthetic control over

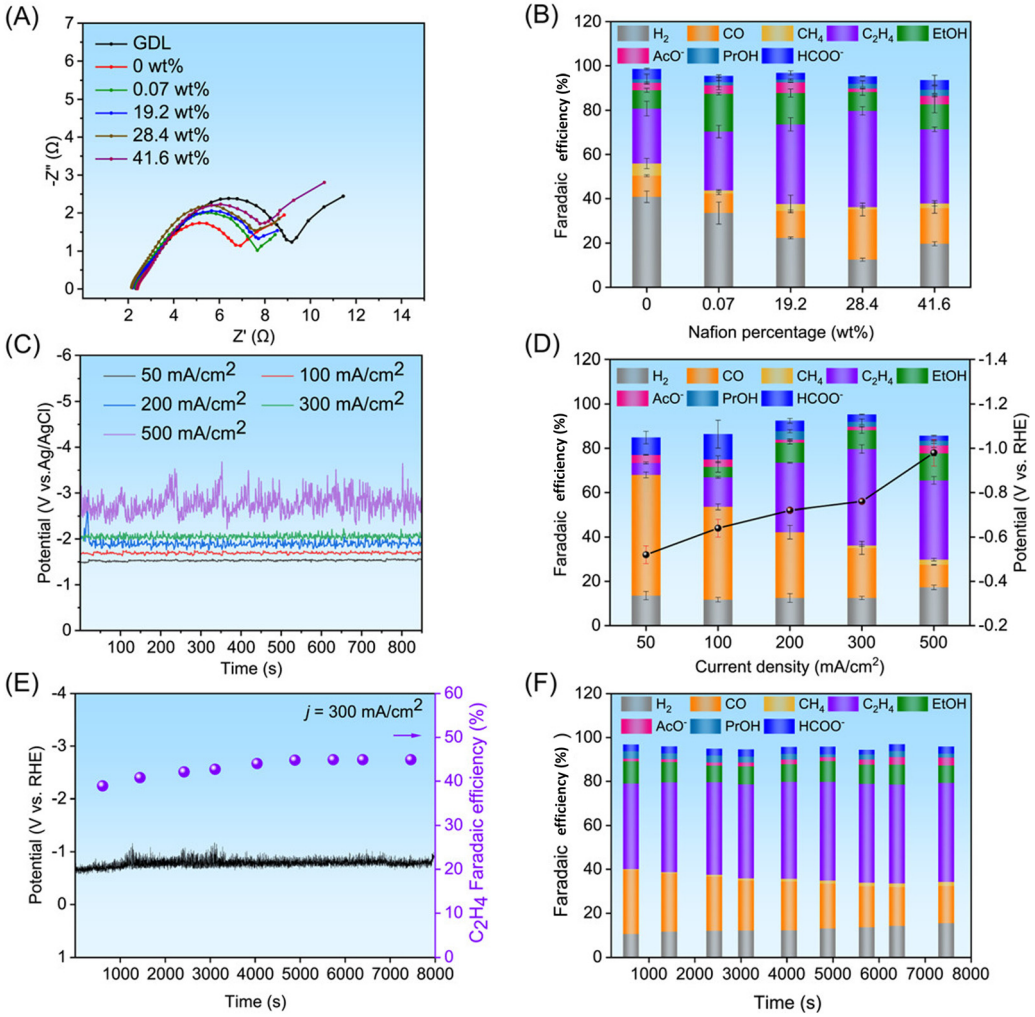

Fig. 10 ANCu@Nafion catalysts with varying Nafion percentages were fabricated at 0.1 V, and their Nyquist plots from 0.01 Hz to 100 kHz (A) and their product distribution FEs at 300 mA cm^{-2} (B) were plotted. The CO_2 reduction kinetics of ANCu@Nafion-28.4 wt% in a 1 M KOH electrolyte (C) along with the corresponding current density *versus* product distribution kinetics (D), voltage profile and C_2H_4 kinetics (E), and product distribution kinetics (F) over the course of an 8000-second test. Reproduced from ref. 119. Open access article, Wiley.

Cu and Ag nanoparticle counterparts. Remarkably, $Ag_1Cu_{1.1}$ NDs exhibited a transformative 3.4-fold surge in FE toward C_2H_4, along with a twofold increase in total CO_2RR activity compared to similar-sized Cu NPs.[126] A meticulous approach involving the electrodeposition of Sn onto porous Cu hollow fibers illuminated pathways to enhancing current density and reaction selectivity in electrochemical CO_2R. Skilled optimization of the Sn^{2+}/Sn^{4+} ratio on the HFGDE surface yielded substantial enhancements in the FE of formate.[127] Unveiling a pathway to dual-loop CO_2 capture during gasification, Rahman *et al.* showcased the potential of pellets merging CuO and limestone. Intriguingly, core-in-shell $Ca_{50}Cu_{40}$Cem10 pellets exhibited rapid CuO reduction in the presence of CO and H_2.[128]

Continuing this scientific journey, elevated-temperature pyrolysis in a reducing atmosphere was harnessed to successfully produce monometallic Cu/C, Ni/C, and intermetallic $Cu_{0.85}Ni_{0.15}$/C nanomaterials from phase-pure MOFs Cu–BTC, Ni–BTC, and $Cu_{0.85}Ni_{0.15}$–BTC. Structural analyses unveiled the creation of a substitutional solid solution, the $Cu_{0.85}Ni_{0.15}$/C nanoalloy, within these MOF-derived nanomaterials, showcasing a significant dispersion of active metal sites on the carbonaceous substrate. With an impressive selectivity for CH_3OH and a high FE reaching up to 60% at 0.40 V, the intermetallic nanoalloy outperformed conventional monometallic catalysts in enhancing the efficiency of CO_2RR.[129] In a parallel exploration, Wannakao *et al.* expressed in the field of e-CO_2R on metal/WC surfaces, employing density functional theory simulations to unravel activity and selectivity trends involving 13 different metal species. The findings revealed that metals such as Zn/WC, Ag/WC, and Au/WC, known for their limited interactions with reaction intermediates, produced CO as a significant product with a limiting potential similar to their pristine metal surfaces. These core–shell M/WC systems showcased potential to reduce the demand for costly metals in contemporary catalytic processes. Conversely, Cu/WC and Pd/WC surfaces exhibited a comparatively low capability for reducing CO_2 to CO.[130] In another facet of investigations, Zhang *et al.* explored the functions of Cu and Sn in selective e-CO_2R by designing a

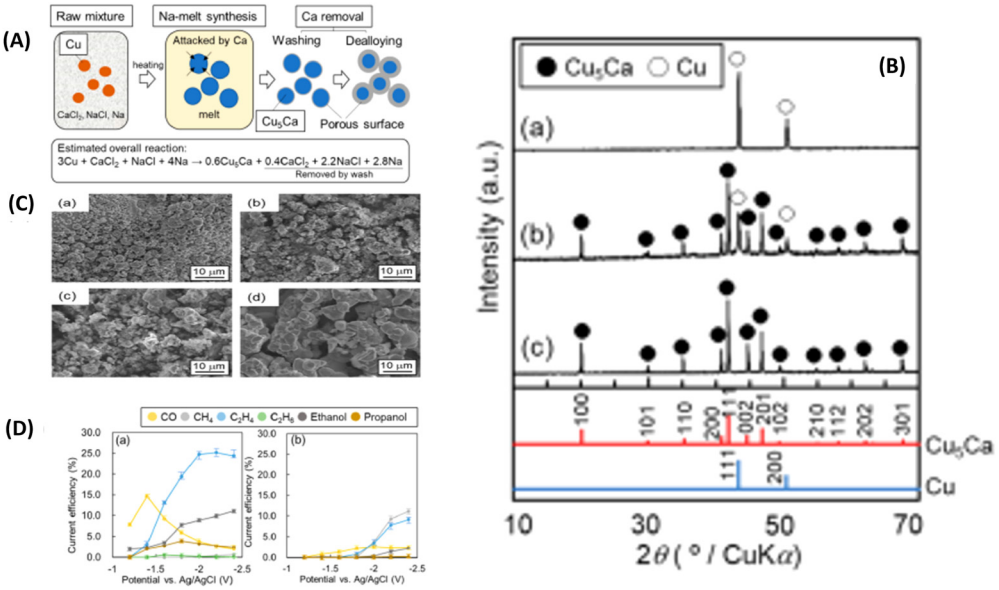

Fig. 11 Schematic representation of the synthesis of Cu_5Ca and its derivatives (A). The P-XRD patterns for Cu_5Ca (PDF 04-007-1585) and Cu (PDF 00-004-0836) synthesized at 400, 600, and 750 °C from a Na melt-synthesized sample with a nominal molar ratio of Cu/Ca = 3/1 (B). SEM micrographs of raw Cu powder (a), 400 (b), 600 (c), and 750 °C (d) Na-melt-synthesized samples (C). Current efficiencies for CO_2R products at different potentials for (a) Cu_5Ca and (b) Cu samples. Each applied potential lasted for 1 hour (D). Reproduced with permission from ref. 121. Copyright 2022, American Chemical Society.

series of Cu–Sn-based composites as model catalysts. By varying the ratio of copper to silver, e-CO_2RR's products can be adjusted to produce either formate or carbon monoxide. Remarkably, both Cu_1Sn_1 and $Cu_{20}Sn_1$ emerged as excellent catalysts for formate and CO oxidation, exhibiting high selectivity and partial current density. While $Cu_{20}Sn_1$ featured a structure consisting of a single Sn atom doped into a Cu atom, characterization of Cu_1Sn_1 unveiled a CuSn alloy core with a minimal quantity of a Cu-doped SnO shell.[131] Table 4 provides a complete summary of different designed electrocatalysts for e-CO_2RR following the compound alloying approach on Cu-based materials.

6.5. Composite engineering approach

Engineering strategies enable designing electrocatalysts for e-CO_2R providing adaptable solutions to improve catalytic performance. The composite engineering approach involves integrating materials or phases with functionalities into one catalyst system. By selecting and combining these components researchers can optimize the activity, selectivity and stability of catalysis effectively addressing the challenges associated with CO_2R. The significance of composite engineering lies in its ability to harness the strength of various materials to create synergistic effects. For instance, a composite catalyst may include supports, active catalytic sites and promoters to enhance CO_2 adsorption, electron transfer and intermediate binding. This tailored approach enables adjustment of catalyst properties to meet requirements, for reducing CO_2R. Different methods such as co-precipitation, sol–gel synthesis and chemical vapor deposition can be employed to produce composite catalysts with controlled structures. Overall composite engineering plays a role in advancing electrocatalysis by providing pathways for developing sustainable technologies for converting CO_2 that are essential, in combating climate change and transitioning towards a greener energy future.

The research group of Cao and co have utilized microporous nitrogen-rich MOFs known as Cu-BTT to serve as precursors for the synthesis of Fe–Cu-BTT. Through a meticulously controlled pyrolysis process, this endeavor yielded Fe_xCu–N–C compounds featuring a diverse array of Fe–N_x sites. The introduction of Fe induced notable structural alterations, including an increase in the BET surface area and total pore volume, a reduction in Cu nanoparticle density, and an augmentation of Fe–N_x sites within the carbon matrix. This structural evolution resulted in an enhanced CO generation, with $Fe_{0.07}$Cu–N–C800 exhibiting the highest CO_2 transfer efficiency at 48.5%.[134] In the context of e-CO_2RR conducted in neutral aqueous solutions, a novel organic–inorganic composite was crafted by Li *et al.* *via* a hydrothermal synthesis method. Remarkably, this composite demonstrated sustained performance without degradation even after 24 hours of continuous e-CO_2R. It comprised a 3D g-C_3N_4 nanosheet-CNT interconnected framework adorned with a polymeric CoPc layer. This reported innovative method offered several advantages, including an increased electrochemically active surface area with numerous active sites, improved homogeneous immobilization at high catalyst loading, and reinforced contacts between the molecular catalyst and the conductive support.[135] Furthermore, CoPc-based and O-linked MOFs were predicted to exhibit reduced activation energies in the synthesis of the carboxyl intermediate, as evidenced by density functional theory calculations. This reduction in activation energy translated into improved catalytic activity and selectivity. These findings underscored the potential for fine-tuning MOFs' activity and selectivity in catalysis through

Table 4 This table provides a summary of the compound alloy strategy employed for developing electrocatalysts and their corresponding electrochemical efficiency. It offers information on approaches for environmentally sustainable conversion of CO_2

				≈FE%									
No.	Material	Electrolyte	V *vs.* RHE	H_2	CO	CH_4	C_2H_4	$HCOO^-$	$C_2H_5^+$	CH_3OH	C_2H_5OH	$C_2H_3O_2^-$	Ref.
1	Cu-Raw	0.1 M $KHCO_3$	−1.0	48	7	12	—	—	—	—	—	—	132
2	Cu-50			38	11	11	—	—	—	—	—	—	
3	Cu-100			33	10	8	—	—	—	—	—	—	
4	Cu-200			37	7	6	—	—	—	—	—	—	
5	Flat-Cu–Sn	0.1 M $KHCO_3$	−1.0		75	—	—	—	—	—	—	—	100
6	Cu–Sn rod				51	—	—	—	—	—	—	—	
7	3D-h Cu–Sn				68	—	—	—	—	—	—	—	
8	AN-Cu	1 M KOH	−0.1	41	9	6	24	3	—	—	10	2	119
9	AN-Cu@Nafion (0.07)			35	8	1	26	2	—	—	17	4	
10	Ah NPs	0.1 M $KHCO_3$	−1.16	29	63	—	—	—	—	—	—	—	120
11	Ag@Cu-5			29	68	—	—	—	—	—	—	—	
12	Ag@Cu-7			29	70	2	—	—	—	—	—	—	
13	Ag@Cu-10			53	21	13	4	—	—	—	—	—	
14	Ag@Cu-15			53	10	20	13	—	—	—	—	—	
15	Ag@Cu-20			45	5	23	16	—	—	—	—	—	
16	Ag@Cu-25			44	5	21	17	—	—	—	—	—	
17	Cu NPs			58	7	17	19	—	—	—	—	—	
18	Cu_5Ca	0.5 M $KHCO_3$	−2.5 Ag/AgCl	—	3	1	24	—	—	—	11	—	121
19	Cu samples			—	3	11	8	—	—	—	3	—	
20	Cu	0.1 M $KHCO_3$	−1.2	—	2	—	—	8	—	—	—	—	122
21	Cu/*p*-Sn 3 nm			—	52	—	—	12	—	—	—	—	
22	Cu/*p*-Sn 20 nm			—	36	—	—	62	—	—	—	—	
23	Cu/*p*-Sn 30 nm			—	3	—	—	98	—	—	—	—	
24	CeO_2/CuO-50%	1 M KOH	250 mA cm^{-2}	—	—	—	—	42	—	—	—	—	123
25	CuO			—	—	—	—	2	—	—	—	—	
26	CeO_2/CuO-50%-PM			—	—	—	—	1	—	—	—	—	
27	CeO_2/CuO-50%-bulk			—	—	—	—	14	—	—	—	—	
28	CeO_2/CuO-20%			—	—	—	—	32	—	—	—	—	
29	CeO_2/CuO-37.5%			—	—	—	—	38	—	—	—	—	
30	CeO_2/CuO-50%			—	—	—	—	42	—	—	—	—	
31	CeO_2/CuO-70%			—	—	—	—	28	—	—	—	—	
32	Ag NPs	0.1 M $KHCO_3$	−1.1	45	68		1	—	—	—	—	—	126
33	Cu NPs			52	13	8	12	12	—	—	—	—	
34	Ag_1–$Cu_{1.1}$ NDs			34	18	19	41	19	—	—	—	—	
35	CuSn (50 s) HFGDEs	0.5 M $KHCO_3$	−1.4	—	—	—	—	50	—	—	—	—	127
36	CeO_2	0.1 M $KHCO_3$	−1.4	78	3	—	—	2	—	—	2	—	133
37	5-CuO/CeO_2			57	17	2	3	1	—	2	9	—	
38	60-CuO/CeO_2			45	2	27	55	1	—	2	3	—	
39	CuO			39	2	10	21	5	—	—	16	—	
40	Cu/C		−1.0	—	10	10	—	—	—	13	—	—	129
41	$Cu_{0.85}Ni_{0.15}$/C			—	3	4	—	—	—	2	—	—	
42	Ni/C			—	16		—	—	—	2	—	—	
43	Pure Sn	0.5 M $KHCO_3$	−1.1	9	15	—	—	70	—	—	—	—	131
44	Pure Cu			41	41	—	—	16	—	—	—	—	
45	Cu_1Sn_1			4	9	—	—	87	—	—	—	—	
46	$Cu_{20}Sn_1$			5	78	—	—	25	—	—	—	—	

the meticulous design and selection of functional ligands, offering a significant degree of modular tunability. Notably, for the e-CO_2R to CO using reticular framework materials, it was demonstrated that these materials served as exceptional cathode materials, boasting high current density and excellent selectivity toward the CO product at a relatively low overpotential of 0.63 V.[136]

To optimize support connections and catalytic efficiency, He *et al.* developed a dimer catalyst, a minimal bimetallic catalyst structure. This innovation opened up the possibility of breaking scaling relationships by expanding the parameter space for optimizing attributes while retaining non-monotonic property correlations. The dimers, formed from Group 10 (Ni, Pd, Pt) and Group 11 (Cu, Ag, Au) elements, were supported at single vacancy sites of graphene. These dimers featured an anchoring atom that transferred a large number of electrons to the graphene and an antenna atom that was much less positively charged and protruded from the graphene surface. All clusters exhibited strong binding energies to the defective graphene, indicating their stability. Notably, the stability of the alloy dimers, such as Cu_2, Ag_2, and Au_2, was significantly improved compared to their monometallic forms. These dimers were selected for further investigation as potential candidates for the e-CO_2R to CH_4 using the first-principles approach and the computational hydrogen electrode model. Among the options studied, Pt_2, AgNi, Pd_2, and AgPt showed the lowest overpotential values when compared to standard Cu electrodes. While the oxygen binding strength of the catalytic dimer provided a semi-quantitative description of the reactivity of the supported dimers, the free energies of OCHO* and OH* correlated well with O*, whereas the free energies of CHO* and HCOOH* exhibited significant variations in their reactivity.[137]

Further, for the e-CO_2R to carbon, an inexpensive and robust Cu-based hybrid catalyst was created. The catalyst, a polymer of Cu phthalocyanine coated on carbon nanotubes, showed 80% faradaic yield for CO synthesis at low overpotentials and was selective for CO production. Since Cu phthalocyanine polymerization was selective for proton reduction under the same conditions, this resulted in a marked increase in reaction selectivity. Although the material initially displayed isolated Cu sites in phthalocyanine-like CuN_4 coordination, the Cu atoms were transformed to Cu nanoparticles under operational conditions.[138] In addition, the research findings showed that CoP_2O_6 played a crucial role in enhancing the efficiency of the Cu/C catalyst for formate production through e-CO_2R (Fig. 12). Utilizing ZIF-67 as the carbon precursor, the resulting CoP_2O_6/HCS–Cu catalyst not only increased current density but also reduced overpotential. Importantly, the catalyst's efficiency in e-CO_2R was found to be modulated by the Cu/Co ratio. Impressively, this catalyst exhibited the most negative overpotential (−0.4 mV) and achieved the highest current density (34.5 mA cm^{-2}) for formate production during e-CO_2R. Furthermore, at −0.66 V *vs.* RHE, formate was generated with an exceptional FE of 89.9%.[139]

In a separate study, solvothermal processing was employed to vulcanize copper hydroxide nanowire arrays (S–CNWs) with a specific amount of cuprous sulfide. These S–CNWs were subsequently investigated for their e-CO_2R under neutral conditions. The research revealed a strong correlation between the degree of vulcanization of the catalyst and formate selectivity. When vulcanized to an optimal extent, the FE could exceed 60%, with almost no generation of additional e-CO_2RR products. Further, the introduction of a small quantity of sulfur was found to facilitate the formation of formate by lowering the energy barrier associated with generating the OCHO intermediate.[140] In a related endeavor, hydrothermal processing followed by pyrolysis was employed to synthesize various Cu–Ni alloys tailored for e-CO_2R. In a 0.5 M $KHCO_3$ electrolyte, the optimized CuNi/NCNT catalyst exhibited a remarkable FE_{CO} of 94.8% for CO_2R and a

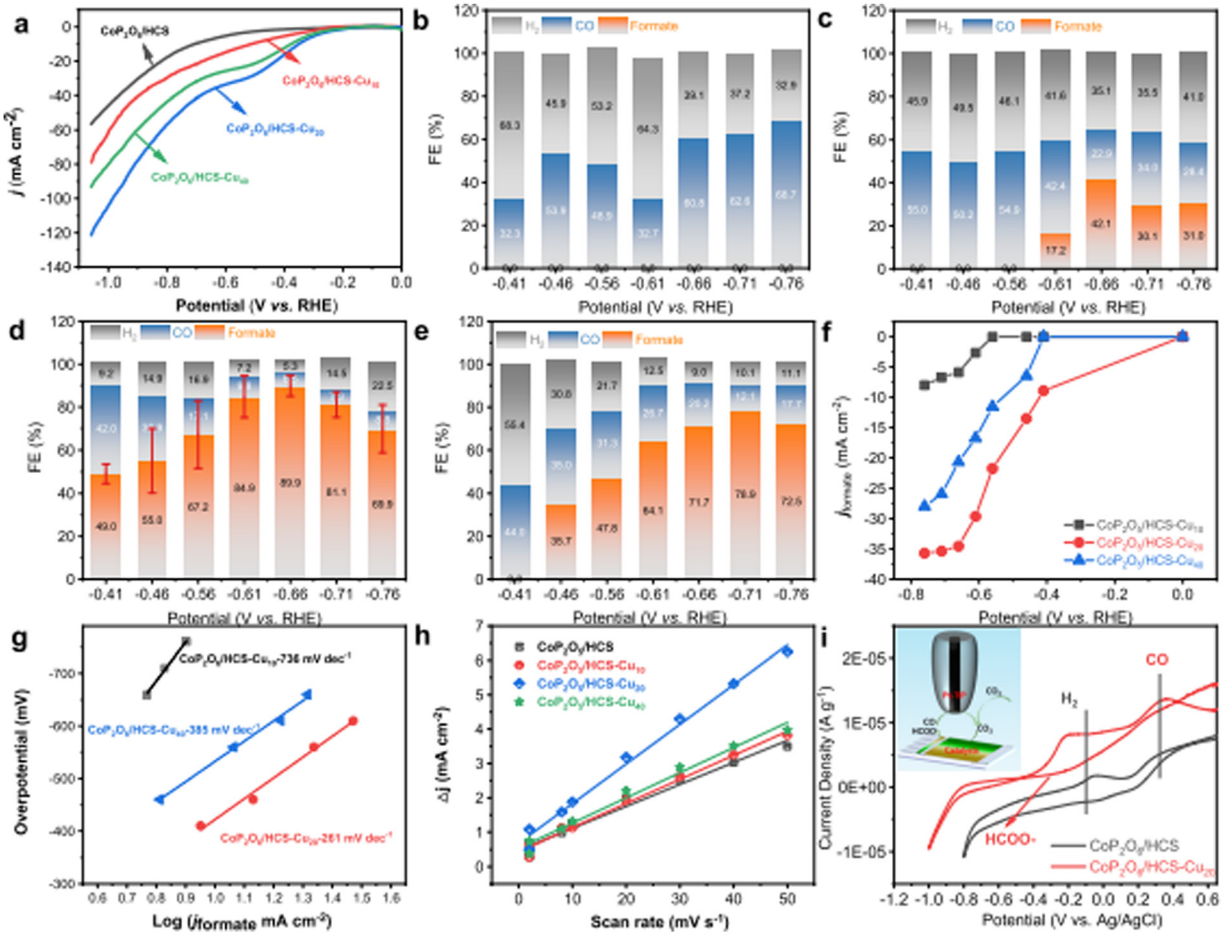

Fig. 12 The LSV curves were generated through experiments conducted in a CO_2-saturated 0.5 M $KHCO_3$ electrolyte using a scan rate of 10 mV s^{-1} (a). The formate, CO, and H_2 FEs were determined at a specific potential for the CoP_2O_6/HCS and CoP_2O_6/HCS–Cu catalysts (b)–(e). The current density (f), Tafel slopes (g), and electrochemically active surface area were determined for the CoP_2O_6/HCS and CoP_2O_6/HCS–Cu catalysts. The detection of products resulting from e-CO_2R on the CoP_2O_6/HCS and CoP_2O_6/HCS–Cu20 catalysts was carried out *in situ* (i). This was achieved by utilizing a Pt UME tip CV response, with a scan rate of 10 mV s^{-1}, at a substrate potential of −1.1 V *vs.* Ag/AgCl. The electrolyte employed was a 0.5 M solution of $KHCO_3$ that was saturated with CO_2 under atmospheric pressure. The experiments were carried out at a temperature of 293 K. Reproduced with permission from ref. 139. Copyright 2023, American Chemical Society.

substantial current density of 26.6 mA cm^{-2}. The addition of nickel to copper facilitated the formation of a crucial intermediate, COOH*, which played a pivotal role in boosting e-CO_2RR activity. Promisingly, the current density further increased to 124.6 mA cm^{-2} with an FE_{CO} of 92.8% at 1.1 V *versus* RHE.[141]

Additionally, Daiyan *et al.* created metal–carbon composites with dual active sites to produce H_2 and CO during e-CO_2RR. Co@CoNC-900 composites exhibited a wide potential window within which they could produce a tunable syngas ratio of 1 : 1. By adjusting the HER active sites, this syngas ratio could be shifted from 1 : 1 to 3 : 2, unlocking new possibilities for the production of a diverse range of fuels and chemicals using the well-established FT process in the industry.[142] In a separate research effort, the impact of Nafion/solvent formulation on CO_2 electrolysis employing CuO as a model catalyst was examined. The composition of Nafion/solvent exerted a significant influence on the activity, selectivity, and stability of e-CO_2RR. The effects of Nafion/solvent formulation on CO_2 electrolysis were attributed to three primary factors: the evolution of the catalyst structure, alteration of the local microenvironment, and accumulation of surface adsorbates. Nafion played a stabilizing role in preserving product distributions by preventing morphological rearrangement and delamination of weakly bound catalysts. The surface coverage of CO and local concentrations of CO_2 and H_2O in the reaction microenvironment were influenced by adjusting the thickness of Nafion coatings and the connectivity of their inner networks *via* modifications to the catalyst ink formulations.[143] Furthermore, researchers produced catalysts derived from CuO for e-CO_2RR, which exhibited resistance to a single thermal treatment but could be removed in two steps. g-C_3N_4-supported CuO catalysts favored the production of CH_4, whereas CuO displayed the highest selectivity toward C_2H_4. Various factors, including particle growth, the ensemble effect due to varying catalyst loading densities, and hybridization and stabilization of the catalyst–support relationship, contributed to this disparity. Scientists aimed to design catalyst systems that would result in a more tightly regulated product distribution of hydrocarbons over H_2 or CO by carefully controlling experimental conditions.[144]

Another research study reports on the reaction of the metal precursor with the nitrogen-doped carbon support to generate (sub)nanosized metal oxide clusters under *ex situ* conditions. The study encompassed a variety of M/NC catalysts. The results indicated that the catalytic activity for CO formation increased while using transition metal based electrocatalysts. Co/NC exhibited the highest activity at 0.5 V *vs.* RHE, while Ni/NC demonstrated good activity and selectivity. Fe/NC, Co/NC, and Ni/NC outperformed other metal hydroxides due to phase contraction and HCO_3 insertion into the layered structure of metal hydroxides.[145] Furthermore, nanophase-separated Cu#ZrO_2 was successfully produced through the internal oxidation of the $Cu_{51}Zr_{14}$ precursor composite alloy (Fig. 13). The material featured nanoscale lamellae of Cu metal and tetragonal ZrO_2, creating a stable Cu–ZrO_2 interface. Its uniformly dispersed catalytic sites and abundant metal–oxide interfaces contributed to increased selectivity for e-CO_2RR-to-FA conversion. CO_2 adsorption led to protonation over the nearby Cu sites, generating FA through the formation of O(CH)O.[146]

Furthermore, another research study explored the use of a triphenylene-core porous structure as a means to modify the

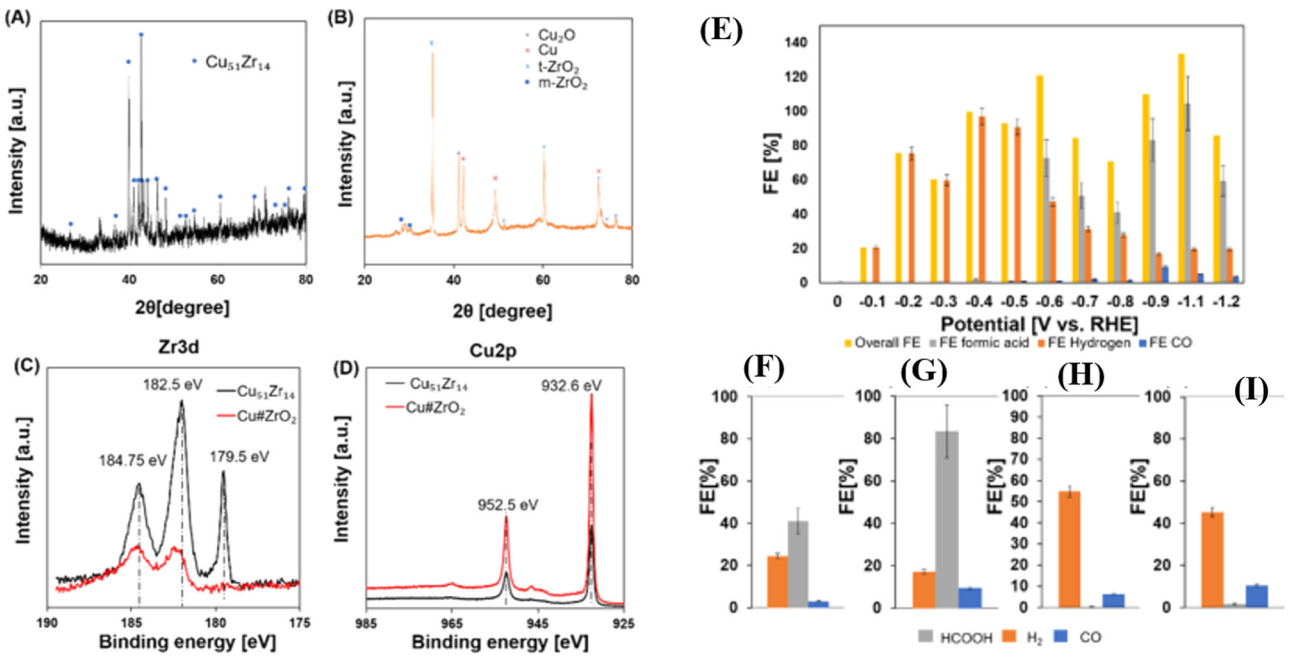

Fig. 13 The p-XRD patterns of the $Cu_{51}Zr_{14}$ composite alloy (A) and Cu#ZrO_2 (B) were analyzed. The HAXPES profiles of the $Cu_{51}Zr_{14}$ precursor alloy (black) and Cu#ZrO_2 (red) were analyzed in the Zr 3d region (C) and the Cu 2p region (D). The product distribution of e-CO_2RR over Cu#ZrO_2 was quantified after 3 hours of electrolysis at a potential of −0.9 V *vs.* RHE (E). The e-CO_2RR performance was evaluated for different catalysts, including a mixture of Cu and YSZ (F), Cu#ZrO_2 (G), commercial Cu (H), and Cu_2O (I). Reproduced from ref. 146. Open access article, American Chemical Society.

performance of Cu atomic catalysts in e-CO_2RR. The triangular pores within this structure served as anchoring sites for Cu atoms, forming complexes that facilitated the hydrogenation of CO_2, a rate-limiting step in e-CO_2RR. Functionalization of these structures with oxygen and nitrogen resulted in reduced overpotentials for e-CO_2RR on Cu@TPGDY, which decreased from 0.26 V to 0.16 V and 0.08 V, respectively.[147] In another facet of e-CO_2RR research, scientists devised a novel catalyst model using a Cu nanosheet coated with a thin layer of carbon. This carbon coating acted as a barrier, inhibiting surface reconstruction at high reducing potentials and preventing the surface oxidation of metallic Cu. Operating at 1.0 V and a current density of 20.3 mA cm^{-2}, the C/Cu/C nanosheet exhibited remarkable stability and a high FE of 47.8% for the production of CH_4. The carbon layers not only enhanced the catalyst's electrical conductivity but also facilitated streamlined electron transport.[148] Furthermore, another research study showcased the synthesis and application of ultrasmall Cu nanocrystals uniformly distributed in nitrogen-doped carbon as catalysts for e-CO_2RR to produce ethanol and formate. These compounds' selective production necessitated specific potentials. At a low potential, the FE for ethanol reached 43.7%, while that for formate was 63.5%. The electronic environment of Cu was influenced by the nitrogen-doped carbon, facilitating proton–electron transport.[149] The overview of the composite engineering strategy utilized to create a number of electrocatalysts for e-CO_2RR to different sustainable products is given in Table 5.

Table 5 Composite engineering is a technique used to create catalysts for CO_2R. The table presents an analysis of electrocatalyst materials specifically designed for this process. It thoroughly examines the properties of these materials and investigates how metal doping affects the distribution of products under different reaction conditions

				≈FE%									
No.	Material	Electrolyte	V *vs.* RHE	H_2	CO	CH_4	C_2H_4	$HCOO^-$	$C_2H_5^+$	CH_3OH	C_2H_5OH	$C_2H_3O_2^-$	Ref.
1	Cu–N–C800	0.1 M $KHCO_3$	−1.2 Ag/AgCl	58	11	—	—	22	—	—	—	—	134
2	$Fe_{0.01}$Cu–N–C800			49	27	—	—	20	—	—	—	—	
3	$Fe_{0.07}$Cu–N–C800			44	48	—	—	4	—	—	—	—	
4	$Fe_{0.13}$Cu–N–C800			41	46	—	—	5	—	—	—	—	
5	CoPPc@g-C_3N_4–CNTs	0.5 M $KHCO_3$	−0.55	35	43	—	—	—	—	—	—	—	135
6	CoPc–Cu–NH	$KHCO_3$	−0.95	41	59	—	—	—	—	—	—	—	136
7	CoPc–Cu–O			42	59	—	—	—	—	—	—	—	
8	NiPc–Cu–NH			62	37	—	—	—	—	—	—	—	
9	NiPc–Cu–O			50	48	—	—	—	—	—	—	—	
10	CuPolyPc@CNT	0.1 M $CsHCO_3$	−1.1	42	53	—	—	—	—	—	—	—	138
11	CoP_2O_6/HCS	0.5 M $KHCO_3$	−0.76	68	32	—	—	—	—	—	—	—	139
12	CoP_2O_6/HCS–Cu10			41	28	—	—	31	—	—	—	—	
13	CoP_2O_6/HCS–Cu20			25	9	—	—	70	—	—	—	—	
14	CoP_2O_6/HCS–Cu40			11	18	—	—	73	—	—	—	—	
15	CF	$KHCO_3$	−1.1	62	1	—	—	3	—	—	2		140
16	CNWs			62		—	1	22	—	—	3		
17	S–CNWs-2			23	1	—	—	60	—	—	—	—	
18	$Cu_{2.4}$Ni/NCNT	0.5 M $KHCO_3$	−0.9 V	8	92	—	—	—	—	—	—	—	141
19	CuNi/NCNT			5	95	—	—	—	—	—	—	—	
20	$Cu_{0.36}$Ni/NCNT			25	75	—	—	—	—	—	—	—	
21	Cu/NCNT			16	84	—	—	—	—	—	—	—	
22	Ni/NCNT			16	84	—	—	—	—	—	—	—	
23	NCNT			6	92	—	—	—	—	—	—	—	
24	Co–N–C	0.1 M $KHCO_3$	−0.8	76	19	—	—	—	—	—	—	—	142
25	Co@ CoNC-800			61	38	—	—	—	—	—	—	—	
26	Co@ CoNC-900			48	43	—	—	—	—	—	—	—	
27	Co@ CoNC-1000			38	59	—	—	—	—	—	—	—	
28	CuO/Nafion/solvent formulations (0.5 : 75 vol)	0.1 M K_2SO_4	−50 mA cm^{-2}	28	10	1	39	7	—	—	6	—	143
29	g-C_3N_4		−1.2	92	—	—	—	—	—	—	—	—	144
30	as-syn CuO			65	4	6	11	—	—	—	—	—	
31	as-syn CuO/C_3N_4			78	4	6	2	—	—	—	—	—	
32	as-syn Cu/C_3N			77	5	11	2	—	—	—	—	—	
33	Mn/N–C	1 M $KHCO_3$	20 mA cm^{-2}	82	18	—	—	—	—	—	—	—	145
34	Fe/N–C			79	19	—	—	—	—	—	—	—	
35	Co/N–C			70	25	—	—	—	—	—	—	—	
36	Ni/N–C			90	10	—	—	—	—	—	—	—	
37	Cu/N–C			79	26	—	—	—	—	—	—	—	
38	Zn/N–C			71	19	—	—	—	—	—	—	—	
39	Cu + YSZ	0.1 M $KHCO_3$	−0.9 Ag/AgCl	21	2	—	—	42	—	—	—	—	146
40	Cu#ZrO_2			19	8	—	—	82	—	—	—	—	
41	Commercial Cu			55	5	—	—	—	—	—	—	—	
42	Cu_2O			43	1	—	—	8	—	—	—	—	
43	CuNCs@p-Cu/g-Cu	0.1 M $KHCO_3$	−1.15	45	1	9	41	5	—	—	—	—	48
44	Cu nanosheet	0.5 M $KHCO_3$	−1.0	—	—	27	24	—	—	—	—	—	148
45	C/Cu/C nanosheet			—	—	48	10	—	—	—	—	—	
46	Cu/NC–NSs	KOH	−0.37	—	—	—	—	3	—	—	45	—	149

6.6. Surface engineering approach

Surface engineering is a multifaceted strategy employed in the design of electrocatalysts for e-CO_2R. Its importance stems from the critical role of catalyst surfaces in dictating reaction pathways and kinetics during electrochemical CO_2 conversion. Surface engineering encompasses various techniques aimed at tailoring the catalyst's surface properties to enhance its activity, selectivity, and stability. Among these techniques are surface anchoring, molecular surface functionalization, interfacial engineering and speciation of Cu surface, which involve the precise attachment of catalytic sites, often metal nanoparticles, onto a support material.

6.6.1. Surface anchoring. The strategy of anchoring the surface plays a role in designing electrocatalysts for CO_2R. It has implications for improving the performance and selectivity of these catalysts. The main idea behind this approach is to attach sites, such as metal nanoparticles or single atoms, to support materials like graphene or metal oxides. This prevents their detachment during the process, enhancing the stability of the catalysts, which is essential for long term and efficient CO_2R. Various techniques, such as chemical binding, physical adsorption or covalent bonding, are used to achieve surface anchoring. By controlling the strength and density of anchoring, researchers can customize the behavior of catalysts for CO_2R reduction reactions. Surface anchoring not only enhances the activity but also addresses the challenges in sustainable energy conversion. It leads to efficiency by preventing aggregation or dissolution of active sites during reactions. This ensures that target fuels or chemicals are produced with by-products. Furthermore, surface anchoring offers the advantage of using affordable materials as catalysts. This is because the support provides stability to sites that may be less stable on their own. Another benefit is that it allows for the integration of sites onto a single support, which encourages cooperative catalysis and enhances reaction kinetics.

A comparison of CO_2RR performance of blank Cu, Cu modified with PPT (Cu-PPT), and Cu modified with QAPPT (Cu-QAPPT) revealed that attaching Pip+ cations onto the Cu electrode reduced competing HER and enhanced CO_2RR selectivity. This enhancement was attributed to reduced interfacial water concentration, an increase in ''ice-like'' water, and the presence of $*CO_{atop}$, $*CO_{bridge}$, and CO–CO dimer species at the Cu/QAPPT interface.[150] Additionally, Ye *et al.* successfully engineered a bi-phasic p-Cu@Cu_2O nanosphere, comprising a Cu nanocrystal core and a Cu_2O nanoprism shell. These nanospheres exhibited exceptional e-CO_2R, with a maximum $FE_{C_2H_4}$ of 79% at −1.18 V *vs.* RHE. Phase engineering facilitated synergistic control of the CO_2 reactant and *CO intermediate adsorption behaviors, resulting in improved CO–CO coupling and increased production of C_{2+} products. During e-CO_2R, CO_2 molecules were absorbed by the faceted Cu_2O shell, where they underwent reduction to *CO intermediates capable of escaping.[151]

In another study, Cu dendrites were coated with PTFE at varying concentrations to create a hydrophobic structure with a stable WCC wetting state. This hydrophobic coating enabled the catalyst surface to efficiently take in gas, increasing the number of triphase contacts for gas diffusion. Consequently, the reaction of *CO was enhanced, with an increase in CO_2 and intermediate *CO on the catalyst surface. Hydrophobic Cu dendrites exhibited a twofold increase in the intrinsic electrochemical activity of their active sites compared to untreated Cu dendrites, leading to more efficient conversion of CO_2 into liquid fuel products such as CH_3OH and C_2H_5OH.[152] Xie *et al.* also unveiled that increased activity and selectivity for C_2H_4 generation were achieved by creating C–Cu nanosheets through the *in situ* reduction of C–CuO nanosheets during e-CO_2RR (Fig. 14). In a gas diffusion flow cell, $FE_{C_2H_4}$ reached 56.2%, and the current density reached 171.0 mA cm^{-2}. Both electrochemical measurements and XAS spectra confirmed the presence of uncoordinated edge sites in the nanosheets. C–Cu nanosheets displayed exceptional activity and selectivity for e-CO_2RR to C_2H_4. They disclosed that Cu atoms with a coordination number of around 5 played a crucial role in assisting the development of a *CHO intermediate, thereby enhancing the coupling reaction of *CO and *CHO intermediates.[153]

In a separate development, researchers devised a method to modify Cu_2O nanocubes to encapsulate carbon dioxide and reduce its concentration. This molecular-scale wrapping was made possible by the CuAAC layer development, transitioning from surface-confined to random as a function of temperature. As a result of this modification, the increased hydrophobicity of the nanocubes dampened hydrogen evolution, making self-controlled modification the optimal condition for CO_2 reduction electrocatalysis.[154] In a different study, Cu nanocubes had been synthesized with rGO modifications through a straightforward electrochemical method. This modification had shifted the post-C–C coupling selectivity from ethylene to ethanol, enhancing local CO concentration on Cu sites. The tandem electrocatalysis approach had led to reduced formate synthesis, increased selectivity, and intrinsic activity towards C_{2+} products during e-CO_2R. Notably, at 0.9 V, the Cu NCbs rGO-60 catalyst had exhibited the highest C–C bond coupling efficiency, favoring ethanol with a 76.84% FE. NCbs rGO-120 and NCbs rGO-60 catalysts had achieved selectivity ratios of approximately 107 and 85.34 for C_{2+} oxygenates/C_{2+} hydrocarbon (ethylene) products, respectively.[155]

In an overarching overview, the utilization of organic chemicals to modify the Cu surface for e-CO_2 conversion had been explored. Catalytic activity had been found to be heavily influenced by the local microenvironment of the electrode surface, encompassing factors like hydrophobicity, electric field, pH, and intermediate coverage. The tunability and designability of organic compounds had offered numerous avenues for enhancing the catalytic activity of Cu-based catalysts. However, challenges remained, such as improving the conductivity and stability of organic compounds. The enhancement of catalytic activity of organic/inorganic hybrid catalysts would benefit from the design and synthesis of well-defined organic molecules or polymers with excellent conductivity and durability. Machine learning with artificial intelligence has the potential

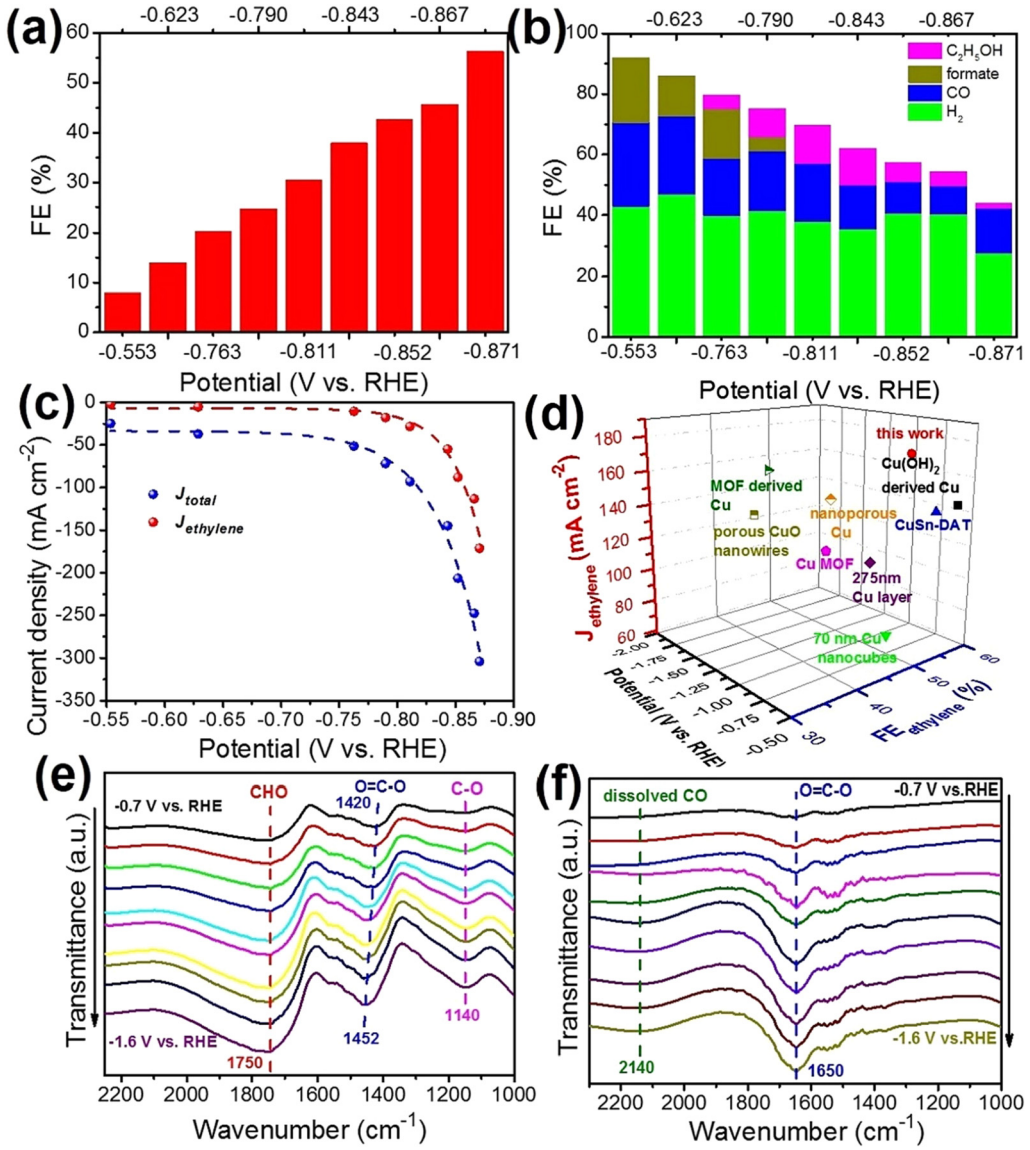

Fig. 14 Gas diffusion flow cell with a 1.0 M KOH electrolyte with FEs of (a) C_2H_4 (a) and (b) H_2, CO, C_6H_5OH, and formate on C–Cu nanosheets. In a gas diffusion flow cell with an Ar-saturated 1.0 M KOH electrolyte, the corresponding total and ethylene currents (J_{total} and $J_{ethylene}$) are measured at varying potentials and the differences between them are *iR* compensated (c). When utilizing a gas diffusion flow cell and an electrolyte of 1.0 M KOH, a summary of the performance of Cu-based electrocatalysts for the formation of C_2H_4 is provided (d). ATR-FTIR spectra of C–Cu nanosheets (e) and Cu powder (f) taken *in situ* during e-CO_2RR at varying potentials in a CO_2-saturated 0.1 M $KHCO_3$ electrolyte. Reproduced with permission from ref. 153. Copyright 2023, Elsevier.

to expedite catalyst manufacturing by predicting crucial reaction parameters, ultimately leading to Cu-based catalysts with high activity, selectivity, and stability for CO_2RR.[156] In the meantime, the discussion also underscored the need to move beyond single-crystal studies and design Cu nanocrystals (NCs) in order to better understand the structural dependence of CO_2RR. The view of NCs is a necessary tool, elucidating the reaction pathway and identifying size-dependent selectivity trends for C_2 products. Most studies have focused on shapes exposing high-index facets. Therefore, it is extremely important to enrich the family of Cu NC shapes. The steps for rebuilding the catalyst, primarily driven by a dissolution–redeposition cycle, can be better understood by using NCs to identify the transient species involved.[157]

In another study, rough-edged Ag NPs/CuO MNSs were synthesized on a Cu foil for e-CO_2R to CO. The heterostructure exhibited high electrical conductivity, abundant active sites, and a superior electronic structure, leading to enhanced CO_2 adsorption and activation. The critical COOH intermediate in the pathway from e-CO_2R to CO was stabilized at the Ag–CuO contact. The best Ag1.01%/CuO catalyst achieved a maximum FE_{CO} of 91.2% at a partial current density of 10.5 mA cm^{-2} and 0.7 V in 0.1 M $KHCO_3$. The catalyst demonstrated good catalytic stability, maintaining a FE_{CO} of over 80% in the potential region.[158] Additionally, a novel bimetallic InSn catalyst was developed using a potential-driven volume diffusion approach at room temperature (Fig. 15). This catalyst effectively increased

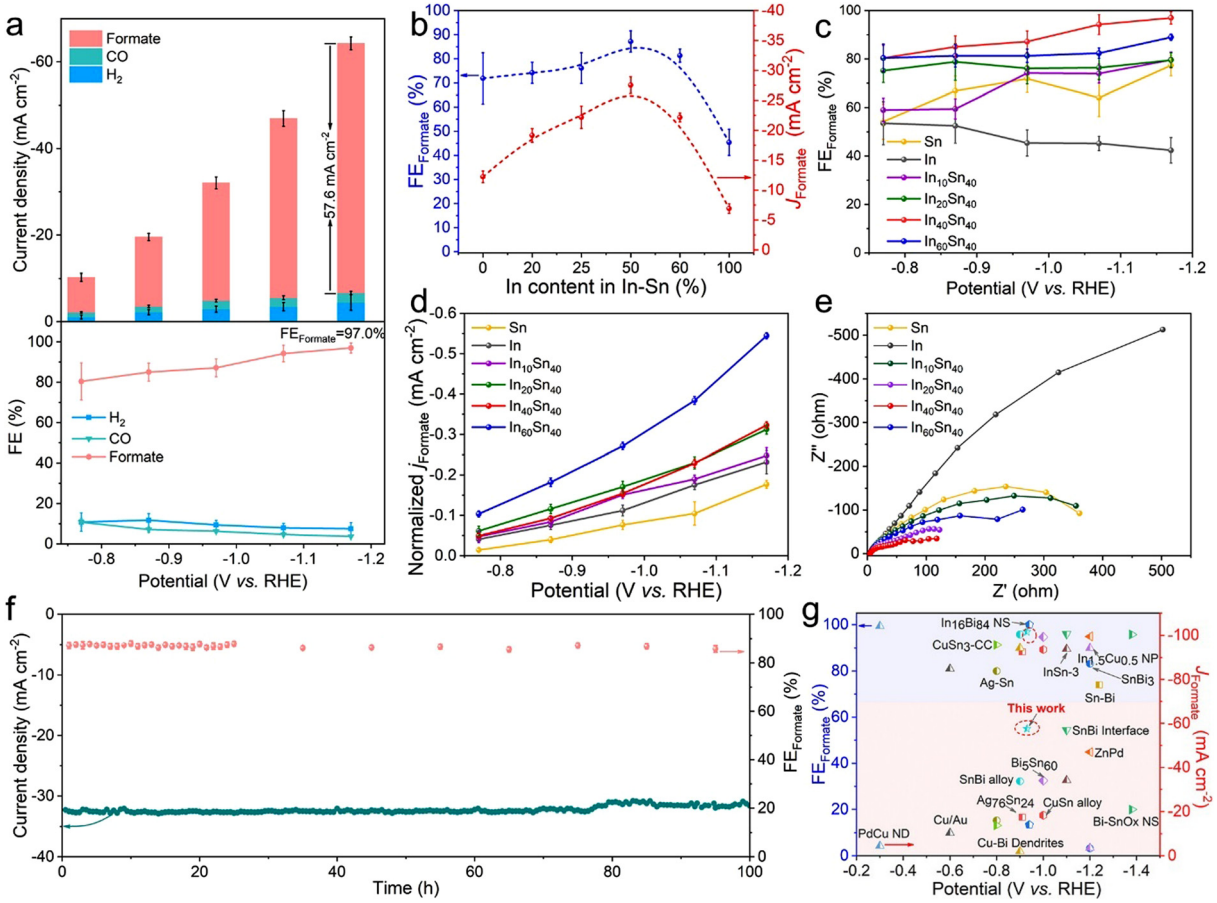

Fig. 15 CO_2RR effectiveness. Current density (top) and FE of CO, H_2, and formate on $In_{40}Sn_{40}$ at different applied potentials (a). Formate production FE values and partial current densities for In, Sn, and InSn catalysts *vs.* various In concentrations at 0.97 V *vs.* RHE (b). Each catalyst's $FE_{formate}$ at varying potentials (c). Partial current densities of each catalyst, expressed in a formate formation (d). EIS plots of all the produced samples were analyzed (e). Electrolysis of $In_{40}Sn_{40}$ for 100 hours at 0.97 V *vs.* RHE (f). Comparison with literature in terms of formate current density and $FE_{formate}$ with 90% *iR*-correction (g). Standard deviations from at least three separate measurements of the sample are used to create the error bars. Reproduced with permission from ref. 159. Copyright 2023, American Chemical Society.

current density by selectively reducing CO_2 to formate. The catalyst featured an InSn hybrid core, a nanoshell structure with multiple interfaces, a multicomponent core–shell heterostructure, and a novel configuration that potentially accelerated CO_2 and HCO_3 equilibrium on the InSn interface.[159]

In addition, the effectiveness of GDEs loaded with copper nanocubes for e-CO_2R in a zero-gap, MEA-type electrolyzer was investigated. These GDEs produced ethylene ($j_{C_2H_4}$ up to about 80 mA cm^{-2}) and propylene, a valuable industrial product, at higher rates compared to nanocube and sputtered Cu catalysts. Although flooding occurred in nanocube GDEs at current densities exceeding 150 mA cm^{-2}, they maintained high ethylene production rates even during flooded operation. Researchers are currently focusing on optimizing mass loading and developing mitigation methods to prevent the loss of ethylene selectivity in Cu nanocube-loaded electrodes due to flooding.[160] In a separate study, electrocatalytic TDPA-capped CuAg NCs were synthesized using a novel approach that involved investigating near-stoichiometric ligand-to-copper (P/Cu) ratios and utilizing Cu(II) acetate monohydrate. Depending on the diameter of the Cu NC precursor, one or two galvanic replacement steps were employed to form sub-10 nm Cu@Ag core–shells and Cu/Ag nanodimers, as confirmed through HRTEM and spectroscopy. The relationship between composition and selectivity was explored in the range of 14 to 41% Ag by spreading the nanocrystals on carbon black at high packing densities. The CO_2RR selectivity transitioned from ethylene to ethanol production between CuNCs/C and CuAg/C-based electrodes, resulting in a 2- to 3-fold increase in the oxygenate-to-hydrocarbon ratio at moderate Ag atom %age levels. $Cu/Ag_{0.14}$/C nanodimers and $Cu@Ag_{0.17}$/C core–shells achieved a total C_2 and C_3 selectivity of 50% at neutral bulk pH and 0.1 A cm^{-2}, suggesting a substantial impact from local CO concentration and CO-spillover on catalytic patterns at high CO_2RR rates.[161]

Moreover, another research endeavor proposed that the e-CO_2R to ethylene can be significantly improved by utilizing an ionic liquid (IL) in combination with a Cu electrocatalyst. The IL was demonstrated to alter the electronic structure of the Cu catalyst, facilitating *CO dimerization and enhancing ethylene generation. This method achieved a remarkably high

77.3% $FE_{ethylene}$ in a water-based electrolyte and a standard H-type cell.[162] Additionally, researchers have coated a layer of PTFE that conforms itself to a Cu nanoneedle (NN). By increasing the amount of PTFE at the end of a nanoneedle, the electric and thermal field strength rapidly varies. This in turn accelerates the C–C coupling of C_2 and CO intermediate production. This method also enabled C_2 generation at a TOF of 11.5 ± 0.3 s^{-1} Cu_site^{-1} and a FE_{C_2} of 85.4 ± 1.5% under partial currents exceeding 250 mA cm^{-2}.[163] The effect of plasma pretreatment of the Cu surface on the overall surface was unusual. This, in turn, caused huge differences in the way the CO_2RR products distributed. The observed differences in CO_2RR activity seen across the series are related to changes in the electrochemically active surface area. The roughened surface has a stronger inclination to CO formed through e-CO_2R than does the electrochemically polished surface. This phenomenon implies that as the size of the surface increased, the percentage of the adsorbed H to CO showed a decreasing trend. As surface roughness increased, the fractions of products containing two or more carbons also changes. The ratio of current densities for C_{2+} to C_1 products displayed an increasing trend with increasing surface roughness, mainly due to the production of CH_4 increasing on substrates with roughness levels above 3.[164]

Meanwhile, during the course of e-CO_2R, the selectivity to C_2H_4 was greatly improved through the formation of the Cu nanoparticle substructure from spheres to cubes. The development was initiated by a weak adhesion of Cu NPs to the graphene oxide substrate. However, with time these Cu nanocubes turned into smaller, less organized nanoparticles, thus reducing the tendency to select for C_2H_4. To meet this challenge, an innovative approach appeared in which 2D- or ''flat''-graphene with nitrogen doping served as an anchoring framework for Cu nanocubes. This relied on the strong interactions between Cu NPs and the pyridinic nitrogen atoms that covered the surface of 2D graphene.[165] Simultaneously, Cu_2O nanostructures with precisely controlled crystal facets were synthesized through a hydrothermal methodology. The catalytic ability and alcohol selectivity of these catalysts were responsible to the exposed crystal facets, ultimately dictating their performance in e-CO_2R. The electrochemical evaluation of the Cu_2O-o catalyst, decorated with (111) crystal facets, revealed an impressive high partial current density and 35.4% selectivity for alcohol generation at 0.3 V *vs.* RHE.[166] Transitioning to the TB catalyst, the most elongated among the examined 1D active sites, it was synthesized with density adjustments ranging from 0 to 105 cm^{-1}. Research findings illuminated TB's remarkable electrocatalytic ability, characterized by an exceedingly high local j_{CH_4} of 1294 mA cm^{-2}, accompanied by inherent CH_4 selectivity fixed at 92%. Computational simulations, in alignment with DFT, affirmed that TB atoms outpaced flat atoms by a staggering factor of 104 in protonating CO*.[167]

In a comprehensive comparative analysis deploying gas-diffusion electrodes and flowing alkaline catholytes, researchers meticulously scrutinized the electrocatalytic performance of Cu nanocubes and nanospheres in CO_2R. While an uptick in catalytic efficiency ensued with the use of a more concentrated alkaline catholyte, it became evidently clear that Cu nanocubes surpassed their nanospheric counterparts when catalyzing CO_2R toward ethylene.[168] Furthermore, the research unveiled that liquid C_{2+} products could be produced at a significantly accelerated rate due to the synergistic interplay of Cu and Pb within Cu/Pb core/shell nanocrystals. The partial current density for CO_2RR in a flow cell system over CuPb-0.7/C reached an impressive 294.4 mA cm^{-2}, and the total free energy associated with C_{2+} products stood at 73.5 kJ mol^{-1}. Notably, in terms of generating C_{2+} liquid products, the total free energy achieved an outstanding 49.5%, accompanied by a partial current density of 196.8 mA cm^{-2}. These results surpassed the performance of most reported Cu-based catalysts for CO_2RR. When CuPb-0.7/C was used as a catalyst for CO_2 reduction, the cooperation between Cu and Pb made it easier to pass through the intermediate product of COOH and then into C_{2+} products through the production of *OCCOH.[169]

In the search for affordable and environmentally friendly e-CO_2R catalysts, research teams have developed a new bimetallic alloy/oxide nanowire catalyst with a core–shell structure. The core of this catalyst boasts high electrical conductivity, while the catalytic activity and selectivity are guaranteed by the amorphous Cu-doped SnO_2 shell. Computational analyses underscored the pivotal role of the Cu-doped SnO_2 layer in curbing the electrocatalytic generation of formate and hydrogen. Remarkably, when operating at 0.9 V *versus* RHE, this electrocatalyst achieved an impressive FE of 78% for formate production at a partial current density of 30 mA cm^{-2}.[170] Another noteworthy development in the field of CO_2R was the monodisperse core/shell Cu/In_2O_3 nanoparticles, resulting in the effective production of syngas. The H_2/CO ratios in syngas could be fine-tuned over a broad range, with a FE for syngas generation exceeding 90% through adjustments in the thickness of the In_2O_3 shell and applied voltage. Compared to other reported electrocatalysts for syngas production, the C–Cu/In_2O_3-0.4 catalyst emerged as the top performer, delivering high current densities at remarkably low overpotentials. The incorporation of compression strain along with Cu doping in the In_2O_3 shell was identified as a key factor responsible for elevating CO production activity and enhancing the H_2/CO ratio.[171] Table 6 presents the properties of different electrocatalysts for e-CO_2R to sustainable products designed by following the surface anchoring strategy.

6.6.2. Molecular surface functionalization. The strategy of modifying the surface of electrocatalysts at the atomic level is a technique that offers precise control over the catalyst's properties. By attaching groups or molecules to the catalyst surface researchers can fine-tune its reactivity and selectivity towards converting CO_2. This method can produce high-performance selective catalysts, which might help turn carbon dioxide into valuable chemicals or fuels. Precise engineering at atomic levels reduces back or side reactions, and improves the overall performance of CO_2 conversion. It is conceptually equal to addressing the main difficulties in clean energy conversion and controlling greenhouse gas emissions. The importance of molecular surface functionalization is found in its capacity to regulate bonding sites and bonding strength for CO_2 and its

Table 6 The table provides an overview of electrocatalyst materials used in CO_2R making it a valuable resource for navigating this field. It presents an analysis of the properties of these materials with an emphasis on how surface anchoring influences the distribution of reaction products under different conditions

				≈FE%									
No.	Material	Electrolyte	V *vs.* RHE	H_2	CO	CH_4	C_2H_4	$HCOO^-$	$C_2H_5^+$	CH_3OH	C_2H_5OH	$C_2H_3O_2^-$	Ref.
1	Blank Cu	0.1 M $KHCO_3$	−1.0	1	83	—	—	—	—	—	—	—	150
2	Cu-PPT			1	87	—	—	—	—	—	—	—	
3	Cu-QAPPT			42	16	—	—	20	—	—	—	—	
4	p-Cu@Cu_2O	0.1 M $KHCO_3$	−0.98	18	18	1	35	3	—	—	13		151
5	i-Cu@Cu_2O			—	—	—	4	—	—	—	—	—	
6	r-Cu@Cu_2O			—	—	—	2	—	—	—	—	—	
7	Untreated Cu dendrite	0.1 M $KHCO_3$	−1.0	—	—	—	—	3.5	—	3	2	—	152
8	Hydrophobic Cu dendrite			—	—	—	—	—	—	4.5	2.8	—	
9	C–Cu nanosheets	0.1 M $KHCO_3$	−1.0	25	22	1	31	—	—	—	—	—	153
10	Cu powder			62	2	1	10	—	—	—	—	—	
11	@3AZ rt-1h	0.1 M $KHCO_3$	−1.4	65	1	28	2	—	—	—	—	—	154
12	@3AZ rt-20h			37	1	43	2	—	—	—	—	—	
13	@3AZ 80 °C 1 h			37	1	40	4	—	—	—	—	—	
14	@3AZ 80 °C 20 h			33	1	43	1	—	—	—	—	—	
15	@2AZ r-t 20 h			41	1	35	2	—	—	—	—	—	
16	Cu NCbs	0.1 M $KHCO_3$	−1.1	—	—	20	33	—	—	13	34	—	155
17	Cu NCbs-rGO/60			—	—	10	32	4	—	2	35	—	
18	Cu NCbs-rGO/120			—	—	18	55	1	—	—	45	—	
19	Ag1.55%/CuO	0.1 M $KHCO_3$	−0.4	59	40	—	—	—	—	—	—	—	158
20	Ago.68%/CuO			32	63	—	—	—	—	—	—	—	
21	Ag1.01%/CuO			41	56	—	—	—	—	—	—	—	
22	CuO			40	53	—	—	—	—	—	—	—	
23	Sn	0.5 M $KHCO_3$	−1.1	—	—	—	—	65	—	—	—	—	159
24	In			—	—	—	—	44	—	—	—	—	
25	$In_{10}Sn_{40}$			—	—	—	—	72	—	—	—	—	
26	$In_{20}Sn_{40}$			—	—	—	—	73	—	—	—	—	
27	$In_{40}Sn_{40}$			5	3	—	—	86	—	—	—	—	
28	$In_{60}Sn_{40}$			—	—	—	—	80	—	—	—	—	
29	Cu-Cubes GDE (loading 440 μg cm^{-2})	0.1 M $KHCO_3$	100 mA cm^{-2}	—	62	—	10	—	—	—	—	—	160
30	$Cu/Ag_{0.14}$	0.1 M $CsHCO_3$	0.1 A cm^{-2}	11	50	6	18	2	—	—	15	—	161
31	$Cu/Ag_{0.17}$			8	83	1	1	2	—	—	3	—	
32	$Cu/Ag_{0.41}$			13	84	—	—	2	—	—	—	—	
33	IL@Cu	0.1 M $KHCO_3$	−1.19	49	10	1	40	—	—	—	—	—	162
34	Cu			62	8	2	22	—	—	—	—	—	
35	Cu-NP	0.1 M $KHCO_3$	−1.5	43	2	3	16	20	—	—	6	—	163
36	Cu-NN			43	4	4	24	4	—	—	21	—	
37	Cu-PTFE NNs (70%)			25	2	3	37	2	—	—	33	—	
38	Cu-PTFE NNs (90%)			18	2	2	34	2	—	—	43	—	
39	Cu-PTFE NNs (99%)			10	1	1	55	1	—	—	41	—	
40	EC polished Cu	0.1 M $CsHCO_3$	−1.0	34	17	4	25	7	—	—	5	—	164
41	After N_2 plasma			30	8	4	34	6	—	—	5	—	
42	After Ar plasma			28	3	2	43	4	—	—	10	—	
43	After O_2 plasma			33	3	3	42	3	—	—	11	—	
44	20 wt% Cu/GO			66	3	2	10	10	—	—	2	—	165
45	40 wt% Cu/GO			53	4	4	8	20	—	—	—	—	
46	60 wt% Cu/GO			45	12	9	22	5	—	—	—	—	
47	80 wt% Cu/GO			51	10		8	25	—	—	—	—	
48	Cu_2O-c	0.5 M $KHCO_3$	−0.3	2	21	28	—	2	—	5	—	—	166
49	Cu_2O-o			11	40	5	—	5	—	6	—	—	
50	Cu_2O-t			5	37	1	—	4	—	11	—	—	
51	Cu_2O-u			4	10	16	—	—	—	2	—	—	
52	Cu			1	25	—	—	—	—	20	—	—	
53	CuO			1	—	—	—	—	—	4	—	—	
54	Nt-16	0.2 M $KHCO_3$	−1.6	20	1.9	59	3.6	19	—	—	—	—	167
55	Nt-43			26	1.6	49	1.4	16	—	—	—	—	
56	Nt-77			40	1.5	38	1.2	15	—	—	—	—	
57	Nt-265			42	0.8	32	1.8	18	—	—	—	—	
58	Ut-Cu			47	0.38	28	1.5	20	—	—	—	—	
59	Cu nanocubes	0.1 M $KHCO_3$	−0.8	5	24		51	5	—	—	—	—	168
	Cu nanospheres			5	34	1	20	22	—	—	—	—	
60	$CuPd_{0.5}$/C	1 M KOH	100 mA cm^{-2}	10	20	—	34	—	—	—	18	—	169
61	Cu_3Sn/CF	0.5 M $KHCO_3$	−0.9	64	4	—	—	37	—	—	—	—	170
62	C–Cu	0.5 M $KHCO_3$	−0.9	64	4	—	—	32	—	—	—	—	171
63	C–Cu/In_2O_3-0.4			38	52	—	—	10	—	—	—	—	
64	C–Cu/In_2O_3-0.8			42	48	—	—	10	—	—	—	—	
65	C–Cu/In_2O_3-1.5			34	21	—	—	40	—	—	—	—	
66	Acid-treated In foil			88	—	—	—	17	—	—	—	—	

intermediates. It helps facilitate binding. Self-assembly, chemical modification, and atomic layer deposition are techniques that allow amines, carboxylates, or imidazoles to be introduced onto the catalyst surface. These catalytic methods use these functional groups as adsorption sites for CO_2. By facilitating its conversion, reaction pathways can be optimized to bring about the desired products, such as methane and ethylene. This approach lays the groundwork for creating tandem reactions through the catalyst it employs, which will take us beyond just one molecule to whatever other valuable chemicals can be derived from CO_2.

The e-CO_2R into enantiomeric amino acids had represented one of the earliest instances of producing complex C_{3+} products with C–N bonds. This achievement was made possible by reducing reaction barriers in the synthesis of C_{3+} compounds through the utilization of chiral twist sites on catalyst surfaces. This discovery underscored the viability of a universal strategy aimed at enhancing the intrinsic catalytic activities of materials for the production of C_{3+} species, while also showcasing the potential of chiral twist sites for generating specific biomolecules starting from CO_2 and ammonium bicarbonate.[172] In a significant development, inorganic CuNCs underwent functionalization with an imidazolium ligand, resulting in the creation of hybrid CO_2RR catalysts that were subject to comprehensive investigation. The findings revealed that, at higher applied potentials, the $ImPF_6$ ligand exhibited a preference for CO_2RR over HER and formates over ethylene across the studied potential range. The structural stability of cubic CuNCs and their strong interactions with the ligands facilitated surface modification experiments. However, it was noteworthy that the promoter effect of the imidazolium ligand dissipated during the reconstruction of spherical CuNCs. These insights highlighted the pressing need for hybrid catalysts characterized by either ligands impeding the rebuilding processes or stable NC morphologies.[173]

In a stunning revelation of scientific achievement, previous researches unveiled the remarkable enhancement of copper catalytic activity through the application of various imidazolium salts. These chemical modifications yielded impressive improvements in ethylene selectivity, all while effectively suppressing the production of H_2, CH_4, and ethanol by skillfully manipulating substituents in organic modifiers. Amazingly, the modified electrodes exhibited an ethylene selectivity of up to 73%, with C_2 product selectivity rising as high as 82%. Even after a demanding 19 hours of continuous use, the total current densities remained virtually indistinguishable between the modified electrodes and their bare copper counterparts. The nuanced steric and electronic characteristics of substituents on imidazolium nitrogen atoms took center stage, dictating product distribution with the finesse to fine-tune selectivity through adjustments in film deposition potential and alkyl chain length.[174]

To explore this further, researchers entered the e-CO_2R process excitedly in a novel way using Cu/SnO_x heterostructured nanoparticles combined with CNTs. As the ratio of Cu/SnO_x was carefully adjusted, the potential for modulating the primary product was revealed – intermediate hydrocarbons, CO_2, formaldehyde or formic acid.[175] Further, the addition of CTAB to an electrolyte was found to significantly change the selectivity of unmodified Cu for formate production during e-CO_2R. In near-neutral aqueous electrolytes, this produced a remarkable 82% selectivity and a 56-fold increase in partial current density.[176]

Moreover, an innovative technique was described for manufacturing a catalyst containing Ni/Cu dual sites on MOF-templated porous carbon. This approach facilitated uniform dispersion of dual sites with adjacent NiN_4 and CuN_4 moieties. The presence of Cu sites was found to lower the formation barrier of *COOH on surrounding Ni sites, making the rate-limiting step more accessible. As a result, the Ni/CuNC catalyst with N_4Ni/CuN_4 moieties exhibited an exceptionally high intrinsic activity and achieved impressive FE_{CO} values (99.2% at 0.79 V *versus* RHE and greater than 95% from 0.39 to 1.09 V *vs.* RHE).[177] In addition to these findings, shed light on the role of metal–supramolecular couples constructed *via* stacking interactions in facilitating a pivotal phase of C_{2+} product production, specifically C–C coupling (Fig. 16). The selectivity towards C_{2+} products was attributed to the paired structure of metal sites and the van der Waals interaction between the secondary coordination sphere and the adsorbed intermediates. Remarkably, they marked the first detailed exploration of engineering metal–supramolecular couples with catalytic activity for multicarbon-selective electrochemical reduction.[178]

Moreover, the research proposed an approach aimed at enhancing the selectivity of e-CO_2R, with a specific focus on C_2 products, notably ethanol. Impressively, CuBr treated with DDT molecules yielded remarkable results, a high ethanol-to-ethylene ratio and an impressive FE of 72%. This achievement stemmed from the inhibition of Br migration and the complete reduction of CuBr through DDT adsorption onto CuBr, leading to the formation of a novel and highly stable Br-doped Cu–thiol interface during the catalytic process. Additionally, the incorporation of Br species into Cu was hypothesized to stabilize high-valence Cu species and direct selectivity towards C_2 products, particularly ethanol, as evidenced in the study.[179] In parallel, another research study's findings unveiled a significant breakthrough in the realm of e-CO_2R. The incorporation of ZrO_2 and the meticulous tuning of nanocavities within CuO were identified as critical factors that facilitated the dimerization and protonation of CO, ultimately yielding C_2H_4. Notably, this approach also acted as an impediment to the antagonistic HER. The capacity for rational manipulation of e-CO_2R performance was established through the modulation of ZrO_2 incorporation levels and the control of flaws in CuO. Notably, over CuO@ZrO_2 in an H-cell configuration, the FE and cathodic energy efficiency (EE) for C_2H_4 generation witnessed substantial enhancements compared to bare CuO, with FE increasing from 19.7% to 47.6% and cathodic EE from 11% to 26.8%. Furthermore, with a flow cell architecture operating at a high current density of 250 mA cm^{-2}, the overall FE and EE for C_2H_4 were significantly boosted to 84.3% and 54.7%, respectively.[180]

In a related domain, the e-CO_2R to CO in an aqueous environment, utilizing metal nanoparticle catalysts such as

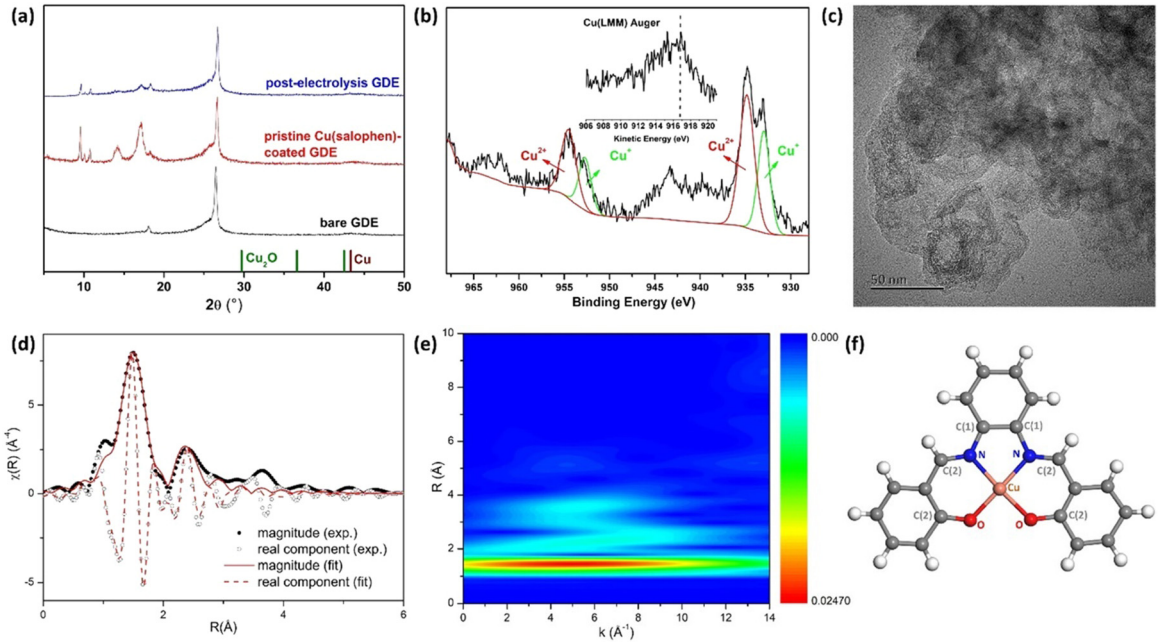

Fig. 16 The P-XRD patterns of the GDE without any modification and the GDEs with the Cu(salophen)–carbon composite catalyst were analyzed before and after electrolysis (a). The Cu 2p XPS spectrum was examined, and the Cu LMM Auger spectrum was included as an inset (b). A TEM image was taken to visualize the structure of the catalyst (c). The Cu K-edge EXAFS spectrum was analyzed, and the fit in *R*-space was determined (d). The Cauchy wavelet transform of the Cu K-edge X-ray absorption spectrum was studied for the post-electrolysis Cu(salophen)–carbon composite catalyst (e). A structural model was used for EXAFS fitting (f). Reproduced with permission from ref. 178. Copyright 2023, American Chemical Society.

Au nanoparticles, witnessed significant advancement through the implementation of a molecular surface functionalization strategy.[181] Concurrently, the research delved into the utilization of a one-step solvothermal methodology for the synthesis of copper hydroxyphosphate catalysts tailored for deployment in e-CO_2RR. Electrochemical investigations brought to light the remarkable component-specific efficiency of these catalysts. The FE exhibited by polyhydroxyl $Cu_5(OH)_4(PO_4)_2$ reached 37.4% at −1.6 V, surpassing that of $Cu_2(OH)PO_4$ by over 100% in terms of current density.[182]

In a parallel research avenue, an innovative strategy revolved around surface molecule functionalization, presenting a potential breakthrough for catalytic applications. Specifically, the 4H/fcc Au-MMT configuration outperformed its counterpart, 4H/fcc Au-OAm, by a significant margin in terms of e-CO_2RR performance within H-type cells. This surface functionalization strategy also exhibited the capacity to enhance the selectivity of the flow cell for CO. DFT simulations conducted on 4H/fcc Au nanorods functionalized with OAm and MMT ligands revealed opposing modulation effects. In both the fcc and 4H phases, surface MMT activation of Au was observed, resulting in a e-CO_2RR process characterized by minimal reaction barriers. In contrast, OAm exerted effects such as reduced electroactivity and the introduction of spatial barriers for intermediate adsorption on the surface.[183] An overview of electrocatalysts designed by following the molecular surface functionalization approach is tabulated in Table 7.

6.6.3. Interfacial engineering. Interfacial engineering represents an innovative strategy when it comes to designing electrocatalysts for CO_2R. Its main focus is on manipulating and optimizing the interface between the catalyst and the electrolyte. The significance of this approach lies in its ability to enhance activity, selectivity and stability, all of which are factors in efficiently converting CO_2 into valuable products. By adjusting the properties of this interface researchers can influence how CO_2 and its intermediates are adsorbed, thereby controlling the reaction pathways. This level of control is vital in addressing the challenges associated with CO_2R, contributing to the production of fuels and chemicals sustainably. There are various techniques that can be utilized for engineering catalyst design. For example, using molecules to modify a surface, such as with electrodes, allows for the introduction of specific binding sites and active groups that help CO_2 capture or conversion. The choice among various support materials and catalyst substrates can also play a role in property determinants. Nanostructuring roughened surfaces or producing heterojunctions is among the ways to engineer the interface between the cathode material and the electrolyte leading to increased catalytic performance. The importance of engineering is that it may allow electrocatalysts to be tailored for CO_2R reactions like methane production or ethylene focusing on practical applications on the one hand and towards sustainability energy solutions on the other hand. And it reduces CO_2 emissions, mitigating climate change.

Zhang *et al.* designed a Cu–Zn alloy/Cu–Zn aluminate oxide composite system for the e-CO_2R to valuable C_{2+} products. Decomposition of the Cu–Zn–Al-LDH precursor signals the beginning of this novel composite system. Following this, the precursory catalyst was transformed into a composite catalyst

Table 7 The table offers an overview of electrocatalysts specifically designed for CO_2R focusing on the approach of molecular surface functionalization. It highlights the range of materials used in electrocatalysis for CO_2R and provides a review of their electrochemical behavior, product selectivity and efficiency. This information provides insights across variable reaction conditions

				≈FE%									
No.	Material	Electrolyte	V *vs.* RHE	H_2	CO	CH_4	C_2H_4	$HCOO^-$	$C_2H_5^+$	CH_3OH	C_2H_5OH	$C_2H_3O_2^-$	Ref.
1	L-CCFs	0.25 M $NH_3{\cdot}H_2O$		—	—	—	—	1	—	—	10	—	172
2	ACFs			—	—	—	—	1	—	—	4	—	
3	Cu_{cub}	0.1 M $KHCO_3$	−1.05	65	7	2	20	3	—	—	1	—	173
4	Cu_{cub}–$ImPF_6$			67	7	1	14	10	—	—		—	
5	Modified polycrystalline copper (12)	0.1 M $KHCO_3$	−1.14	39	5	10	20	21	—	—	3	—	174
6	CuO_y-CNT-#1	0.1 M $KHCO_3$	−1.09	46	4	35	10	6	—	—	—	—	175
7	CuO_y/SnO_x-CNT-#2			50	5	25	10	10	—	—	—	—	
8	CuO_y/SnO_x-CNT-#7			12	76	—	—	12	—	—	—	—	
9	CuO_y/SnO_x-CNT-#12			14	13	—	—	80	—	—	—	—	
10	SnO_x-CNT-#13			23	25	—	—	52	—	—	—	—	
11	Oxide-derived Cu	0.5 M $KHCO_3$	−0.9	45	2	2	1	50	—	—	—	—	176
12	Cu-CTAB			48	1	—	—	54	—	—	—	—	
13	N/C			—	25	—	—	—	—	—	—	—	177
14	Cu–N–C			—	50	—	—	—	—	—	—	—	
15	Ni–N–C			—	51	—	—	—	—	—	—	—	
16	Ni/Cu–N–C			—	85	—	—	—	—	—	—	—	
17	Cu(salophen)-coated GDE	1 M KOH	−1.0	30	20	3	38	6	—	—	3	—	178
18	CuBr	—	−1.10	24	4		25	—	—	—	—	—	179
19	CuBr-DDT			18	20		18	—	—	—	—	—	
20	CuO@ZrO_2	0.1 M $KHCO_3$	−1.1	—	9	7	48	7	—	—	—	—	180
21	CuO			—	2	2	25	9	—	—	—	—	
22	ZrO_2			—	—	—	—	7	—	—	—	—	
23	$Cu_2(OH)PO_4$	0.1 M $KHCO_3$	−1.0	38	8	—	—	—	—	—	—	—	182
24	$Cu_5(OH)_4(PO_4)_2$			46	8	—	9	—	—	—	—	—	
25	4H/fcc Au-MMT	1.0 M $KHCO_3$	−1.0		70	—	—	—	—	—	—	—	183
26	4H/fcc Au-OAm				53	—	—	—	—	—	—	—	

consisting of the Cu–Zn alloy and Cu–Zn aluminate oxide. These two components were replicated in a lattice that results in interface after interface crisscrossing. An optimized $Cu_9Zn_1/Cu_{0.8}Zn_{0.2}Al_2O_4$ catalyst displayed massive current and atom-light effects (though only for C_{2+} products): 88.5% FE at 400 mA cm^{-2} when operating at 1.15 V *vs.* RHE.[184] Simultaneously, another study delved into the e-CO_2R into methane, leveraging a Cu foil modified with ZnO_x nanoparticles. Notably, the peak FE for methane production was achieved at 1.1 V, reaching approximately 36%, and it exhibited no significant deterioration over time. This catalytic activity was attributed to the induction of active sites for methane production, identified as cupric ions, at the Cu/ZnO_x interface. The interaction between Cu and ZnO_x provided stability to these active species, prolonging their catalytic lifespan. Importantly, the synthesis process for this system was characterized by its swiftness, simplicity, cost-effectiveness, and straightforwardness. Furthermore, the scalability of methane production was achieved by expanding the surface area of the Cu foil.[185]

Furthermore, in the pursuit of achieving exceptional selectivity and stability in the e-CO_2R to C_{2+} products, Liu *et al.* developed a heterostructured catalyst comprising 2D Cu MOFs and Cu_2O nanoparticles (Cu_2O@Cu-BDC). This catalyst consistently generated stable C_{2+} products with remarkable FE of 72.1% in an H-type cell and 58.2% in a flow cell setup. The key to its success lay in the stabilization of Cu^+ active sites at the interfaces formed between Cu_2O and Cu-BDC within the 2D Cu MOFs. This stabilization, in turn, enhanced C–C coupling reactions and improved the adsorption of critical intermediates involved in the production of C_{2+} products.[186] Additionally, a one-step reduction technique had been employed to create a bimetallic Cu and SnO_x nanocomposite on an amorphous rGO support, aiming to enhance formate synthesis through the interplay between the materials, heterointerfaces, high oxophilicity, and electrochemical surface area. The production of SnO_x nanoparticles had hindered C–C coupling and had reduced H_2 and CO generation, ultimately leading to enhanced formate selectivity and endurance. Remarkably, even after 6 hours of electrolysis, the nanocomposite had maintained 85% of its original current density.[187] In the quest to improve C_{2+} selectivity in e-CO_2R, researchers had devised a method for *in situ* modification of the Cu^+/Cu^0 interface within oxide-derived Cu catalysts. Tests of the R-Cu with Br catalyst's performance in e-CO_2R had unveiled outstanding stability, complemented by its excellent activity and selectivity in producing C_{2+} products. The cooperative Cu^+/Cu^0 interface, which played a pivotal role in conferring remarkable selectivity for C_{2+} products, had substantially lowered the energy barrier for CO–CO coupling and had repressed the HER, thereby enhancing the efficiency of CO–CO coupling.[188]

In a related context, the interactions between Cu and the electrolyte were found to be of paramount importance in the context of CO_2R in aqueous solutions. When CuO electrodes were modified with various polymers such as PVDF, PE, PVA, and PVP, the FE for C_2H_4 generation doubled, and the partial current density nearly tripled. This advantageous effect was primarily governed by the hydrophobic environments created by PVDF and PE polymers on the Cu surface. Hydrophobic

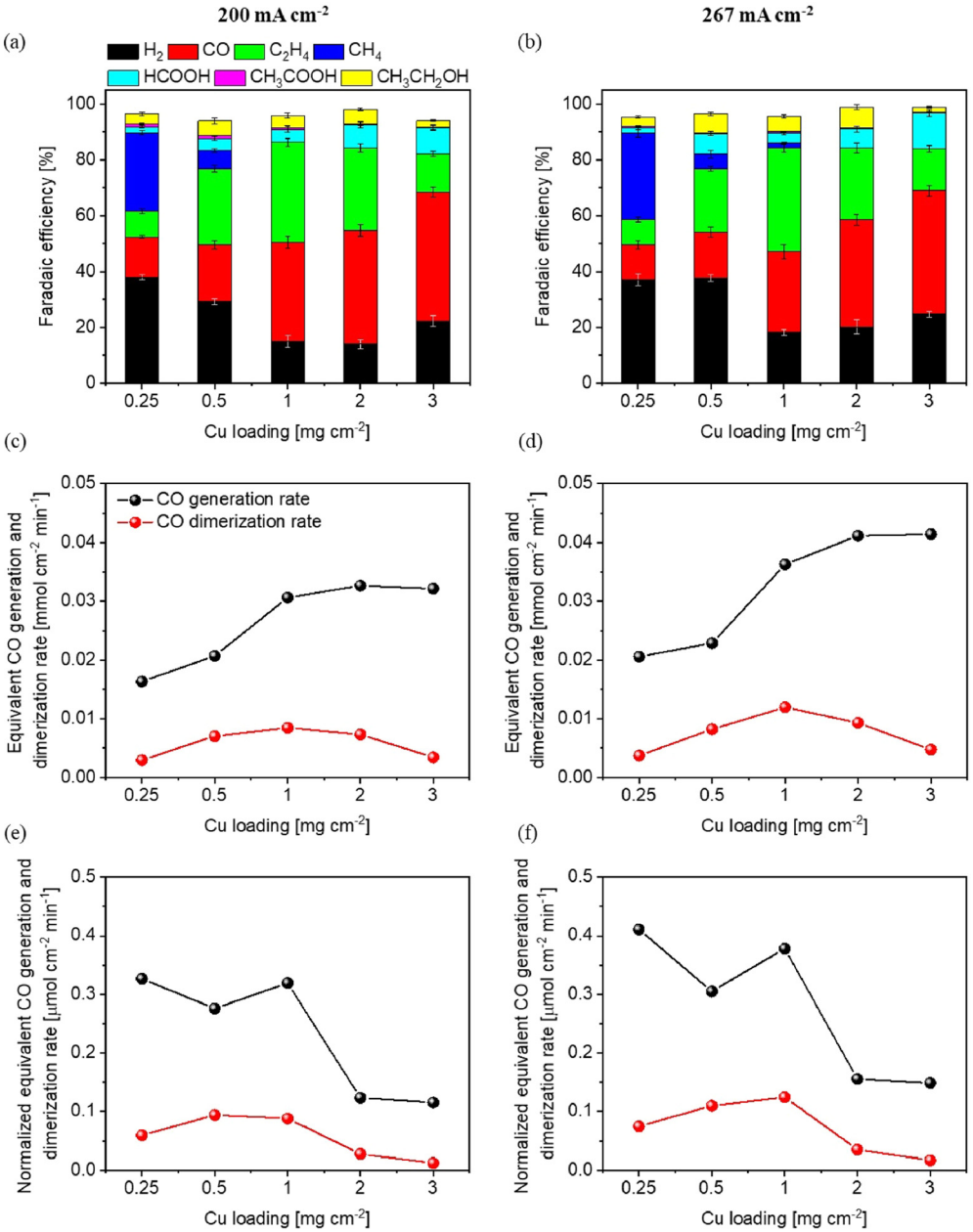

Fig. 17 Comparison of electrodes consisting of 25 nm nanoparticles (NPs) with varying loadings: at 200 mA cm^{-2}, (a) assessing selectivity, (c) evaluating equivalent bulk CO generation and dimerization rates and (e) normalizing equivalent CO generation and dimerization rates to the electrode's electrochemically active surface area (ECSA); at 267 mA cm^{-2}, (b) analyzing selectivity, (d) calculating equivalent bulk CO generation and dimerization rates, and (f) ECSA-normalized equivalent CO generation and dimerization rates. Each electrode underwent testing on multiple occasions. The bulk and ECSA-normalized equivalent CO generation and dimerization rates in (c)–(f) were computed based on the average selectivity values from at least two sets of experiments conducted at different catalyst loadings and current densities. Reproduced with permission from ref. 194. Copyright 2023, Elsevier.

polymer coatings resulted in a higher surface pH, inhibiting HER and promoting the reduction of CO_2 to C_2H_4.[189] To illustrate uniform Cu dispersion onto the CeO_2 support and the fine-tuning of interfacial characteristics, Yin *et al.* had demonstrated the fabrication of heterostructured Cu_y/CeO_2 nanorods through chemical prelithiation and galvanic displacement. The Cu decoration had facilitated the activation of CO_2 and its subsequent conversion to the *CO intermediate on the surrounding Cu surface, generating a new strong-binding site at the Cu and CeO_2 interface. The trends in the production of C_1 and C_{2+} products in e-CO_2R had exhibited a decreasing and volcano-shaped pattern as the extent of Cu decoration had increased. Through *in situ* ATR-SEIRAS and Raman measurements, it had been found that the Cu surface had generated two distinct types of *COLFB and *COHFB intermediates, with a high coverage of *COHFB promoting the creation of C_1 products and a high coverage of *COLFB contributing to the formation of C_{2+} products.[190] Moreover, it was found that

during e-CO_2RR the S–CuSn catalyst goes through dynamic changes. There are five stages in this complicated process: CuS reduction; S leaching from Cu_2SnS_3; $Cu_{24}Sn_{20}$ alloy generation; Sn metal formation; and the constitution of a stable structure in the form of co-doped $Cu_{24}Sn_{20}$ alloys with S/Sn. This reconstructed S–CuSn catalyst gave a maximum CO_2 FE of 91.5% and formate FE of 96.4%, owing to its exemplary activity in the e-CO_2R toward formate.[191]

Furthermore, metallurgy-dealloying techniques were employed to craft a novel CeO_2Cu amorphous heterostructure. This catalyst, through its interfacial sites, increased the adsorption strength of CO and stabilized CH_2CHO, guiding the reaction toward C_{2+} alcohol production. The catalyst significantly enhanced the inherent activity and selectivity of Cu-based catalysts in the synthesis of C_{2+} alcohols, achieving a remarkable FE of 32.9% at a low potential.[192] Besides, Rudd *et al.* investigated the creation of foams and their morphology, crystal structure, and catalytic efficiency under varying conditions. They also studied how foams reacted to CO_2 electrolysis and examined the potential impact of urea as an additive. Both s unmodified and urea-treated foam electrodes exhibited a variety of cub-octahedra and dendrites. However, changes in the shape, crystallinity, and surface content of copper foams after 35 minutes of electrolysis resulted in their deactivation as catalytic materials.[193]

Additionally, the study examined two electrode families comprised of Cu NPs loaded at varying concentrations (ranging from 0.25 to 2.0 mg cm^{-2}) as e-CO_2RR catalysts (Fig. 17). At low loadings, the predominant reduction product at the electrodes was CH_4, while at higher loadings, CO became the dominant product. Interestingly, at moderate concentrations (0.5 to 1.0 mg cm^{-2}), C_2H_4 selectivity was maximized. This behavior was attributed to the presence of low-density NPs, which reduced the likelihood of CO dimerization, ultimately leading to increased CH_4 generation. Bulk CO generation increased with higher loading, increasing the probability of dimerization and thus favoring C_2H_4 synthesis. Additionally, capacitance was found to slow the outward flow of charges from the electrode as NP loading increased further.[194]

Likewise, Tafazoli *et al.* highlighted a substantial difference in the FEs of C_2 products between low and high current density electrodeposited Cu oxides. *In situ* SERS was employed to monitor changes in surface chemistry under CO_2RR conditions, revealing rapid shifts in Cu oxidation states on porous high current density electrodes but not on low current density electrodes. The formation of $Cu_2(CO_3)(OH)_2$ was linked to Cu oxidation states, surface intermediates, and product analyses, affecting adsorbed intermediates and C_2 products based on local HCO^{3-} concentration and pH during $Cu_2(CO_3)(OH)_2$ production. The high current density surface was easily terminated by $Cu_2(CO_3)(OH)_2$, inhibiting further CO_2RR. As a result, HER was enhanced at the expense of C_2 products due to decreased CO_2 concentration near the surface, driven by HCO^{3-} consumption and resulting in higher alkalinity over the electrode. The strong adsorption of CO molecules over the high current density electrode terminated by $Cu_2(CO_3)(OH)_2$ might account for the removal of the C_2 pathway.[195]

In addition, Yang *et al.* demonstrated increased selective adsorption of Cl at dual-phase interfaces using a Cu-based catalyst with abundant Cu^+ species. This facilitated CO_2-to-C_{2+} conversion in neutral fluids by providing local *CO coverage, which favored energetically advantageous CO dimerization. The employment of the dual-phase method to enhance *CO intermediates' coverage has broader implications for improving CO_2R catalysis in various electrolytes and other electrochemical processes.[196] Also, single-atom-thick Cu–Sn surface alloys ($Cu_{97}Sn_3$ and $Cu_{99}Sn_1$) were created for effective e-CO_2R. These alloys exhibited different catalytic selectivity compared to pure Cu100 and $Cu_{70}Sn_{30}$ bulk alloys due to their distinct geometric and electronic structures. The $Cu_{97}Sn_3$ catalyst achieved 98% FE_{CO} at low overpotential, showcasing the influence of the local coordinating environment in isolated Cu–Sn bonding, as demonstrated by density functional theory simulations.[197]

Additionally, a practical method for stabilizing copper with silica and producing $CuSiO_x$ amorphous nanotube catalysts that are resistant to rebuilding was introduced by Tan *et al.* The Cu–O–Si interfacial sites are ultra-stable in the CO_2RR without evident reconstruction due to the strong interfacial connection between Cu and silica, resulting in high CO_2-to-CH_4 selectivity (72.5% after 12 hours of testing) and stability (FE_{CH_4} remains over 60% after 12 hours of testing) (Fig. 18). In a flow cell device, an impressive CO_2-to-CH_4 conversion rate of 0.22 mol cm^{-2} s^{-1} was also attained, suggesting a viable path toward the development of highly active and stable Cu-based CO_2R catalysts.[198] Table 8 presents a comparative overview of different electrocatalysts synthesized by the interfacial engineering approach for e-CO_2R to sustainable products.

6.6.4. Speciation of Cu surface. In the design of catalysts for e-CO_2R, the arrangement of copper surfaces is completely different from bulk materials. Since the selectivity, activity, and stability of the catalyst in converting CO_2 into useful chemicals and fuels are directly influenced by the surface configuration of Cu, it is important to understand and control this. The key to this approach lies in the fact that through it we can tailor the properties of Cu surfaces and thereby control the reaction pathways and side reactions. By manipulating the surface configuration researchers can enhance the performance of the catalyst making it more energy efficient and economically viable for large scale CO_2RR applications. Additionally, by modifying the configuration of the Cu surface, it can be made into a selective catalyst, which can selectively convert C_2 into ethylene or ethanol, and suppress the production of competing by-products. To design CO_2RR catalysts, a variety of methods are available to control and manipulate Cu's surface configuration. One way is to use electrodeposition techniques to create thin films or nanostructured Cu surfaces having controlled crystallographic orientations, grain size and defect types. In addition, adding foreign elements/molecules, such as in atomic layer deposition of metal oxide or formation of surface alloys, can change Cu's electronic structure and coordination environments to change its responsiveness to CO_2. One possible approach is to use electrochemical potential control and pH adjustment as a way to synthesize and operate Cu-based

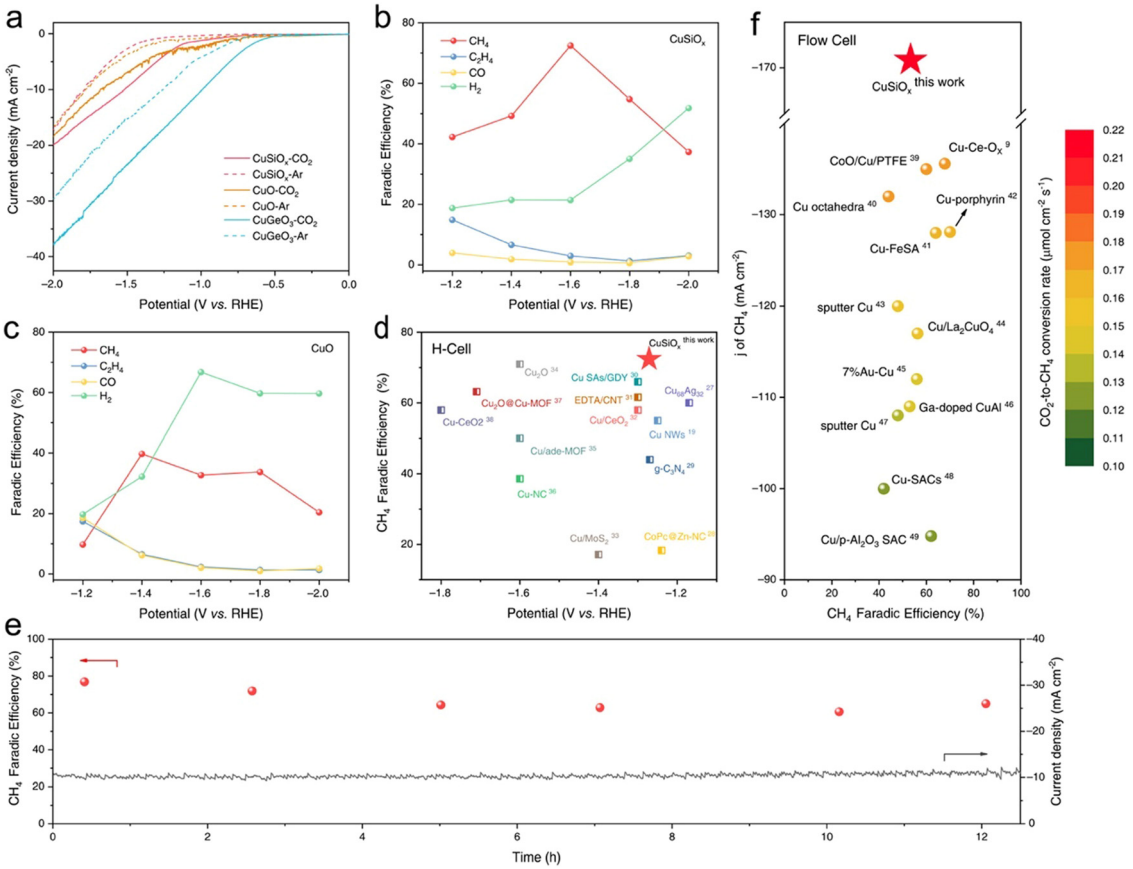

Fig. 18 e-CO_2R performance: LSV curves of $CuSiO_x$, $CuGeO_3$, and CuO under CO_2 or Ar purging conditions (a). FEs of CO_2R products at varying potentials (b) and (c). FE for CH_4 production by $CuSiO_x$ compared with other catalysts from previous studies after *iR* corrections (d). Time-dependent total current density and FE_{CH_4} generated by $CuSiO_x$ measured at −1.6 V *vs.* RHE over a 12-hour period (e). A comparative analysis of this research with prior investigations regarding electrocatalytic CO_2-to-CH_4 conversion, conducted in a flow cell device (f). Reproduced with permission from ref. 198. Copyright 2023, American Chemical Society.

catalysts. This can mediate specific surface speciation and stabilize reactive intermediates.

Continuing with this line of investigation, tin doped CuO NSs were prepared and their catalytic activity was found to be higher than that of pure CuO catalysts. The excellent performance of the NSs was mainly attributed to the increased $CO_2^{\bullet}$ adsorption. The synergistic relationships between SnO_2 and CuO were found to be beneficial for e-CO_2R.[200] In another facet of research, La_2CuO_4 perovskites with engineered grain boundaries (GBs) were developed as effective electrocatalysts for e-CO_2RR. These tailored nanoparticles exhibited a strong FE toward C_2H_4, a desirable product of CO_2R. The enhanced selectivity for the C_2 product was attributed to their high adsorption affinity for CO intermediates. The introduction of strain generated by the twin boundaries (TBs) in La_2CuO_4 nanoparticles led to increased CuO and CuLa bond lengths, further improving $FE_{C_2H_4}$.[201] Advancing this research, a microfluidic flow cell was utilized to reduce Cu_2O precursors under CO_2RR conditions, resulting in the formation of catalysts with a porous Cu cavity (Fig. 19). These catalysts exhibited a Cu(111) facetted cavity with dimensions of approximately 108 ± 23 nm. Remarkably, these structures led to an increase in both the FE for C_{2+} products and the partial current density, all achieved at a low applied voltage. This was attributed to the entrapment of numerous *CO intermediates within the cavities, preventing their easy migration between cavities. DFT calculations and electrochemical Raman spectra suggested that C–C coupling primarily occurred *via* the CO–CHO coupling mechanism.[202]

In the realm of catalytic advancements, a groundbreaking achievement was made by immobilizing OH_{ad}-introduced non-covalent interactions (NCI) in the reduction of CO_2 on SnO nanosheet catalysts. This innovative approach yielded remarkable results, including a high FE of 90.5% and a substantial partial current density of 61.8 mA cm^{-2}. The catalytic mechanism revolved around the rapid protonation of CO_2 into formate on the SnO(001) surface through activation. The introduction of NCI by OH_{ad}, coupled with its role in enhancing hydrogen adsorption, facilitated efficient regeneration, enabling continuous operation. Notably, OH_{ad}-induced NCIs outperformed their H_2-annealed counterparts in promoting formate reduction across various catalysts, including CuO, Bi_2O_3, and TiO_2.[203] Another notable advancement in catalytic science involved the creation of a Cu_2O(CO) nanocubic catalyst through controlled thermal topological transformation of Cu_2O nanocubes under a

Table 8 The table showcases the performance of materials in terms of their properties. It specifically focuses on how the interfacial engineering approach affects the selectivity and efficiency of the resulting products. The findings from this table provide insights for advancing sustainable solutions in the field of energy conversion technologies

				≈FE%									
No.	Material	Electrolyte	V *vs.* RHE	H_2	CO	CH_4	C_2H_4	$HCOO^-$	$C_2H_5^+$	CH_3OH	C_2H_5OH	$C_2H_3O_2^-$	Ref.
1	$CuZn/CuZnAl_2O_4$	2 M KOH	−1.1	4	4	—	38	2	—	—	34	—	184
2	$Cu/CuAl_2O_4$			18	4	—	35	4	—	—	25	—	
3	CuZn			17	18	2	17	2	—	—	21	—	
4	0D-CuZn	0.1 M $KHCO_3$	−1.1	—	—	35	18	—	—	—	—	—	185
5	0D-Cu			—	—	8	30	—	—	—	—	—	
6	Cu			—	—	6	2	—	—	—	—	—	
7	Cu_2O@Cu-BDC	0.1 M KBr	−1.1	17	21	2	25	6	—	—	—	—	186
8	Cu-BDC			38	6	5	14	2	—	—	—	—	
9	Cu_2O			40	5	8	26	5	—	—	—	—	
10	Ni–N–C@900 °C	0.1 M $KHCO_3$	−1.1	93	12	—	—	—	—	—	—	—	199
11	Ni–N–C@700 °C			77	8	—	—	—	—	—	—	—	
12	NiNPs–N–C			94	7	—	—	—	—	—	—	—	
13	N–C			85	6	—	—	—	—	—	—	—	
14	$CuSnO_x$/rGO	0.5 M $KHCO_3$	−0.99	2	21	—	—	22	—	—	—	—	187
15	Cu_3SnO_x/rGO			3	28	—	—	28	—	—	—	—	
16	$Cu_{0.33}SnO_x$/rGO			3	27	—	—	69	—	—	—	—	
17	R–Cu	0.1 M $KHCO_3$	1.0	18	1	1	52	2	—	—	12	—	188
18	R–Cu–Br			38	1	8	38	1	—	—	5	—	
19	CuO	0.5 M $KHCO_3$	−1.02	51	12	2	18	—	—	—	—	—	189
20	CuO-PVDF			40	10	2	25	—	—	—	—	—	
21	$Cu_{0.04}/CeO_2$	0.1 M $KHCO_3$	−1.0	23	32	—	2	33	—	—	—	—	190
22	$Cu_{0.12}/CeO_2$			31	17	—	24	22	—	—	—	—	
23	$Cu_{0.32}/CeO_2$			25	20	—	20	23	—	—	7	—	
24	$Cu_{0.4}/CeO_2$			24	10	4	23	24	—	—	7	—	
25	$Cu_{0.6}/CeO_2$			29	18	—	13	38	—	—	—	—	
26	S–CuSn	0.5 M $KHCO_3$	−0.8	8	10	—	—	50	—	—	—	—	191
27	S–Cu		−0.65	66	—	—	—	3	—	—	—	—	
28	S–Sn		−0.99	9	9	—	—	41	—	—	—	—	
29	CeO_2–Cu	1.0 M KOH	−0.6	—	—	—	—	—	—	—	30	—	192
30	CuZn		−0.7	—	—	—	—	—	—	—	38	—	
31	Grain boundary rich Cu		−0.8	—	—	—	—	—	—	—	17	—	
32	CuAg		−0.8	—	—	—	—	—	—	—	19	—	
33	Cu_2S–Cu–V		−1.0	—	—	—	—	—	—	—	19	—	
34	Nanoporous Cu		−0.7	—	—	—	—	—	—	—	10	—	
35	CuAg wires		−0.7	—	—	—	—	—	—	—	10	—	
36	Cu nanoparticles		−0.8	—	—	—	—	—	—	—	15	—	
37	Porous Cu		−0.8	—	—	—	—	—	—	—	15	—	
38	CuAu		−1.0	—	—	—	—	—	—	—	25	—	
39	CF-18H	0.1 M $KHCO_3$	−1.05	74.3	1.7	0.3	11.6	2.6	—	—	2.5	—	193
40	CF-18H-100U			90.9	0.8	0.7	8	2.4	—	—	1.5	—	
41	$CuZn/CuZnAl_2O$	2 M KOH	−1.1	4	6	—	38	2	—	—	34	—	184
42	$Cu/CuAl_2O_4$			26	4	—	33	4	—	—	27	—	
43	CuZn			17	20	4	16	—	—	—	21	—	
44	Cu NPs (3 mg cm^{-2})	1.0 M KOH	200 mA cm^{-2}	22	44	—	16	10	—	—	—	—	194
45	S–ZnO	1 M KOH	−1.06	38	30	—	—	8	—	—	—	—	50
46	S–CuO			21	5	3	40	—	—	—	12	—	
47	$S–Cu_5Zn_1O_x$			48	12	2	18	—	—	—	6	—	
48	$S–Cu_1Zn_3O_x$			28	14	3	16	—	—	—	7	—	
49	$CuSiO_x$	1 M KOH	−1.3	19	4	43	16	—	—	—	—	—	198
50	CuO			20	18	10	18	—	—	—	—	—	
51	Cu_{100}	0.5 M $KHCO_3$	−1.0	22	18	—	28	28	—	—	—	—	197
52	$Cu_{97}Sn_3$			5	84	—	—	9	—	—	—	—	
53	$Cu_{70}Sn_{30}$			2	5	—	—	90	—	—	—	—	

CO atmosphere at 275 °C. This catalyst exhibited a unique structural configuration characterized by high-density nanograin boundaries, which exposed Cu(100) facets, Cu[n(100) × (110)] step sites, and Cu^0/Cu^+ interfaces. During the CO_2RR process, it demonstrated exceptional performance, achieving a $FE_{C_{2+}}$ of 77.4%, and showcased remarkable stability even under high polarization and current densities. The abundance of Cu^0/Cu^+ interfaces played a pivotal role in increasing the adsorption density of *CO intermediates, thereby contributing to the high selectivity for C_{2+} products. Furthermore, the presence of rich nanograin boundaries significantly improved the catalytic stability, underscoring the critical importance of surface structures in Cu-based catalysts for achieving high C_{2+} selectivity during CO_2RR, especially under industrially relevant current densities.[204]

Synthesis of methanol using $Cu/ZnO/Al_2O_3$ catalysts at an industrial level has long been a mystery, and it is mainly because we are not certain of where the active sites are located. A large-scale machine learning atomic simulation was harnessed to investigate

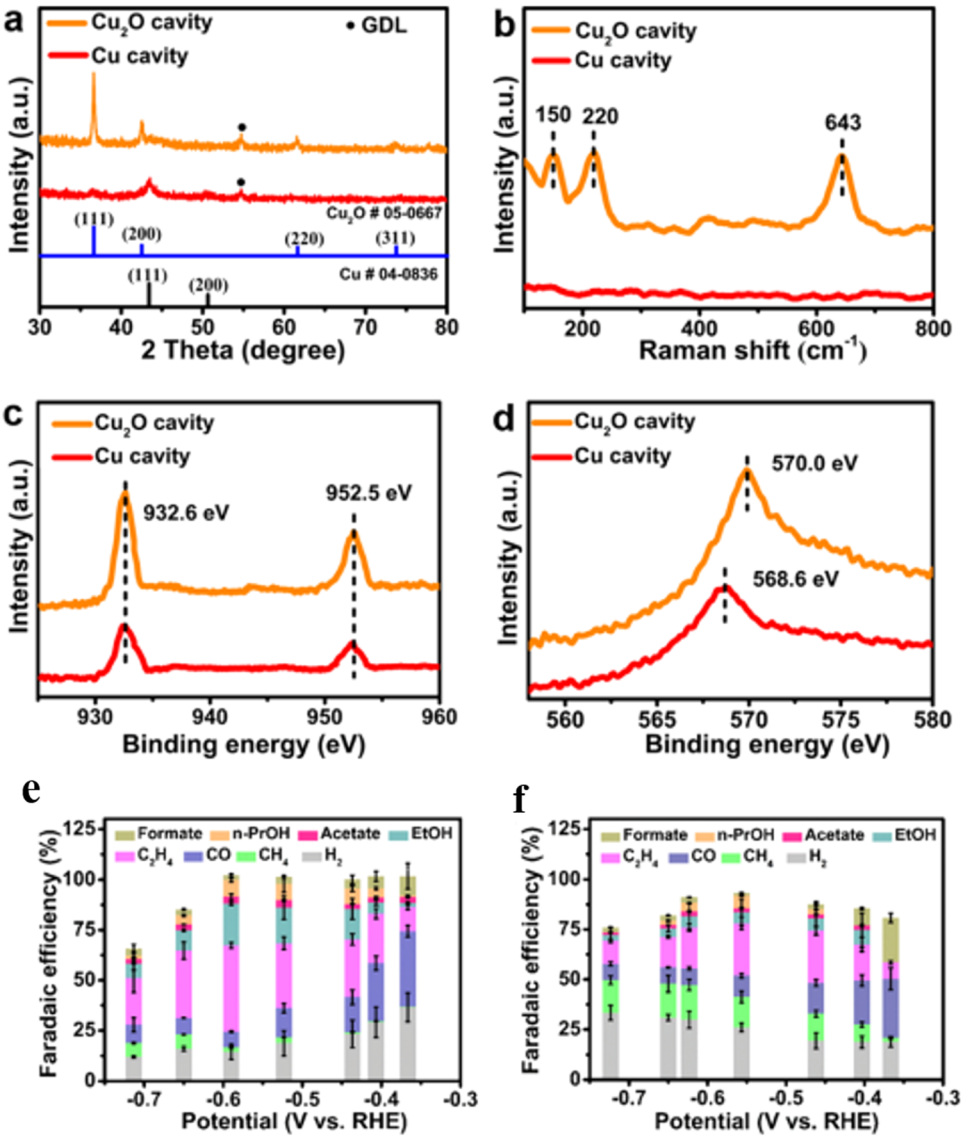

Fig. 19 The study focuses on characterizing the synthesized Cu_2O pre-catalyst and the Cu cavity catalysts. The XRD pattern (a), Raman spectra (b), and XPS of Cu 2P (c) and Cu LMM (d) were obtained for the synthesized Cu_2O precatalyst and the Cu cavity catalysts. "GDL" refers to the commercial gas diffusion layer. The performance of e-CO_2RR was tested in a flow cell reactor. The major products of the e-CO_2RR were studied on both cavity Cu (e) and solid Cu (f) surfaces at various applied potentials in a 1 M KOH solution. Reproduced with permission from ref. 202. Copyright 2023, American Chemical Society.

thousands of reaction paths connected to both CO_2 and CO hydrogenations on Cu–Zn surfaces predicted by thermodynamic calculations to be stable. This extensive study revealed several key insights. Firstly, under reaction conditions, Zn decorates at the step-edge of Cu(211) up to 0.22 monolayers (ML), indicating a dynamic surface modification process. Additionally, the investigation highlighted that CO_2 hydrogenation overwhelmingly governs the methanol synthesis process. Moreover, the formation of [–Zn–OH–Zn–] chains on Cu(111) surfaces was observed under reaction conditions, suggesting the pivotal role of CO in the mixed gas environment.[205] Transitioning to the selectivity of the carbon reduction reaction (CRR) aimed at producing C_{2+} products on oxidized Cu-based catalysts, it was discovered that the oxidation state of the surface Cu active site plays a pivotal role. At lower oxidation states, weak *CHO adsorption is observed at the Cu site, rendering the transition from *CO to *CHO unfavorable. As the oxidation state of Cu increases, the C–C coupling step shifts toward *CHO dimerization, and the *CO to *CHO transition becomes more favorable. Remarkably, the optimal oxidation state for CC coupling was identified to be around +0.5. Importantly, the selectivity for C_{2+} products can be tailored through doping with transition metals, which have the capacity to alter the Cu oxidation state. The presence of these metal dopants can be discerned through the utilization of artificial intelligence clustering based on physical characteristics.[206] Notably, one promising avenue for enhancing the electrocatalytic performance of copper involves surface promotion of copper with alumina (AlO_x) clusters. This strategy has led to the development of highly selective and stable catalysts capable of catalyzing the

Table 9 By examining the details of the materials used the table investigates how surface engineering strategies for copper impact CO_2R. It offers an analysis of electrocatalyst materials designed specifically to convert CO_2. The main focus lies on studying their properties selectivity in product formation and overall efficiency under different reaction conditions

				≈FE%									
No.	Material	Electrolyte	V *vs.* RHE	H_2	CO	CH_4	C_2H_4	$HCOO^-$	$C_2H_5^+$	CH_3OH	C_2H_5OH	$C_2H_3O_2^-$	Ref.
1	La_2CuO_4 NBs	0.1 M $KHCO_3$	−1.1	38	10	4	43	—	—	—	—	—	201
2	La_2CuO_4 NRs			55	7	8	25	—	—	—	—	—	
3	Bulk La_2CuO_4			18	84	2	—	—	—	—	—	—	
4	Bulk CuO	0.5 M $KHCO_3$	−1.0	—	—	8	—	—	—	—	—	—	200
5	CuO NS			—	—	12	4	—	—	—	—	—	
6	1% SnO_2–CuO NS			—	—	12	21	—	—	—	—	—	
7	3% SnO_2–CuO NS			—	—	15	24	—	—	—	—	—	
8	5% SnO_2–CuO NS			—	—	13	13	—	—	—	—	—	
9	10% SnO_2–CuO NS			—	—	11	8	—	—	—	—	—	
10	Cavity Cu	1 M KOH	−0.7	11	9	8	23	4	—	—	6	—	202
11	Solid Cu			31	7	19	15	3	—	—	2	—	
12	Sn	0.5 M $KHCO_3$	−0.95	—	—	—	—	37	—	—	—	—	203
13	H–SnO			—	—	—	—	40	—	—	—	—	
14	SnO			10	20	—	—	41	—	—	—	—	
15	SnO_2			—	—	—	—	41	—	—	—	—	
16	Ag-as prepared	0.1 M $KHCO_3$	−1.1	63	2	8	—	18	—	—	6	—	208
17	Ag-5 mint O_2 plasma			75	1	2	—	13	—	—	16	—	
18	Pt-as prepared			83	1	2	—	10	—	—	3	—	
19	Pt-5 mint O_2 plasma			91	1	1	—	8	—	—	2	—	
20	Cu_2O	0.1 M $KHCO_3$	−1.0	—	—	—	45	—	—	—	17	—	204
21	Cu_2O(CO)			—	—	—	55	—	—	—	13	—	
22	$Cu_2O(H_2)$			—	—	—	38	—	—	—	17	—	
23	Cu after 1 hour	0.1 M $KHCO_3$	−1.0	—	1.6	—	0.25	—	—	—	—	—	209
24	Cu_2O after 1 hour			—	8	—	1.5	—	—	—	—	—	
25	NH_2–Cu after 1 hour			—	22	—	12	—	—	—	—	—	
26	NH_2–Cu after 12 hours			—	15	—	14	—	—	—	—	—	
27	4H Au@Cu	0.1 M $KHCO_3$	−1.06	18	52	—	14	9	—	—	—	—	71
28	4H/fcc Au@Cu			22	23	3	43	7	—	—	—	—	
29	Od-Cu	0.1 M $KHCO_3$	−1.05	—	—	—	38	—	—	—	—	—	207
30	AP-Cu			—	—	—	32	—	—	—	—	—	
31	Hd-Cu			—	—	—	50	—	—	—	—	—	

transformation of CO_2 into ethylene and other multicarbon compounds. The catalyst, formed from Cu–aluminum (Cu–Al) layered double hydroxide nanosheets and promoted with AlO_x, has demonstrated remarkable performance in this regard, offering potential solutions for sustainable carbon utilization and emission reduction.[207] Table 9 presents an overview of different materials designed by following the Cu surface engineering strategy for e-CO_2R to different valuable products.

6.7. Doping strategy

Doping plays a role in developing e-CO_2R. It involves intentionally introducing foreign atoms, such as metals or non-metals, into the catalyst structure to modify its electronic and chemical properties. This technique is extremely significant in the field of electrocatalysis because it allows for adjustment of the catalyst's ability to react with and select CO_2 conversion products.

6.7.1. Metal doping. The strategy of incorporating metals into electrocatalysts for e-CO_2R is a means to enhance their performance. By introducing metal atoms into the catalyst structure we can modify its electronic properties, surface reactivity and how strongly it binds with CO_2 intermediates. Metal doping holds significance as it allows us to fine-tune catalysts for CO_2 conversion. Through selection of dopants researchers can adjust the catalysts' structure leading to stronger interactions with CO_2 molecules and intermediate species. This results in improved activity and selectivity, effectively addressing the challenges associated with CO_2R. There are methods available such as wet impregnation, chemical vapor deposition and atomic layer deposition that enable precise control over dopant concentrations when creating metal doped catalysts. This approach not only contributes to the development of energy conversion technologies but also enhances our understanding of the fundamental catalytic mechanisms involved in CO_2R reactions. Ultimately metal doping offers a pathway towards developing selective electrocatalysts that are essential for a more sustainable and environmentally friendly future.

Xu *et al.* have investigated the e-CO_2R efficiency of Cu, Ni, and Mn doped CNTs. The overpotential values of Cu, Ni, and Mn doped CNT(8,0) and CNT(6,6) catalysts were found to be lower than those obtained with individual metal catalysts.[210] Additionally, the Ce–Cu nanoparticles (NPs) exhibited exceptional performance in e-CO_2RR, particularly in the production of the C_2H_4 product, with Ce–Cu-2 NPs achieving an impressive 53% FE for C_2H_4 at 150 mA cm^{-2}. The addition of Ce to Cu resulted in an increase in the number of sites for catalysis and a reduction in particle size. This played a role in enhancing the activity of Ce–Cu NPs. Experimental evidence, including XANES and XPS analyses, indicated that the presence of Ce altered the oxidation state of Cu and caused the formation of OVs. Furthermore *in situ* SERS experiments supported the idea that

Ce doping helped to stabilize CuO_x species enabling adsorption of CO and subsequent interactions between carbon atoms.[211]

In order to explore how various compositions and structures of Cu–ZrO_2 catalysts affect the conversion of CO_2 to CH_3OH through hydrogenation, a group of researchers led by Mao synthesized a range of catalysts. The catalytic performance of these catalysts was found to be influenced by factors like OVs, low valence copper species, the surfaces of ZrO_2 and the size of pores. Methanol selectivity was particularly impacted by the interface between low-valence Cu species and ZrO_2, where OVs were abundant.[212] In another study, the research focused on the synthesis of Pd and Cu doped g-C_3N_4 nanotubes with a porous structure. These nanotubes exhibited exceptional gas-phase CO oxidation activity and durability, along with enhanced e-CO_2R activity attributed to their high surface area.[213] In a different study, a hydrothermal synthesis method was used to prepare a Cu-doped $BiVO_4$ catalyst for e-CO_2R (Fig. 20). This catalyst had excellent electrocatalytic performance, with the highest FE_{HCOO^-} of 87.15% at −1.0 V *versus* RHE, and a maximum current density of −20.68 mA cm^{-2} at …1.3 V *versus* RHE. The introduction of Cu was conducive to changing the electronic structure of $BiVO_4$ and produced more active adsorption sites. Also, in a photo-electrocatalytic system, a WO_3 nanotube array was made into a photoanode, which further improved the catalyst's performance. In the PEC system, formate yield was 3.3-fold higher at −0.9 V *versus* RHE than in the electrochemical system. Reflecting this fact is that there is a synergistic effect between photocatalysis and electrocatalysis.[214]

A remarkable C_{2+} FE of 76.4% was found for Cu–Al MONFs at a high current density of 600 mA cm^{-2}, demonstrating their superior ability in the electrocatalytic reduction of e-CO_2R to C_{2+} products. This marked a significant difference compared to

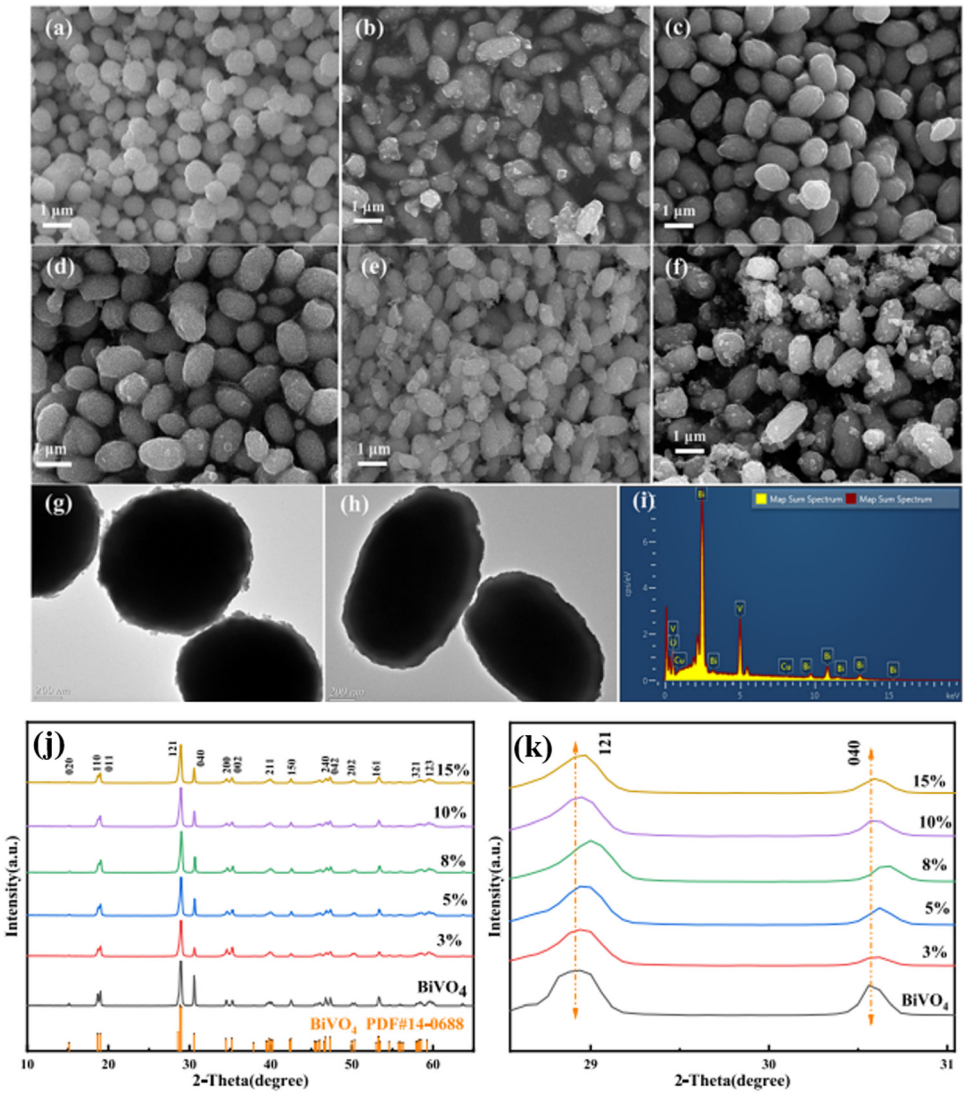

Fig. 20 The provided images (a)–(f) display SEM images of $BiVO_4$ samples doped with varying concentrations of copper (Cu), including pristine (a) and 3% (b), 5% (c), 8% (d), 10% (e), and 15% (f) Cu-doped $BiVO_4$. TEM images of undoped $BiVO_4$ (g) and $BiVO_4$ doped with 8% Cu (h). EDS of 8% Cu-doped $BiVO_4$ (i). The study also examines the XRD pattern of pristine $BiVO_4$ and Cu-doped $BiVO_4$ (j and k). Reproduced with permission from ref. 214. Copyright 2023, Elsevier.

CuO nanofibers, which exhibited weak C_{2+} products and excessive hydrogen evolution. The introduction of aluminum through doping modified the electronic structure of Cu, optimizing intermediate binding and CC coupling, while also creating a mesoporous structure during the etching process.[215] The study explored the *in situ* activation of Sn-doped Cu bimetallic electrocatalysts using pristine SnO_2-decorated CuO nanoparticles. These catalysts demonstrated near-unity selectivity for CO_2 to CO conversion and maintained steady performance for up to 15 hours. *Ex situ* electron microscopy, X-ray spectroscopy, and diffraction experiments shed light on the native shape and structure of these electrocatalysts. The *in situ* activated Sn-doped Cu electrocatalysts significantly enhanced the electrochemical conversion of CO_2 to CO, achieving a record faradaic efficiency of 98% for CuO-0.4% Sn at 0.75 V applied potential *versus* RHE. *In situ* Raman spectroscopy and XRD measurements revealed catalyst activation and adsorbed species, both dependent on time and potential. The findings indicated that clean surface CuO was rapidly reduced within seconds, paving the way for the development of high-performance, low-cost electrocatalysts by doping Cu-based electrocatalysts with post-transition metals.[216] Another study introduced Cu-doped CeO_2 nanocrystals coated with carbon, synthesized through a one-step pyrolysis of MOFs (Fig. 21). These nanocrystals exhibited a significant CH_4 partial current density of 138.6 mA cm^{-2}, coupled with the highest FE_{CH_4} of 80.3%. The outstanding activity and selectivity of these nanocrystals were attributed to the synergistic effect of carbon encapsulation and the Cu/CeO_2 active component.[217]

Kim *et al.* demonstrated that the production rate of CO over a CoCu SAA catalyst with trace doping levels of Co atoms in Cu could be doubled compared to that based on bare Cu. The material also displayed a high $j_{C_2H_4}$ of 282 mA cm^{-2} at 1.01 V *vs.* RHE in a neutral electrolyte. This alloy improved the coverage of *CO intermediates necessary for the synthesis of multicarbon products and accelerated the conversion of CO_2 to CO. The

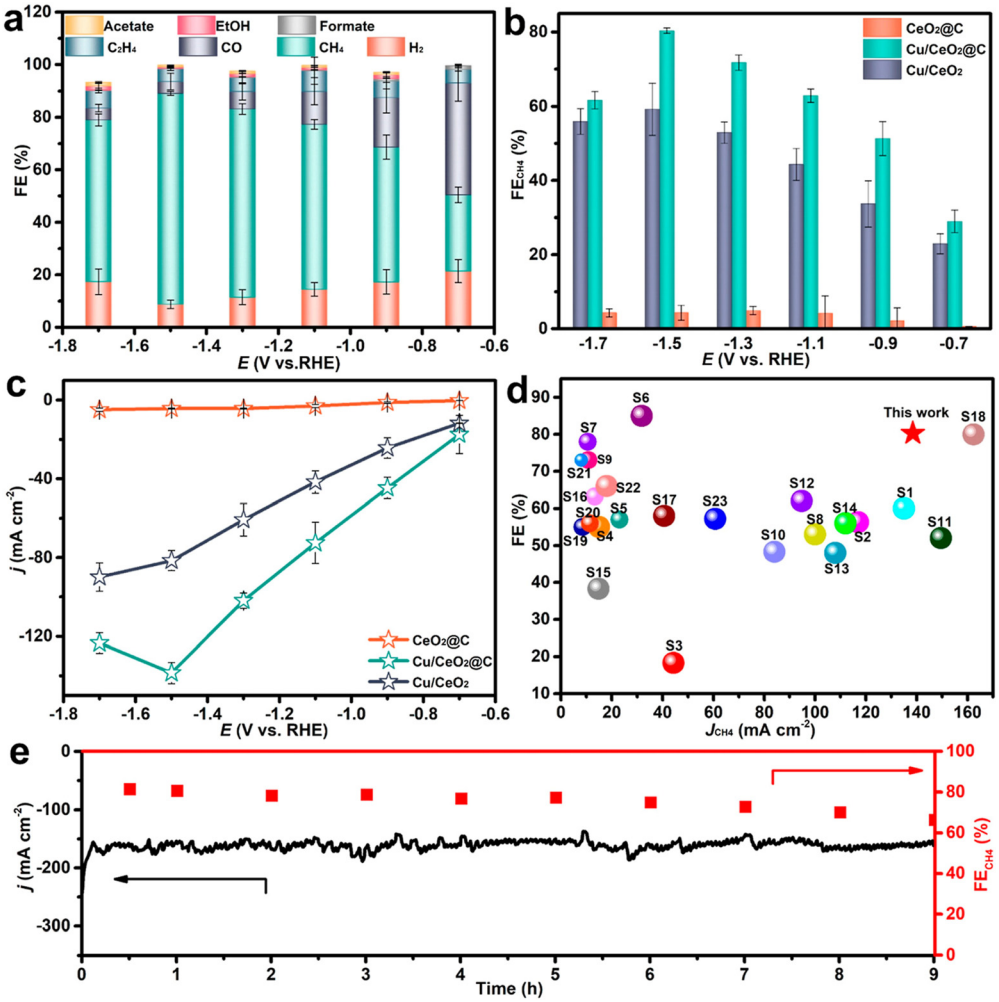

Fig. 21 The performance of e-CO_2RR was evaluated for various samples in the flow cell. The FEs of all the products for the Cu/CeO_2@C catalyst were measured at different applied potentials (a) and (b). The comparison of CH_4 selectivity and CH_4 partial current density among various samples (c). The CH_4 selectivity and partial current density of Cu/CeO_2@C were compared to those of previously reported electrocatalysts (d). A long-term stability test was conducted on Cu/CeO_2@C at a potential of −1.5 V for a duration of 9 hours (e). Reproduced with permission from ref. 217. Copyright 2023, American Chemical Society.

selectivity of CoCu SAA was enhanced toward ethylene over ethanol due to its active sites, which promoted the deoxygenation of *HOCCH, resulting in a yield of 15.6% ethylene.[218] A high-performance Vo-CuO(Sn) catalyst containing OVs for e-CO_2RR-to-CO conversion was produced using one-pot synthesis. The electrode's FE_{CO} was greater than 95% across a broad range of operating potentials, and its partial current density for CO was 35.22 mA cm^{-2}. The catalyst's high activity was further demonstrated by its ability to achieve an optimal 99.9% FE at a low potential.[219] Through *in situ* structural rebuilding of a CuS–Bi_2S_3 heterojunction precursor, a CDB electrocatalyst with an ampere-level current density and remarkable durability for e-CO_2RR to formate was created. The catalyst's high conversion rate can be attributed to the electron-rich surface, a critical point both for its stability and activity, and it could effectively lower the kinetic barrier in the reaction.[220]

In another investigation, researchers explored the Cu/Sn ratio for e-CO_2RR to CO. In undertaking experiments to use Sn-decorated Cu electrodes, they found that the catalyst is believed to be a Cu–SnO overlayer. These studies showed that for particle shaped electrodes, the CO partial current density becomes saturated at high overpotentials and then decreases. However, this phenomenon was not seen in dendritic shaped electrodes. Dendrite morphology increased the concentration of CO_2 at the electrode surface, thus maintaining relatively constant FE_{CO} over a wide potential range.[221] Another study explored electrochemically produced C_2H_6 from CO_2 using a Cu_2O-derived Cu working electrode and $PdCl_2$ in a 0.1 M $KHCO_3$ catholyte. A FE of up to 30.1% at a potential of 1.0 V was achieved. The process involved the initial reduction of CO_2 at Cu sites, followed by hydrogenation using $PdCl_x$ to produce C_2H_6. This approach required the presence of both copper and $PdCl_x$ sites for effective reduction, and the conversion efficiency of other palladium-based particles was found to be comparatively lower.[222] In another investigation, the study had revealed extremely porous Fe-CNPs through a process of amorphous SiO_2 coating, carbonizing, and acid leaching. The presence of these nanoparticles had greatly aided the e-CO_2RR to CO process, with their FE in a 1.0 M $KHCO_3$ electrolyte reaching 98.8%. The research had also shown that the selectivity for e-CO_2R had changed with porosity. Additional investigations on ZIF-derived carbon catalysts with Ni- and Co-doping had indicated that mesopores and macropores might enhance CO selectivity.[223]

Furthermore, Li *et al.* had demonstrated that doping Cu with p-block metal atoms could enhance e-CO_2R to C_{2+} products at high current density by inducing p-d orbital hybridization. At a potential of −1.07 V *vs.* RHE, the CuGa catalyst had achieved a remarkable C_{2+} FE of 81.5% at a current density of 0.9 A cm^{-2}. The catalyst had maintained its high C_{2+} productivity at 1.1 A cm^{-2} and a FE of 76.9%. P-d hybridization between Cu and Ga had increased C_{2+} selectivity, strengthened binding to the *CO intermediate, reduced the reaction energy barrier for CC coupling, and guaranteed an abundance of catalytic reactive sites.[224] In a different study, Ni-substituted CuO and CuO catalysts had been synthesized using solution combustion synthesis. The research had demonstrated the significance of ionic nickel substitution through electrochemical analyses of $Cu_{0.9}Ni_{0.1}O$ and $Cu_{0.95}Ni_{0.05}O$, both of which had exhibited exceptional redox-active behavior and higher electrocatalytic performance compared to CuO. Ionic connection between Ni^{2+} and Cu^{2+} had been crucial, as evidenced by the enhanced electrocatalytic activities of $Cu_{0.9}Ni_{0.1}O$ and $Cu_{0.95}Ni_{0.05}O$ in comparison to Ni metal and NiO-supported CuO. Steady-state chronoamperometry at a fixed potential of 0.2 V *vs.* RHE in a CO_2-saturated electrolyte had also revealed the high activity and stability of nickel-doped catalysts. On $Cu_{0.9}Ni_{0.1}O$, the FE% values of CH_4 and C_2H_4 had been roughly 3 and 4 times higher than those on CuO, significantly increasing the hydrocarbon selectivity.[225] In another investigation, Al-PILC doped with Cu^{2+} ions and mixed metal pillars had both increased basal spacing, indicating effective dispersion of aluminum and copper. This increased surface area and volume had facilitated the adsorption and reduction of CO_2. It is noteworthy that the CO_2R reaction activity has been found to increase with the proportion of copper in the composite electrode.[226] Information on a number of representative catalysts prepared through metal doping to convert CO_2 into organic fuel is given in Table 10.

6.7.2. Non-metal doping. In terms of e-CO_2R catalysts, incorporating metal elements is a crucial technique for increasing their performance characteristics. Elements like nitrogen, sulfur or phosphorus are able to alter the behavior of the catalyst, making them essential in certain cases. CO_2RR activity and selectivity depend on the right amount of non-metal doping. However, the method improves performance by making it easier to bind CO_2 molecules and their intermediates on catalyst surfaces. It also promotes more rapid electron transfer. This leads to better efficiency and higher yields of methane or ethylene. Different techniques like chemical vapor deposition, ion exchange or solvothermal synthesis allow us to precisely control the distribution of metal dopants within the catalyst structure. This strategy holds importance in advancing energy technologies by making electrochemical CO_2R more efficient and sustainable while deepening our understanding of catalytic mechanisms at a molecular level.

In a study, Yuan *et al.* explored novel materials for electrochemical reduction; they investigated Cu_2S–X materials with varying starting morphologies (Fig. 22). These materials were successfully transformed into S–Cu_2O–*X* through electrochemical reduction. By strategically optimizing the electronic structure and increasing the surface area *via* microstructure rebuilding, the efficiency of the catalyst in e-CO_2R reduction and formate selectivity was significantly enhanced. Notably, the team demonstrated the ability of S–Cu_2O-14 catalysts in formate synthesis, achieving an impressive 18% increase in current and a remarkable selectivity of 66.1%.[227]

In a parallel effort, using a co-doping approach Dai *et al.* converted CO_2 to CH_4 using copper-based catalysts. The Cu–N_2B_2 planar unit within their B-doped Cu–N_x set-up was the main focus of concern. Incorporation of boron into the coordination layer facilitated methane synthesis by increasing the strength of binding towards both CO* and CHO* intermediates. This strategic approach has been very successful, with the maximum FE for methane reaching as high as 73%

Table 10 The potential, selectivity, and efficiency of the product are also listed in the table. This information provides clues as to how CO_2 might be turned into other fuels by adopting the metal doping strategy

No.	Material	Electrolyte	V *vs.* RHE	≈FE%									Ref.
				H_2	CO	CH_4	C_2H_4	$HCOO^-$	$C_2H_5^+$	CH_3OH	C_2H_5OH	$C_2H_3O_2^-$	
1	Ce–Cu-3 NPs	1 M KOH	100 mA cm^{-2}	—	35	—	47	—	—	—	—	—	211
2	Ce–Cu-2 NPs			—	38	—	47	—	—	—	—	—	
3	Ce–Cu-1 NPs			—	42	—	38	—	—	—	—	—	
4	Cu NPs			—	69	—	12	—	—	—	—	—	
5	Cu-doped $BiVO_4$	0.5 mol L^{-1} $NaHCO_3$	−1.0	7	—	—	—	16	—	—	—	—	214
6	Cu-doped $BiVO_4$-3%			3	—	—	—	48	—	—	—	—	
7	Cu-doped $BiVO_4$-5%			4	—	—	—	67	—	—	—	—	
8	Cu-doped $BiVO_4$-8%			1	—	—	—	87	—	—	—	—	
9	Cu-doped $BiVO_4$-10%			5	—	—	—	60	—	—	—	—	
10	Cu-doped $BiVO_4$-15%			16	—	—	—	45	—	—	—	—	
11	Cu_3Al MONFs	1 M KOH	100 mA cm^{-2}	12	51		18	9	—	—	8	1	215
12	Cu ONFs			30	13	1	19	15	—	—	13	2	
13	Cu foil	0.1 M $KHCO_3$	−0.75	57	19	—	9	13	—	—	—	—	216
14	CuO			41	40	—	3	14	—	—	—	—	
15	CuO-0.4% Sn			3	98	—	—	—	—	—	—	—	
16	CuO-0.6% Sn			17	77	—	—	—	—	—	—	—	
17	CuO-0.8% Sn			27	68	—	—	—	—	—	—	—	
18	CeO@C	0.1 M KOH	−1.1	—	—	5	—	—	—	—	—	—	217
19	Cu/CeO@C			13	12	60	9	—	—	—	1	1	
20	Cu/CeO			—	—	45	—	—	—	—	—	—	
21	Bare CuO	1 M $KHCO_3$	100 mA cm^{-2}	40	32		8	13	—	0.2	4	—	218
22	0.2% Co-doped CuO			27	41	0.4	8	19	—	0.2	3	—	
23	1.0% Co-doped CuO			27	32	—	9	26	—	0.2	3	—	
24	3.0% Co-doped CuO			30	26	0.3	5	35	—	0.1	2	—	
25	5.0% Co-doped CuO			50	6	0.3	7	27	—	0.5	5	—	
26	Vo–CuO(Sn)	0.1 M $KHCO_3$	−1.03	9	91	—	—	—	—	—	—	—	219
27	Vo–CuO			15	75	—	2	8	—	—	—	—	
28	CuO			31	19	—	5	45	—	—	—	—	220
29	Cu-doped bismuth	1 M KOH	−1.05	—	—	—	—	92	—	—	—	—	
30	Cu–Sn dendrite	0.1 M $KHCO_3$	−1.1	18	75	—	2	4	—	—	2	—	221
31	Cu–Sn particle			62	2	—	19	10	—	—	8	—	
32	Electropolished Cu			24	1	6	20	3	—	—	10		
33	Cu_2O-derived Cu			85	1	1	10	1	—	—	8		
34	Cu_2O-derived Cu with $PdCl_2$			26	1	1	4	2	—	—	10		
35	Fe-CNPs-w/o	1.0 M $KHCO_3$	−0.88		48	—	—	—	—	—	—	—	223
36	Fe-CNPs			—	59	—	—	—	—	—	—	—	
37	Ni-CNPs			—	60	—	—	—	—	—	—	—	
38	Ni-CNPs-w/o			—	45	—	—	—	—	—	—	—	
39	Co-CNPs			—	38	—	—	—	—	—	—	—	
40	Co-CNPs-w/o			—	15	—	—	—	—	—	—	—	
41	Cu	1 M KOH	1.1	38	10	—	29	2	—	—	19	—	224
42	CuGa-II			20	2	—	46	2	—	—	22	—	
43	$Cu_{0.9}Ni_{0.1}O$	0.5 M $NaHCO_3$	−0.2	25	2	29	13	—	—	—	—	—	225
44	$Cu_{0.95}Ni_{0.05}O$			28	3	19	8	—	—	—	—	—	
45	CuO			35	3	9	5	—	—	—	—	—	

and a peak methane partial current density of −462 mA cm^{-2} at −1.94 V *vs.* RHE. This demonstrates the excellent methane yield of the B-doped Cu–N_x material. The underlying reaction mechanism of the Cu–N_2B_2 coordination complex was exactly analyzed, employing a comprehensive two-dimensional reaction phase diagram. This multifaceted investigation contributes valuable insights into the design and performance of copper-based catalysts for efficient and sustainable CO_2 conversion processes.[81] Another research study led to alternative breakthrough as scientists ingeniously dispersed Cu and Zn onto microporous N-doped carbon, resulting in a remarkable catalyst tailored for the e-CO_2R to produce CH_4. The catalyst's performance metrics surpassed expectations, showcasing above-average efficiency, production rate, partial current density, and an exceptional 45-hour lifespan. The success was attributed to the unique combination of microporosity, excellent electrical conductivity, and the synergistic effect of Cu and Zn surface areas, which played pivotal roles in elevating its overall effectiveness.[228] Simultaneously, Zhang *et al.* delved into the electrocatalytic landscape, scrutinizing the potential of various SACs and DACs for CO_2RR. The results unveiled the secure attachment of Cu and Er atoms to the graphene framework, with ErNC emerging as the prime choice for facilitating the conversion of CO_2 to CO. Among these options, CuErNC-I exhibited remarkable catalytic ability, favoring the production of CO molecules with minimal energy barriers.[229] In a parallel endeavor, scientists harnessed the power of a Cu electrocatalyst supported by Ni–Ni–C, facilitating the transformation of carbon dioxide into hydrocarbons. Through ammonia-driven deposition precipitation, they effectively deposited copper nanoparticles onto carbon black and nickel–nitrogen-doped

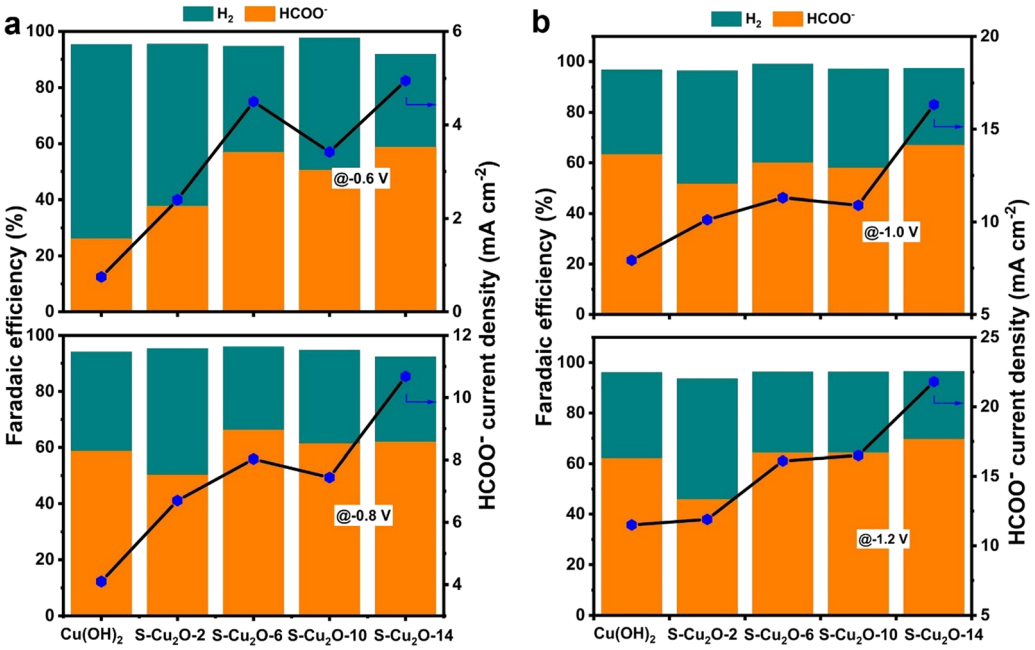

Fig. 22 The FE_{HCOO^-} and partial current density were measured for $Cu(OH)_2$, S-Cu_2O-2, S-Cu_2O-6, S-Cu_2O-10, and S-Cu_2O-14 electrodes at various applied potentials ranging from −0.6 V to −1.2 V *vs.* RHE. Reproduced with permission from ref. 227. Copyright 2023, Elsevier.

carbon substrates. The results, presented at potentials of −1.0 V *vs.* RHE, unveiled the impressive activity of these particles in driving the synthesis of methane and ethylene. Particularly notable, Cu nanoparticles supported by Ni–N–AC demonstrated a reduced C_1/C_2 product ratio, leading to a tenfold increase in CO generation and a twofold increase in partial ethylene current density.[230]

In a separate investigation, Patra *et al.* observed a phenomenon of high selectivity for C_{2+} hydrocarbons in boron-doped CuO, achieved along with a simultaneous reduction in overpotential requirements. The operational spectra of ATR-SEIRAS unveiled distinct CO intermediate species present on BCuO, attributed to the active sites of Cu^+ and Cu^0. This nuanced insight was linked to the availability of multiple CO adsorption sites and heightened CO binding energy within BCuO.[231] In a separate advancement, Yang *et al.* introduced an innovative approach to CO_2R through the utilization of copper selenide nanocatalysts. This introduction marked a novel path to methanol synthesis, boasting exceptional FE and current density at remarkably low overpotentials.[232] Another study offered a method to fabricate Br-doped CuO multilamellar mesoporous nanosheets on Cu foam for e-CO_2R. These nanosheets showcased a prolonged retention time for carbonaceous intermediates and provided numerous active sites for CO_2 adsorption. Through the incorporation of Br ions, the electronic structure of CuO was transformed, inducing the formation of OVs and thereby amplifying CO_2 adsorption capacity. With an admirable FE of 53.3%, the optimized $Br_{1.95\%}$–CuO emerged as a catalyst of choice for driving the e-CO_2R to C_2H_5OH.[233] Saxena *et al.* demonstrated that $CuCo_2Se_4$ was a highly selective catalyst for converting carbon dioxide into carbon-rich, high-value compounds. It generated acetic acid and ethanol at low potentials and formic acid in trace amounts at high potentials.[234]

Another study highlighted a high-performance e-CO_2RR electrocatalyst (ONCuO) sustaining good selectivity for the C_{2+} product over time. Utilizing oxide-derived CuO and heteroatom doping, oxygen-assisted nitrogen doping on CuO resulted in defects such as OVs and grain boundaries. The selectivity for the C_{2+} product was 77%, and ONCuO remained stable for 22 hours.[235] Ma *et al.* revealed that sulfur-modified Cu_2O electrocatalysts could provide more targeted product dispersion (Fig. 23). The selectivity of these electrocatalysts for formate was extremely sensitive to the orientation of the Cu_2O crystal faces. The improved S_3-Cu_2O-70 electrocatalyst displayed a formate efficiency of 90% and an extended lifetime.[236]

The mechanism of the e-CO_2RR for the formation of highly selective formic acid was studied using sulfur-modified Cu electrodes. It was discovered that most sulfur existed in unstable forms, with the stability of individual sulfur atoms dependent on their immediate surroundings and symmetry. The study observed that CO* coverage was up to 3.9 times higher than on clean Cu surfaces due to the significant adsorption of CO* by sulfur atoms.[237] The selective production of formate using a sulfide-derived copper (SD-Cu) catalyst was attributed to stronger CO intermediate binding from subsurface sulfur atoms.[238] Table 11 provides an overview for evaluating the electrochemical performance of different electrocatalysts designed by following the non-metal doping strategy for conversion of CO_2 to sustainable fuel.

6.8. Facet engineering approach

The facet engineering is particularly important in catalyst design for e-CO_2R because it can control the catalytic properties of designed materials. In this technique, the faces of catalyst materials are responsible for the reactivity towards desired reaction products. In the facet engineering approach, the basic

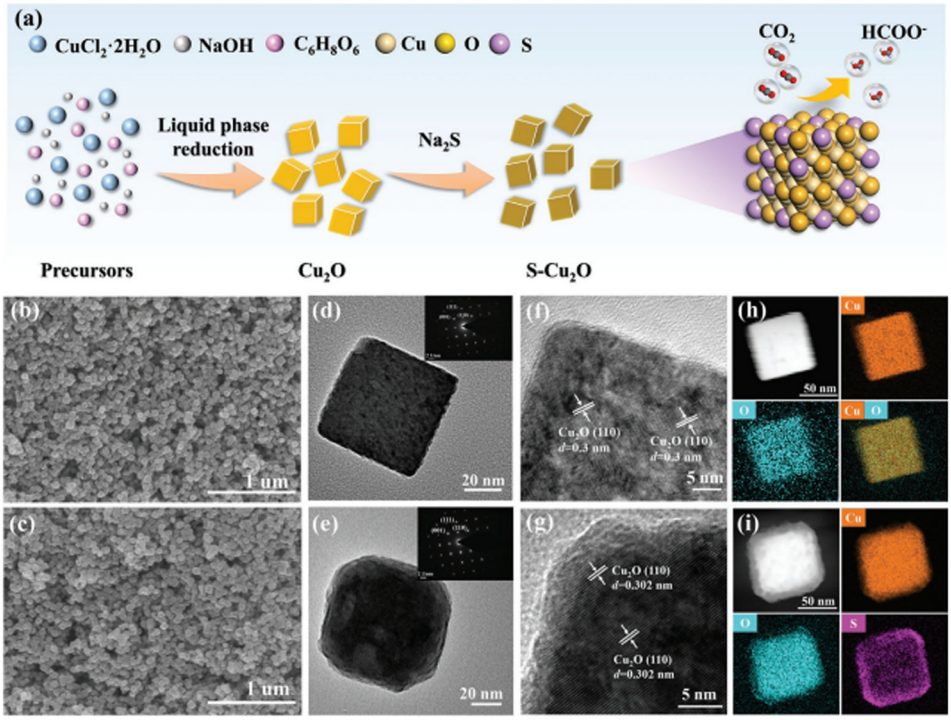

Fig. 23 The synthesis and subsequent characterization of a particular structure. Schematic representation of the process for preparing electrocatalysts (a). The SEM images of S_0-Cu_2O-70 (b) and S_3-Cu_2O-70 (c) are shown. TEM images of S_0-Cu_2O-70 and S_3-Cu_2O-70, along with their corresponding SAED patterns as insets, are presented. The HRTEM images of S_0-Cu_2O-70 (f) and S_3-Cu_2O-70 (g) are shown. The elemental mappings for S_0-Cu_2O-70 (h) and S_3-Cu_2O-70 (i) are also shown. Reproduced with permission from ref. 236. Copyright 2023, Wiley.

idea is to pick crystalline faces for making catalysts that facilitate pathways while minimizing undesired side reactions. On a larger scale, this approach also optimizes the efficiency and cost-effectiveness of CO_2 capture and conversion systems. There are various methods available for incorporating the facet engineering strategy into CO_2RR catalyst designs. A typical way is to synthesize catalyst materials under controlled growth conditions so as to have specific crystal planes exposed, or by using templates to do it. Another approach would be to selectively etch facets already present in the catalysts, thereby bringing out the reactive site(s) of interest instead. Additionally surface modification techniques like depositing layers of metals or oxides onto facets can be utilized to engineer the surface properties of the catalysts. Researchers can tap into the power of facet engineering to fully utilize catalyst materials. This opens up opportunities for developing selective catalysts for CO_2RR, which play a vital role in reducing greenhouse gas emissions and advancing sustainable energy conversion technologies.

Gao *et al.* have introduced a novel approach to immobilize ionic liquids on Cu, forming a collaborative "Cu-ionic liquid heterointerface" for e-CO_2RR. The process involves dissolving Cu^{2+} and AFIL in a H_2SO_4 electrolyte, directing their positive ions toward the GDL cathode, and embedding the deposited Cu. This embedding effect enhances Cu(100) production and incorporates more AFIL due to AFIL's capping influence. Consequently, Cu-IL/GDL exhibits smaller Cu particles with embedded AFIL, resulting in a lamellar particle structure. Operating under a total current density of 73.59 mA cm^{-2} at 1.17 V *vs.* RHE, this synergistic interaction between Cu and AFIL yields high selectivity for C_2 products, notably C_2H_4 (40.67%). Especially, Cu-IL/GDL maintains relatively stable performance, with only a 3.8% decrease in current density observed after 5 hours of operation.[240] Yu *et al.* have developed copper nanosheet arrays on copper foils, which promote the formation of multi-carbon products, resulting in a remarkable multi-carbon to single-carbon ratio of 7.2 (Fig. 24). Notably, potassium ions exhibit a fivefold higher adsorption density on the surfaces of copper nanosheets compared to pure copper foils.[241]

Additionally, researchers have harnessed colloidal techniques to craft Cu-based nanocrystals with tailored dimensions, shapes, compositions, and interior structures. Importantly, their exceptional activity and selectivity for C_{2+} during CO_2R make them promising candidates for electrocatalysis.[242] Shifting the focus to a different investigation, Mangione *et al.* investigated the geometry of copper electrodes in the context of e-CO_2R, particularly over copper nanocubes. These cube-shaped copper catalysts, characterized by 100-degree terraces, 110-degree edges, and 111-degree corners, exhibit enhanced activity and selectivity in the production of ethylene. Nevertheless, the molecular mechanisms underlying this behavior have remained elusive. They also uncovered a dual facet mechanism occurring at the interface of the 100 terraces and 110 edges, highlighting that the reactivity of shape-controlled nano-catalysts extends beyond facet selectivity observed in single crystals.[243] In a separate study examining the effectiveness of Cu(111) ML as a catalyst in the CO_2 hydrogenation process, it is revealed that the Cu(111) ML surface exhibits higher adsorption

Table 11 In essence the table offers an overview of non-metal doping specifically engineered for sustainable CO_2 conversion. It focuses on evaluating electrocatalysts designed to facilitate conversion of CO_2 as depicted in the accompanying table. The research dives into the behavior of these tailored electrocatalysts providing valuable insights for advancing energy conversion applications with sustainability

				≈FE%									
No.	Material	Electrolyte	V *vs.* RHE	H_2	CO	CH_4	C_2H_4	$HCOO^-$	$C_2H_5^+$	CH_3OH	C_2H_5OH	$C_2H_3O_2^-$	Ref.
1	$Cu(OH)_2$	0.1 M $KHCO_3$	−1.2	37	—	—	—	61	—	—	—	—	227
2	S-Cu_2O-2			54	—	—	—	43	—	—	—	—	
3	S-Cu_2O-6			35	—	—	—	63	—	—	—	—	
4	S-Cu_2O-10			35	—	—	—	63	—	—	—	—	
5	S-Cu_2O-14			33	—	—	—	65	—	—	—	—	
6	Cu–SAs/NC	$KHCO_3$	−1.2	—	—	11	—	—	—	—	—	—	228
7	Zn-SAs/NC			—	—	12	—	—	—	—	—	—	
8	CuZn-SAs/NC			—	—	70	—	—	—	—	—	—	
9	Ni–N-AC	0.1 M $KHCO_3$	−1.07	48	52	—	—	—	—	—	—	—	230
10	Ni–N-EC			46	46	—	—	—	—	—	—	—	
11	Cu-VC			—	3	12	14	12	—	—	—	—	
12	Cu-EC			—	3	22	15	8	—	—	—	—	
13	Cu–Ni–N-AC			—	10	15	30	—	—	—	—	—	
14	CuO	1 M KOH	−0.6	20	31	2	23	15	—	—	3	1	231
15	B–CuO			13	35	2	32	7	—	—	4	1	
16	Cu_2O	0.5 M H_2SO_4 [Bmim]PF_6–CH_3CN–H_2O	−2.1. Ag/Ag^+	78	5	—	—	11	—	6	—	—	232
17	Cu_2S			43	20	—	—	17	—	19	—	—	
18	Cu_2Se			33	12	—	—	31	—	23	—	—	
19	$Cu_{1.63}Se$(1/3)				2	—	—	21	—	78	—	—	
20	CuSe			35	28	—	—	22	—	19	—	—	
21	CuS			63	15	—	—	10	—	12	—	—	
22	CuO			42	23	—	—	22	—	5	—	—	
23	Cu			62	20	—	—	10	—	3	—	—	
24	CuO	0.1 M $KHCO_3$	−1.2	62	32	—	—	—	—	—	—	—	233
25	Br1.95%–CuO			—	18	8		37	—	—	31	—	
26	$CuCo_2Se_4$	0.3 M $NaHCO_3$	−0.9	2	—	—	—	26	—	17	24	26	234
27	CuO	0.1 M $KHCO_3$	−1.0	26	6	—	43	5	—	—	10	—	235
28	5-N–CuO			58	8	—	24	24	—	—	3	—	
29	15-N–CuO			45	8	—	35	35	—	—	6	—	
30	25-N–CuO			38	6	—	38	38	—	—	7	—	
31	5-ON–CuO			23	8	—	49	49	—	—	9	—	
32	15-ON–CuO			24	5	—	54	54	—	—	9	—	
33	25-ON–CuO			21	5	—	52	52	—	—	10	—	
34	c-Cu_2O	0.1 M $KHCO_3$	−1.1	20	21	—	25	20	—	—	—	—	236
35	t-Cu_2O			23	18	—	32	18	—	—	—	—	
36	o-Cu_2O			33	16	—	19	22	—	—	—	—	
37	S_3-c-Cu_2O			23	1	—	1	77	—	—	—	—	
38	S_3-t-Cu_2O			24	3	—	—	74	—	—	—	—	
39	S_3-o-Cu_2O			24	1	—	—	73	—	—	—	—	
40	N–Cu	KOH	−1100 mA cm^{-2}	18	11	—	48	1	—	—	19	—	239
41	P–Cu			80	1	3	4	1	—	—	5	—	
42	S–Cu			43	3	2	28	2	—	—	21	—	
43	O–Cu			43	2	28	15	1	—	—	9	—	
44	Cu			53	3	1	23	3	—	—	11	—	
45	Cu-Foil	0.1 M $KHCO_3$	−0.9	38	11	—	—	14	—	—	—	—	238
46	SD-Cu1			38	45	—	—	—	—	—	—	—	
46	S-DCu_2			39	37	—	—	—	—	—	—	—	

energies for intermediates compared to the bulk Cu(111) surface. This preference for the creation of the *CO intermediate over the *COH intermediate leads to selective hydrogenation to CH_3OH. The study identifies two rate-limiting processes in CO_2 hydrogenation: the hydrogenation of CO_2 to COOH and the hydrogenation of CO to CHO. Notably, when compared to bulk Cu and Cu nanocrystal-based catalysts, the predicted working potential for selective CO_2 hydrogenation to CH_3OH is lower on the Cu(111) ML surface.[244]

In another study, Cu nano-catalysts were tested in a gas-fed flow cell, showcasing their facet-dependent selectivity. When compared to a standard H-cell setup, this configuration reduced hydrogen generation while increasing FE towards CO_2 reduction products. The interplay between the system and catalyst effects yielded cutting-edge product selectivity even at low applied voltage and high current densities. In 1 M KOH, Cu cubes exhibited a mass activity of 700 mA mg^{-1} and a selectivity of up to 57% for ethylene, while Cu octahedra achieved a selectivity of up to 51% for methane.[245] In a related effort, Kim *et al.* employed a modified CVD graphene growth technique to create a Cu catalyst featuring a high density of step-sites and a high-facet atomic arrangement. This catalyst stood out for its remarkable ethanol productivity, achieving 40% FE at 0.9 V *vs.* RHE. This represents one of the highest values reported for copper-catalyzed CO_2 conversion to ethanol. Furthermore, the fabrication process for this catalyst is simple and scalable.[246]

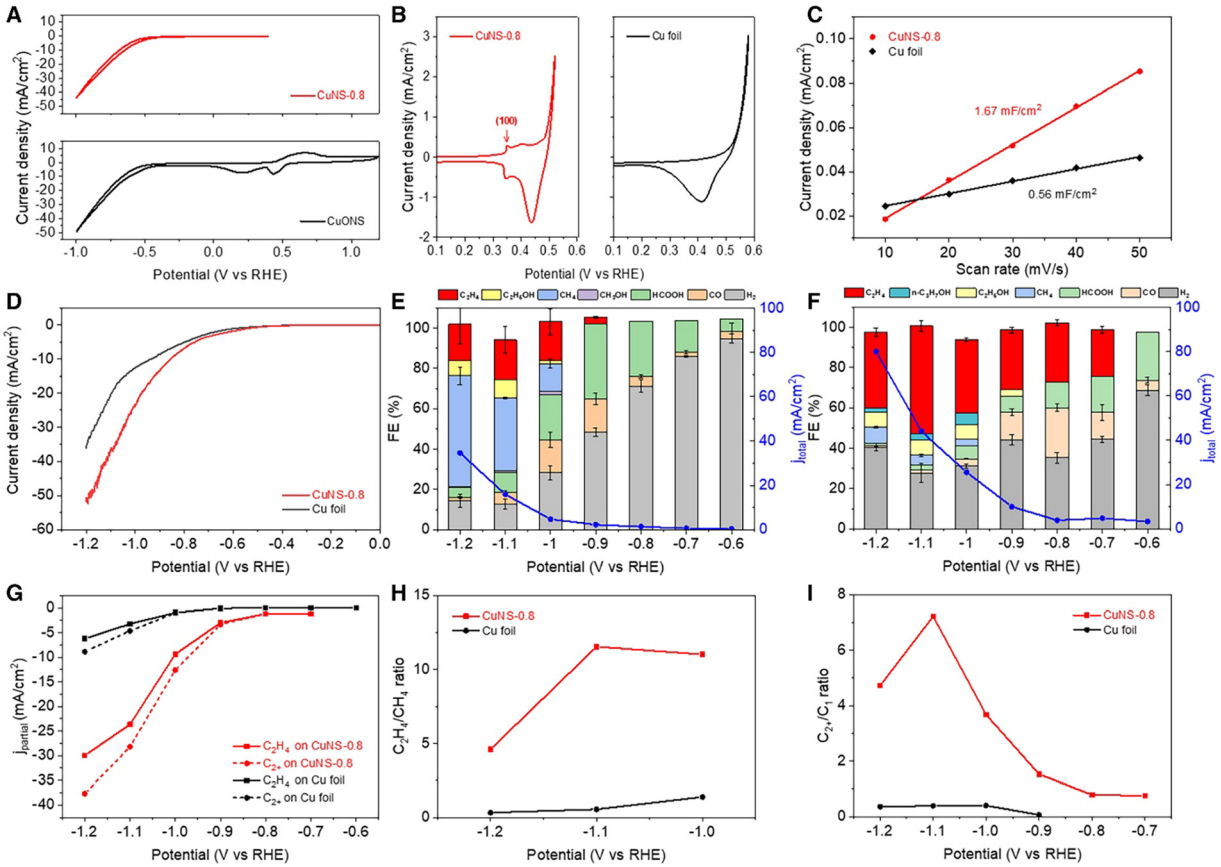

Fig. 24 Illustration of the electrochemical characteristics and efficacy of Cu foil and CuNS-0.8 (A). The CV curves of CuNS were obtained after reducing the CuONS at a potential of −0.8 V *vs.* RHE (B). The OH^- adsorption profiles of CuNS-0.8 and Cu foil are shown in the left and right panels, respectively (C). The plot shows the differences in charging current density between CuNS-0.8 and Cu foil as a function of scan rates (D). The LSV curves of CuNS-0.8 and Cu foil were obtained in a CO_2-saturated 0.1 M $KHCO_3$ electrolyte using a scan rate of 10 mV s^{-1} (E). This study examines the product distributions and current densities of Cu foil and CuNS-0.8 at various potentials. The error bars indicate the standard deviation of three measurements (F). The partial current densities of C_2H_4 and C_{2+} products were measured on CuNS-0.8 and Cu foil at various potentials (G). The study also investigates the variation in the C_2H_4 to CH_4 ratio on CuNS-0.8 and Cu foil under different potentials (H). The study investigates the variation in the ratio of C_{2+} products to C_1 products on CuNS-0.8 and Cu foil under different potentials (I). Reproduced with permission from ref. 241. Copyright 2023, Elsevier.

In another investigation, the researchers explored the selectivity of Cu catalysts for CO_2RR by employing Cu_{oh} and Cu_{cub} in a tandem arrangement with CO-producing Ag_{sph}. Both Cu–Ag catalyst configurations exhibited greater selectivity and activity toward C_2H_5OH and C_2H_4 compared to CH_4 and H_2. Cu_{oh}–Ag catalysts displayed higher selectivity for C_2H_5OH than Cu_{cub}–Ag, with the C_2H_5OH to C_2H_4 ratio reaching 2.4. DFT calculations and a simple model revealed that active sites on the Cu_{cub}–Ag catalyst preferred $*CH_x$ and *CO coupling, followed by subsequent reduction, while more extended facets continued to promote ethylene. Cu_{oh}–Ag catalysts exhibited higher selectivity toward ethanol.[247] Furthermore, DFT simulations shed light on the facet-dependent nature of Cu electrode reactions, electrochemical potential, and product selectivity in CO_2R. Cu(111) facilitates the synthesis of both methane and ethylene from a single CH_2 species by promoting the formation of a COH* intermediate. In contrast, Cu(100) exhibits a preference for generating the CHO* intermediate at lower potentials, leading to ethylene production through C–C coupling and the reduction of C_2 species. The competition between COH* and CHO* intermediates depends on the applied potential, impacting reaction rates and potential requirements, particularly involving the breaking of the C–OH bond. The partial reconstruction of the Cu(100) surface is proposed as a factor contributing to the observed differences between density functional theory predictions and electrokinetic studies.[248]

In another research endeavor, Cu_2O NPs with tunable morphology were synthesized for efficient electrocatalysis in the conversion of CO_2 to C_{2+} products. Among various Cu_2O catalyst forms, the o-Cu_2O catalyst exhibited superior efficiency and current density for C_{2+} generation during CO_2RR. Impressively, it demonstrated stability during electrolysis at −1.1 V *vs.* RHE for 12 hours without destabilization. The abundance of active sites and the preservation of high-index faces in o-Cu_2O led to increased C–C coupling during CO_2RR.[249] Additionally, the synthesis of three distinct Ag–Cu JNS-100s was achieved through confined growth of Cu on one of the six symmetrical faces of Ag NCs. Among these, the Ag_{65}–Cu_{35} JNS-100 demonstrated the highest $FE_{C_2H_4}$ (54%) and $FE_{C_{2+}}$ product (72%), showcasing its superior performance in CO_2R towards C_{2+}

products. The observed shifts in C_2H_4 production and the C_{2+}/C_1 product ratio hold promise for improved CO_2RR outcomes.[250]

In a separate study, two nanoscale forms of copper molybdate ($CuMoO_4$ and $Cu_3Mo_2O_9$) were synthesized, with their crystal structures significantly influencing their electrochemical properties. In a 0.1 M alkaline solution, $Cu_3Mo_2O_9$ exhibited improved catalytic performance for both HER and OER, indicating its potential as a bifunctional water splitting catalyst in alkaline environments. The enhanced activity was attributed to the presence of more active sites, potentially arising from OVs or the unique structure of $Cu_3Mo_2O_9$ crystals.[251] In another investigation, a new Cu_2O NP film was produced using square-wave electrochemical redox cycling of high-purity Cu foils. This cathode achieved up to 98% FE for e-CO_2R to practically pure formate under 45 atm of CO_2 in bicarbonate catholytes. A two-electrode high-pressure electrolysis cell, combined with a recently designed NiFe hydroxide–carbonate anode in a KOH/borate anolyte, achieved a high energy conversion efficiency of up to 55.8% for continuous formate synthesis. Importantly, it was discovered that a $Cu_2O(111)$ oriented film was crucial for reducing CO_2 efficiently when producing formate.[2]

Using density functional theory, Zheng *et al.* conducted an analysis of the e-CO_2R on four distinct Pd_3Au alloy bimetal catalyst surfaces. The findings demonstrated that the catalytic activity and selectivity were influenced by the catalysts' d-band populations, charge distributions, and morphologies. The $Pd_3Au(100)$ surface exhibited strong HER selectivity at low applied potentials, while the $Pd_3Au(110)$ surface was more active in formic acid production. The (211) surface exhibited high selectivity for methanol synthesis during e-CO_2RR.[252] In another study, a dynamic deposition-etch-bombardment approach was employed to regulate Cu(100) facets in e-CO_2R, achieving a FE of 86.5% and a full-cell electricity conversion efficiency of 36.5% towards C_{2+} products in a flow cell setup. The single-pass yield for C_{2+} products from the electrode assembly system reached 13.2% at 12 A.[253] Additionally, in another investigation, the impact of high-index facets on e-CO_2R was explored. Through SWP treatment, copper NW catalysts with high selectivity for C_{2+} products and excellent suppression of side reactions were synthesized (Fig. 25). The FE of SW-Cu NWs at −1.1 V was found to be 57%, surpassing the FE of the original Cu NWs.[254] Table 12 offers a broad overview of different designed electrocatalysts for e-CO_2RR following the facet engineering approach on Cu-based materials.

6.9. Coordination engineering approach

In the design of e-CO_2RR catalysts, coordination engineering has taken on great importance as a means of achieving control over the behavior of the materials involved. This approach works through influencing the coordination environments surrounding metal atoms in catalyst structures. Coordination environment manipulation, however, can have a great effect on reaction rate and selectivity. Accordingly, the importance of coordination engineering lies in its potential to fine-tune the binding energies of CO_2 and reaction intermediates so as to steer the pathways of reactions. These coordination sites designed by scientists are able to be observed as selective for

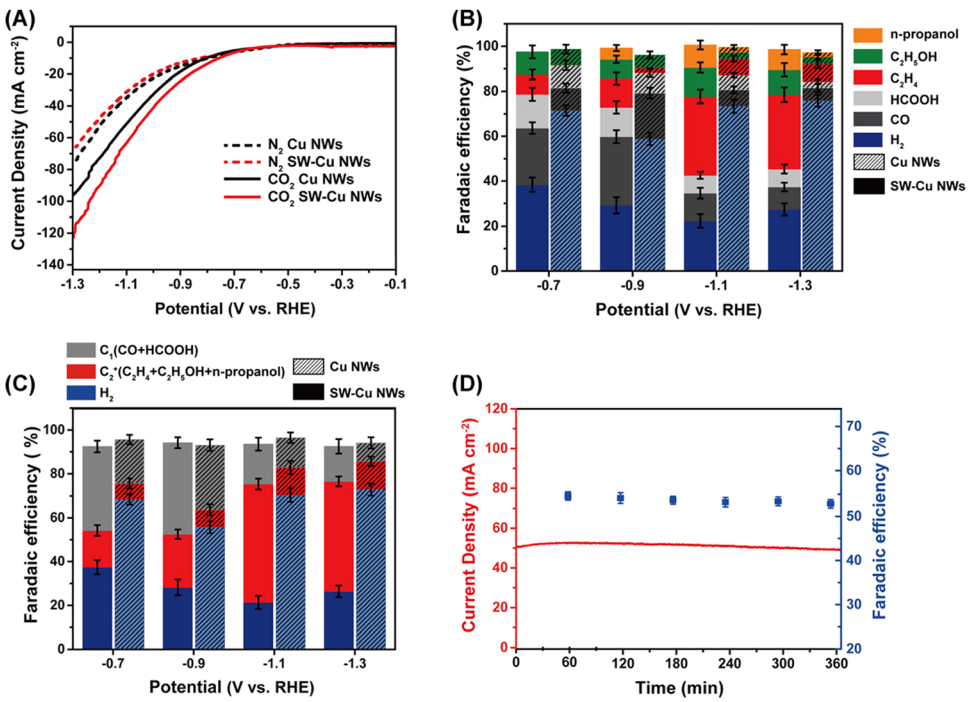

Fig. 25 LSV curves were obtained for Cu NWs and single-walled copper NWs (SW-Cu NWs) in N_2- and CO_2-saturated aqueous 1 mol L^{-1} KCl electrolytes. The scanning rate used in this study was 5 mV s^{-1} (A). The FE of each product was measured on both Cu NWs and SW-Cu NWs electrodes at various applied potentials (B). The distribution of Cu NWs and SW-Cu NWs in terms of product distribution is examined. The gray C_1 compound consists of CO and HCOOH, while the red C_{2+} compound is composed of C_2H_4, C_2H_5OH, and *n*-propanol. The blue compound is H_2 (C). The stability of SW-Cu NWs was tested at a potential of −1.1 V *vs.* RHE (D). Reproduced with permission from ref. 254. Copyright 2022, Wiley.

Table 12 This table digs deep into materials created through facet engineering for use as electrocatalysts. It focuses on their performance, describing how facet engineering can affect the distribution

				≈FE%									
No.	Material	Electrolyte	V *vs.* RHE	H_2	CO	CH_4	C_2H_4	$HCOO^-$	$C_2H_5^+$	CH_3OH	C_2H_5OH	$C_2H_3O_2^-$	Ref.
1	GDL	KCl $KHCO_3$	—	90.5	—	—	2.5	—	—	—	—	—	255
2	IL/GDL		−1.18	82.9	—	—	2.6	—	—	—	—	—	
3	Cu/GDL		−1.16	31.2	—	—	22.8	—	—	—	—	—	
4	Cu-IL/GDL		−1.17	15.7	—	—	40.6	—	—	—	—	—	
5	Cu foil	0.1 M $KHCO_3$	−1.0	29	16	16	19	23	—	1	1	—	256
6	CuNS-0.8			32	2	3	37	7	—	—	9	—	
7	A-CuNWs	0.5 M $KHCO_3$	−1.02	7	1	3	56	—	—	—	—	—	242
8	H-CuNWs			12	4	3	50	—	—	—	—	—	
9	Cu_{sph}	0.1 M $KHCO_3$	−0.79	47	4	6	24	3	—	—	3	—	245
10	Cu_{cub}		−0.75	12	10	3	60	2	—	—	3	—	
11	Cu_{oh}		−0.96	40	10	40	5	2	—	—		—	
12	Cu film	0.1 M $KHCO_3$	−1.2	20	2	55	10	5	—	—	2	—	246
13	Wrinkled Cu			30	2	32	10	5	—	—	5	—	
14	Cu film	0.1 M KCl		10	2	32	24	3	—	—	30	—	
15	Wrinkled Cu			15	2	32	23	8	—	—	30	—	
16	Cu_{oh}	0.1 M $KHCO_3$	−1.1	39	3	15	10	8	—	—	7	—	247
17	Cu_{oh}–Ag			32	50	—	2	2	—	—	—	—	
18	Ag			38	52	—	—	—	—	—	—	—	
19	Cu_{cu}			22	3	13	32	13	—	—	5	—	
20	Cu_{cu}–Ag			20	55	1	8	—	—	—	—	—	
21	Ag			38	52	—	—	—	—	—	—	—	
22	o-Cu_2O	1.0 M KCl	−1.1	25	7		34	13	—	—	15	—	249
23	d-Cu_2O			27	5	3	19	29	—	—	9	—	
24	c-Cu_2O			28	8	2	15	32	—	—	9	—	
25	Ag_{65}–Cu_{35} JNS-100	0.1 M $KHCO_3$	−1.0	18	22	4	52	14	—	—	—	—	257
26	Ag_{50}–Cu_{50} JNS-100			16	23	1	54	16	—	—	—	—	
27	Ag_{25}–Cu_{75} JNS-100			25	21	1	34	22	—	—	—	—	
28	0.5h-SW-Cu_2O/Cu @ 1 atm CO_2	0.5 M $KHCO_3$	−1.04	68.9	1	8.9	—	16.1	—	—	4.9	—	2
29	0.5h-SW-Cu_2O/Cu @ 45 atm CO_2			8.4	1	—	—	79.4	—	—	3.7	—	
30	0.5h-SW-Cu_2O/Cu @ 60 atm CO_2			16	1	—	—	81.2	—	—	1	—	
31	HRS-Cu	0.1 M $KHCO_3$	−0.95	10	1	2	53	—	—	—	22	—	253
32	Cu NWs	1 M KCl	−1.1	78	2	—	8	1	—	—	2	—	258
33	SW-Cu NW			28	10	—	32	4	—	—	10	—	

specific e-CO_2R products. However, to implement the coordination engineering strategy for designing electrocatalysts, there are several methods that can be employed. One used approach involves designing coordination polymers where the coordination environment around metal centers might be set up *via* ligand choices and metal ions in the medium. Another technique involves modifying surfaces using techniques like layer deposition, which allows for controlled deposition of catalytically active metal atoms onto support materials enabling the creation of well-defined sites for coordination reactions. Furthermore, when two distinct metals are deliberately combined the creation of catalysts can result in improved performance by leveraging synergistic effects. By employing coordination engineering techniques, we can effectively optimize CO_2R catalysts thereby promoting the advancement of sustainable carbon capture and utilization technologies and facilitating the transition towards a low carbon future.

In a comprehensive exploration of e-CO_2R, multiple Cu-doped ZIF-8 samples were synthesized. These Cu-doped ZIF-8 catalysts exhibited excellent selectivity for methane and carbon monoxide, with the highest FE_{CH_4} achieved by Cu30%ZIF-8 at −1.6 V *vs.* Ag/AgCl. Furthermore, Cu30%ZIF-8 demonstrated a peak current density of −40 mA cm^{-2} at −2.1 V *vs.* Ag/AgCl, indicating high catalytic efficiency.[259] Furthermore, the copper(II) bis-triazine bipyridine complex supported on carbon black was designed by Garcia *et al.* for e-CO_2R. The electrocatalytic performance of the catalyst was monitored using differential mass spectrometry. They exposed the simultaneous production of methanol, formic acid, formaldehyde, carbon monoxide, and methane, indicating that the catalyst lacked product selectivity. Optimal results, with a FE of around 22%, were achieved with both 2.5% and 5% composition of the Cu complex on carbon black, making them suitable for polymeric electrolytic reactor fuel cell applications.[260] Furthermore, a separate investigation showcased the potential of porphyrin-based catalysts for CO_2 conversion. For this, a molecular Cu–porphyrin built porous framework demonstrated an excellent FE of 73.6%, indicating the promise of porphyrin-based catalysts in CO_2 conversion (Fig. 26). Interestingly, this system produced only carbon monoxide as a hydrocarbon on the Cu–porphyrin support. Abundant copper-active sites efficiently absorbed CO_2, and finite-element modeling highlighted the importance of isolating CO intermediates for hydrocarbon production.[261]

Furthermore, the research proposed the utilization of the generalized coordination number (GCN) as an activity descriptor for e-CO_2RR on Cu surfaces. This approach established linear scaling relationships between CO_2RR intermediates and GCN at various surface sites, including cavities, step edges, twists, and adatoms. The activity-GCN volcano plot was employed to calculate the theoretical overpotential limit on

Cu surfaces, revealing that overpotentials exceeding 0.12 V could not be reduced by surface engineering alone. It was suggested that dimerized surfaces might minimize the overpotential for converting CO_2 to methane. Adatom surface engineering showed potential for reducing CO_2RR overpotentials while inhibiting competitive HER.[262] In a complementary effort, Zhou *et al.* have proposed the optimization of cobalt–nitrogen functionalized materials for CO_2R processes through coordination engineering. This approach involved constructing a volcano diagram to assess activity levels in relation to CO adsorption energies. The study revealed that the absence of bonding in Co–O bonds, in contrast to Co–C or Co–N bonds in cobalt-centered motifs, contributed to increased catalytic activity. Moreover, the variation in vacancy formation energy of the cobalt atom emerged as a predictive factor for catalytic activity.[263]

Besides, another experiment showed that porous hollow copper microspheres (H-Cu MPs) were produced by combining the properties of EDTA-2Na to chelate ions and their natural ability to self-assemble. The adsorption of EDTA anions induced modifications in the geometrical structure and electronic distribution of H-Cu MPs, facilitating the selective production of ethene.[264] In a related development, the Cu_2O@Cu-MOF system was created through *in situ* etching, dissolving, and restructuring, resulting in a hybrid catalyst for the e-CO_2R. The system exhibited an impressive overall FE of 79.4%, particularly excelling in forming hydrocarbon products, notably CH_4. The remarkable FE ratio of 3.89 for CH_4 to C_2H_2 underscores the excellent selectivity of this catalyst.[265] Moreover, the results of another investigation unveiled the potential of Cu catalysts with varying Sn molar ratios for CO_2RR. Cu/Sn catalysts containing less than 1.5% Sn exhibited higher FE in CO production, while maintaining nearly identical FEs in hydrocarbon production. Notably, the Cu/Sn-1.5 sample achieved a substantial CH_4 partial current density of -27.5 mA cm^{-2} at -1.25 V *vs.* RHE.[266] Furthermore, the research demonstrated the remarkable e-CO_2R to C_2H_4 facilitated by a crystalline CuPc/C catalyst, which exhibited both high selectivity and reactivity. The crystallinity of CuPc was identified as a critical factor for efficient and selective C_2H_4 synthesis.[267]

In a related study, crystalline single-chain models (Cu-PzH, Cu-PzCl, Cu-PzBr, and CuPzI) were constructed to investigate product selectivity during e-CO_2 in a flow cell. Predictions indicated different selectivity for CH_4 and C_2H_4 due to variations in the lengths and dihedral angles between bi-copper atoms, which were contingent on the coordination microenvironment. Cu-PzH, at 1.0 V and a high current density, exhibited the highest $FE_{C_2H_4}$ (60%) among all materials, while Cu-PzI, under the same conditions, showed the highest FE_{CH_4} (52%). These selectivity differences were found to be due to the synergistic effects between the surrounding catalytic active sites and the adsorption ability of the catalytically active center on critical reaction intermediates.[268] Furthermore, excellent performance in selective CO_2R into C_2 compounds has been demonstrated when using a metal-azolate framework with a tetranuclear copper(I) cluster as a catalyst for e-CO_2R. The multinuclear copper cluster in CuBPZ, which may encourage C–C coupling to create C_2 chemicals, is believed to be responsible for the observed performance.[269] In a complementary effort to enhance the selectivity of e-CO_2R to CH_4, Zhang *et al.* developed a single crystal of a copper(II) complex containing hydroxy groups, known as 5,10,15,20-tetrakis(3,4-dihydroxyphenyl)porphyrin copper(II) (Cu-PorOH). Cu-PorOH was found to serve as a highly efficient heterogeneous electrocatalyst for catalyzing the e-CO_2R to methane. The hydroxy groups within Cu-PorOH construct solid three-dimensional frameworks and stabilize intermediate species, resulting in a remarkable FE of 51.3% for CH_4 and a substantial partial current density of 23.2 mA cm^{-2} at 1.5 V *vs.* RHE in an H-cell.[270]

Additionally, the research highlights that ligand-protected Cu-hydride nanoclusters, such as $Cu_{32}H_{20}L_{12}$, exhibit exceptional selectivity for e-CO_2R at modest overpotentials. When copper clusters contain negatively charged hydrides, HCOOH becomes the preferred reduction product due to its lower overpotential compared to CO. However, at low overpotentials, hydrogen evolution competes more favorably than the lattice hydride process. Electrochemical studies of the $Cu_{32}H_{20}L_{12}$ cluster support these predictions, indicating that HCOOH is the dominant product at low overpotential, while hydrogen production becomes more prominent at higher overpotentials.[271] In a related effort to enhance the activity and stability of GDE for CO_2 gas diffusion electrolysis, a hydrophobic molecule was incorporated into the Cu catalyst layer. This modification enabled strong-current electrolysis without flooding, due to the 1-octadecanethiol-modified Cu catalyst layer on the GDE. The modified GDE exhibited robust C_{2+} FEs of over 70.0% in the current density range of 100 to 800 mA cm^{-2}, with a peak $FE_{C_{2+}}$ of 85.2% at 800 mA cm^{-2}.[272] In another study aimed at enhancing e-CO_2R to acetic acid, Xiao *et al.* developed helical porphyrinic MOF CuTCPP on the surface of $Cu(OH)_2$ nanoarrays. Electrodeposition was employed to create the nanoarrays on Cu foil, followed by immersion in a TCPP solution to assemble the chiral HCuTCPP@$Cu(OH)_2$ nanoarrays. The electrocatalytic results demonstrated a high $FE_{acetic\ acid}$ of 26.1% at a potential of -1.6 V *vs.* Ag/Ag$^+$, surpassing the performance of nHCuTCPP@$Cu(OH)_2$ (19.8%).[273]

In a related research effort, the feasibility of e-CO_2R into valuable alcohols was investigated. The study employed an elongated and fluorinated porphyrin structure to single out three model bicentric copper complexes, elucidating the relationship between their structure, properties, and performance. It was found that complexes with strong intramolecular tension and coordination asymmetry exhibited more active Cu centers. The hybrid structure of a Cu cluster and a partly reduced O-containing hexaphyrin ligand enabled the production of up to 32.5% ethanol and 18.3% *n*-propanol from CO_2.[274]

In another research endeavor, a method was used to generate ultra-stable copper dendrites (Cu CF) with a high FE_{C_2}. The Cu CF was found to have a FE_{C_2} of 90.6% and the partial current density was 453.3 mA cm^{-2}. A 400 h stable electrolysis at 800 mA and even a ground-breaking stable operation at a large industrial current of 10 A were achieved in the membrane electrode assembly (MEA) form. The formation of a coordination compound was credited with having solved the problem. It generates

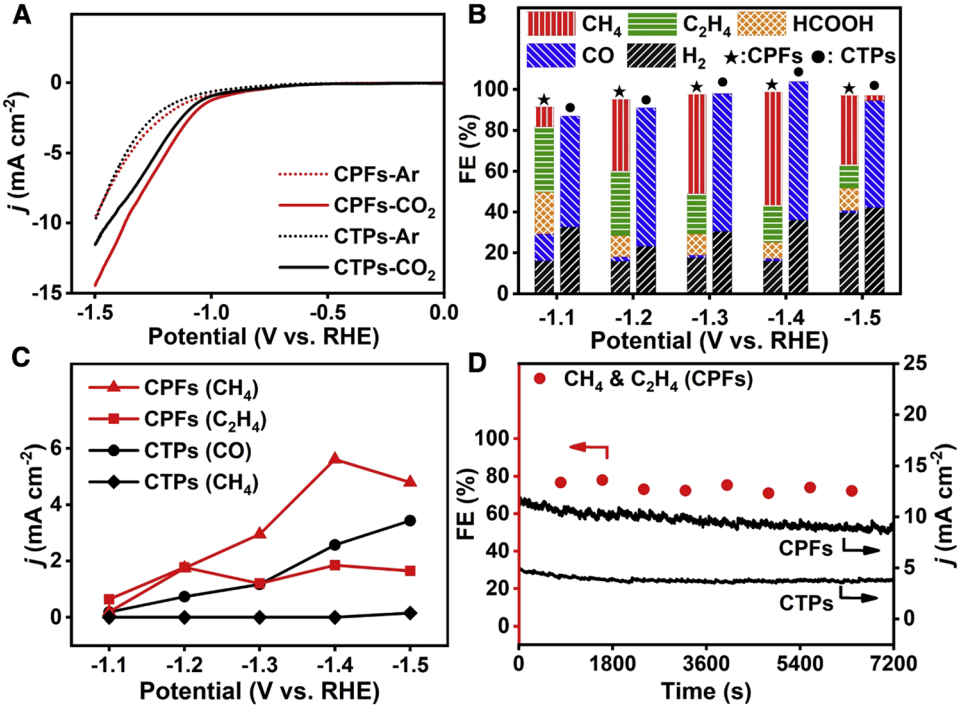

Fig. 26 e-CO_2R performance of carbon-based transition metal catalysts (CTPs) and carbon-based precious metal-free catalysts (CPFs) was evaluated by LSV curves at a scan rate of 10 mV s^{-1} in both Ar- and CO_2-saturated solution (A). The FEs of various products (B). The partial current densities of various products (C). The FE and current density of CPFs and CTPs were measured at a potential of 1.4 V *versus* RHE (D). Reproduced from ref. 261. Open access article, Elsevier.

a Cu(II) carboxylate on the surface of Cu CF, ensuring the stability of the Cu^+ state and the material's hydrophobicity.[275] Furthermore, the electrocatalyst is critical to obtaining and managing product selectivity in e-CO_2R. In their study, two types of 2D MOFs were investigated, copper naphthalenedicarboxylate (Cu-UNDC) and copper benzenedicarboxylate (Cu-UBDC), to see how their ligand environment affected their selective properties and themselves. When ligand modifications were made, the MOF structure was altered, as well as the electrical environment around the copper center. This resulted in changes to product selectivity. The research team found that ligand modifications changed the structure of the MOF and thereby also its electrical environment around the copper center – which affected product selectivity. Under light exposure, Cu-UNDC had a FE of 24.3% for C_2 products, and Cu-UBDC 26.2%.[276] In addition, Han *et al.* combined the traditional HKUST-1 layout using the atomic layer infiltration (ALI) method to control the determining conditions at the Cu metal location. When Zn–O–Zn sites were added uniformly to HKUST-1, its FECO increased significantly from 20–30% to 70–80%. This change was made by reinforcing contact bonds and thus increasing the enthalpy of CO_2 adsorption, as evidenced by density functional theory simulations.[277]

In another study related to the e-CO_2R to high-energy-density C_{2+} products, the creation of carbon–carbon bonds was explored, particularly the OC–COH coupling pathway over the CO dimerization pathway. Density functional theory simulations in this study demonstrated that the adsorption of *CO species coupled with their hydrogenation species, *COH, took precedence over CO dimerization on low-coordinated copper sites. Remarkably, at 300 mA cm^{-2}, the researchers achieved a FE_{C_2} of 77.8% using a fragmented Cu catalyst with an abundance of low-coordinated sites.[278] In a separate study, Cu_2SnS_3 nanoplates were synthesized and shown to be formate-selective over a wide potential and current range. When tested in a flow cell with a gas-diffusion electrode, the thiocyanate-capped Cu_2SnS_3 nanoplates exhibited a maximum formate FE of 92% and partial current densities of up to 181 mA cm^{-2}. The high formate selectivity was attributed to favorable adsorption of HCOO* intermediates on cationic Sn sites, which were electrically regulated by thiocyanates coupled to neighboring Cu sites.[279]

Furthermore, the research evaluated the performance of MOFs for the e-CO_2RR, contrasting those based on square–pyramidal CuO_5 nodes with those based on square-planar CuO_4 nodes. With a FE of 56% and a current density of 11.4 mA cm^{-2} at 1.4 V *vs.* RHE, the MOF (Cu-DBC) built from CuO_5 nodes and catechol-derived ligands demonstrated excellent performance in the e-CO_2R to CH_4. On the other hand, Cu-HHTP and Cu-THQ were two additional MOFs that only produced CO as a reduced product. The study also showed that the CuO_5 active sites can effectively hydrogenate CO into CH_4 because the energy levels of metal d-orbitals in the square–pyramidal CuO_5 site are higher than those in the square-planar CuO_4 site, leading to the formation of CH_4 rather than CO.[280] Moreover, oxide-derived Cu (OD-Cu)-type catalysts were designed by Lu *et al.* which showed improved C_{2+} production, maybe due to Cu sites that are undercoordinated. Undercoordinated Cu sites have not been

Table 13 The table provides an overview of electrocatalysts designed for CO_2R by utilizing the coordination engineering techniques. It investigates their performance and evaluates how these techniques impact product selectivity and efficiency across various reaction conditions

				≈FE%									
No.	Material	Electrolyte	V *vs.* RHE	H_2	CO	CH_4	C_2H_4	$HCOO^-$	$C_2H_5^+$	CH_3OH	C_2H_5OH	$C_2H_3O_2^-$	Ref.
1	$Cu_{30\%}$ZIF-8	0.1 M $KHCO_3$	−1.2 Ag/AgCl	84	7	1	—	—	—	—	—	—	259
2	$Cu_{20\%}$ZIF-8			80	8	2	—	—	—	—	—	—	
3	$Cu_{10\%}$ZIF-8			82	8	—	—	—	—	—	—	—	
4	1% Cu complex	—	−1.2	—	—	—	—	—	—	9	—	—	282
5	2.5% Cu complex			—	—	—	—	—	—	21	—	—	
6	5% Cu complex			—	—	—	—	—	—	13	—	—	
7	10% Cu complex			—	—	—	—	—	—	20	—	—	
8	20% Cu complex			—	—	—	—	—	—	19	—	—	
9	CPFs	0.1 $KHCO_3$	−1.1	18	12		31	20	—	9	—	—	283
10	CTPs			33	55	—	—	—	—	—	—	—	
11	H-Cu MPs	0.1 M $KHCO_3$	−0.91	22	4	17	50	4	—	—	—	—	264
12	Cu_2O@Cu-MOF	0.1 M $KHCO_3$	−1.71	—	—	62	17	—	—	—	—	—	284
13	Cu-MOF			—	—	35	11	—	—	—	—	—	
14	Cu_2O			—	—	3	42	—	—	—	—	—	
15	Cu		−1.25	22	16	12	12	—	—	—	—	—	266
16	Cu/Sn-0.5			9	31	13	3	—	—	—	—	—	
17	CuSn-1.5			7	43	15	3	—	—	—	—	—	
18	Crystalline CuPC	$KHCO_3$	−1.6 Ag/AgCl	—	5	5	26	—	—	—	—	—	285
19	Non-crystalline CuPC			—	28	2	6	—	—	—	—	—	
20	Crystalline CuPC (restored)			—	5	5	35	—	—	—	—	—	
21	I-Cu-PzH	1 M KOH	−1.1	10	23	9	48	—	—	—	—	—	286
22	II-Cu-PzCl			22	20	18	30	—	—	—	—	—	
23	III-Cu-PzBr			20	18	20	30	—	—	—	—	—	
24	IV-Cu-PzI			22	14	39	20	—	—	—	—	—	
25	CuBPZ	0.1 M $KHCO_3$	−1.1	20	28	2	—	2	—	—	45	—	287
26	Cu-PorOH	$KHCO_3$	−1.2	—	8	7	8	—	—	—		—	288
27	H-GDE	1.0 M KOH	100 mA cm^{-2}	13	10	1	26	2	—	—	38	—	289
28	$Cu(OH)_2$	—	−1.4	—	—	—	—	19	—	—	—	—	273
29	nH-CuTCPP@$Cu(OH)_2$			—	—	—	—	14	—	—	—	—	
30	H-CuTCPP@$Cu(OH)_2$			—	—	—	—	6	—	—	—	—	
31	Hex-2Cu–O	0.1 M $KHCO_3$	−1.0	13	28	—	4	27	—	—	7	—	274
32	Hex-2Cu–2O			45	—	—	5	33	—	—		—	
33	Oct-2Cu			60	38	—	—	—	—	—		—	

investigated for their stability in alkaline e-CO_2R environments. Different crystalline phases and Sr/Cu ratios in strontium copper oxide catalysts were prepared. The C_{2+} FE of a $SrCuO_2$ tetragonal phase catalyst is 53%, demonstrating its remarkable selectivity for C_{2+} products. $SrCuO_2$ catalysts can retain or recover oxidized Cu species after being subjected to reductive e-CO_2R conditions, as shown by *ex situ* X-ray absorption spectroscopy.[281] The different electrocatalysts designed by following the coordination engineering approach are summarized in accordance with their CO_2 conversion to different valuable products in Table 13.

6.10. Site engineering approach

Site engineering can be used to design e-CO_2R catalysts by precisely controlling the catalytic sites on the surface of a material. In this method, the sites such as metal atoms and defects are selectively used. By doing that, the reactivity and selectivity of the catalyst in reducing CO_2 into different products can be optimized. Researchers can enhance the ability of these catalysts to facilitate desired chemical transformations while minimizing side reactions by designing and engineering these sites. Such a level of control is needed for shaping catalysts to produce CO_2RR products and, therefore, site engineering is a powerful tool for developing sustainable energy conversion and carbon capture technologies. Many methods can be used to put the site engineering tactics into practice for designing CO_2RR catalysts. The favored approach is to deposit metal nanoparticles or single metal atoms onto a support material to gain control over the sites. On the catalyst surface, as pointed out earlier, defect engineering can also be considered as a form of site engineering. This strategy involves developing catalysts within a molecular framework that show promise for a defined and specific active site. Researchers can improve the efficiency of catalysts by tuning the arrangement and properties of these sites. As a matter of fact, it facilitates the design of catalysts, which produce CO_2RR products that are indispensable in the energy-efficient use of captured carbon dioxide and in response to the global demand to address the problem of climate change.

To enhance CO_2RR performance under a range of calcination conditions, MOF Cu(BTC) was designed with tunable valence states of Cu(II), Cu(I), and Cu(0) sites. Catalysts for the reactions of air, hydrogen, and nitrogen were all created using variations of the Cu/C-T-gas system. C_2H_4 was generated by Cu/C-T-air catalysts, which may have been due to the presence of both Cu(I) and Cu(II) and an abundance of V_O. After 12 hours, the Cu/C-450-air demonstrated remarkable CO_2RR characteristics, with a $FE_{C_2H_4}$ of 34.8% at 1.1 V *vs.* RHE. Smaller grain size and a thinner carbon layer may have led to greater exposure to active sites and faster electron transport in the Cu/C-T-H_2 system,

leading to the production of C_2H_4, while in the Cu/C-T-N_2 system, CH_4 was generated.[290]

In parallel work, Liu *et al.* have provided a framework for exploring intrinsic activity differences between e-ND-Fe(II) and c-ND-Fe(II) in the context of CO_2-to-CO conversion. Atomic Fe catalysts with changeable porosity architecture were synthesized *via* the pyrolysis of N-rich bimetallic Fe/Zn 2D ZIF, shedding light on the impact of ND configurations on the CO_2RR activity of Fe–N_4 active sites. Electrochemical studies revealed that the concentration of e-ND-Fe(II) in A-Fe@NG-Li_xK_y catalysts was positively correlated with CO_2RR activity. DFT calculations and *in situ* ATR-IR spectroscopy studies demonstrated higher electron density surrounding e-ND-Fe(II), which reduced CO bonding on metal sites, favoring CO_2RR. The optimized sample A-Fe@NG-Li_1K_3 showed excellent performance, with a maximum FE_{CO} of 95%.[291] Furthermore, Zhu *et al.* have optimized electrosynthesis pathways for selective fuel production by studying aqueous e-CO_2R on Cu. Electrocatalysts with voltage- and facet-dependent CO_2R selectivity were devised and produced from nine large-area single-crystal Cu foils with different surface orientations.[292] Furthermore, the 2Bn-Cu@UiO-67 catalyst, doped with N-heterocyclic carbene (NHC), was designed and it achieved the e-CO_2R to CH_4 at a current density of 420 mA cm^{-2} with an outstanding FE of 81%. The catalyst maintained a FE_{CH_4} of greater than 70%, and it achieved a record-breaking turnover frequency of 16.3 s^{-1}.[293]

Moreover, Cheng *et al.* investigated the active sites of OD-Cu catalysts for e-CO_2R to multi-carbon compounds. Utilizing molecular dynamics simulation and density functional theory computations, they described realistic models of the OD-Cu surface and explored more than 150 surface locations. Ethylene formation was observed at planar-square sites and convex-square sites, while alcohol formation was favored at step-square sites due to the geometric influence of stabilizing acetaldehyde intermediates and destabilizing Cu–O interactions.[294] Furthermore, lamellae of copper phyllosilicate were created in this research with CuO particles that were uniformly scattered and hence readily reducible to Cu^+ and Cu^0. Synthesizing a series of CuO/$CuSiO_3$ with varying Cu loadings yielded Cu^+–Cu^0 sites. On 20% Cu/$CuSiO_3$, the e-CO_2R activity was greatly improved, with a $FE_{C_2H_4}$ of 51.8% and a $FE_{C_2+C_2}$ of 82% being attained. Activation of CO_2, adsorption of *CO, and C–C coupling were all shown to involve Cu^0 and Cu^+, as calculated by *in situ* ATR-IR and DFT.[295]

Furthermore, Guan *et al.* showed that a nitrogen-coordination technique can be used to evenly distribute single-atom Cu catalysts over nitrogen-doped carbon. Nitrogen in nitrogen-doped carbon frameworks with Cu–N_x topologies promotes efficient dispersion and attachment of atomic Cu species. The pyrolysis temperature allows for fine-tuning of the doping concentrations and Cu–N_x combinations. For C–C coupling to occur and C_2H_4 to be produced, a very high concentration of Cu (4.9% mol) is required. The production of CH_4 as C_1 products is favored at low Cu concentrations due to the considerable distance between Cu and N_x species.[296] Moreover, another research study investigated physical vapor deposition as a viable method for growing large-format Cu thin films intended for e-CO_2R. These films epitaxially grew on Al_2O_3(0001), Si(100), and Si(111) substrates, each exhibiting a distinct out-of-plane orientation. X-ray pole figures revealed that Cu can be oriented in both low and high Miller index directions depending on the single-crystal substrate's orientation. *In situ* structural investigations identified three distinct Cu surface structures. Electrochemical tests demonstrated that thin-film orientations with more undercoordinated sites exhibit higher activity and selectivity for C–C coupling. Cu(751), characterized by fewer nearest neighbors on the Cu(S) − [*n*(110) (100)] surface, achieved the highest oxygenate/hydrocarbon ratio at 0.89 V *vs.* RHE.[297]

Additionally, the creation of a conductive di-nuclear cuprous complex with a short CuCu contact, formed by combining 1*H*-[1,10]phenanthrolin-2-one with Cu(I) ions, resulted in Cuophen. This complex demonstrated robust activity for the e-CO_2R to C_2H_4, achieving a FE of 55.11% and a current density of 580 mA cm^{-2}. Notably, a *CO species bridged two copper ions, forming a stable intermediate transition state and facilitating C–C interaction due to the reduced CuCu distance.[298] In addition to this, a novel single-site copper coordination polymer known as Cu(OH)BTA was formed from e-CO_2R using renewable electricity (Fig. 27). This polymer demonstrated a C_2H_4 selectivity 1.5 times higher than its metallic analogue and maintained a stable structure during the reaction. The presence of adjacent Cu in the polymer allows for the formation of a *OCCHO intermediate after CO hydrogenation, acting as a dual site. These polymers enable full-device CO_2 electrolysis to run for 67 hours at an applicable current within a membrane electrode assembly.[299]

Moreover, a technique has been established to achieve the site-selective generation of AgPd nanodendrites on Au nanoparticles by using H_2PdCl_4 to galvanically replace the Ag layers on Au@Ag nanoprisms and a coreduction process involving silver and palladium ions. The selectivity of AgPd nanodendrite deposition on Au nanoprisms is determined by the concentration of H_2PdCl_4. These nanoprisms exhibit a strong electrochemical activity for CO_2R, particularly at the most favorable reduction potential for CO_2 at 0.18 V *vs.* RHE.[300] Furthermore, a novel technique has been developed to create atomically scattered Fe–N_5 sites on defect-rich porous carbon nanofibers through electrospinning and annealing. The Fe–N_5/DPCF electrocatalyst exhibits exceptional e-CO_2RR, with a substantial j_{CO} of 9.4 mA cm^{-2}, high FE_{CO} (>90%), and sustained stability even after 25 hours of electrolysis. This catalyst operates reliably for an extended period and provides a high power density of 1.3 mW cm^{-2}.[301] Additionally, Varandili *et al.* have introduced Cu/CeO_{2-x} heterodimers (HDs) to illustrate the synergistic effects at metal/metal oxide interfaces that enhance selectivity in the e-CO_2RR. The Cu/CeO_{2-x} HDs achieve up to 80% selectivity against CO_2RR and 54% FE for methane at −1.2 V *vs.* RHE, which is five times higher than that in the case of physically mixed Cu and CeO_{2-x} nanocrystals. *In situ* and *in operando* X-ray absorption spectroscopy studies reveal the partial conversion of Ce^{4+} to Ce^{3+} in the HDs during CO_2RR.[302] Furthermore, to construct catalysts with high selectivity towards C_2 products in e-CO_2R, a Cu foil kinetic model featuring numerous nanocavities and a larger reaction rate

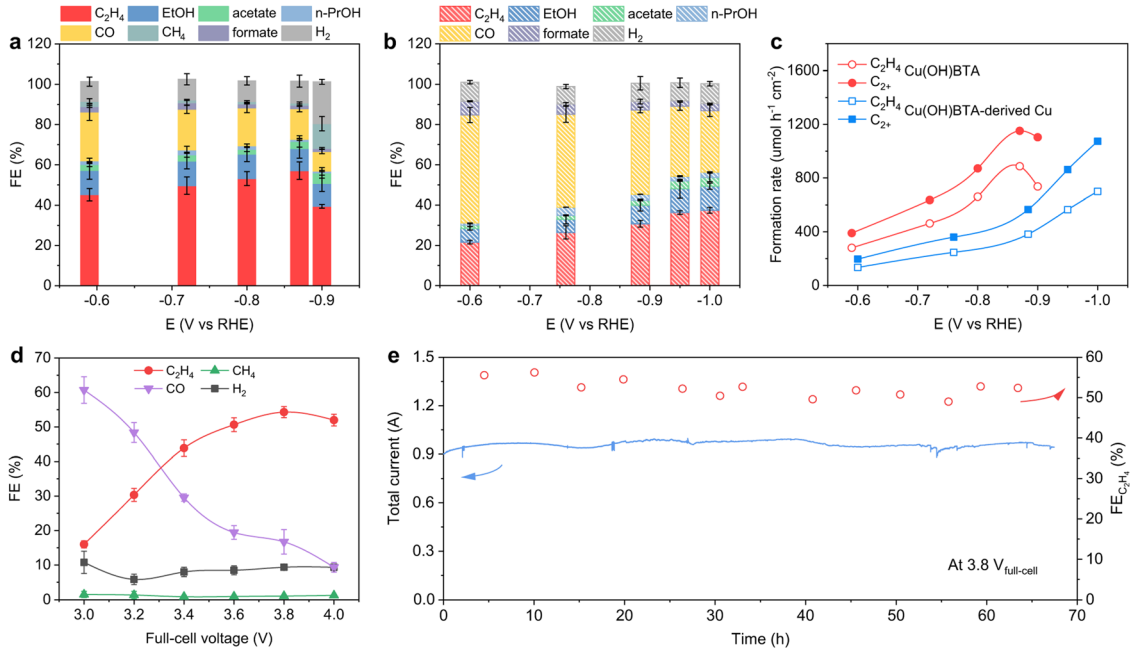

Fig. 27 The study investigated the FEs of various products at different applied potentials using Cu(OH)BTA (a) and Cu(OH)BTA-derived Cu (b) in a 1 M KOH electrolyte. The study also investigated the formation rates of C_{2+} products and C_2H_4 under various applied potentials using Cu(OH)BTA and Cu(OH)BTA-derived Cu in a 1 M KOH electrolyte (c). The study also measured the FEs of various gas products within the voltage range of 3.0–4.0 V using a membrane-electrode assembly (MEA) device (d). The electrosynthesis of C_2H_4 was performed in a MEA with a geometric electrode area of 4 cm^{-2}. The catalyst maintained its overall current and ethylene FE for a duration of 67 hours (e). The error bars for the uncertainty in FE represent one standard deviation, which is calculated using three independent runs. Reproduced from ref. 299. Open access article, Nature.

constant k is presented by Han *et al.* This model promotes the production of C_2H_4 by increasing the concentration of adsorbed CO and decreasing the C–C coupling barrier for CO intermediates. The C_2H_4/CH_4 ratio on commercial Cu foil treated with cyclic voltammetry is 4.11, aligning with this concept and representing an 18-fold increase compared to untreated Cu foil.[303]

Further, a Cu-based MOF as a catalyst was used by Zhu *et al.* with a FE of 92%/88%, and the partial current density was 9.8/18.3 mA cm^{-2} at a potential of 1.2/−1.3 V, making it the most active system for producing methane. The trigonal pyramidal Cu(I)N_3 produced on-site acts as the electrochemical active site, stabilizing critical intermediates and suppressing HER.[304] Furthermore, three Cu-MOFs with varying copper(II) site distributions were reported. The FE of Cu_1 was four times higher than that of FE_{H_2}, while the FE of Cu_2 was twice as high.[305] The different electrocatalysts and their e-CO_2R products developed by the site engineering approach are tabulated in Table 14.

6.11. Strain engineering approach

The approach of strain engineering has become a strategy for designing catalysts for e-CO_2R. Its significance lies in the ability to finely adjust the properties of materials, especially copper and other metal catalysts, to enhance CO_2RR performance. By incorporating controlled strains into the crystal structure of catalyst materials, researchers can manipulate the arrangement of atoms on the surface. This has an effect on the selectivity and activity of the catalyst allowing for the production of carbon-based products like ethylene or ethanol while minimizing unwanted byproducts. The goal of strain engineering is to improve the efficiency of CO_2R by developing new catalyst formulations. Thus, it holds promise as a sustainable path toward energy solutions based on chemistry and also possible new carbon capture technologies. There is a way to practice strain engineering on CO_2RR catalyst design. One common technique is nano-structuring through methods such as electrodeposition and chemical vapor deposition, which create nanomaterials with specific shapes and sizes. Another effective method is surface doping or alloying, which involves introducing atoms or molecules onto the catalyst surface to induce strain and alter its properties. Furthermore, subjecting the catalyst material to stress or pressure can induce strain, which has demonstrated potential in improving the performance of CO_2RR.

Kim *et al.* have shown that CO_2 distribution on model-strained Cu(001) surfaces can be controlled using strain engineering (Fig. 28). The kinetics of CO_2R to single-carbon products are influenced by tensile strain, which moves the center of the d-band closer to the Fermi level as the film thickness decreases. While C_{2+} product activity remains stable, CO_2R reduction kinetics slow down, leading to fewer single-carbon products. Increases in adsorption energy and surface coverage of CO and H are suggested by the greater d-band center, which improves selectivity for C_{2+} products relative to CO and CH_4. Hydrogen adsorption becomes more attractive as tensile strain rises, surpassing the faradaic current for CO_2R.[314]

Additionally, Kang *et al.* have demonstrated the effectiveness of self-supported PS–Cu catalysts with tensile strain and a

Table 14 The table provides an overview of electrocatalyst materials developed using site engineering strategies for CO_2R. It thoroughly analyzes their characteristics with a particular emphasis on understanding how site engineering influences the resulting products

				≈FE%									
No.	Material	Electrolyte	V *vs.* RHE	H_2	CO	CH_4	C_2H_4	$HCOO^-$	$C_2H_5^+$	CH_3OH	C_2H_5OH	$C_2H_3O_2^-$	Ref.
1	Cu/C-550-air	0.1 M $KHCO_3$	−1.1	—	—	—	27	—	—	—	—	—	306
2	Cu/C-450-air			—	—	—	35	—	—	—	—	—	
3	Cu/C-350-air			—	—	—	26	—	—	—	—	—	
4	Cu/C-550-N_2			—	—	20	6	—	—	—	—	—	
5	Cu/C-450-N_2			—	—	35	11	—	—	—	—	—	
6	Cu/C-350-N_2			—	—	12	25	—	—	—	—	—	
7	Cu/C-550-H_2			—	—	—	28	—	—	—	—	—	
8	Cu/C-450-H_2			—	—	—	33	—	—	—	—	—	
9	Cu/C-350-H_2			—	—	—	16	—	—	—	—	—	
10	Cu_2S/CM	0.1 M $KHCO_3$	−1.1	50	—	—	—	—	—	—	—	—	307
11	A-Fe@NG-Li_1K_3	0.5 M $KHCO_3$	−0.75		22	—	—	—	—	—	—	—	291
12	Fe/Mn–N–C	0.1 M $KHCO_3$	−1.0	33	65	—	—	—	—	—	—	—	308
13	Fe–N–C			75	30	—	—	—	—	—	—	—	
14	Mn–N–C			85	12	—	—	—	—	—	—	—	
15	N–C			68	10	—	—	—	—	—	—	—	
16	20% Cu/$CuSiO_3$	0.1 M $KHCO_3$	−1.1	16	14	4	53	—	—	—	8	—	309
17	Cu–N–C-800	0.1 M $KHCO_3$	−1.0	—	—	3	9	—	—	—	—	—	296
18	Cu–N–C-900			—	—	7	1	—	—	—	—	—	
19	Cuophen	0.1 M $KHCO_3$	−1.0	69	2	6	10	—	—	—	—	—	310
20	Cu(OH)BTA	0.1 M $KHCO_3$	−0.9	35	10	1	42	2	—	—	8	—	311
21	Cu(OH)BTA-derived Cu			10	43	—	30	5	—	—	2	—	
22	DPCF	0.5 M $KHCO_3$	−0.7	—	82	—	—	—	—	—	—	—	312
23	Fe–N_x–/PCF			—	50	—	—	—	—	—	—	—	
24	Fe–N_5–/DPCF			—	63	—	—	—	—	—	—	—	
25	Cu (15 nm)/CeO_2 HDs	0.1 M $KHCO_3$	−1.1	40	1	9	25	15	—	—	1		302
26	Cu (24 nm)/CeO_2 HDs			25	16	12	31	4	—	—	—	—	
27	Cu (36 nm)/CeO_2 HDs			20	5	40	18	1	—	—	—	—	
28	Cu (54 nm)/CeO_2 HDs			35	14	23	8	13	—	—	—	—	
29	Fe–N–C	—	−0.7	65	43	—	—	—	—	—	—	—	313
30	Ni–N–C			10	80	—	—	—	—	—	—	—	
31	Mn–N–C			72	30	—	—	—	—	—	—	—	
32	Co–N–C			92	10	—	—	—	—	—	—	—	
33	Cu–N–C			62	28	—	—	—	—	—	—	—	

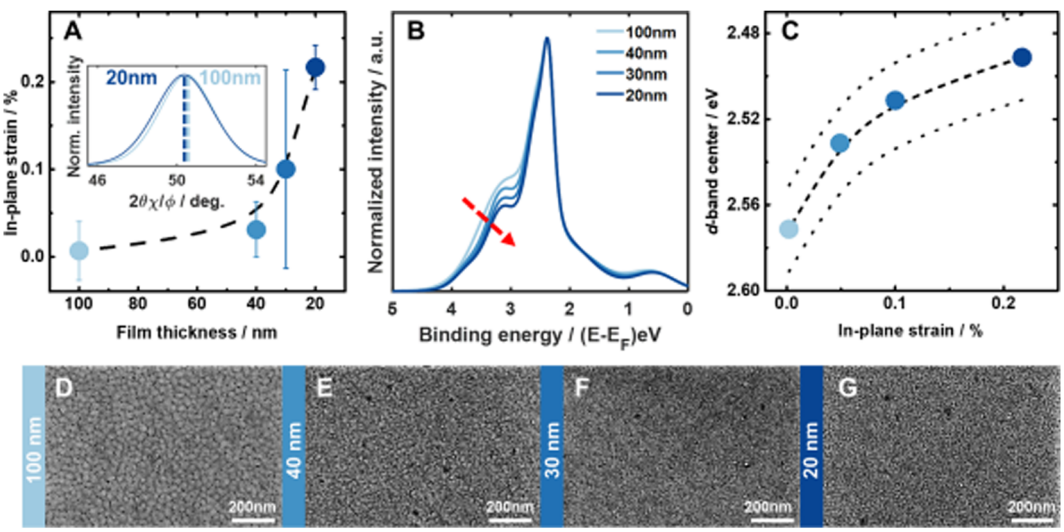

Fig. 28 The study examines the structural properties of epitaxial Cu(001) on single-crystal Si(001). The in-plane strain at the surface was measured as a function of film thickness using grazing-incidence XRD. The inset illustrates the decrease in the angle of the Bragg peak as the film thickness decreases (A). The obtained He–I ultraviolet photoelectron spectroscopic valence band spectra is represented in (B). The d-band center from the ultraviolet photoelectron spectroscopy is examined as a function of in-plane strain (C). The 99% confidence interval is represented by dotted lines. SEM images of Cu(001) films with varying thicknesses were obtained. The thicknesses of the films are as follows: (D) 100 nm, (E) 40 nm, (F) 30 nm, and (G) 20 nm. Reproduced with permission from ref. 314. Copyright 2021, American Chemical Society.

porous microstructure. These catalysts outperform Pt foil at high current densities and exhibit superior pH-universal catalytic activity for the HER compared to Cu NPs and Cu foam. Importantly, PS–Cu displays resistance to corrosion and remains stable over time.[315] Moreover, an analysis of the impact of water solvation and uniaxial lattice strain on CO_2RR across Cu(211) and Cu(100) surfaces has been conducted by Du and An. The results reveal that tensile strain enhances the binding strength of COOH and CHO, while diminishing the binding strength of CO and COH. This phenomenon arises due to the distinct strain effects induced at the surface site by their respective binding arrangements. Notably, the study highlights the variability between implicit solvation corrections and explicit water solvation, which is crucial for accurately estimating the solvation effect on CO_2RR.[316]

By analyzing the pure ligand effect on Cu and the combined influence of ligand and strain effects on Cu, Maark *et al.* have investigated two types of bimetallic hetero-surfaces: $Cu_i/M_j/Cu_k$ sandwiched surfaces and Cu/M_j overlayers. To mitigate the ligand impact independently, several strategies were employed, including moving the M layer deeper into the Cu lattice, placing two MLs of M directly below the top Cu layer, and combining these two strategies in the sandwiched surfaces. By doubling the number of Cu MLs in the overlayers, the ligand impact was effectively reduced. The research findings indicate that the ligand effect strengthens the binding energies of all adsorbates in $Cu_1/M_1/Cu_4$ and Cu_1/M_5, leading to an increase in overpotential for Rh and a slight decrease for Ni.[317] Furthermore, another study delves into the investigation of adsorption energies for critical intermediates in CO_2R processes over core–shell type heterostructure catalysts. It explores the impacts of strain and ligand effects on these adsorption energies. Notably, the research observes that the adsorption of *CO and *COH is less sensitive to strain compared to the adsorption of *COOH and *CHO on the Cu(111) surface, revealing that the adsorption energy variations are dependent on the specific adsorbate. The findings highlight certain catalyst models among Cu–M hetero-layered slab structures that exhibit promise for reducing overpotential during e-CO_2R due to the interplay of strain and ligand effects. Additionally, the research emphasizes that strain-insensitive adsorbates like *CO and *COH tend to benefit more from the ligand effect.[318]

In a separate study, an initial metastable Au overlayer was synthesized using a two-step solution approach. The success of this approach is attributed to the significant interface strain within the $AuCu_3$@Au core–shell structure, which provided support for the overlayer. The metastable Au exhibited increased FE and enhanced specific activity for CO_2R to CO. This increase in the reaction rate can be attributed to the downshift of the energy barrier for the production of the intermediate COOH* due to the upshift in the d-band center.[319] Another line of research focuses on the e-CO_2RR facilitated by heteroatom-doped Cu-based catalysts, known for their high activity and selectivity. However, the complexity of Cu-based materials often makes it challenging to pinpoint the specific factors responsible for performance improvements. This study highlights that lattice strain adjustment in Cu-based catalysts can be used to control the activity and selectivity of e-CO_2RR. Specifically, tensile-strained Sn/Cu alloy catalysts, by suppressing the dimerization process and promoting the formation of HCOOH and H_2, enhance CO production due to the predominant adsorption of CO and lower adsorption free energies of COOH.[320] Furthermore, in a separate study, a synthetic method is presented to maintain tensile strain in a copper/ceria heterostructure, thereby increasing selectivity for CO_2R. This approach employs metal/metal oxides. The research demonstrates that carbonaceous intermediates are better adsorbed due to the tensile strain in the copper domain, and it facilitates *CO dimerization by creating an inadequate electron environment around interfacial Cu sites. Consequently, this method leads to a maximum FE of 76.4% and increases the efficiency of converting half-cell power to 49.1%.[321]

In a separate investigation, Feng *et al.* explore the influence of atomic dopants on the activity of copper-based electrocatalysts during CO_2R processes. Notably, doping Cu_2O with atomic Gd is found to significantly enhance the catalyst's performance. To achieve this, Gd_1/CuO_x catalysts were developed, taking advantage of the unique electrical structure and large ion radii of Gd. Gd doping induces tensile strain during the reaction, stabilizing the Cu^+ species and resulting in superior catalytic performance. These catalysts achieved a partial current density of 444.3 mA cm^{-2} at 0.8 V against a hydrogen electrode, with a remarkable FE of 81.4% for C_{2+} products.[322] In another study, bimetallic alloy structures with engineered strain played a crucial role. A remarkable FE of 96.6% for CO_2-to-CO conversion was achieved by strategically managing lattice stresses in bimetal MNi alloys using a strain relaxation technique. Molecular dynamics simulations were employed to reveal that the relaxation of strained PdNi alloys can be controlled by increasing the synthesis temperature. DFT simulations further demonstrated that strain relaxation, by maximizing the energies of intermediate production, enhances CO_2RR activity and selectivity.[323] Furthermore, a novel class of Pd/Cu core/shell icosahedra with a tensile-strained Cu shell has enabled the efficient production of syngas with controllable compositions *via* the CO_2RR. By adjusting the Pd/Cu composition, the molar ratio of H_2/CO in syngas can be tuned from 1/1 to 2/1 and 3/1.[324] Table 15 shows the effect of strain on different electrocatalysts synthesized by the strain engineering approach upon CO_2 conversion products.

6.12. Precursor derived approach

In the development of catalysts for e-CO_2R, the approach that relies on precursor materials is becoming increasingly important. It makes possible the composition and structure of catalysts to be controlled. That involves the creation of catalyst materials by synthesizing them from selected precursor compounds, from which these compounds can be separated once they have been prepared. The main benefit of this method is that it enables the creation of designated catalysts, with chemical compositions, atomic structures and surface properties displayed in an orderly array. And by selecting precursor compounds, and optimizing synthesis conditions, researchers are free to tailor the properties of catalysts to achieve high selectivity and activity in converting CO_2 to valuable products such as hydrocarbons or alcohols. There are also scalability and

Table 15 The table delves into the utilization of strain engineered materials as a solution for CO_2R. It thoroughly investigates designed electrocatalyst materials and examines how the strain-induced changes in these materials affect their catalytic performance under different reaction conditions

				≈FE%									
No.	Material	Electrolyte	V *vs.* RHE	H_2	CO	CH_4	C_2H_4	$HCOO^-$	$C_2H_5^+$	CH_3OH	C_2H_5OH	$C_2H_3O_2^-$	Ref.
1	fcc Au	0.1 M $KHCO_3$	−1.0	—	60	—	—	—	—	—	—	—	319
2	o-$AuCu_3$@fct Au			—	88	—	—	—	—	—	—	—	
3	Cu_2O/CeO_2-0.18	KOH	−0.75	12	16	2	38	2	—	—	15	—	321
4	Pd ico/C	0.1 M $KHCO_3$	−1.0	78	17	—	—	—	—	—	—	—	324
5	$Pd_{2.2}Cu$ ico/C			48	37	—	—	—	—	—	—	—	
6	$Pd_{6.1}Cu$ ico/C			51	17	—	—	—	—	—	—	—	
7	$Pd_{4.3}Cu$ ico/C			63	21	—	—	—	—	—	—	—	
8	CuO_x	2 M KOH	−1.0	25	9	—	40	2	—	—	20	—	322
9	6.5% GD1/CuO_x			18	8	1	40	1	—	—	30	—	
10	s-PdNi/CNFs-1000	0.1 M $KHCO_3$	−1.18	—	52	—	—	—	—	—	—	—	323
11	s-PdNi/CNFs-800			—	64	—	—	—	—	—	—	—	
12	PdNi/C			—	83	—	—	—	—	—	—	—	
13	s-AuNi/CNFs			—	90	—	—	—	—	—	—	—	
14	s-AgNi/CNFs			—	68	—	—	—	—	—	—	—	
15	CuO	1 M KOH	−1.0	26	19	—	28	22	—	—	5	—	320
16	Sn–CuO-7.5			13	75	—		15	—	—		—	

affordability benefits to the precursor-based approach, which therefore provides an encouraging possibility for solving the problems associated with carbon capture and utilization. The precursor-based approach also has a number of techniques for designing CO_2 reduction catalysts. In one method, inorganic precursor materials are decomposed to carbon-based catalysts having defined structures and active sites by controlled heating at a temperature or by pyrolysis. Another process is called sol–gel, in which precursor compounds are mixed in a solution and then, by controlled drying and controlled thermal processing, transformed into catalytic materials. Chemical vapor deposition (CVD) is a method that allows the placement of catalysts derived from precursors onto substrates. This enables integration of these catalysts into setups promoting their usefulness in achieving a sustainable and low carbon future. Researchers can effectively utilize the potential of the precursor derived approach, by selecting precursor compounds and optimizing synthesis parameters resulting in the development of highly efficient and selective CO_2RR catalysts.

In a specific study, using ultrasonic irradiation, Guzmán *et al.* have developed novel catalysts for e-CO_2R, achieving increased selectivity towards H_2 and C_1 products (CO and formate) in aqueous media (Fig. 29). These catalysts harnessed the synergistic interaction between ZnO and CuO metal oxides, resulting in over a 1.4-fold increase in syngas productivity for the ultrasound-prepared CuZ catalysts. Furthermore, adjusting ultrasonic amplitudes increased the BET surface area by 100%, leading to a more than 14% improvement in FE towards alcohols in the RDE system at a catalyst loading of 0.2 mg cm^{-2}. They have also discussed the electroactivity in terms of precursor concentration, duration of ultrasound-assisted precipitation, and calcination temperature of the synthesized powders, allowing fine-tuning of the physical and chemical properties of the nanoparticles. To optimize the synthesis of *CO intermediates and facilitate their dimerization into multi-carbon products, mesoporous materials with a mean pore size of approximately 20 were engineered to create ideal conditions.[325]

In the quest for phase-pure solid Cu_3P NPs, Downes *et al.* have developed a molecular precursor method. This approach involves using a mixture of hydrocarbons and amines as a solvent for the high-temperature decomposition of $[Cu(H)(PPh_3)]_6$ to produce Cu_3P NPs. The electrocatalytic efficiency of Cu_3P NPs for CO_2R in CO_2-saturated $KHCO_3$ aqueous solutions was thoroughly examined. Cu_3P NPs demonstrated exceptional dispersibility, allowing them to be easily deposited onto carbon paper electrodes. However, it was observed that Cu_3P NPs exhibited instability under electrocatalytic conditions. Further investigations revealed that increasing the phosphorus content improved electrochemical stability, while decreasing the Cu_3P content enhanced stability.[326] In another study, nanocomposites of ZIF-L (zeolitic imidazolate framework with large cavities) and GO (graphene oxide) were developed, showcasing excellent electrical conductivity, a substantial active surface area, and robust electrocatalytic performance. Particularly, Cu GNC-VL (Cu zeolitic imidazolate framework-derived nitrogen-doped porous carbon) exhibited a remarkably high current density of 10.4 mA cm^{-2} at −0.87 V *vs.* RHE and an impressive FE for ethanol production of 70.52%.[327]

In a related study, Dou *et al.* have developed a method for creating CuS nanosheet arrays on a brass mesh through a single-step chemical bath deposition process. When subjected to e-CO_2R at the CuS/BM electrode, increased production of $HCOO^-$ was observed. This electrochemical process induced reconstruction, resulting in a nanowire network with multiple active centers. The reconstituted Cu(111)/CuS(102) structure was identified as a key contributor to the electrode's strong selectivity towards $HCOO^-$ generation. Moreover, the presence of sulfur (S) beneath the Cu^0 layer led to reduced binding energies of HCOO* and *COOH compared to the Cu(111) plane, facilitating the production of HCOOH or $HCOO^-$.[328] In another innovative approach, synthetic control over Cu NPs and Ag NPs has been achieved through a newly developed seeded-growth colloidal method, resulting in the production of AgCu nanodimers (NDs) with varying Cu domain sizes. This method also applies to other

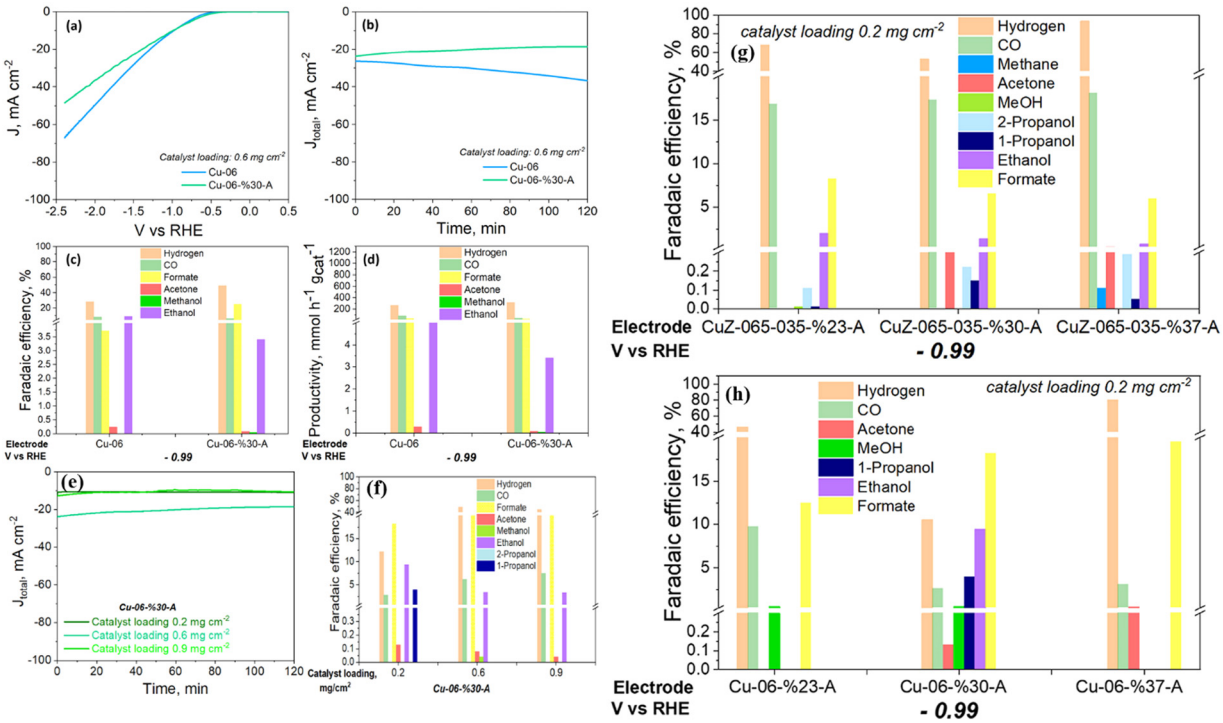

Fig. 29 The LSV responses, evolution time of total current density for the e-CO_2R, FE, and productivity of gas and liquid products were measured for Cu-06 and Cu-06-%30-A (0.6 mg cm^{-2}) in a 1 M $KHCO_3$ aqueous electrolyte at a potential of −0.99 V *vs.* RHE (a–d). The chronoamperometry responses (e) and FEs were measured for a Cu-06-%30-A catalyst with varying catalyst loading. The tests were conducted in a 1 M $KHCO_3$ aqueous electrolyte at a potential of −0.99 V *vs.* RHE (f). The FE of the US-prepared CuZ-06-035 (g) and US-prepared Cu-06 (h) catalysts, with a loading of 0.2 mg cm^{-2}, was evaluated in a 1 M $KHCO_3$ aqueous electrolyte at a potential of −0.99 V *vs.* RHE. Reproduced with permission from ref. 325. Copyright 2023, Elsevier.

dimer systems like Cu–Ru, Cu–Rh, and Cu–Ir, where two metals are traditionally unmixable in the bulk phase. To examine the compositional and structural sensitivity of e-CO_2R in this bimetallic system, model catalysts were made from Ag/Cu nanocrystals. In particular, the $Ag_1Cu_{1.1}$ NDs displayed a 3.4-fold increase in FE for C_2H_4 and a 2.0-fold improvement in the combined e-CO_2RR activity over Cu NPs of comparable size and shape.[126]

In another research study, Chen *et al.* controlled the aspect ratio and composition of alloyed nanorods made of Cu through a co-reduction synthesis process using seeds. They demonstrated different catalytic activities for p-nitrophenol reduction by the Cu_3Au nanorods tuning across the visible to infrared spectrum.[329] Zheng *et al.* have made significant progress in synthesizing e-CO_2RR catalyst materials and created highly efficient Au–Cu knot structures, referred to as NSs in this study. NSs of all types were formed by Cu growth on the concave surface of a Au seed. The final products are obtained by using *o*-phenylenediamine (OPDA) as a capping agent and $Cu(acac)_2$ as a precursor. A growth mode and high exposure to Au are typical of the anisotropic nature of the products. The Au–Cu NSs exhibited remarkable selectivity for C_{2+} product generation, with an optimum FE_{2+} of 67% and a C_{2+} partial current density of 0.29 A cm^{-2} at 0.75 V *vs.* RHE.[330] In a separate study, Wang *et al.* have developed effective catalysts for e-CO_2R by generating dense OD-Cu NPs using a three-step process (Fig. 30). This process involved the thermal oxidation of CuO_x on a Cu mesh, followed by reduction through annealing, and finally the conversion to OD-Cu by applying a cathodic potential to the partially reduced CuO_x. These OD-Cu NPs maintained their shape and exhibited the capability to produce various types of syngas at high rates with modest overpotentials.[331]

Additionally, Wang *et al.* have grown scalable arrays of metallic 2D Cu_2Te nanosheets on copper foils. During the growth process, chemical etching and vapor deposition, exposure to potential active sites at the edges of these nanosheets facilitated CO_2R to CH_4 at lower overpotentials.[332] Moreover, Han *et al.* have employed the atomic layer infiltration method using the HKUST-1 template. By uniformly adding Zn–O–Zn sites throughout HKUST-1, the FE for CO increased from 20–30% to 70–80%. Computational density-functional-theory studies revealed that this modification lowered the activation energy barrier for the reaction and accelerated CO production by increasing the enthalpy of CO_2 adsorption.[277] Furthermore, a potential electrocatalyst for CO_2R has been introduced by Sirisomboonchai *et al.* This electrocatalyst, consisting of In and Zn deposited over Cu foam, exhibited improved CO_2R to CO with a remarkable FE of 93.7% and a 100-hour operational lifetime.[333] In a related study, the impact of various sulfur precursors on the structure–property–activity relationship of copper-based catalysts for e-CO_2 conversion was investigated by Gao *et al.* The CuS-TU catalyst, synthesized using thiourea as the sulfur precursor, exhibited a distinctive flower-like structure and the highest sulfur vacancy concentration. This unique structure facilitated interfacial mass transfer during CO_2R. The abundance of sulfur vacancies on the

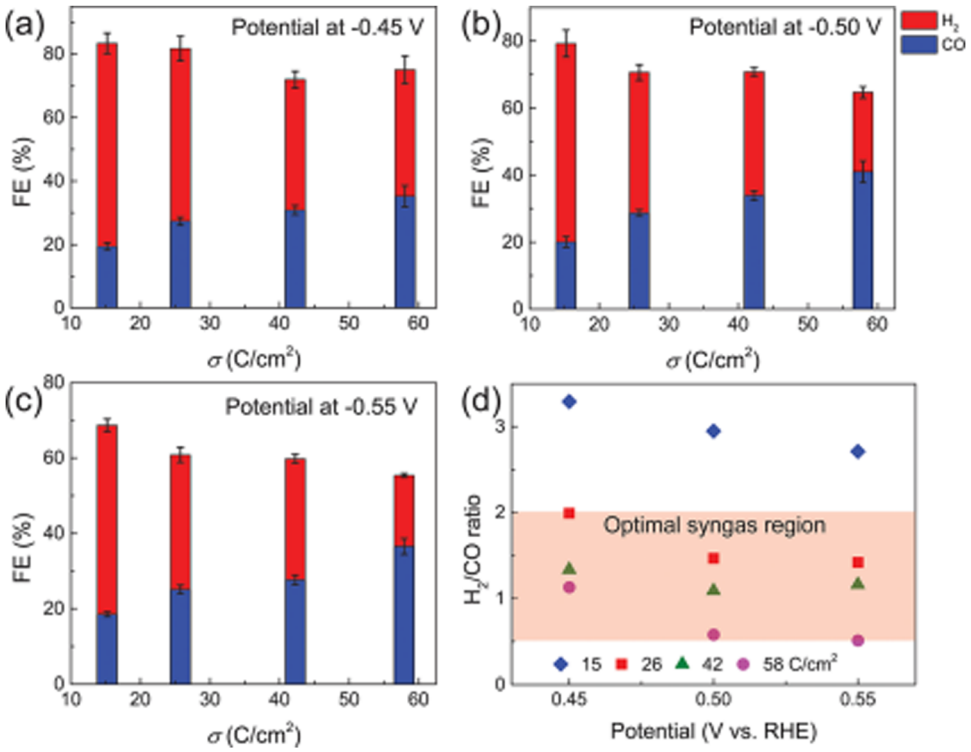

Fig. 30 The FEs of H_2 and CO production on OD-Cu NPs were measured at different applied potentials: (a) −0.45 V, (b) −0.50 V, and (c) −0.55 V. The controllable composition of syngas varies depending on the applied potentials (d). Reproduced with permission from ref. 331. Copyright 2020, American Chemical Society.

Table 16 This resourceful table provides an examination of electrocatalyst materials employed in CO_2 conversion processes. It simplifies exploration and comprehension within this domain by scrutinizing the electrochemical properties of catalysts, particularly how different precursor derived approaches influence product distribution

				≈FE%									
No.	Material	Electrolyte	V *vs.* RHE	H_2	CO	CH_4	C_2H_4	$HCOO^-$	$C_2H_5^+$	CH_3OH	C_2H_5OH	$C_2H_3O_2^-$	Ref.
1	CuZ-065-035	1 M $KHCO_3$	−0.99	52	22	—	—	5	—	—	10	—	325
2	CuZ-065-035-%30-A			80	22	—	—	2	—	—	2	—	
3	Cu GNC-VL	0.5 M $KHCO_3$	−1.07	40	—	—	—	5	—	13	42	—	327
4	Cu ZIFL@GO			60	5	—	—	9	—	14	12	—	
5	CuS/BM	0.5 M $KHCO_3$	−1.0	60	—	—	—	48	—	—	—	—	328
6	Ag NPs	0.1 M $KHCO_3$	−1.4	92	10	—	—	—	—	—	—	—	126
7	Cu NPs			34	1	32	8	1	—	—	—	—	
8	Ag_1–$Cu_{1.1}$-NDs			50	2	30	12	2	—	—	—	—	
9	Au–Cu Janus	3 M KOH	−0.75	—	—	—	37	—	—	—	20	—	330
10	Au@Cu core–shell		−0.95	—	—	—	20	—	—	—	10	—	
11	Cu NPs		−0.81	—	—	—	37	—	—	—	17	—	
12	OD-Cu NA	0.1 M $KHCO_3$	−0.55	60	19	—	—	—	—	—	—	—	331

catalyst's surface played a crucial role in increasing CO generation through the *COOH route by enhancing the adsorption of COOH intermediates. Subsequently, the CuS-TU catalyst achieved a CO selectivity of 72.67% at −0.51 V *vs.* RHE.[334] Table 16 shows different materials designed by the precursor derived approach for e-CO_2R.

6.13. Polymer modification approach

The utilization of polymer modification is an approach in the development of e-CO_2R catalysts. It plays a role in enhancing the selectivity, activity and stability of these catalysts. When researchers incorporate polymers into the structure or surface of the catalyst, they achieve some advantages. Polymers serve as stabilizers too, preventing the aggregation or dissolution of species during the CO_2RR process. This makes the catalyst more durable. Polymers also are effective as templates for controlling the nanostructure and catalyst material morphology, influencing its performance. Furthermore, the modification of polymers promotes the formation of active sites essential for efficient conversion of CO_2 into more valuable products like hydrocarbons or alcohols. The reason this is important is that making CO_2RR catalysts better and more efficient by means of such

engineering will foster sustainable carbon capture and utilization technologies. Polymer-modified catalysts with catalytic metal cores can be synthesized by multiple methods for designing CO_2RR catalysts. One of these is electrochemical deposition, in which polymer films grow onto a catalyst surface allowing precise control of thickness and composition. In another method, polymers can be incorporated into the catalyst matrix when synthesized to produce the material combining the characteristics of metals together with the stabilizing and templating effects caused by polymers. Additionally, researchers may go with a couple of possible synthesis techniques, such as chemical or physical adsorption, to introduce polymer modifiers on the catalyst surface.

Poly(ionic liquid) (PIL) NPs with multilamellar chain stacking were prepared by free radical homopolymerization. By manipulating the carbon used in the polymerization process, PIL NPs of various sizes and shell thicknesses could be synthesized. Molecular dynamics simulations corroborated the mechanism of PIL NV formation, emphasizing the role of the polymerization degree of PIL chains in determining assembly behavior. These well-defined PIL NVs with hollow interiors allowed for high loading amounts of ultra-small Cu NPs for e-CO_2R. The strong electronic interactions between PIL units and Cu atoms on the surface of Cu NPs resulted in a high FE toward C_1 products, primarily CH_4.[335] In another study, the impact of a poly(4-vinylpyridine) (P4VP) layer on the e-CO_2RR on both poly Cu and Au electrodes was investigated by Ye *et al.* The research revealed that the P4VP layer inhibits the HER and enhances CO_2RR, particularly the production of HCOOH. In *in situ* ATR-SEIRAS tests, fewer CO adsorption bands were observed on P4VP-modified Cu electrodes, while higher ICO_2/$IHCO_3$ ratios were detected on P4VP-modified Au electrodes. These observations suggest that the mass transfer of H_2O and HCO_3 from the bulk to active sites is impeded by the P4VP modification. Importantly, the hydrophilicity of the electrode surface is altered by the presence of P4VP, leading to increased HCOOH production at low overpotentials.[336] Furthermore, polymer coatings can modify local pH levels, hydrophilicity/hydrophobicity, and reactant concentrations. Jun *et al.* have demonstrated that polymer coatings can enhance the catalytic selectivity of Cu-based catalysts in CO_2RR while also improving electrocatalytic stability.[337]

Additionally, the impact of three different ionomers on Cu-catalyzed CO_2RR under high-current conditions was investigated. In this investigation, it was observed that the anionic ionomer Nafion had a negligible effect on CO_2RR, likely due to the negatively charged nature of the electrode/catalyst interface. However, the cationic ionomers XA-9 and PTP had significant effects on the selectivity of CO_2RR with Cu catalysts. Specifically, PTP led to increased HER and formate synthesis, likely due to decreased mass transport. In contrast, XA-9 favored the production of CO at the expense of C_{2+} products.[338] Moreover, another study highlighted the influence of different polymeric binders used during electrode fabrication on the selectivity of CO_2RR on Cu electrodes (Fig. 31). The research findings demonstrate that the choice of binder material can significantly modify the selectivity of CO_2RR products. Specifically, it was observed that Cu electrodes with polyvinylidene fluoride as the binder favored the production of CH_4, while Cu electrodes with polyacrylic acid as the binder exhibited greater selectivity for HCOOH generation.[339]

Liang *et al.* have developed a novel single-site copper coordination polymer known as Cu(OH)BTA. Notably, this polymer exhibits a 1.5 times higher selectivity for producing C_2H_4 compared to its metallic counterpart (Fig. 32). An interesting feature of this catalyst is that it maintains its structural integrity throughout the reaction. This advantageous characteristic allows for the formation of an energetically favorable *OCCHO intermediate during CO hydrogenation, facilitated by suitably distanced dual sites provided by adjacent copper atoms in the polymer. The study also demonstrates the practical applicability of this polymers by running full-device CO_2 electrolysis for 67 hours at an appropriate current in a membrane electrode assembly.[311]

Additionally, Wang *et al.* have explored a unique approach for enhancing the selectivity of heterogeneous Cu catalysts for CO_2RR employing random copolymers as surface modifiers. Among these copolymers, a tricomponent variant demonstrated superior performance in maximizing the FE for ethylene and C_{2+} products during CO_2RR. Surface characterization conducted under CO_2RR conditions highlighted the copolymer's resilience, attributed to the presence of a phenylpyridinium component. Advanced techniques, including AFM, SEM, and XPS, were utilized to counter the presence of nanostructuring and electrical effects. Molecular dynamics simulations illustrated that the optimal polymer modifier led to localized increases in CO_2 content. Moreover, compared to block copolymers, random copolymers exhibited greater porosity, facilitating improved access and mass transport of reactants.[340] Furthermore, Wei *et al.* demonstrated that coating Cu surfaces with a PANI thin film can significantly alter the catalytic activity and selectivity for CO_2RR. The NH group on PANI interacts with CO_2 molecules, enriching the presence of CO_2 and inhibiting the HER on Cu surfaces. Consequently, the CO_2RR current density at the Cu/PANI interface experiences a substantial increase. This transformation leads to a shift from 15% C_{2+} hydrocarbon production on pure Cu to over 60% on Cu-PANI, making C_{2+} hydrocarbons the dominant products.[341]

On another front, researchers have synthesized and evaluated two stable Cu(I)-based coordination polymer electrocatalysts, NNU-32 and NNU-33(H), designed for e-CO_2RR within a flow-cell electrolyzer. These electrocatalysts exhibit exceptional selectivity for converting CO_2 into CH_4, achieving a FE of 82% at −0.9 V *vs.* RHE. The outstanding selectivity is attributed to the presence of cuprophilic interactions within the catalysts. Furthermore, a dynamic *in situ* crystal structure transformation from NNU-33(S) to NNU-33(H) enhances cuprophilic interactions and CO_2 adsorption. This structural change, involving the substitution of hydroxyl radicals for sulfate radicals, significantly contributes to the superior performance of these electrocatalysts. It is worth noting that cuprophilic contacts play a pivotal role in CH_4 production, and the selectivity for CH_4 varies with the number and proximity of interacting cuprophiles.[342] Furthermore, Li *et al.* have found that by stabilizing a metal-

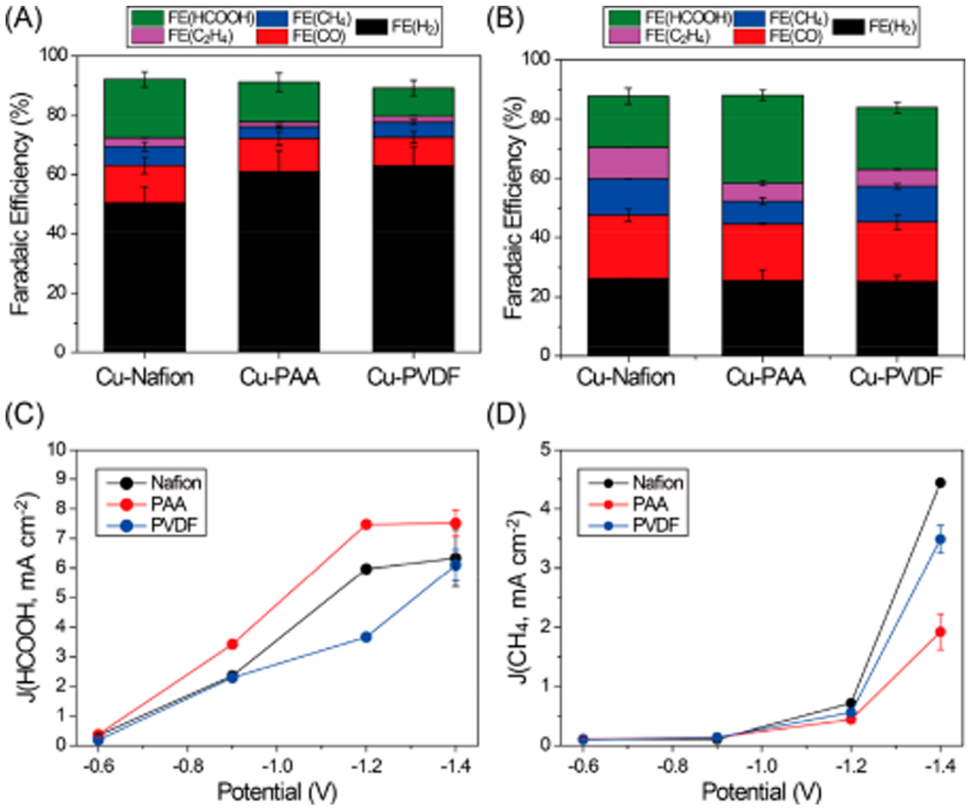

Fig. 31 The CO_2RR performance of various Cu/C catalysts with different binders was evaluated. The FE of HCOOH, CO, CH_4, C_2H_4, and H_2 was evaluated at two different potentials: −0.6 V and −1.4 V (A and B). The partial current density profiles of HCOOH and CH_4 are presented (C and D). Reproduced from ref. 339. Open access article, American Chemical Society.

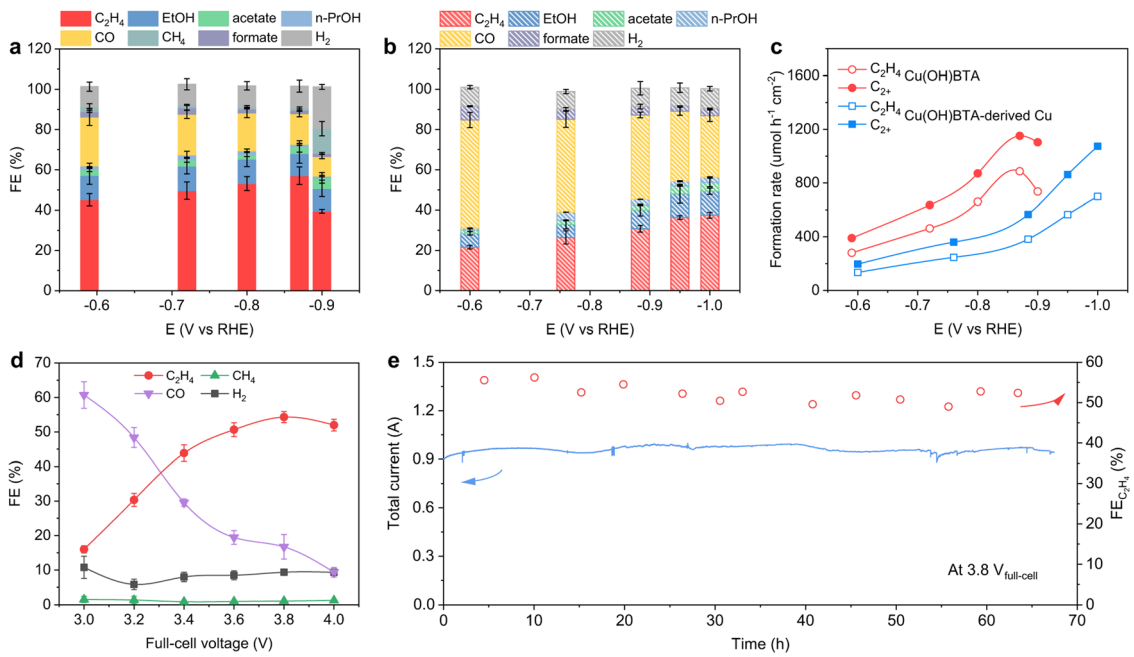

Fig. 32 The study investigated the FEs of various products at different applied potentials using Cu(OH)BTA (a) and Cu(OH)BTA-derived Cu (b) in a 1 M KOH electrolyte. The study also investigated the formation rates of C_{2+} products and C_2H_4 under varying applied potentials using Cu(OH)BTA and Cu(OH)BTA-derived Cu in a 1 M KOH electrolyte (c). The study also measured the FEs of various gas products within the voltage range of 3.0–4.0 V using a membrane-electrode assembly device (d). The electrosynthesis of C_2H_4 was conducted in a membrane-electrode assembly with a geometric electrode area of 4 cm^{-2}. The catalyst maintained its overall current and ethylene FE for a duration of 67 hours (e). The error bars for the uncertainty of the FE analysis represent one standard deviation, which is calculated based on three independent samples. Reproduced from ref. 311. Open access article, Nature.

Table 17 The table comprehensively summarizes electrocatalyst materials explicitly designed for reducing CO_2 emissions with a focus on polymer modification techniques. It explores the performance of polymers and investigates how modifications impact both selectivity and efficiency, in producing desired products

				≈FE%									
No.	Material	Electrolyte	V *vs.* RHE	H_2	CO	CH_4	C_2H_4	$HCOO^-$	$C_2H_5^+$	CH_3OH	C_2H_5OH	$C_2H_3O_2^-$	Ref.
1	NWs/Cu	0.1 M $KHCO_3$	−1.0	27	34	7	14	—	—	—	—	—	335
2	Pristine CuNPs			30	15	3	22	—	—	—	—	—	
3	Poly Cu	0.1 M $KHCO_3$	−0.9	57	12	4	2	27	—	—	—	—	336
4	P4VP-modified Cu			95	5	3	2	32	—	—	—	—	
5	Cu-P1	1 M KOH	−0.97	1	5	—	73	1	—	—	1	—	337
6	Cu-P4			30	3	2	35	15	—	—	1	—	
7	Cu	0.5 M $KHCO_3$	−0.86	—	6	—	7	15	—	—	3	—	338
8	Cu/Nafion			—	5	—	7	6	—	—	1	—	
9	Cu/XA-9			—	12	—	8	20	—	—	2	—	
10	Cu/PTP			—	2	—	—	10	—	—	—	—	
11	Cu-Nafion	0.1 M $KHCO_3$	−1.4	28	20	12	10	18	—	—	—	—	339
12	Cu-PAA			28	18	6	4	34	—	—	—	—	
13	Cu-PVDF			28	20	12	4	18	—	—	—	—	
14	Cu(OH)BTA	0.1 M $KHCO_3$	−0.6	10	23	2	45	2	—	—	13	—	311
15	Cu(OH)BTA-derived Cu			10	55	—	20	7	—	—	8	—	
16	Cu	0.1 M $KHCO_3$	−1.04	39.7	0.5	25.6	22.3	1.8	—	—	5.9	—	340
17	Cu-1			94.6	—	1.5	—	0.7	—	—	—	—	
18	Cu-2			69.3	1	14.1	5.3	6.6	—	—	—	—	
19	Cu-3			37.8	2.8	14	21.5	11.1	—	—	3.4	—	
20	Cu-4			34.1	0.4	33.1	19	3.8	—	—	3.9	—	
21	Cu-5			33.6	0.5	28.1	25.4	1.1	—	—	6	—	
22	Cu-6			32.5	1.1	22.3	30.4	1	—	—	9.3	—	
23	Cu-7			16.5	1.2	4.7	49.5	2.2	—	—	16	—	
24	Cu-8			11.9	0.7	1.9	55.6	1.9	—	—	17.4	—	
25	Cu-9			19.2	0.4	2.8	53.8	0.9	—	—	15.5	—	
26	Cu-10			35	1	11.5	36.8	1.8	—	—	9.5	—	
27	Cu-11			36.2	2.3	8.7	31.7	9	—	—	4.3	—	
28	Cu-12			44.8	0.5	25	20.4	1.4	—	—	5.2	—	
29	Cu-13			21.9	0.6	5.7	59.8	1.3	—	—	11.8	—	
30	Cu-*block*-8			30.5	0.6	14.1	34.5	2.4	—	—	11	—	
31	Cu	0.1 M $KHCO_3$	−1.1	45	3	5	5	27	—	—	10	—	341
32	Cu-PANI			17	2	11	30	10	—	—	13	—	
33	NNU-33(H)	1 M KOH	−1.0	13	12	63	13	—	—	—	—	—	342

bound CO intermediate, Nafion-modified electrodes can significantly enhance the production of CH_4. To precisely regulate the transfer of protons to the metal–CO intermediate, Cu electrodes were constructed using a polymer blend of Nafion and polyvinylidene fluoride. This precise control mechanism leads to increased rates of production for C_{2+} products such as ethylene, ethanol, and 1-propanol. Importantly, under these controlled conditions, hydrogen evolution does not occur, as almost all carbon-containing products can be extracted from Cu electrodes equipped with a 15 m Nafion overlayer.[343] Furthermore, the e-CO_2R to high-energy-density C_{2+} products necessitates carbon–carbon interactions. In this context, Zhang *et al.* have explored the use of capping agents and electrochemical treatment to fabricate polycrystalline Cu catalysts. These catalysts exhibit a 34% FE for the production of C_2H_4 at −1.5 V *vs.* RHE. Importantly, a critical *COOH intermediate was observed on the Cu surfaces, as confirmed by quasi-*in situ* total reflection FTIR analysis.[344] Different polymers were used for modification of e-CO_2R performance of different materials, which is summarized in Table 17.

6.14. Support engineering approach

Support engineering plays a role in the design of e-CO_2R catalysts as it focuses on selecting and modifying support materials to improve catalytic performance. This approach enables researchers to optimize the sites of the catalyst by providing a conductive platform for reactions. By choosing support materials and manipulating their properties scientists can enhance the efficiency, durability and economic viability of CO_2RR catalysts for sustainable carbon capture and utilization technologies. In the strategy of support engineering for CO_2RR catalyst design, there are methods that can be employed. One common approach is depositing nanoparticles or single atoms onto support materials like graphene, carbon nanotubes or metal oxides such as TiO_2 and ZnO. Another method involves modifying support materials through surface functionalization or doping to influence the binding energies of CO_2 and reaction intermediates, thereby customizing the selectivity of the catalyst. Additionally creating materials by combining components with suitable supports offers a versatile solution that combines advantages from both components. In the quest for effective e-CO_2R to value-added syngas, a technique has been devised utilizing anion-regulated self-supported Cu_3Se_2 nanosheet-assembled fibers (Fig. 33). These fibers exhibit an excellent TOF of 1303 h^{-1} over a wide potential window and accommodate a broad range of H_2-to-CO ratios from 0.8 to 6.0. Remarkably, they can sustain bulk electrolysis for 10 hours, owing to their high current density and minimal attenuation.[345]

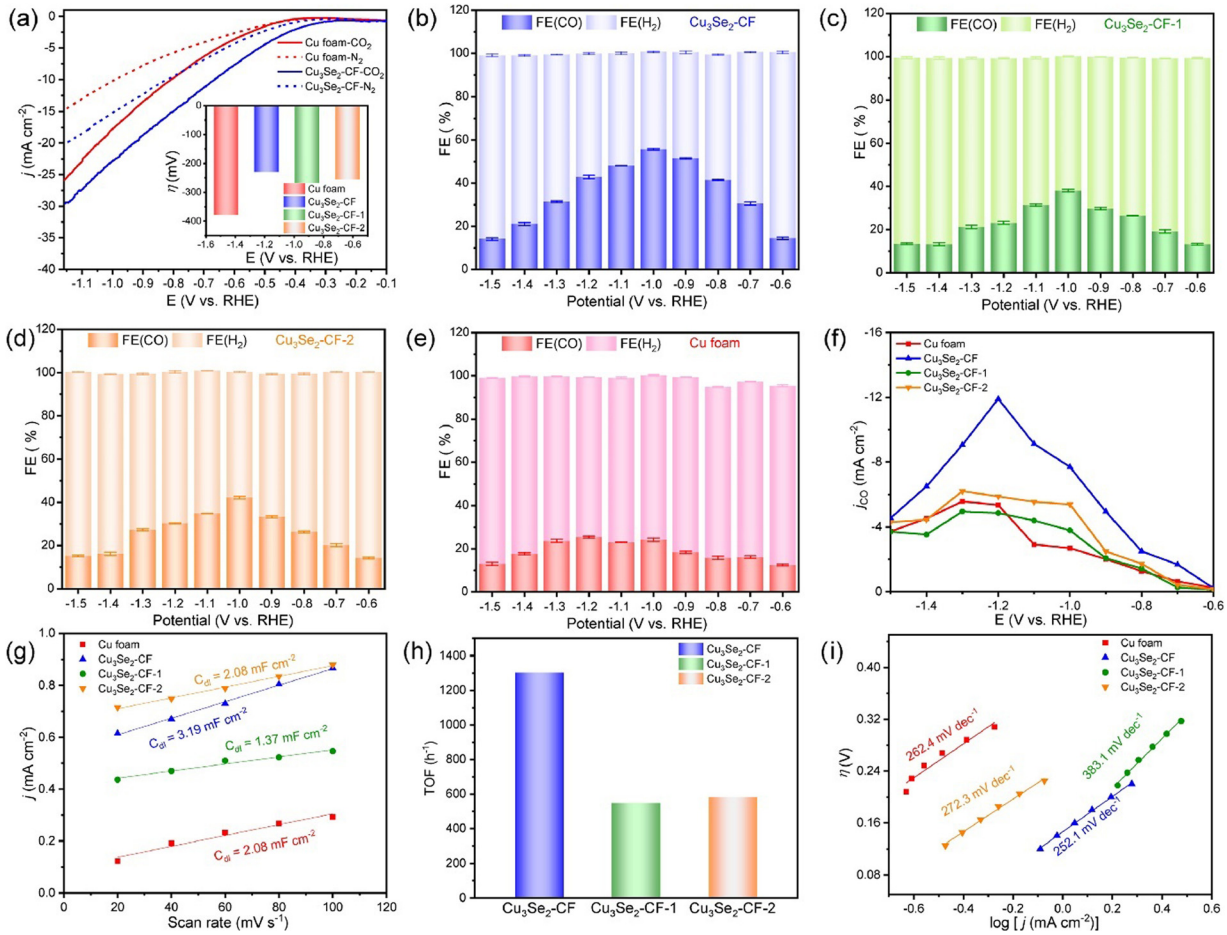

Fig. 33 The CO_2R of Cu foam and Cu_3Se_2-CF nanocatalysts. LSV traces were obtained in a CO_2-saturated or N_2-saturated electrolyte using a scan rate of 5 mV s^{-1} (a). The inset in (a) shows the onset potential. The total FE was determined for gaseous products only, specifically H_2 and CO (b)–(e). The j_{CO} was measured at different applied potentials (f). The double-layer capacitance was measured (g). TOFs were calculated (h). Tafel slopes were determined for Cu foam, Cu_3Se_2-CF, Cu_3Se_2-CF-1, and Cu_3Se_2-CF-2 (i). The data were collected under standard ambient temperature and pressure conditions, using a CO_2 stream with a flow rate of 20 sccm. Error bars represent the standard deviation of a minimum of three independent measurements. Reproduced with permission from ref. 345. Copyright 2023, Elsevier.

Furthermore, an oxide-derived composite material supported on N-doped graphene was designed by Dongare *et al.* It was found that by adjusting the Cu to Zn ratio during the coprecipitation process, one can customize the electrocatalyst's composition to meet specific requirements. Notably, an electrode containing 20 wt% Zn in conjunction with copper exhibits the highest selectivity for ethanol production (FE = 34.25%), while the CuO/NGN electrode demonstrates lower selectivity for ethanol and other C_2 compounds.[346] Furthermore, pyrolyzing mixed precursors of $Cu(NO_3)_2$ and polyvinyl pyrrolidone produces Cu/NC composite electrocatalysts for catalyzing CO_2 reduction. Among these, Cu-20/NC stands out due to its substantial Cu nanoparticle size and extensive coverage of the carbon support surface, resulting in highly competitive HER activity. Conversely, Cu-5/NC, with its nanoparticle morphology, favors poor C–C coupling activity and CH_4 formation. Meanwhile, Cu-10/NC exhibits remarkable selectivity for CO and hydrocarbons, leading to an impressive 37% $FE_{C_2H_4}$ at −1.2 V and enhanced e-CO_2R to C_2H_4 conversion activity, selectivity, and durability.[347] Moreover, Gu *et al.* have demonstrated that the incorporation of Cu onto PCC supports yields intriguing e-CO_2R outcomes, particularly with improved selectivity for C_2 products like ethanol and ethylene. Among Cu_5-PCC, Cu_{10}-PCC, and Cu_{20}-PCC, Cu_{15}-PCC outperforms in various applied potentials, offering a more cost-effective approach to e-CO_2R by leveraging affordable and abundant minerals as the foundation for suitable electrocatalysts.[348]

In another study, Lim *et al.* have developed a CuS_x catalyst for e-CO_2R by dipping Cu foil into an industrial CO_2-purged electrolyte containing H_2S gas. Increasing the H_2S concentration significantly improved the maximum FE_{HCOOH} from 22.7% to 71.8%, attributed to the reaction between Cu foil and sulfur species. Notably, these catalysts demonstrated excellent performance in both pure CO_2-purged electrolytes and industrial CO_2-purged electrolytes, maintaining stability for 12 hours.[349] Furthermore, Kim *et al.* have explored the e-CO_2R on copper through pulsed electrolysis. The cathode's potential was cyclically shifted between −0.8 V *vs.* RHE and −1.15 V *versus* RHE over durations ranging from 5 seconds to 25 seconds. Notably, static electrolysis at −1.15 V *vs.* RHE resulted in a decreased FE_{HER} while simultaneously increasing the FE for the

CO_2RR. However, when pulsed electrolysis was employed, the FE_{HER} decreased, whereas the FE for CO_2RR increased. The optimal duration for pulsed electrolysis was found to be 10 s at each potential, achieving the lowest FE for the HER and the highest FE for the CO_2RR. Additionally, pulsed electrolysis introduced changes in the ratio of oxygenated to hydrocarbon products and significantly boosted the FE for C_{2+} products.[350]

Moreover, by enhancing the geometric partial current density of hydrocarbons through surface modification of copper foam with poly(acrylamide), the faradaic output of ethylene can be doubled. While poly(allylamine) completely impedes CO_2R, poly(acrylic acid) exerts only a transient impact. Through mechanisms such as CO activation for dimerization, stabilization of CO dimers *via* hydrogen bond interactions, and facilitation of CO adsorption in proximity to the polymer, poly(acrylamide) adheres to copper through oxygen on carbonyl groups, thereby increasing the efficiency of ethylene formation. Achieving high CO_2 mass transfer rates, utilizing modified poly(acrylamide), and employing porous copper catalysts all contribute to improved ethylene production.[351] In another study, the e-CO_2R was demonstrated using Bi-doped SnO nanosheets on a Cu foam substrate. Remarkably, the Bi–SnO/Cu foam electrode achieved the highest FE (93%) and HCOOH selectivity (99%), with exceptional long-term stability over 30 hours of operation. The Bi doping played a pivotal role in stabilizing divalent tin on the electrocatalyst, making its reduction to metallic tin more challenging. Additionally, the presence of Cu foam influenced the catalysis by promoting electron transfer, thereby maintaining tin in a positively oxidized state favorable for the adsorption of *OOCH intermediates.[352]

In a separate investigation, various synthetic approaches were employed to produce Cu nanoparticles with sizes ranging from 10 to 30 nm, supported by VC, KB, and SWNTs. Importantly, these carbon-supported Cu nanocatalysts demonstrated higher selectivity for C_2H_4 production compared to electrodeposited Cu. The onset potentials for C_2H_4 generation exhibited significant shifts for well-dispersed 40 wt% Cu/VC and 20 wt% Cu/SWNT catalysts in comparison to electrodeposited Cu.[353] In another work, a porous Cu-NC composite catalyst for e-CO_2R was synthesized using a scalable glucose blowing process. The catalyst exhibited remarkable efficiency (69% at 590 mV) in converting CO_2 to C_1 products, underscoring its strong catalytic activity.[354] Furthermore, the one-step pyrolysis synthesis of Cu Ps/BCF from butterfly wing carbon fibers and copper salt resulted in a material with unusual geometric features, including low-coordinated active spots at stepped surfaces. Increased conductivity from nitrogen dopants allows CO_2 to be reduced to C_2H_4 at a low applied voltage while maintaining excellent selectivity and long lifetime.[355]

Additionally, Kordus *et al.* have analyzed the activity and selectivity of ZnO-supported Cu nanoparticles in methanol synthesis, revealing that the shape of the pre-catalyst (cubic *vs.* spherical) played a significant role. Cubic Cu particles exhibited higher activity for methanol synthesis but significantly reduced selectivity compared to spherical particles, underscoring the substantial changes in the morphology and composition of the shaped pre-catalysts under reaction conditions.[356] Also, another research study has demonstrated that $Cu_{1.8}Se$ nanowires on Cu foam serve as effective electrocatalysts for the selective CO_2R to higher-value C_2 products, such as C_2H_4 and EtOH, with promising applications in the chemical and fuel industries. These nanowires exhibit impressive FE of 55% and 24% at −1.1 V and maintain exceptional stability over extended periods. The presence of significant concentrations of CO_2 and Se species was likely responsible for the observed high selectivity toward the C_2/C_1 product.[357]

In a related study, a series of Cu catalysts with adjustable particle sizes were constructed within a Zn, N-doped carbon matrix generated from ZIF-8. Crystal diameters ranging from 8.9 to 27.3 nm were observed in the enclosed Cu metal catalysts. Notably, catalysts with a grain size of 15.7 nm exhibited the highest FE_{CO} (approximately 80%), directly correlating with their performance in the CO_2RR.[358] In a separate investigation, Lou *et al.* have conducted experiments in an H-type reaction cell and a continuous-flow membrane electrode assembly (MEA) reactor to evaluate the performance of CuBi bimetallic catalysts in selectively reducing CO_2 to formate. The study revealed that co-electrodeposition potentials of 0.6 V yielded the best performance, with the catalyst achieving a remarkable $FE_{formate}$ (98.3%) at a current density of 56.6 mA cm^{-2} in the continuous-flow MEA reactor, outperforming the H-type reaction cell. Additionally, the study identified the optimal elemental ratio of Cu to Bi at 0.6 V to maximize the catalyst's activity.[359]

In another breakthrough, a novel fast-reduction approach was employed to create a Cu-decorated porous Bi/Bi_2O_3 nanofoam, denoted as P-Cu-BiNF. The nanoparticles forming the 3D porous network architecture of P-Cu-BiNF are consistently sized at 15–20 nm. The inclusion of Cu into P-Cu-BiNF enhances CO_2R performance by controlling the morphology and local electronic state of Bi/Bi_2O_3. Remarkably, P-Cu-BiNF exhibits a CO_2-to-formate FE exceeding 90% across a wide potential range of 0.78 to 1.08 V, providing a high formate partial current density of 62.7 mA cm^{-2} at 1.18 V while maintaining exceptional stability over time.[360] Additionally, another research study investigated nano-sized Cu_2O on three different carbon-based substrates, namely BG (positively charged), NG (negatively charged), and rGO (weakly negatively charged), for e-CO_2R with promising results. The use of these substrates led to an increase in the FE of C_2 products, with the FE_{C_2}/FE_{C_1} ratio ranging from 0.2 to 7.1, where rGO/Cu > BG/Cu > pure Cu > NG/Cu. Notably, under CO_2R conditions, the negatively charged NG stabilized Cu^+ species, thereby improving CO* adsorption and enhancing C–C coupling for C_2 products. Consequently, at high current densities, the $FE_{C_{2+}}$ was significantly increased to around 68%.[361] Moreover, it is proposed that introducing different functional groups to Cu based electrocatalysts (N-, G-, COOH, NH_2, and OH) can modify their selectivity and, in turn, their ability to adsorb crucial intermediates. Catalysts containing N and OH functional groups exhibit selectivity for C_1 products close to 90% during e-CO_2R catalysis.[362] Conclusively, the support engineering approach is considered as an efficient approach for designing e-CO_2R catalysts. An overview of different materials designed by following this approach is given in Table 18.

Table 18 This table explores how support engineering approaches influence electrocatalyst materials within the context of CO_2R. The table showcases a range of electrocatalyst materials that have been specifically created for CO_2R. By examining the behavior, product selectivity and efficiency of these materials, valuable insights are gained

				≈FE%									
No.	Material	Electrolyte	V *vs.* RHE	H_2	CO	CH_4	C_2H_4	$HCOO^-$	$C_2H_5^+$	CH_3OH	C_2H_5OH	$C_2H_3O_2^-$	Ref.
1	Cu foam	0.1 M $KHCO_3$	−1.1	76	24	—	—	—	—	—	—	—	345
2	Cu_3Se_2-CF			52	48	—	—	—	—	—	—	—	
3	Cu_3Se_2-CF-1			33	67	—	—	—	—	—	—	—	
4	Cu_3Se_2-CF-2			65	35	—	—	—	—	—	—	—	
5	CuO-NGN	0.1 M $KHCO_3$	−1.0	—	—	—	—	—	—	—	3	—	346
6	$CuZn_{10}$-NGN			—	—	—	—	—	—	—	7	—	
7	$CuZn_{20}$-NGN			—	—	—	—	—	—	—	13	—	
8	$CuZn_{30}$-NGN			—	—	—	—	—	—	—	3	—	
9	$CuZn_{40}$-NGN			—	—	—	—	—	—	—	3	—	
10	Cu-0/NC	0.1 M $KHCO_3$	−1.0	65	3	—	14	—	—	—	—	—	347
11	Cu-5/NC			22	23	5	19	—	—	—	—	—	
12	Cu-10/NC			16	18	3	8	—	—	—	—	—	
13	Cu-15/NC			38	20	1	7	—	—	—	—	—	
14	Cu-20/NC			62	6	1	3	—	—	—	—	—	
15	Pure Cu samples			25	7	1	17	—	—	—	—	—	
16	Cu5-PCC	0.1 M $KHCO_3$	−1.0		18		2	27	—	—	6	—	348
17	Cu10-PCC				10		5	23	—	—	6	—	
18	Cu15-PCC				22	2	12	26	—	—	16	—	
19	Cu20-PCC				15		8	20	—	—	5	—	
20	CuS_x	0.1 M $KHCO_3$	−1.0	—	32	—	—	15	—	—	—	—	363
21	Cu foam	0.1 M $NaHCO_3$	−0.96	15	1	4	13	—	—	—	—	—	351
22	Cu-P-acrylamide			15	2	2	27	—	—	—	—	—	
23	Cu-P-acrylic acid			16	1	3	17	—	—	—	—	—	
24	Cu-P-allylamine			30	—	0.5	—	—	—	—	—	—	
25	Bi-SnO/Cu foam	0.1 M $KHCO_3$	−1.6 Ag/AgCl	10	2	—	—	87	—	—	—	—	352
26	SnO/Cu foam			17	3	—	—	77	—	—	—	—	
27	Cu foam			58	4	—	—	15	—	—	—	—	
28	Electrodeposited Cu	0.1 M $KHCO_3$	−1.6	38	37	1	2	—	—	—	—	—	364
29	20 wt% Cu/VC			50	10	1	2	—	—	—	—	—	
30	40 wt% Cu/VC			30	20	1	11	—	—	—	—	—	
31	20 wt% Cu/SWNT			40	18	1	17	—	—	—	—	—	
32	50 wt% Cu/KB			41	17	5	10	—	—	—	—	—	
33	Cu-NC 1 : 1	0.1 M $KHCO_3$	−1.0	—	10	—	—	43	—	—	—	—	365
34	Cu-NC 2 : 1			—	13	—	—	35	—	—	—	—	
35	Cu-NC 1 : 2			—	13	—	—	42	—	—	—	—	
36	NC			—	12	—	—	—	—	—	—	—	
37	Cu@Vul	0.5 M $KHCO_3$	−1.0	52	28	8	3		—	—	—	—	366
38	Cu@KB			43	49	2	5		—	—	—	—	
39	Cu@MGS			42	48	5	1		—	—	—	—	
40	Cu Ps/BCF	0.1 M $KHCO_3$	−1.0	35	2	1	54	8	—	—	—	—	355
41	$Cu_{1.8}Se$	0.1 M $KHCO_3$	−1.0	—	2	—	30	3	—	—	20	—	367
42	ZNC	0.1 M $KHCO_3$	−0.7	80	20	—	—	—	—	—	—	—	358
43	Cu@ZNC-1			55	42	—	—	—	—	—	—	—	
44	Cu@ZNC-2			38	65	—	—	—	—	—	—	—	
45	Cu@ZNC-3			23	80	—	—	—	—	—	—	—	
46	Cu@ZNC-4			43	60	—	—	—	—	—	—	—	
47	CuBi	0.5 M $KHCO_3$	−1.07	—	—	—	—	98.3	—	—	—	—	359
48	Bulk BI	0.5 M $KHCO_3$	−1.0	—	—	—	—	91	—	—	—	—	368
49	P-Bi			—	—	—	—	85	—	—	—	—	
50	P-Cu-BiNF			—	—	—	—	90	—	—	—	—	

6.15. Defect engineering approach

Defect engineering plays a role in designing e-CO_2R catalysts as it greatly influences their reactivity, selectivity and overall performance. Defects like vacancies, dislocations and grain boundaries serve as sites for reactions affecting the binding energies of reactants and intermediates. The significance of this approach lies in its ability to customize the surface chemistry of catalyst materials promoting reaction pathways and desired products while minimizing side reactions. By introducing and controlling defects, researchers can enhance the efficiency of CO_2 conversion into chemicals and fuels contributing to sustainable energy conversion and carbon capture technologies. To incorporate engineering into CO_2RR catalyst design, several methods can be employed. One approach involves synthesizing nanostructured materials with defects like metal nanoparticles with lattice imperfections. Another approach includes treating catalysts after synthesis through annealing in atmospheres to induce formation. Surface modification techniques such as chemical functionalization or atomic layer deposition can also be utilized to introduce

controlled defects onto the catalyst surface. Furthermore, combining strain engineering with defect engineering can lead to CO_2RR performance improvement.

In a related investigation, the study focused on faulty graphene-supported Cu_4S_2 clusters and isolated Cu_4Xn clusters for e-CO_2R to C_1 products. DFT simulations reveal that among the C_1 products on Cu_4X_2 clusters, CH_3OH exhibits the most favorable limiting potential, spanning from Cu_4S_2 to Cu_4Se. When it comes to selectivity and catalytic activity (−0.48 V), the Cu_4S_2 cluster stands out in the CO_2 conversion process. The introduction of defect-engineered graphene increases the robust interaction between the cluster and the substrate, leading to enhanced catalytic performance. Crucially, the Cu_4S_2/SV catalyst excels in suppressing competing reactions such as HER, CO, and HCOOH generation, thereby exhibiting superior activity in producing CH_3OH at low potential.[369] In a related study, Zhang *et al.* investigated e-CO_2R, with a specific focus on the use of nano-defective Cu nanosheets as catalysts, aiming to enhance the production of ethylene efficiently. Remarkably, the results demonstrate that at a current density of approximately 60 mA cm^{-2}, the ethylene FE can be significantly increased to an impressive 83.2% when employing these nano-defective Cu nanosheets as catalysts. The key role played by these nano-defects involves providing highly concentrated atomic defects that enrich reaction intermediates while limiting OH^- availability. This dual effect facilitates C–C coupling reactions and ultimately enhances ethylene production.[24]

Simultaneously, another study has successfully synthesized and dispersed CeO_2 nanotubes with diameters ranging from 100 to 300 nm and 30 to 50 nm. Importantly, these nanotubes maintain their morphology even after being loaded with Cu and Ni. The interaction between these metals leads to enhanced dispersion and reducibility within the bimetallic Cu–Ni system, effectively reducing the activation barrier for CO adsorption and promoting hydrogenation to CH_3OH. Notably, robust Cu–Ni alloy–CeO_2 interactions further increase the reducibility of surface CeO_2, facilitating the transition from Ce^{4+} to Ce^{3+}.[370] In another significant development, Zhou *et al.* have conducted hydrothermal synthesis to create catalysts based on MoS_2 with varying levels of Cu doping. The incorporation of metallic Cu into the catalyst resulted in improved crystallinity, increased layer thickness, and an increased number of sulfur vacancies. Notably, the 5% Cu-MoS_2 catalyst exhibited CH_3OH production that was 2.27 times higher than that of the pure catalyst, indicating its superior efficiency in converting CO_2 to methanol.[371] Furthermore, a La_2CuO_4 perovskite catalyst was also designed for e-CO_2R, leading to the generation of CH_4. At −1.4 V *vs.* RHE, this catalyst achieved a partial current density of 117 mA cm^{-2} for CH_4 production, with a high FE of 56.3%. Interestingly, during cathodic CO_2 methanation, the perovskite structure evolves simultaneously with the formation of a Cu/La_2CuO_4 heterostructure.[372]

Additionally, Deng *et al.* have explored the e-CO_2R to formate using a sulfur-doped copper catalyst. Sulfur dopants were found to play a crucial role in enhancing the AC–CuS_x catalyst's ability to selectively produce formate. The presence of sulfur on the copper surface altered the adsorption strength of adsorbed HCOO*, resulting in increased formate synthesis and reduced *COOH generation, which is an intermediate in the pathway to CO production.[373] In another significant development, Wang *et al.* have successfully created a Cu-doped CeO_2 electrocatalyst for the selective CO_2R to CH_4. The strong interaction between CeO_2 and Cu results in the formation of single-atomic-distributed Cu species, which in turn generate numerous OVs in close proximity to one another (Fig. 34). This atomic dispersion of electrocatalytic Cu sites, coupled with the surrounding OVs and the cooperative effect from the CeO_2 framework, accounts for the exceptional efficiency of this catalytic site in converting CO_2 molecules into CH_4.[374]

In the quest for more efficient catalysts for CO_2R, Yang *et al.* have explored the synthesis of a (Cu, N) co-doped SnO_2 material through hydrothermal synthesis and calcination (Fig. 35). This doping strategy significantly improved the catalyst's activity, selectivity, and long-term stability. Notably, the catalyst achieved its highest catalytic activity, reaching 54.97%, when co-doped with 7% Cu and N. Furthermore, this doping strategy reduced the material's band gap from 1.058 eV (pure SnO_2) to 0.518 eV (7% doped SnO_x), enhancing its ability to absorb visible light.[375]

Zhang *et al.* have developed copper nanowires with a high density of flaws for e-CO_2R to C_2H_4. These nanowires exhibit a broad potential window for C_2H_4 synthesis and a high selectivity for C_2 products.[376] In a related study, Wu *et al.* have inserted point defects and planar defects into the Cu substrate. These defects are then used to successfully construct a highly diluted SnCu polycrystal. The electrical effect is optimized through the combined use of Sn doping and grain boundaries, which prevent H_2 evolution and encourage CO_2 hydrogenation.[377] In another research endeavor, density functional theory calculations were employed to examine CO_2R over three defective facets in Cu_2O. OVs were found to significantly reduce the activation barrier for C–O bond breakage, from 3.2 to approximately 1 eV. Furthermore, when Cu_2O is combined with plasmonic metals, the remaining barrier is further reduced or even eliminated under plasmon-excited states.[378] Furthermore, Wang *et al.* revealed a method for producing binder-free, OV-rich Cu/CuO_x in-plane heterostructured nanosheet arrays (Cu/CuO_x/CF) using Cu foam as a support. The nanosheet morphology plays a crucial role during electrocatalysis by promoting efficient mass and charge transfer through the exposure of active sites. The electronic structure of these active sites is modified through the synergistic effects of in-plane heterojunctions and OVs, influencing adsorption characteristics and preventing the formation of byproducts.[379]

Moreover, Zhang *et al.* have developed a CuPc/DG composite for the e-CO_2R into formic acid. The presence of defective graphene in the composite plays a significant role in altering the electronic structure of Cu active centers through π-stacking interactions. The composite exhibits a partial current density of 5.28 mA cm^{-2} for HCOOH production, a remarkable FE of 44.6% at 0.78 V *vs.* RHE for CO_2RR to HCOOH, and exceptional stability, maintaining its performance for at least 20 hours of continuous reaction.[380] Furthermore, in the pursuit of methane generation at single-atomic Cu active sites, Patra *et al.* have

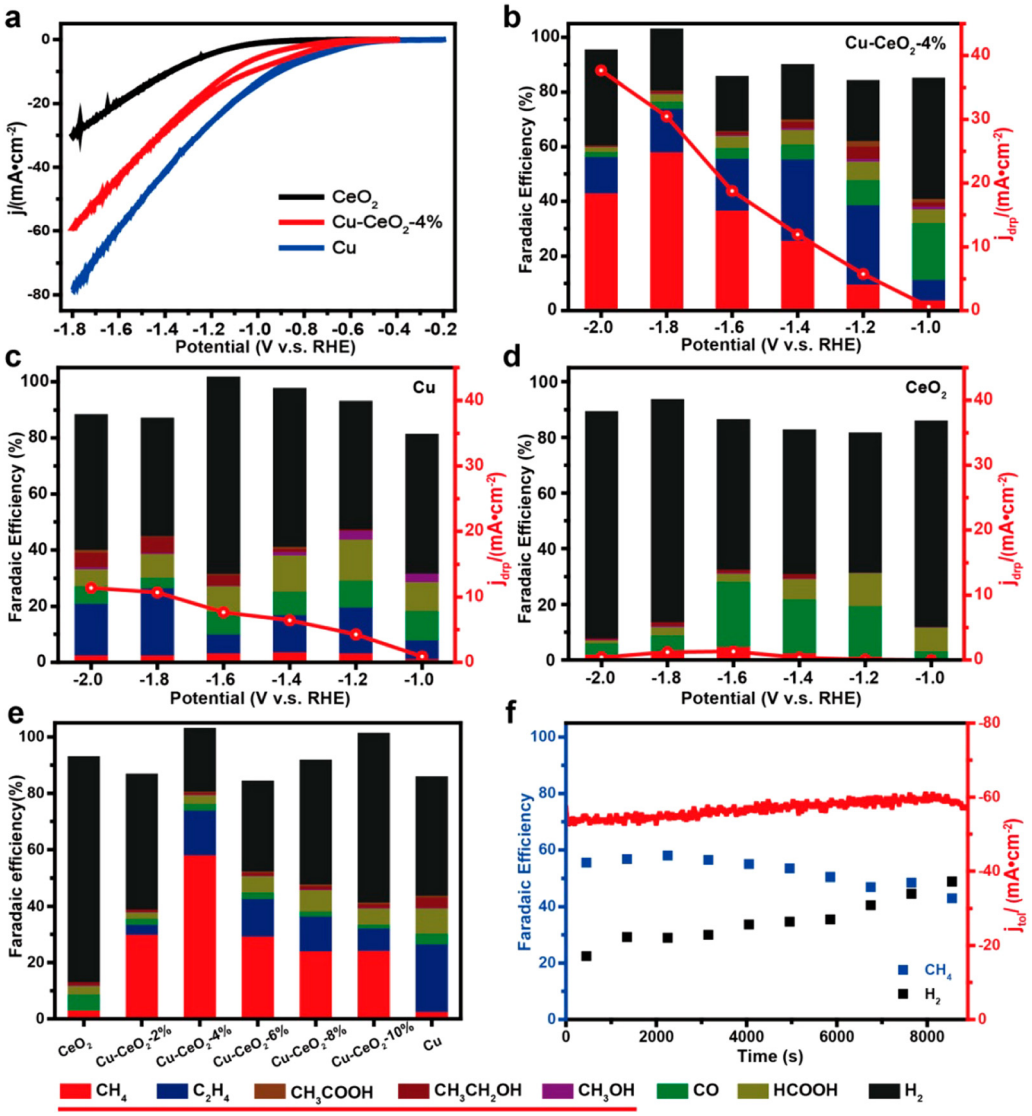

Fig. 34 Performances of e-CO_2R. CV curves for Cu–CeO_2, CeO_2, and Cu (a). FE (bars, left y-axis) and j_{drp} (red curves, right y-axis) of Cu–CeO_2-4% (b), pure Cu (c), and undoped CeO_2 (d) at different overpotentials. The first five products in the legends at the bottom, which are marked with a red line, are the deep reduction products. A comparison of the FE of samples with different amounts of Cu doping (e). On the left side of the y-axis, the squares show how stable are FE_{CH_4} (blue) and FE_{H_2} (black) (f). Total current density (j_{total}) of Cu–CeO_2-4% at 1.8 V is shown by the red arcs on the right side of the y-axis. Reproduced with permission from ref. 374. Copyright 2018, American Chemical Society.

successfully developed a Cu/ceria catalyst with excellent selectivity. It was found that high selectivity during CO_2RR is regulated by the calcination temperature due to the increased concentration of OVs on the catalyst surface. Additionally, it was observed that a higher alkaline pH creates more active sites for hydrogen evolution, supporting the hypothesis that pH plays a crucial role in regulating surface termination.[381] In a related study, the importance of the Zr–O–Cu interface for CO_2R was highlighted. This study utilized Cu nanoparticles for CO_2R reduction on a UiO-66 MOF with missing-linker defects. The research revealed that the presence and quantity of linker defects significantly influence the kinetics, efficiency, and side-product production in CO_2R. An optimal range of five to seven missing linkers per unit cell was identified, striking a balance between steric effects and binding at the Zr node.[382] The crystalline or morphological defect engineering strategy has been adopted as described earlier and a number of designed electrocatalysts are summarized in Table 19. Defect engineering can focus on both crystalline and morphological aspects. The strategies are stated before. Table 19 contains several designed electrocatalysts.

6.16. Metal organic framework (MOF) derived approach

The MOF based method to design e-CO_2R catalysts is important because researchers can use it to design more environmentally friendly products. What's interesting about MOFs is that they provide a platform that can be easily adjusted to meet the demands of catalyst development. There are lots of MOFs which consist of metal ions bound to ligands, differing in qualitative properties from each other because of their unique

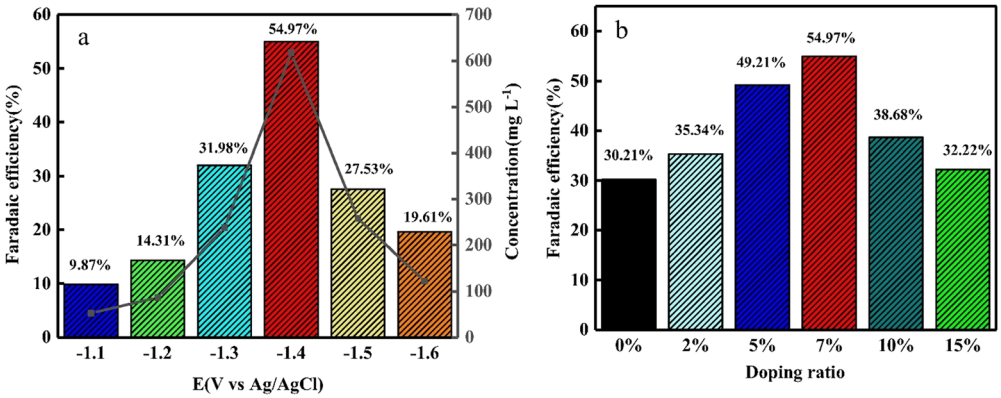

Fig. 35 The FE of CO_2 reduction to formate was investigated using a carbon paper electrode loaded with 7%-(Cu, N)–SnO_x at various potentials (a). The faradaic efficiency of CO_2R to formate was studied using different electrodes with varying amounts of (Cu, N) doping at a potential of −1.4 V, with an electrolysis time of 1 hour (b). Reproduced with permission from ref. 375. Copyright 2020, Elsevier.

Table 19 The key target is now to study how defect engineering can modify the properties of catalysts to a high precision. The table analyses the properties sanely, foregrounding what role defects play in addressing sustainable energy challenges

				≈FE%									
No.	Material	Electrolyte	V *vs.* RHE	H_2	CO	CH_4	C_2H_4	$HCOO^-$	$C_2H_5^+$	CH_3OH	C_2H_5OH	$C_2H_3O_2^-$	Ref.
1	n-CuNS	0.1 M $KHCO_3$	−1.0	27	—	—	73	—	—	—	—	—	24
2	OD-Cu	0.1 M $KHCO_3$	−0.95 V	37.4	1.17	1.3	30.5	6.4	—	—	12.5	—	383
3	La_2CuO_4	0.1 M $KHCO_3$	−1.4	—	—	50	—	—	—	—	—	—	372
4	Cu bare	0.1 M $KHCO_3$	−2.54 mA cm^{-2}	70.1	—	7.1	4.4	—	—	—	—	—	373
5	AC–CuS_x		−7.49 mA cm^{-2}	88.4	—	1.6	1.6	0.2	—	—	—	—	
6	DS-CuS_x		−10.45	90.9	—	0.4	2.5	—	—	—	—	—	
7	0%-(Cu, N)–SnO_x	0.1 M $KHCO_3$	−1.4 *vs.* Ag/AgCl	—	—	—	—	30.21	—	—	—	—	375
8	2%-(Cu, N)–SnO_x			—	—	—	—	35.34	—	—	—	—	
9	5%-(Cu, N)–SnO_x			—	—	—	—	49.21	—	—	—	—	
10	7%-(Cu, N)–SnO_x			—	—	—	—	54.97	—	—	—	—	
11	10%-(Cu, N)–SnO_x			—	—	—	—	38.68	—	—	—	—	
12	15%-(Cu, N)–SnO_x			—	—	—	—	32.22	—	—	—	—	
13	10h-CuNWs	1 M KOH	−1.0	—	—	—	55	—	—	—	—	—	376
14	15h-CuNWs			—	—	—	58	—	—	—	—	—	
15	20h-CuNWs			—	—	—	38	—	—	—	—	—	
16	25h-CuNWs			—	—	—	47	—	—	—	—	—	
17	Cu	2.5 M KOH	−0.9	78	23	—	—	—	—	—	—	—	377
18	SnCu			63	37		5	—	—	—	—	—	
19	pc-SnCu			20	30	11	45	—	—	—	—	—	
20	0%-Cu/CeO_2	1 M KOH	−0.89	85	2	—	—	—	—	—	—	—	381
21	0.5%-Cu/CeO_2			48	4	32	3	—	—	—	—	—	
22	1%-Cu/CeO_2			43	2	42	2	—	—	—	—	—	
23	1.6%-Cu/CeO_2			50	5	25	4	—	—	—	—	—	
24	2.3%-Cu/CeO_2			65	3	8	10	—	—	—	—	—	

structures. By choosing appropriate metal ions and ligands researchers can prepare MOFs that can be used as catalytic materials. The method which is advocated here has control over the composition, structure and surface properties of the catalyst. The MOF derived approach can be used in many ways in the design of CO_2RR catalysts. One method widely used is that in which MOFs are thermochemically decomposed by calcination in a controlled atmosphere, hence forming carbon-related materials which have a definite structure and active sites. In situations MOFs can serve as templates, for depositing metal nanoparticles or individual atoms. This enables the development of catalysts that exhibit improved properties. The approach derived from MOFs offers a foundation for designing CO_2RR catalysts. By leveraging the characteristics of these materials, we can tackle the urgent issues related to carbon capture and conversion while fostering a sustainable and environmentally friendly future, with reduced carbon emissions.

Zhao *et al.* offered a strategy by using a Cu-based MOF (HKUST-1) and created oxide-derived Cu/carbon (OD Cu/C) catalysts. At −0.1 to −0.7 V *vs.* RHE, the resultant materials exhibited a total FE of 45.2–71.2%, demonstrating highly selective CO_2R to alcohol molecules. Ethanol and methanol yields were optimized to 3.7–13.4 mg L^{-1} h^{-1} and 5.1–12.4 mg L^{-1} h^{-1}, respectively. Near −0.1 V, or 190 mV overpotential, C_2H_5OH production began to occur.[384] In another work, $Cu_3(BTC)_2$ (Cu-MOF) was incorporated into carbon paper-based GDEs as a CO_2 capture agent. This incorporation resulted in higher FEs of CH_4 on GDEs with Cu-MOF weight ratios, greatly improving the conversion efficiency

and product selectivity of CO_2 electroreduction.[385] In a related field, Ma *et al.* designed CTF-B constrained Cu catalysts with an impressive maximum FE of 81.3% for CO_2R. Their investigations revealed the dynamic development of Cu-ACs, active sites for CO_2RR, in response to potential, as demonstrated through *in vivo* XAFS investigations.[386] In a complementary study, Kim *et al.* successfully controlled the shape of Cu-MOFs into nanoparticles with diameters of 80 nm using a seed-mediated solvothermal polyol method. During more than 10 hours of e-CO_2RR under neutral conditions, the MOF-based copper catalysts exhibited maximum selectivity towards ethylene and C_{2+} products. By employing a GDE technique, they maintained high FE and generated a high partial geometric current density toward C_{2+} products in alkaline environments.[387]

In a related investigation, a thin film of organic additives like *N*-toylpyridinium could effectively restrict H^+ mass passage to the electrode without impeding CO_2 transit. This strategic modification leads to improved production of C_{2+} products and a reduction in the competitive HER. Modified copper electrodes enhance selective CO_2R to C_{2+} products, even in very acidic electrolytes and at low alkali cation concentrations and operating current densities.[388] In a separate investigation, another study explored the effectiveness of electrolysis at a constant potential in six different electrolytes ($KHCO_3/H_2O$, TBAB/DMF, KBr/CH_3OH, CH_3COOK/CH_3OH, TBAB/CH_3OH, and TBAP/CH_3OH) for the CO_2R. Notably, $KHCO_3/H_2O$ and TBAB/CH_3OH showed a lower onset potential. Across all electrolytes, the primary product generated was HCOOH, although with varying maximum formic acid concentrations. Interestingly, when using a 0.1 M TBAB/DMF electrolyte, the synthesized MOF material exhibited a high efficiency of 58% in forming both HCOOH and CH_3COOH products.[389] Furthermore, through a novel approach of carbonizing Cu–BTC at steady temperatures, a new catalyst (Cu_2O/Cu@NC-800) was developed. Carbonizing the catalyst at 800 °C significantly increased its activity and selectivity toward formate production. The formation of low-index facets and the uniform distribution of metallic nanoparticles within N-doped carbon frameworks played a key role in enhancing the catalyst's activity. The increased nitrogen content in the Cu_2O lattice lowered the binding energy of *OCHO, facilitating easier formate synthesis *via* the *OCHO pathway.[390]

In a related context, another research study focused on regulating the structural evolution of porous materials during e-CO_2RR to develop new electrocatalysts. To promote the coupling of C radical intermediates for the creation of C_{2+} products, TCNQ was introduced as a second electron acceptor to expedite the reduction of Cu(II) sites to Cu(I) species. The resulting TCNQ@CuMOP-p/CP catalyst exhibited a high selectivity of 68% for C_{2+} products at a total current density of 268 mA cm^{-2} and 2.27 V *vs.* RHE, making it competitive with the best Cu(II)-MOF-derived catalysts for CO_2RR.[391] Furthermore, Cheng *et al.* revealed that the e-CO_2RR performance of Cu catalysts derived from MOFs is greatly influenced by the amount and types of nitrogen present in the carbon shell. The remarkable selectivity for the production of ethylene and ethanol can be attributed to the high pyrrolic-N and Cu–N doping in the carbon support, which provides numerous CO_2 adsorption sites and facilitates carbon–carbon coupling processes. However, an abundance of graphitic-N and oxidized-N atoms can lead to severe competition from the HER. Therefore, enhancing the synergy between Cu and the nitrogen-doped carbon support requires modifications to the N structure.[392]

In related research, the synthesis of a single-atom copper catalyst based on MOFs *via* plasma activation was described by Wei *et al.* The plasma bombardment increases low-coordinated copper sites and creates OVs, while also forming a hierarchically porous structure that effectively adsorbs reactant molecules. This unique combination of features greatly enhances e-CO_2R activity, resulting in a maximum FE of 75.3%. Products with carbon content achieve a total FE of 96.5%.[393] Furthermore, the research reveals that homemade e-CO_2R reactors can be constructed using CuIn-MOF series catalysts coated on carbon paper. These catalysts have low over-potentials, large current densities, and selective activity toward CO and formic acid. The stability can be enhanced by adjusting the relative molar ratio of Cu/In, which results in a current density between 20.1 and 88.4 mA cm^{-2}. Cu_1In_1-MOF-SO_4 exhibits the highest e-CO_2R activity, while Cu_1In_3-MOF-NO_3 and Cu_1In_3-MOF-SO_4 have the highest FE_{CO} and FE_{HCOO^-} values.[394] In another study, MOF-derived In–Cu bimetallic oxides were used in a 0.5 M $KHCO_3$ aqueous solution for the e-CO_2R to CO. With a total current density of 11.2 mA cm^{-2} and a FE of 92.1%, InCuO-0.92 was found to be a very effective and stable catalyst. The improved performance was traced back to the synergistic impact between In and Cu oxides, the increased electrochemical surface area, the greater CO_2 adsorption, the lower charge transfer resistance, and the porous mass diffusion structure.[395] Furthermore, through *in situ* modification of MWCNTs, a novel BiCu bimetallic organic framework composite catalyst, SU-101-Cu@2.5C, was effectively developed and synthesized (Fig. 36). The catalyst's efficiency in converting e-CO_2R to formate was investigated. The combination of BMOFs and MWCNTs created a synergistic effect that facilitated electron transport, ultimately enabling efficient e-CO_2R to formate.[396]

Additionally, Cu-MOF808 was pyrolyzed to produce Cu@ZrO_2 with a hollow structure. This transformation allowed for the control of the porosity structure and metal–support interaction through varying pyrolysis temperatures. Notably, the numerous Cu–ZrO_2 interfaces created during proper calcination were instrumental in facilitating the hydrogenation of CO_2 to methanol. CO_2 primarily found absorption and activation sites at the fundamental locations of Cu–ZrO_2 interfaces, underscoring the significance of the Cu^+/Cu^0 ratio. Among these catalysts, CM-300 at 220 °C demonstrated the most remarkable efficacy for converting CO_2 into methanol, boasting a 5% conversion rate and an 85% selectivity for methanol.[397] Furthermore, electrocatalytic stability and performance in hydrocarbon synthesis can be substantially enhanced by post-synthetic alterations of copper-based MOFs. This improvement involves converting free COOH/–OH groups into amide/amine groups. The modified MOFs exhibit high electrocatalytic performance (total FE = 81%, with FE_{C_1} = 62% and FE_{C_2} = 19%) and remarkable stability.[398]

Moreover, Liu *et al.* have developed Cu–N coordinated MOFs for selective C_2H_4 production, and *in situ* electrochemical reconstruction was employed to construct highly active Cu/Cu_2O nanoclusters. The FE for C_2H_4 production, measured by partial current density at 1.03 V *vs.* RHE in the CO_2RR, reached

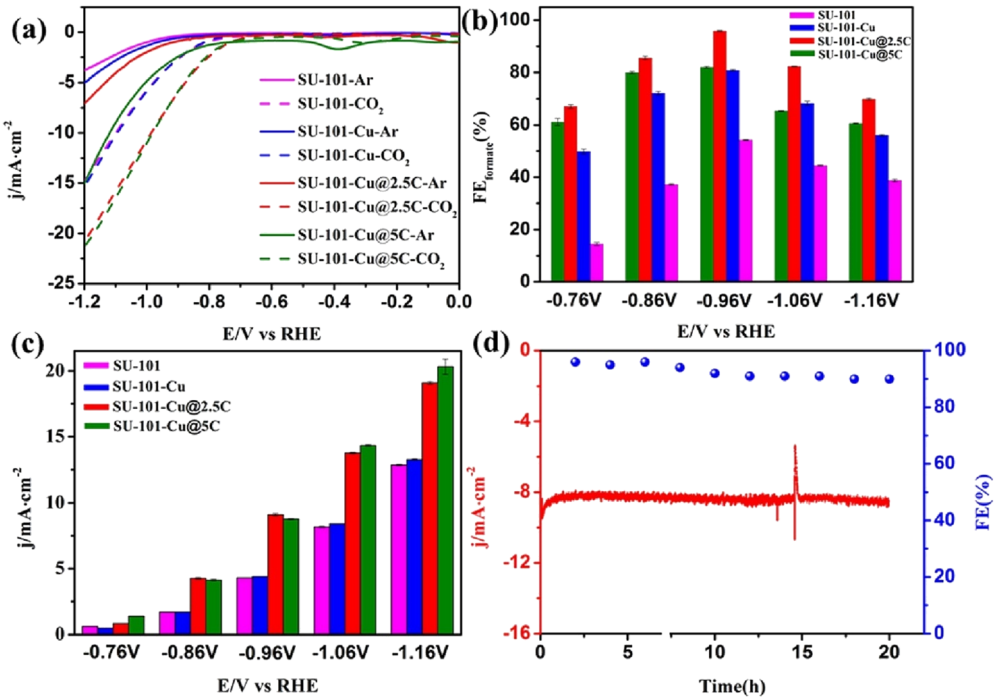

Fig. 36 The electrocatalytic performance of SU-101, SU-101-Cu, and SU-101-Cu@xC was evaluated through LSV measurements in CO_2 and Ar atmospheres (a). The measurements included different applied potentials, $FE_{formate}$ (b), and current density (c). SU-101-Cu@2.5C was tested for long-term durability at a voltage of −0.96 V *vs.* RHE for a duration of 20 hours (d). Reproduced with permission from ref. 396. Copyright 2023, Elsevier.

70.2 ± 1.7%.[399] In addition, Parambath *et al.* have utilized a Cu-based MOF, namely HKUST-1. Remarkably, these materials exhibited high selectivity in CO_2R to alcohol molecules, with total FE ranging from 45.2% to 71.2% at potentials between −0.1 and −0.7 V *vs.* RHE. Ethanol and methanol yields were optimized to 3.7–13.4 mg L^{-1} h^{-1} and 5.1–12.4 mg L^{-1} h^{-1}, respectively. The overpotential for CO_2 reduction, as indicated by the onset potential for C_2H_5OH production, was modest and close to −0.1 V.[400] Table 20 showcases different MOFs designed for e-CO_2R to yield valuable products.

6.17 Alkaline metal cations and halide anions on Cu electrocatalysts

The modification of Cu electrocatalysts through the adsorption of alkaline metal cations and halide anions has shown significant impact on the e-CO_2RR. This section explores the mechanisms and outcomes of such modifications. Alkaline metal cations, such as Li^+, Na^+, K^+, and Cs^+, play a crucial role in CO_2RR. These cations interact with the electric double layer at the catalyst surface, affecting the local electric field and the binding strength of reaction intermediates. The size and hydration energy of these cations influence their specific adsorption properties, which in turn modify the catalytic activity and selectivity.[408] Smaller cations like Li^+ have higher charge densities and stronger hydration energies, leading to different adsorption behaviors compared to larger cations like Cs^+.[409] These differences impact the stabilization of key intermediates such as $CO_2^{\bullet-}$ and *CO. Adsorbed cations can alter the local electric field at the catalyst surface, influencing the electron transfer kinetics. For example, larger cations may create a more diffuse electric field, which could enhance the formation of multi-carbon products by stabilizing the required intermediates.[410]

Halide ions on copper surfaces play a crucial role in e-CO_2RR by weakening the C–O bonds of CO_2, lowering hydrogenation potential barriers. Understanding halide modified copper electrocatalysts (Cu–*X*) can help design efficient Cu–X electrocatalysts for e-CO_2RR. Factors influencing catalytic performance include morphology, oxidation state, and electrolyte pH/composition.[411] Halide anions, including Cl^-, Br^-, and I^-, adsorb on the Cu surface and modify the catalytic properties through electronic and geometric effects. Yuan *et al.* have presented a method to immobilize Cu-based catalysts during the e-CO_2RR, revealing the fundamental mechanism of specific adsorption of halide ions. The method involves pre-reduction in aqueous KX electrolytes and e-CO_2RR using non-buffered K_2SO_4. *In situ* spectroscopy shows that specific adsorption enhances the adsorption of *CO intermediates, achieving a high selectivity of 84.5% for C_{2+} products.[412] Zhang and co have investigated the impact of alkali metal cations and anions on the current density and product selectivity of e-CO_2RR into HCOOH on a SnO_2/carbon paper electrode. The results showed that cations promote current density and faradaic efficiencies, while anions decrease current density and FEs for HCOOH formation.[413] The current density and FE_{HCOOH} were found to be in the order of $Li^+ < Na^+ < K^+ < Cs^+ < Rb^+$. The cation species' effect is attributed to the change in surface charge density influenced by the radius of hydrated cations and the pH values determined by the small number of bare cations. The anions' promotion of

Table 20 The table presents an overview of electrocatalyst materials that have been developed using strategies derived from MOFs for CO_2R. This overview focuses on comprehensively examining the characteristics of MOFs and their influence on the resulting products

No.	Material	Electrolyte	V *vs.* RHE	≈FE%									Ref.
				H_2	CO	CH_4	C_2H_4	$HCOO^-$	$C_2H_5^+$	CH_3OH	C_2H_5OH	$C_2H_3O_2^-$	
1	OD Cu/C-1000	0.1 M $KHCO_3$	−0.7	—	—	—	—	9	—	15	33	—	384
2	Cu/C1000			—	—	—	—	16	—	4	12	—	
3	Cu-MOF-10%	0.5 M $NaHCO_3$	−1.8	47	—	11	16	—	—	—	—	—	385
4	NNU-50	—	−1.1	—	—	66	—	—	—	—	—	—	401
5	Cu_6MePz			—	—	22	—	—	—	—	—	—	
6	n-MDC-225	1.0 M KOH	−1.01	45.9	7.3	9.8	29.6	5.8	—	—	5.2	—	402
7	n-MDC-250			13.4	2.3	1.9	63.1	3.2	—	—	12.5	1.2	
8	n-MDC-300			22.2	5.0	0.5	52.6	9.6	—	—	2.0	7.7	
9	m-MDC-250			36.0	10.4	3.3	34.7	11.7	—	—	5.6	—	
10	m-MDC-265			27.7	2.7	1.4	48.3	5.9	—	—	11.6	0.1	
11	m-MDC-300			27.8	7.7	0.7	25.1	24.6	—	—	7.9	6.0	
12	Cu	H_3PO_4/KH_2PO_4, $[K^+]$ =	−1.29	95	0.14	—	—	1	—	—	—	—	403
13	Cu/10 mM tolyl-pyr	0.1 M	−1.43	23.7	0.7	1.9	24.3	3.4	—	—	23.8	—	
14	Cu_2O/Cu@NC-700	0.1 M $KHCO_3$	−0.88 Ag/	—	—	—	—	28	—	—	—	—	390
15	Cu_2O/Cu@NC-800		AgCl	—	—	—	—	42	—	—	—	—	
16	Cu_2O/Cu@NC-900			—	—	—	—	20	—	—	—	—	
17	TCNQ@CuMOP-p/CP	1.0 M KOH	−1.07	—	18	1	15	10	—	—	6	—	404
18	HKUST-1-p/CP			—	20		10	5	—	—	7	—	
19	TCNQ@HKUST-1-p/CP			—	25		15	8	—	—	6	—	
20	CuMOP-p/CP			—	18	1	12	8	—	—	5	—	
21	PA–CuDBC-1	0.5 M $KHCO_3$	−1.0	15	15	60	10	—	—	—	—	—	405
22	CuDBC			43	42	—	1	—	—	—	—	—	
23	PA–CuDBC-2			30	30	30	10	—	—	—	—	—	
24	CuIn–MOF–SO_4	0.5 M $KHCO_3$	1.06	—	50	—	—	—	—	—	—	—	406
25	CuIn–MOF–NO_3 (Cu/In molar ratio $\frac{1}{4}$ 1 : 3)			—	38	—	—	—	—	—	—	—	
26	In_2O_2	0.5 M $KHCO_3$	−1.0	—	10	—	—	—	—	—	—	—	407
27	InCuO-0.15			—	30	—	—	—	—	—	—	—	
28	InCuO-0.37			—	50	—	—	—	—	—	—	—	
29	InCuO-0.55			—	70	—	—	—	—	—	—	—	
30	InCuO-0.72			—	83	—	—	—	—	—	—	—	
31	InCuO-0.92			—	91	—	—	—	—	—	—	—	
32	SU-101-Cu@5C	0.5 M $KHCO_3$	−1.06	28	2	—	—	65	—	—	—	—	396
33	SU-101-Cu@2.5C			5	2	—	—	82	—	—	—	—	
34	SU-101-Cu			15	10	—	—	70	—	—	—	—	
35	SU-101			43	7	—	—	45	—	—	—	—	

current density was found to be in the order of $NaHCO_3$ < NaCl < NaBr < NaI and $KHCO_3$ < KCl ≈ KI < KBr, and the effect on FE_{HCOOH} was in the order of HCO_3^- < Cl^- < Br^- < I^-. The influence of anions on ER_{CO_2} to HCOOH is mainly due to changes in CO_2, H^+, and OH^- transport, as well as anions' adsorption (Fig. 37).

7. Summary

In the process of developing technology to fight climate change, e-CO_2R copper-based catalysts can be rationally designed, offering hope for the future of this method. Among engineering strategies, the single crystal and atom approach is a standout

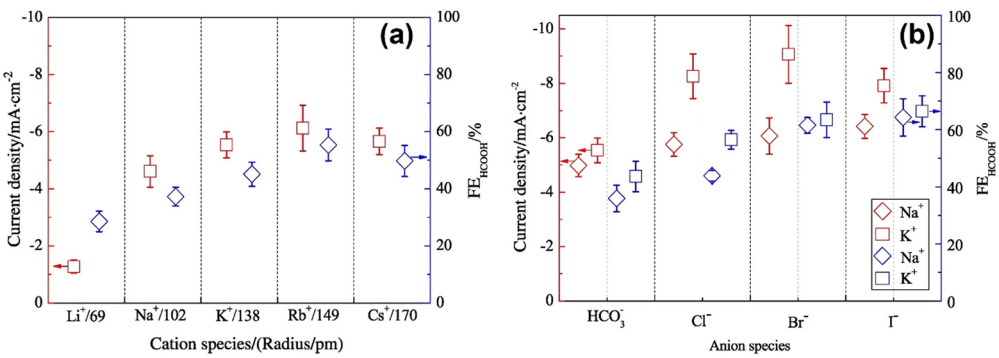

Fig. 37 Current density and FE_{HCOOH} as functions of electrolyte type and the cation size, measured using an SnO_2/C electrode at −1.4 V in 0.1 mol L^{-1} $MHCO_3$ (M = Li^+, Na^+, K^+, Rb^+, Cs^+) and NaX and KX (X = HCO_3^-, Cl^-, Br^- and I^-), respectively (a and b). Reproduced with permission from ref. 413. Copyright 2020, Elsevier.

technique. This innovative technique involves dispersing individual copper atoms onto a support material resulting in efficiency and selectivity for CO_2R. By distributing metal atoms scientists can minimize the use of scarce metals while maximizing catalytic activity. Control over sites and this approach are appropriate to address challenges, and offer opportunities for efficiency and selectivity.

Another important strategy in designing copper-based catalysts is oxidation state engineering. In designing copper-based catalysts, another important possibility is oxidation state manipulation. The structure of the catalyst allows for optimization of e-CO_2R, through tailoring. Balance between activity and selectivity is achieved by this approach. Utilizing alloys is also a robust strategy for designing copper-based catalysts. Copper and metals are strategically combined here. With customized properties, these alloys have been adapted. Compound alloys further take this concept by introducing elements into the alloys, which not only increases their strength but also makes them more accurate. In catalyst design, these strategies allow for fine-tuning of activity and selectivity.

The methods of composite engineering involve the addition of copper-based catalysts to other functional materials in order to increase their stability and activity. Typically, these composites are made up of copper nanoparticles incorporated in a supportive matrix that gives them improved performance. Another way is to add other metals to the structure of copper-based catalysts, to produce changes in their properties and catalytic behavior. This approach may result in high activities and selectivity but sustainability as well as cost are among its drawbacks. On the other hand, nonmetal doping offers an approach to modify the properties of Cu catalysts by introducing nonmetal elements into their structure. This allows researchers to tailor their properties and reactivity for optimized CO_2R efficiency and selectivity. Surface anchoring focuses on attaching metal nanoparticles to support materials preventing agglomeration and enhancing stability.

Molecular surface functionalization involves modifying the surface of the catalyst with molecules to enhance CO_2 adsorption and reactivity. This strategy improves activity and selectivity by customizing the surface properties of the catalyst. Interfacial engineering aims at optimizing interactions between the catalyst and reactants thereby improving CO_2 reduction efficiency. Additionally controlling the chemical species on the surface of Cu through speciation influences its behavior. Facet engineering focuses on manipulating the crystal surfaces of Cu based catalysts to optimize the adsorption and conversion of CO_2. The coordination engineering approach involves adjusting the arrangement of Cu atoms in the catalyst, which affects their reactivity. The site engineering approach aims to control the sites on the catalyst surface to optimize CO_2 adsorption and conversion. Strain engineering employs chemical methods to introduce strain into the catalyst structure, which impacts its properties and catalytic activity. The catalyst pre-oxidation approach involves controlled oxidation to enhance its performance.

The precursor derived methods use precursor materials to fabricate Cu-based catalysts with the properties desired. As an alternative, polymer modification procedures introduce polymers into the catalyst structure and increase stability and reactivity. This research aims to improve catalyst performance by optimizing the support material from an engineering perspective. The defect engineering method involves carefully forming defects within catalysts as sites for the adsorption and reduction of CO_2. By reducing costs, and increasing both activity and selectivity, this process also turns Cu into a primary catalyst material.

8. Conclusions

To sum up, by producing copper-based catalysts for e-CO_2R, one can hit three birds with one stone by fighting global warming, alleviating energy tension and facilitating sustainable technologies. Various engineering techniques, from doping of atoms to changing defects, have been studied to improve these catalysts' performance. The single atom approach controls sites effectively and attains outstanding efficiency and selectivity in CO_2 reduction. Therefore, this approach will prove an asset in future catalyst modification. Moreover, strategies involving oxidation state manipulation, alloy combinations, and composite designs offer flexibility in catalyst development, providing customized properties that match specific needs. Doping with both metal and non-metal additives, as well as surface functionalization techniques, are ways to modify catalysts for greater reactivity. Interfacial, facet, coordination, site, strain, and speciation engineering approaches allow fine-tuning of catalyst behavior. Catalyst preoxidation, precursor-derived approaches, polymer modification, support engineering, and defect engineering help to further improve the optimization of catalysts. Cost effectiveness plays a vital part in making CO_2 utilization a commercial reality. While the costs of such techniques may be raised by approaches like doping with elements, defect engineering with low-cost Cu as the main material offers an economically viable option. For practical applications, stability is essential, and much attention is paid to these problems. Combined with defect engineering, single-atom methods have shown excellent stability, while metal doping with noble metals also helps protect against corrosion and agglomeration. Long-term catalyst reliability can also be achieved through proper defect engineering, strict control of sites for activities, and strain engineering.

Based on the comprehensive analysis presented in this review, it is evident that no single approach stands out as the universally best strategy for designing Cu-based electrocatalysts for e-CO_2R. However, the combination of several engineering strategies appears to be the most promising pathway. Specifically, integrating doping techniques with surface and defect engineering can synergistically enhance the catalytic performance by improving both the activity and selectivity of the catalysts. This multi-faceted approach leverages the strength of each individual strategy, offering a balanced solution that addresses the various challenges associated with CO_2R. Moreover, the incorporation of advanced *in situ* spectroscopic and computational studies provides critical insights into the reaction mechanisms and intermediate species, guiding the rational design of these hybrid catalysts. This combination

not only allows for real-time monitoring and optimization of catalytic processes but also facilitates the prediction and screening of potential modifications at an atomic level. Therefore, a holistic strategy that combines experimental advancements with theoretical insights is recommended as the best approach for the development of high-performance Cu-based electrocatalysts for CO_2 electroreduction.

9. Future outlook

Cu-based e-CO_2R catalysts project a bright future for further innovation and development. There are several main directions and problems we would like to discuss. In addition, given advances in materials science, future catalysts may be designed to carry out various reactions simultaneously, as applications progress in this area. The realizability of Cu-based catalysts is necessary for real-world usage. Researchers must work out high-capacity synthesis methods and steps. Under industrial conditions, maintaining long-term durability and reliability of Cu-based catalysts is all-important. Taking steps to lessen catalyst deterioration ought to be a target of future research. The integration of catalysts into CO_2 capture and utilization systems will facilitate the realization of efficient CO_2R processes. Integrating e-CO_2R with solar and wind power, among other renewable sources, can make the technology more ecological and manageable. We need to tailor Cu-based catalysts so that they can selectively make ethylene or ethanol or other multi-carbon products in order to satisfy various industrial demands. To ensure these techniques' overall sustainability, rigorous assessments of the environmental and energy impacts of Cu-based CO_2 reduction technology are necessary. Regulations and policies should be introduced as Cu-based catalysts and CO_2 utilization technologies mature to support their deployment and promote environmentally sound practices. To accelerate the use of Cu-based catalysts and development of new candidates, a collaborative approach in cooperation with researchers, industry participants, and governments from around the world is required.

Data availability

All data and information related to this review article are presented in the main text and supporting references. No new data were generated or analyzed for this review. All sources are properly cited and listed in the reference section. Therefore, no additional data are available for this article.

Conflicts of interest

There are no conflicts to declare.

References

1 L. J. R. Nunes, The Rising Threat of Atmospheric CO_2: A Review on the Causes, Impacts, and Mitigation Strategies, *Environments*, 2023, **10**(4), 66.
2 J. Li, *et al.*, Electroreduction of CO_2 to Formate on a Copper-Based Electrocatalyst at High Pressures with High Energy Conversion Efficiency, *J. Am. Chem. Soc.*, 2020, **142**(16), 7276–7282.
3 F. Raganati, F. Miccio and P. Ammendola, Adsorption of Carbon Dioxide for Post-combustion Capture: A Review, *Energy Fuels*, 2021, **35**(16), 12845–12868.
4 J. Wu, *et al.*, CO_2 Reduction: From the Electrochemical to Photochemical Approach, *Adv. Sci.*, 2017, **4**(11), 1700194.
5 Y. Wang, J. Liu and G. Zheng, Designing Copper-Based Catalysts for Efficient Carbon Dioxide Electroreduction, *Adv. Mater.*, 2021, **33**(46), 2005798.
6 K. K. Maniam, *et al.*, Progress in Electrodeposited Copper Catalysts for CO_2 Conversion to Valuable Products, *Processes*, 2023, **11**(4), 1148.
7 A. Álvarez, *et al.*, Challenges in the Greener Production of Formates/Formic Acid, Methanol, and DME by Heterogeneously Catalyzed CO_2 Hydrogenation Processes, *Chem. Rev.*, 2017, **117**(14), 9804–9838.
8 P. A. Kempler and A. C. Nielander, Reliable reporting of faradaic efficiencies for electrocatalysis research, *Nat. Commun.*, 2023, **14**(1), 1158.
9 J. Li, *et al.*, Selective CO_2 electrolysis to CO using isolated antimony alloyed copper, *Nat. Commun.*, 2023, **14**(1), 340.
10 J. Medina-Ramos, J. L. DiMeglio and J. Rosenthal, Efficient Reduction of CO_2 to CO with High Current Density Using *in Situ* or *ex Situ* Prepared Bi-Based Materials, *J. Am. Chem. Soc.*, 2014, **136**(23), 8361–8367.
11 S. Nitopi, *et al.*, Progress and Perspectives of Electrochemical CO_2 Reduction on Copper in Aqueous Electrolyte, *Chem. Rev.*, 2019, **119**(12), 7610–7672.
12 H. Yang, *et al.*, Performance and long-term stability of CO_2 conversion to formic acid using a three-compartment electrolyzer design, *J. CO_2 Util.*, 2020, **42**, 101349.
13 S. Kozuch and J. M. L. Martin, ''Turning Over'' Definitions in Catalytic Cycles, *ACS Catal.*, 2012, **2**(12), 2787–2794.
14 S. Anantharaj, P. E. Karthik and S. Noda, The Significance of Properly Reporting Turnover Frequency in Electrocatalysis Research, *Angew. Chem., Int. Ed.*, 2021, **60**(43), 23051–23067.
15 E. Bertheussen, *et al.*, Quantification of liquid products from the electroreduction of CO_2 and CO using static headspace-gas chromatography and nuclear magnetic resonance spectroscopy, *Catal. Today*, 2017, **288**, 54–62.
16 G. Zhang, Y. Cui and A. Kucernak, Real-Time *In Situ* Monitoring of CO_2 Electroreduction in the Liquid and Gas Phases by Coupled Mass Spectrometry and Localized Electrochemistry, *ACS Catal.*, 2022, **12**(10), 6180–6190.
17 A. Marinoiu, *et al.*, Nitrogen-Doped Graphene Oxide as Efficient Metal-Free Electrocatalyst in PEM Fuel Cells, *Nanomaterials*, 2023, **13**(7), 1233.
18 S.-T. Gao, *et al.*, Theoretical understanding of the electrochemical reaction barrier: a kinetic study of CO_2 reduction reaction on copper electrodes, *Phys. Chem. Chem. Phys.*, 2020, **22**(17), 9607–9615.
19 J. Bian, *et al.*, Strategies and reaction systems for solar-driven CO_2 reduction by water, *Carbon Neutrality*, 2022, **1**(1), 5.

20 T. Cheng, H. Xiao and W. A. Goddard, III, Reaction Mechanisms for the Electrochemical Reduction of CO_2 to CO and Formate on the Cu(100) Surface at 298 K from Quantum Mechanics Free Energy Calculations with Explicit Water, *J. Am. Chem. Soc.*, 2016, **138**(42), 13802–13805.
21 X. Cai, *et al.*, Tuning Selectivity in Catalytic Conversion of CO_2 by One-Atom-Switching of Au_9 and Au_8Pd_1 Catalysts, *CCS Chem.*, 2021, **3**(12), 408–420.
22 Y. Pei, H. Zhong and F. Jin, A brief review of electrocatalytic reduction of CO_2—Materials, reaction conditions, and devices, *Energy Sci. Eng.*, 2021, **9**(7), 1012–1032.
23 Y. Zhou and B. S. Yeo, Formation of C–C bonds during electrocatalytic CO_2 reduction on non-copper electrodes, *J. Mater. Chem. A*, 2020, **8**(44), 23162–23186.
24 B. Zhang, *et al.*, Highly Electrocatalytic Ethylene Production from CO_2 on Nanodefective Cu Nanosheets, *J. Am. Chem. Soc.*, 2020, **142**(31), 13606–13613.
25 J. Kim, *et al.*, Branched Copper Oxide Nanoparticles Induce Highly Selective Ethylene Production by Electrochemical Carbon Dioxide Reduction, *J. Am. Chem. Soc.*, 2019, **141**(17), 6986–6994.
26 X. Chen, *et al.*, Electrochemical CO_2-to-ethylene conversion on polyamine-incorporated Cu electrodes, *Nat. Catal.*, 2021, **4**(1), 20–27.
27 J. Cai, *et al.*, Highly Selective Electrochemical Reduction of CO_2 into Methane on Nanotwinned Cu, *J. Am. Chem. Soc.*, 2023, **145**(16), 9136–9143.
28 X.-Q. Wang, *et al.*, Cu-based bimetallic catalysts for CO_2 reduction reaction. Advanced Sensor and Energy, *Materials*, 2022, **1**(3), 100023.
29 Y. Sun, *et al.*, Importance of the Initial Oxidation State of Copper for the Catalytic Hydrogenation of Dimethyl Oxalate to Ethylene Glycol, *ChemistryOpen*, 2018, **7**(12), 969–976.
30 S. D. McCann and S. S. Stahl, Copper-Catalyzed Aerobic Oxidations of Organic Molecules: Pathways for Two-Electron Oxidation with a Four-Electron Oxidant and a One-Electron Redox-Active Catalyst, *Acc. Chem. Res.*, 2015, **48**(6), 1756–1766.
31 W. Hong, *et al.*, Exploring the Parameters Controlling Product Selectivity in Electrochemical CO_2 Reduction in Competition with Hydrogen Evolution Employing Manganese Bipyridine Complexes, *ACS Catal.*, 2023, **13**(5), 3109–3119.
32 Y. Lei, *et al.*, Recent advances on electrocatalytic CO_2 reduction to resources: target products, reaction pathways and typical catalysts, *Chem. Eng. J.*, 2023, **453**, 139663.
33 J. Zeng, *et al.*, Electrochemical Reduction of CO_2 With Good Efficiency on a Nanostructured Cu–Al Catalyst, *Front. Chem.*, 2022, **10**, 931767.
34 D. Xu, *et al.*, Electrocatalytic CO_2 reduction towards industrial applications, *Carbon Energy*, 2023, **5**(1), e230.
35 M. Li, *et al.*, Discovery of single-atom alloy catalysts for CO_2-to-methanol reaction by density functional theory calculations, *Catal. Today*, 2022, **388–389**, 403–409.
36 T. Ahmad, *et al.*, Electrochemical CO_2 reduction to C_{2+} products using Cu-based electrocatalysts: a review, *Nano Res. Energy*, 2022, **1**, e9120021.
37 Y. Jia, *et al.*, Cu-based bimetallic electrocatalysts for CO_2 reduction, *Adv. Powder Mater.*, 2022, **1**(1), 100012.
38 D. S. Ripatti, T. R. Veltman and M. W. Kanan, Carbon Monoxide Gas Diffusion Electrolysis that Produces Concentrated C_2 Products with High Single-Pass Conversion, *Joule*, 2019, **3**(1), 240–256.
39 D. Wakerley, *et al.*, Bio-inspired hydrophobicity promotes CO_2 reduction on a Cu surface, *Nat. Mater.*, 2019, **18**(11), 1222–1227.
40 C. W. Li, J. Ciston and M. W. Kanan, Electroreduction of carbon monoxide to liquid fuel on oxide-derived nanocrystalline copper, *Nature*, 2014, **508**(7497), 504–507.
41 P. Wilde, *et al.*, Is Cu instability during the CO_2 reduction reaction governed by the applied potential or the local CO concentration?, *Chem. Sci.*, 2021, **12**(11), 4028–4033.
42 T. Burdyny and W. A. Smith, CO_2 reduction on gas-diffusion electrodes and why catalytic performance must be assessed at commercially-relevant conditions, *Energy Environ. Sci.*, 2019, **12**(5), 1442–1453.
43 A. Prašnikar, *et al.*, Mechanisms of Copper-Based Catalyst Deactivation during CO_2 Reduction to Methanol, *Ind. Eng. Chem. Res.*, 2019, **58**(29), 13021–13029.
44 J. Zhao, *et al.*, An overview of Cu-based heterogeneous electrocatalysts for CO_2 reduction, *J. Mater. Chem. A*, 2020, **8**(9), 4700–4734.
45 P. Forzatti and L. Lietti, Catalyst deactivation, *Catal. Today*, 1999, **52**(2), 165–181.
46 Y. Yang, *et al.*, Operando Resonant Soft X-ray Scattering Studies of Chemical Environment and Interparticle Dynamics of Cu Nanocatalysts for CO_2 Electroreduction, *J. Am. Chem. Soc.*, 2022, **144**(20), 8927–8931.
47 Y. Sun, *et al.*, Boosting CO_2 Electroreduction to C_2H_4 *via* Unconventional Hybridization: High-Order Ce^{4+} 4f and O 2p Interaction in Ce–Cu_2O for Stabilizing Cu^+, *ACS Nano*, 2023, **17**(14), 13974–13984.
48 T. H. Phan, *et al.*, Emergence of Potential-Controlled Cu-Nanocuboids and Graphene-Covered Cu-Nanocuboids under Operando CO_2 Electroreduction, *Nano Lett.*, 2021, **21**(5), 2059–2065.
49 D. Friebel, *et al.*, Structure, Redox Chemistry, and Interfacial Alloy Formation in Monolayer and Multilayer Cu/Au(111) Model Catalysts for CO_2 Electroreduction, *J. Phys. Chem. C*, 2014, **118**(15), 7954–7961.
50 Y.-P. Huang, *et al.*, *In situ* probing the dynamic reconstruction of copper–zinc electrocatalysts for CO_2 reduction, *Nanoscale*, 2022, **14**(25), 8944–8950.
51 Y. Xu, *et al.*, Low coordination number copper catalysts for electrochemical CO_2 methanation in a membrane electrode assembly, *Nat. Commun.*, 2021, **12**(1), 2932.
52 Q. Lei, *et al.*, Structural evolution and strain generation of derived-Cu catalysts during CO_2 electroreduction, *Nat. Commun.*, 2022, **13**(1), 4857.
53 B. Xiong, *et al.*, Electrochemical conversion of CO_2 to syngas over Cu–M (M = Cd, Zn, Ni, Ag, and Pd) bimetal catalysts, *Fuel*, 2021, **304**, 121341.
54 H. Yang, *et al.*, Scalable Production of Efficient Single-Atom Copper Decorated Carbon Membranes for CO_2

Electroreduction to Methanol, *J. Am. Chem. Soc.*, 2019, **141**(32), 12717–12723.
55 J. G. Rivera de la Cruz and M. Fontecave, Electrochemical CO_2 reduction on Cu single atom catalyst and Cu nanoclusters: an ab initio approach, *Phys. Chem. Chem. Phys.*, 2022, **24**(26), 15767–15775.
56 M. Morimoto, *et al.*, Experimental and Theoretical Elucidation of Electrochemical CO_2 Reduction on an Electrodeposited Cu_3Sn Alloy, *J. Phys. Chem. C*, 2019, **123**(5), 3004–3010.
57 Y. Yang and D. Cheng, Role of Composition and Geometric Relaxation in CO_2 Binding to Cu–Ni Bimetallic Clusters, *J. Phys. Chem. C*, 2014, **118**(1), 250–258.
58 H. Li, *et al.*, Insight into the mechanisms of CO_2 reduction to CHO over Zr-doped Cu nanoparticle, *Chem. Phys.*, 2021, **540**, 111012.
59 J.-S. Wang, *et al.*, Strong Boron–Carbon Bonding Interaction Drives CO_2 Reduction to Ethanol over the Boron-Doped Cu(111) Surface: An Insight from the First-Principles Calculations, *J. Phys. Chem. C*, 2021, **125**(1), 572–582.
60 X. Zhi, *et al.*, Directing the selectivity of CO_2 electroreduction to target C_2 products *via* non-metal doping on Cu surfaces, *J. Mater. Chem. A*, 2021, **9**(10), 6345–6351.
61 C.-C. Chang and M.-S. Ku, Role of high-index facet Cu(711) surface in controlling the C_2 selectivity for CO_2 reduction reaction—a DFT study, *J. Phys. Chem. C*, 2021, **125**(20), 10919–10925.
62 F. Zhou, *et al.*, Synergetic effects of Cu cluster-doped g-C_3N_4 with multiple active sites for CO_2 reduction to C_2 products: a DFT study, *Fuel*, 2023, **353**, 129202.
63 W. Xue, *et al.*, Theoretical Screening of CO_2 Electroreduction over MOF-808-Supported Self-Adaptive Dual-Metal-Site Pairs, *Inorg. Chem.*, 2023, **62**(2), 930–941.
64 R. Duan, *et al.*, Effects of *CO Coverage on Selective Electrocatalytic Reduction of CO_2 to Ethylene over Cu_2O with Undercoordinated Cu Sites, *J. Phys. Chem. C*, 2022, **126**(49), 20878–20885.
65 A. Das, *et al.*, Ga and Zn Atom-Doped $CuAl_2O_4$(111) Surface-Catalyzed CO_2 Conversion to Dimethyl Ether: Importance of Acidic Sites, *J. Phys. Chem. C*, 2022, **126**(51), 21628–21637.
66 X. Dong, *et al.*, Screening of bimetallic M–Cu–BTC MOFs for CO_2 activation and mechanistic study of CO_2 hydrogenation to formic acid: a DFT study, *J. CO_2 Util.*, 2018, **24**, 64–72.
67 Z. Zhao and G. Lu, Cu-Based Single-Atom Catalysts Boost Electroreduction of CO_2 to CH_3OH: First-Principles Predictions, *J. Phys. Chem. C*, 2019, **123**(7), 4380–4387.
68 M. Sassenburg, *et al.*, Characterizing CO_2 Reduction Catalysts on Gas Diffusion Electrodes: Comparing Activity, Selectivity, and Stability of Transition Metal Catalysts, *ACS Appl. Energy Mater.*, 2022, **5**(5), 5983–5994.
69 X. Lyu, *et al.*, Trace level of atomic copper in N-doped graphene quantum dots switching the selectivity from C1 to C_2 products in CO electroreduction, *Mater. Today Chem.*, 2023, **29**, 101398.
70 P. Qi, *et al.*, Revisiting the Grain and Valence Effect of Oxide-Derived Copper on Electrocatalytic CO_2 Reduction Using Single Crystal Cu(111) Foils, *J. Phys. Chem. Lett.*, 2021, **12**(16), 3941–3950.
71 Y. Chen, *et al.*, Ethylene Selectivity in Electrocatalytic CO_2 Reduction on Cu Nanomaterials: A Crystal Phase-Dependent Study, *J. Am. Chem. Soc.*, 2020, **142**(29), 12760–12766.
72 S. Chen, *et al.*, Lewis Acid Site-Promoted Single-Atomic Cu Catalyzes Electrochemical CO_2 Methanation, *Nano Lett.*, 2021, **21**(17), 7325–7331.
73 Q. Zhao, *et al.*, Selective Etching Quaternary MAX Phase toward Single Atom Copper Immobilized MXene ($Ti_3C_2Cl_x$) for Efficient CO_2 Electroreduction to Methanol, *ACS Nano*, 2021, **15**(3), 4927–4936.
74 D. Karapinar, *et al.*, Electroreduction of CO_2 on Single-Site Copper-Nitrogen-Doped Carbon Material: Selective Formation of Ethanol and Reversible Restructuration of the Metal Sites, *Angew. Chem., Int. Ed.*, 2019, **58**(42), 15098–15103.
75 H. Bao, *et al.*, Isolated copper single sites for high-performance electroreduction of carbon monoxide to multicarbon products, *Nat. Commun.*, 2021, **12**(1), 238.
76 Z. Ma, *et al.*, Atomically Dispersed Cu Catalysts on Sulfide-Derived Defective Ag Nanowires for Electrochemical CO_2 Reduction, *ACS Nano*, 2023, **17**(3), 2387–2398.
77 T. Zheng, *et al.*, Copper-catalysed exclusive CO_2 to pure formic acid conversion *via* single-atom alloying, *Nat. Nanotechnol.*, 2021, **16**(12), 1386–1393.
78 P. Song, *et al.*, Modulating the Asymmetric Atomic Interface of Copper Single Atoms for Efficient CO_2 Electroreduction, *ACS Nano*, 2023, **17**(5), 4619–4628.
79 A. Guan, *et al.*, Nitrogen-Adsorbed Hydrogen Species Promote CO_2 Methanation on Cu Single-Atom Electrocatalyst, *ACS Mater. Lett.*, 2023, **5**(1), 19–26.
80 X. Hu, *et al.*, Tandem Electroreduction of CO_2 to Programmable Acetate and Syngas *via* Single-Nickel-Atom-Encapsulated Copper Nanocatalysts, *ACS Mater. Lett.*, 2023, **5**(1), 85–94.
81 Y. Dai, *et al.*, Manipulating local coordination of copper single atom catalyst enables efficient CO_2-to-CH_4 conversion, *Nat. Commun.*, 2023, **14**(1), 3382.
82 W. Ni, *et al.*, Efficient electrocatalytic reduction of CO_2 on Cu_xO decorated graphene oxides: an insight into the role of multivalent Cu in selectivity and durability, *Appl. Catal., B*, 2019, **259**, 118044.
83 M. Li, *et al.*, Modulated Sn Oxidation States over a Cu_2O-Derived Substrate for Selective Electrochemical CO_2 Reduction, *ACS Appl. Mater. Interfaces*, 2020, **12**(20), 22760–22770.
84 H. Guzmán, *et al.*, CO_2 Conversion to Alcohols over Cu/ZnO Catalysts: Prospective Synergies between Electrocatalytic and Thermocatalytic Routes, *ACS Appl. Mater. Interfaces*, 2022, **14**(1), 517–530.
85 J.-J. Velasco-Vélez, *et al.*, On the Activity/Selectivity and Phase Stability of Thermally Grown Copper Oxides during the Electrocatalytic Reduction of CO_2, *ACS Catal.*, 2020, **10**(19), 11510–11518.

86 J. Liu, *et al.*, Metal–Organic-Frameworks-Derived Cu/Cu_2O Catalyst with Ultrahigh Current Density for Continuous-Flow CO_2 Electroreduction, *ACS Sustainable Chem. Eng.*, 2019, **7**(18), 15739–15746.
87 G. Liu, *et al.*, Elucidating Reaction Pathways of the CO_2 Electroreduction *via* Tailorable Tortuosities and Oxidation States of Cu Nanostructures, *Adv. Funct. Mater.*, 2022, **32**(36), 2204993.
88 C. A. Obasanjo, *et al.*, *In situ* regeneration of copper catalysts for long-term electrochemical CO_2 reduction to multiple carbon products, *J. Mater. Chem. A*, 2022, **10**(37), 20059–20070.
89 T.-C. Chou, *et al.*, Controlling the Oxidation State of the Cu Electrode and Reaction Intermediates for Electrochemical CO_2 Reduction to Ethylene, *J. Am. Chem. Soc.*, 2020, **142**(6), 2857–2867.
90 Q. Lei, *et al.*, Investigating the Origin of Enhanced C_{2+} Selectivity in Oxide-/Hydroxide-Derived Copper Electrodes during CO_2 Electroreduction, *J. Am. Chem. Soc.*, 2020, **142**(9), 4213–4222.
91 X. Jiang, *et al.*, Oxidation State Modulation of Bimetallic Tin-Copper Oxide Nanotubes for Selective CO_2 Electroreduction to Formate, *Small*, 2022, **18**(47), 2204148.
92 Y. Yang, *et al.*, Operando Constructing Cu/Cu_2O Electrocatalysts for Efficient CO_2 Electroreduction to Ethanol: CO_2-Assisted Structural Evolution of Octahedral Cu_2O by Operando CV Activation, *ACS Catal.*, 2022, **12**(20), 12942–12953.
93 Z. Zhang, *et al.*, Charge-Separated Pdδ−–Cuδ+ Atom Pairs Promote CO_2 Reduction to C_2, *Nano Lett.*, 2023, **23**(6), 2312–2320.
94 Y. Li, *et al.*, Insight into the Electrochemical CO_2-to-Ethanol Conversion Catalyzed by Cu_2S Nanocrystal-Decorated Cu Nanosheets, *ACS Appl. Mater. Interfaces*, 2023, **15**(15), 18857–18866.
95 F. Yang, *et al.*, Optimizing Copper Oxidation State to Promote Ethylene Generation in Efficient Carbon Dioxide Conversion, *ACS Sustainable Chem. Eng.*, 2022, **10**(14), 4677–4682.
96 H. Pan, *et al.*, Highly Efficient $CuPd_{0.1}/\gamma$-Al_2O_3 Catalyst with Isolated Pd Species for CO_2 Hydrogenation to Methanol, *ACS Sustainable Chem. Eng.*, 2023, **11**(19), 7489–7499.
97 T. Gunji, *et al.*, Preparation of Various Pd-Based Alloys for Electrocatalytic CO_2 Reduction Reaction—Selectivity Depending on Secondary Elements, *Chem. Mater.*, 2020, **32**(16), 6855–6863.
98 S. Ajmal, *et al.*, Zinc-Modified Copper Catalyst for Efficient (Photo-)Electrochemical CO_2 Reduction with High Selectivity of HCOOH Production, *J. Phys. Chem. C*, 2019, **123**(18), 11555–11563.
99 Y. Ding, Y. Xu and L. Zhang, Tin Alloying Enhances Catalytic Selectivity of Copper Surface: A Mechanistic Study Based on First-Principles Calculations, *J. Phys. Chem. Lett.*, 2021, **12**(12), 3031–3037.
100 C. J. Yoo, *et al.*, Compositional and Geometrical Effects of Bimetallic Cu–Sn Catalysts on Selective Electrochemical CO_2 Reduction to CO, *ACS Appl. Energy Mater.*, 2020, **3**(5), 4466–4473.
101 H. Tang, *et al.*, Boosting the Electroreduction of CO_2 to Ethanol *via* the Synergistic Effect of Cu–Ag Bimetallic Catalysts, *ACS Appl. Energy Mater.*, 2022, **5**(11), 14045–14052.
102 G. E. Park, *et al.*, Interfacial Electronic Structures and the Fischer–Tropsch Synthesis Path by Electrochemical CO_2/CO Reduction for Ternary CuNiZn Alloys, *ACS Appl. Energy Mater.*, 2023, **6**(13), 7258–7273.
103 D. Chen, *et al.*, Tailoring the Selectivity of Bimetallic Copper–Palladium Nanoalloys for Electrocatalytic Reduction of CO_2 to CO, *ACS Appl. Energy Mater.*, 2018, **1**(2), 883–890.
104 K. Liu, *et al.*, Electronic Effects Determine the Selectivity of Planar Au–Cu Bimetallic Thin Films for Electrochemical CO_2 Reduction, *ACS Appl. Mater. Interfaces*, 2019, **11**(18), 16546–16555.
105 W. Guo, *et al.*, Highly Selective CO_2 Electroreduction to CO on Cu–Co Bimetallic Catalysts, *ACS Sustainable Chem. Eng.*, 2020, **8**(33), 12561–12567.
106 J.-J. Velasco-Vélez, *et al.*, Cationic Copper Species Stabilized by Zinc during the Electrocatalytic Reduction of CO_2 Revealed by *In Situ* X-Ray Spectroscopy, *Adv. Sustainable Syst.*, 2023, **7**(5), 2200453.
107 M. Bernal, *et al.*, CO_2 electroreduction on copper-cobalt nanoparticles: size and composition effect, *Nano Energy*, 2018, **53**, 27–36.
108 H. Pérez Blanes, *et al.*, High CO_2 reduction activity on AlCrCoCuFeNi multi-principal element alloy nanoparticle electrocatalysts prepared by means of pulsed laser ablation, *J. Mater. Res. Technol.*, 2023, **24**, 9434–9440.
109 V. Okatenko, *et al.*, Alloying as a Strategy to Boost the Stability of Copper Nanocatalysts during the Electrochemical CO_2 Reduction Reaction, *J. Am. Chem. Soc.*, 2023, **145**(9), 5370–5383.
110 A. C. Foucher, *et al.*, Synthesis and Characterization of Stable Cu–Pt Nanoparticles under Reductive and Oxidative Conditions, *J. Am. Chem. Soc.*, 2023, **145**(9), 5410–5421.
111 E. L. Clark, *et al.*, Electrochemical CO_2 Reduction over Compressively Strained CuAg Surface Alloys with Enhanced Multi-Carbon Oxygenate Selectivity, *J. Am. Chem. Soc.*, 2017, **139**(44), 15848–15857.
112 T. T. H. Hoang, *et al.*, Nanoporous Copper–Silver Alloys by Additive-Controlled Electrodeposition for the Selective Electroreduction of CO_2 to Ethylene and Ethanol, *J. Am. Chem. Soc.*, 2018, **140**(17), 5791–5797.
113 Y. Wang, *et al.*, Ensemble Effect in Bimetallic Electrocatalysts for CO_2 Reduction, *J. Am. Chem. Soc.*, 2019, **141**(42), 16635–16642.
114 H. S. Jeon, *et al.*, Operando Insight into the Correlation between the Structure and Composition of CuZn Nanoparticles and Their Selectivity for the Electrochemical CO_2 Reduction, *J. Am. Chem. Soc.*, 2019, **141**(50), 19879–19887.
115 H. Mistry, *et al.*, Size-dependent reactivity of gold-copper bimetallic nanoparticles during CO_2 electroreduction, *Catal. Today*, 2017, **288**, 30–36.
116 J. Zhu, *et al.*, Quasi-Covalently Coupled Ni–Cu Atomic Pair for Synergistic Electroreduction of CO_2, *J. Am. Chem. Soc.*, 2022, **144**(22), 9661–9671.

117 Y. Wang, *et al.*, Tunable selectivity on copper–bismuth bimetallic aerogels for electrochemical CO_2 reduction, *Appl. Catal., B*, 2022, **317**, 121650.
118 Y. Lai, *et al.*, Breaking Scaling Relationships in CO_2 Reduction on Copper Alloys with Organic Additives, *ACS Cent. Sci.*, 2021, **7**(10), 1756–1762.
119 L. Zhou, *et al.*, Synergistic regulation of hydrophobicity and basicity for copper hydroxide-derived copper to promote the CO_2 electroreduction reaction, *Carbon Energy*, 2023, **5**(6), e328.
120 Z. Chang, *et al.*, The Tunable and Highly Selective Reduction Products on Ag@Cu Bimetallic Catalysts Toward CO_2 Electrochemical Reduction Reaction, *J. Phys. Chem. C*, 2017, **121**(21), 11368–11379.
121 H. Itahara, *et al.*, Dealloyed Intermetallic Cu_5Ca Fine Powders as Nanoporous Electrocatalysts for CO_2 Reduction, *ACS Appl. Nano Mater.*, 2022, **5**(8), 11991–11996.
122 W. J. Dong, *et al.*, Evidence of Local Corrosion of Bimetallic Cu–Sn Catalysts and Its Effects on the Selectivity of Electrochemical CO_2 Reduction, *ACS Appl. Energy Mater.*, 2020, **3**(11), 10568–10577.
123 S. Wang, *et al.*, Efficiently Electroreducing CO_2 to Ethylene on Heterostructured CeO_2/CuO, *Ind. Eng. Chem. Res.*, 2022, **61**(44), 16445–16452.
124 H. Farsi, *et al.*, Nanostructured Tungstate-Derived Copper for Hydrogen Evolution Reaction and Electroreduction of CO_2 in Sodium Hydroxide Solutions, *J. Phys. Chem. C*, 2019, **123**(42), 25941–25948.
125 W. Huang, *et al.*, Preparation and Adsorption Performance of GrO@Cu–BTC for Separation of CO_2/CH_4, *Ind. Eng. Chem. Res.*, 2014, **53**(27), 11176–11184.
126 J. Huang, *et al.*, Structural Sensitivities in Bimetallic Catalysts for Electrochemical CO_2 Reduction Revealed by Ag–Cu Nanodimers, *J. Am. Chem. Soc.*, 2019, **141**(6), 2490–2499.
127 H. Rabiee, *et al.*, Tuning the Product Selectivity of the Cu Hollow Fiber Gas Diffusion Electrode for Efficient CO_2 Reduction to Formate by Controlled Surface Sn Electrodeposition, *ACS Appl. Mater. Interfaces*, 2020, **12**(19), 21670–21681.
128 R. A. Rahman, *et al.*, Investigating the Use of CaO/CuO Sorbents for *in Situ* CO_2 Capture in a Biomass Gasifier, *Energy Fuels*, 2015, **29**(6), 3808–3819.
129 S. Payra, *et al.*, Unprecedented Electroreduction of CO_2 over Metal Organic Framework-Derived Intermetallic Nano-Alloy $Cu_{0.85}Ni_{0.15}$/C, *ACS Appl. Energy Mater.*, 2022, **5**(4), 4945–4955.
130 S. Wannakao, *et al.*, Catalytic Activity and Product Selectivity Trends for Carbon Dioxide Electroreduction on Transition Metal-Coated Tungsten Carbides, *J. Phys. Chem. C*, 2017, **121**(37), 20306–20314.
131 M. Zhang, *et al.*, Tunable Selectivity for Electrochemical CO_2 Reduction by Bimetallic Cu–Sn Catalysts: Elucidating the Roles of Cu and Sn, *ACS Catal.*, 2021, **11**(17), 11103–11108.
132 J. Wen, *et al.*, Restructuring of copper catalysts by potential cycling and enhanced two-carbon production for electroreduction of carbon dioxide, *J. CO_2 Util.*, 2022, **56**, 101846.
133 H.-D. Cai, *et al.*, Tuning the Interactions in CuO Nanosheet-Decorated CeO_2 Nanorods for Controlling the Electrochemical Reduction of CO_2 to Methane or Ethylene, *ACS Appl. Nano Mater.*, 2022, **5**(5), 7259–7267.
134 S.-M. Cao, *et al.*, Iron-doping on Cu–N–C composite with enhanced CO Faraday efficiency for the electrochemical reduction of CO_2, *J. CO_2 Util.*, 2021, **44**, 101418.
135 T.-T. Li, *et al.*, Highly Selective and Active Electrochemical Reduction of CO_2 to CO on a Polymeric Co(II) Phthalocyanine@Graphitic Carbon Nitride Nanosheet–Carbon Nanotube Composite, *Inorg. Chem.*, 2020, **59**(19), 14184–14192.
136 Z. Meng, *et al.*, Hierarchical Tuning of the Performance of Electrochemical Carbon Dioxide Reduction Using Conductive Two-Dimensional Metallophthalocyanine Based Metal–Organic Frameworks, *J. Am. Chem. Soc.*, 2020, **142**(52), 21656–21669.
137 H. He, *et al.*, Graphene-Supported Monometallic and Bimetallic Dimers for Electrochemical CO_2 Reduction, *J. Phys. Chem. C*, 2018, **122**(50), 28629–28636.
138 D. Karapinar, *et al.*, Carbon-Nanotube-Supported Copper Polyphthalocyanine for Efficient and Selective Electrocatalytic CO_2 Reduction to CO, *ChemSusChem*, 2020, **13**(1), 173–179.
139 J. Du, *et al.*, CoP_2O_6-Assisted Copper/Carbon Catalyst for Electrocatalytic Reduction of CO_2 to Formate, *ACS Nano*, 2023, **17**(11), 10055–10064.
140 E. Cui, *et al.*, Cu_2S Nanoparticle-Modified Copper Hydroxide Nanowire Arrays for Optimized Electrochemical CO_2 Reduction Selectivity, *ACS Appl. Nano Mater.*, 2023, **6**(11), 9361–9368.
141 Y. Ren, *et al.*, Cu–Ni Alloy Nanoparticles Anchored on Nitrogen-Doped Carbon Nanotubes for Efficient CO_2 Electroreduction to CO, *Energy Fuels*, 2023, **37**(13), 9289–9296.
142 R. Daiyan, *et al.*, Tunable Syngas Production through CO_2 Electroreduction on Cobalt–Carbon Composite Electrocatalyst, *ACS Appl. Mater. Interfaces*, 2020, **12**(8), 9307–9315.
143 P. Ding, *et al.*, Elucidating the Roles of Nafion/Solvent Formulations in Copper-Catalyzed CO_2 Electrolysis, *ACS Catal.*, 2023, **13**(8), 5336–5347.
144 C.-L. Sung, *et al.*, g-C_3N_4 Nanosheet Supported CuO Nanocomposites for the Electrochemical Carbon Dioxide Reduction Reaction, *ACS Omega*, 2023, **8**(8), 7368–7377.
145 J. Li, *et al.*, Metal Oxide Clusters on Nitrogen-Doped Carbon are Highly Selective for CO_2 Electroreduction to CO, *ACS Catal.*, 2021, **11**(15), 10028–10042.
146 A. Strijevskaya, *et al.*, Nanophase-Separated Copper–Zirconia Composites for Bifunctional Electrochemical CO_2 Conversion to Formic Acid, *ACS Appl. Mater. Interfaces*, 2023, **15**(19), 23299–23305.
147 H. Shen and Q. Sun, Tuning CO_2 Electroreduction of Cu Atoms on Triphenylene-Cored Graphdiyne, *J. Phys. Chem. C*, 2019, **123**(49), 29776–29782.
148 W. Ni, *et al.*, Surface Reconstruction with a Sandwich-like C/Cu/C Catalyst for Selective and Stable CO_2 Electroreduction, *ACS Appl. Mater. Interfaces*, 2022, **14**(11), 13261–13270.
149 X. Meng, *et al.*, Ultrasmall Cu Nanocrystals Dispersed in Nitrogen-Doped Carbon as Highly Efficient Catalysts for CO_2 Electroreduction, *ACS Appl. Mater. Interfaces*, 2022, **14**(15), 17240–17248.

150 Z. Gao, *et al.*, Promoting electrocatalytic CO_2 reduction *via* anchoring quaternary piperidinium cations onto copper electrode, *Electrochim. Acta*, 2023, **458**, 142509.
151 M. Ye, *et al.*, Phase engineering of Cu@Cu_2O core–shell nanospheres for boosting tandem electrochemical CO_2 reduction to C_{2+} products, *Appl. Surf. Sci.*, 2023, **622**, 156981.
152 L. Zhao, *et al.*, Regulation of three-dimensional hydrophobic state of copper dendrite adjusts the distribution of liquid products from electrochemical reduction of CO_2, *Appl. Surf. Sci.*, 2023, **628**, 157369.
153 H. Xie, *et al.*, Achieving highly selective electrochemical CO_2 reduction to C_2H_4 on Cu nanosheets, *J. Energy Chem.*, 2023, **79**, 312–320.
154 T. Umeda, *et al.*, Uniform wrapping of copper(I) oxide nanocubes by self-controlled copper-catalyzed azide–alkyne cycloaddition toward selective carbon dioxide electrocatalysis, *Chem. Commun.*, 2022, **58**(58), 8053–8056.
155 E. Mardones-Herrera, *et al.*, Reduced Graphene Oxide Overlayer on Copper Nanocube Electrodes Steers the Selectivity Towards Ethanol in Electrochemical Reduction of Carbon Dioxide, *ChemElectroChem*, 2022, **9**(10), e202200259.
156 C. Lu, *et al.*, Organic-moiety-engineering on copper surface for carbon dioxide reduction, *Chem. Commun.*, 2023, **59**(45), 6827–6836.
157 K. Rossi and R. Buonsanti, Shaping Copper Nanocatalysts to Steer Selectivity in the Electrochemical CO_2 Reduction Reaction, *Acc. Chem. Res.*, 2022, **55**(5), 629–637.
158 W. Zhang, *et al.*, Efficacious CO_2 Adsorption and Activation on Ag Nanoparticles/CuO Mesoporous Nanosheets Heterostructure for CO_2 Electroreduction to CO, *Inorg. Chem.*, 2021, **60**(24), 19356–19364.
159 S. Chang, *et al.*, Bimetallic In–Sn Core–Shell Catalyst Enabling Highly Efficient Electrocatalytic CO_2 Reduction to Formate, *ACS Appl. Eng. Mater.*, 2023, **1**(6), 1514–1523.
160 G. O. Larrazábal, *et al.*, Investigation of Ethylene and Propylene Production from CO_2 Reduction over Copper Nanocubes in an MEA-Type Electrolyzer, *ACS Appl. Mater. Interfaces*, 2022, **14**(6), 7779–7787.
161 D. Choukroun, *et al.*, Mapping Composition–Selectivity Relationships of Supported Sub-10 nm Cu–Ag Nanocrystals for High-Rate CO_2 Electroreduction, *ACS Nano*, 2021, **15**(9), 14858–14872.
162 Y. Sha, *et al.*, Anchoring Ionic Liquid in Copper Electrocatalyst for Improving CO_2 Conversion to Ethylene, *Angew. Chem., Int. Ed.*, 2022, **61**(13), e202200039.
163 B. Yang, *et al.*, Accelerating CO_2 Electroreduction to Multicarbon Products *via* Synergistic Electric–Thermal Field on Copper Nanoneedles, *J. Am. Chem. Soc.*, 2022, **144**(7), 3039–3049.
164 K. Jiang, *et al.*, Effects of Surface Roughness on the Electrochemical Reduction of CO_2 over Cu, *ACS Energy Lett.*, 2020, **5**(4), 1206–1214.
165 S. Kuang, *et al.*, Stable Surface-Anchored Cu Nanocubes for CO_2 Electroreduction to Ethylene, *ACS Appl. Nano Mater.*, 2020, **3**(8), 8328–8334.
166 B. Liu, *et al.*, Synthesis of Cu_2O Nanostructures with Tunable Crystal Facets for Electrochemical CO_2 Reduction to Alcohols, *ACS Appl. Mater. Interfaces*, 2021, **13**(33), 39165–39177.
167 C. Tang, *et al.*, CO_2 Reduction on Copper's Twin Boundary, *ACS Catal.*, 2020, **10**(3), 2026–2032.
168 Y. Wang, *et al.*, Copper Nanocubes for CO_2 Reduction in Gas Diffusion Electrodes, *Nano Lett.*, 2019, **19**(12), 8461–8468.
169 P. Wang, *et al.*, Synergized Cu/Pb Core/Shell Electrocatalyst for High-Efficiency CO_2 Reduction to C_{2+} Liquids, *ACS Nano*, 2021, **15**(1), 1039–1047.
170 Y. Wu, *et al.*, Engineering Bimetallic Copper-Tin Based Core–Shell Alloy@Oxide Nanowire as Efficient Catalyst for Electrochemical CO_2 Reduction, *ChemElectroChem*, 2021, **8**(14), 2701–2707.
171 H. Xie, *et al.*, Boosting Tunable Syngas Formation *via* Electrochemical CO_2 Reduction on Cu/In_2O_3 Core/Shell Nanoparticles, *ACS Appl. Mater. Interfaces*, 2018, **10**(43), 36996–37004.
172 Y. Fang, *et al.*, Synthesis of amino acids by electrocatalytic reduction of CO_2 on chiral Cu surfaces, *Chem*, 2023, **9**(2), 460–471.
173 J. R. Pankhurst, *et al.*, Copper Nanocrystal Morphology Determines the Viability of Molecular Surface Functionalization in Tuning Electrocatalytic Behavior in CO_2 Reduction, *Inorg. Chem.*, 2021, **60**(10), 6939–6945.
174 B. Cheng, *et al.*, Selective CO_2 Reduction to Ethylene Using Imidazolium-Functionalized Copper, *ACS Appl. Mater. Interfaces*, 2022, **14**(24), 27823–27832.
175 S. Huo, *et al.*, Coupled Metal/Oxide Catalysts with Tunable Product Selectivity for Electrocatalytic CO_2 Reduction, *ACS Appl. Mater. Interfaces*, 2017, **9**(34), 28519–28526.
176 Z. Tao, *et al.*, Activating Copper for Electrocatalytic CO_2 Reduction to Formate *via* Molecular Interactions, *ACS Catal.*, 2020, **10**(16), 9271–9275.
177 H. Cheng, *et al.*, Atomically Dispersed Ni/Cu Dual Sites for Boosting the CO_2 Reduction Reaction, *ACS Catal.*, 2021, **11**(20), 12673–12681.
178 L.-J. Zhu, *et al.*, Copper–Supramolecular Pair Catalyst Promoting C_{2+} Product Formation in Electrochemical CO_2 Reduction, *ACS Catal.*, 2023, **13**(8), 5114–5121.
179 J. Wang, *et al.*, Fastening Br–Ions at Copper–Molecule Interface Enables Highly Efficient Electroreduction of CO_2 to Ethanol, *ACS Energy Lett.*, 2021, **6**(2), 437–444.
180 X. Li, *et al.*, Selective Electroreduction of CO_2 and CO to C_2H_4 by Synergistically Tuning Nanocavities and the Surface Charge of Copper Oxide, *ACS Sustainable Chem. Eng.*, 2022, **10**(19), 6466–6475.
181 Z. Cao, *et al.*, A Molecular Surface Functionalization Approach to Tuning Nanoparticle Electrocatalysts for Carbon Dioxide Reduction, *J. Am. Chem. Soc.*, 2016, **138**(26), 8120–8125.
182 Z. Wang, *et al.*, Toward highly active electrochemical CO_2 reduction to C_2H_4 by copper hydroxyphosphate, *J. Solid State Electrochem.*, 2023, **27**(5), 1279–1287.
183 J. Wang, *et al.*, Surface Molecular Functionalization of Unusual Phase Metal Nanomaterials for Highly Efficient Electrochemical Carbon Dioxide Reduction under Industry-Relevant Current Density, *Small*, 2022, **18**(11), 2106766.

184 Z.-Y. Zhang, *et al.*, Cu–Zn-based alloy/oxide interfaces for enhanced electroreduction of CO_2 to C_{2+} products, *J. Energy Chem.*, 2023, **83**, 90–97.
185 R. Wang, *et al.*, Engineering a Cu/ZnO_x Interface for High Methane Selectivity in CO_2 Electrochemical Reduction, *Ind. Eng. Chem. Res.*, 2021, **60**(1), 273–280.
186 C. Liu, *et al.*, Highly Selective CO_2 Electroreduction to C_{2+} Products over Cu_2O-Decorated 2D Metal–Organic Frameworks with Rich Heterogeneous Interfaces, *Nano Lett.*, 2023, **23**(4), 1474–1480.
187 M. Kempasiddaiah, *et al.*, Interface-Rich Highly Oxophilic Copper/Tin–Oxide Nanocomposite on Reduced Graphene Oxide for Efficient Electroreduction of CO_2 to Formate, *ACS Appl. Energy Mater.*, 2023, **6**(5), 3020–3031.
188 R. Du, *et al.*, *In Situ* Engineering of the Cu^+/Cu^0 Interface to Boost C_{2+} Selectivity in CO_2 Electroreduction, *ACS Appl. Mater. Interfaces*, 2022, **14**(32), 36527–36535.
189 H.-Q. Liang, *et al.*, Hydrophobic Copper Interfaces Boost Electroreduction of Carbon Dioxide to Ethylene in Water, *ACS Catal.*, 2021, **11**(2), 958–966.
190 J. Yin, *et al.*, Customizable CO_2 Electroreduction to C_1 or C_{2+} Products through Cuy/CeO_2 Interface Engineering, *ACS Catal.*, 2022, **12**(2), 1004–1011.
191 K. Li, *et al.*, *In Situ* Dynamic Construction of a Copper Tin Sulfide Catalyst for High-Performance Electrochemical CO_2 Conversion to Formate, *ACS Catal.*, 2022, **12**(16), 9922–9932.
192 T. Kou, *et al.*, Amorphous CeO_2–Cu Heterostructure Enhances CO_2 Electroreduction to Multicarbon Alcohols, *ACS Mater. Lett.*, 2022, **4**(10), 1999–2008.
193 J. A. Rudd, *et al.*, Investigation into the Re-Arrangement of Copper Foams Pre- and Post-CO_2, *Electrocatalysis*, 2021, **3**(3), 687–703.
194 J. Zeng, *et al.*, Engineering copper nanoparticle electrodes for tunable electrochemical reduction of carbon dioxide, *Electrochim. Acta*, 2023, **464**, 142862.
195 S. Tafazoli, *et al.*, *In situ* surface enhanced Raman spectroscopy investigations on surface transformations of oxide derived copper electrodes during CO_2RR, *J. Catal.*, 2023, **423**, 118–128.
196 P.-P. Yang, *et al.*, Highly Enhanced Chloride Adsorption Mediates Efficient Neutral CO_2 Electroreduction over a Dual-Phase Copper Catalyst, *J. Am. Chem. Soc.*, 2023, **145**(15), 8714–8725.
197 W. Ren, *et al.*, Isolated copper–tin atomic interfaces tuning electrocatalytic CO_2 conversion, *Nat. Commun.*, 2021, **12**(1), 1449.
198 X. Tan, *et al.*, Stabilizing Copper by a Reconstruction-Resistant Atomic Cu–O–Si Interface for Electrochemical CO_2 Reduction, *J. Am. Chem. Soc.*, 2023, **145**(15), 8656–8664.
199 F. Ismail, *et al.*, Atomically Isolated Nickel–Nitrogen–Carbon Electrocatalysts Derived by the Utilization of Mg^{2+} ions as Spacers in Bimetallic Ni/Mg–Metal–Organic Framework Precursors for Boosting the Electroreduction of CO_2, *ACS Appl. Energy Mater.*, 2022, **5**(8), 9408–9417.
200 Y. Lan, *et al.*, SnO_2-Modified Two-Dimensional CuO for Enhanced Electrochemical Reduction of CO_2 to C_2H_4, *ACS Appl. Mater. Interfaces*, 2020, **12**(32), 36128–36136.
201 J. Wang, *et al.*, Grain-Boundary-Engineered La_2CuO_4 Perovskite Nanobamboos for Efficient CO_2 Reduction Reaction, *Nano Lett.*, 2021, **21**(2), 980–987.
202 L.-X. Liu, *et al.*, Enriching the Local Concentration of CO Intermediates on Cu Cavities for the Electrocatalytic Reduction of CO_2 to C_{2+} Products, *ACS Appl. Mater. Interfaces*, 2023, **15**(13), 16673–16679.
203 X.-C. Liu, *et al.*, Tailoring the Electrochemical Protonation Behavior of CO_2 by Tuning Surface Noncovalent Interactions, *ACS Catal.*, 2021, **11**(24), 14986–14994.
204 Q. Wu, *et al.*, Nanograin-Boundary-Abundant Cu_2O–Cu Nanocubes with High C_{2+} Selectivity and Good Stability during Electrochemical CO_2 Reduction at a Current Density of 500 mA cm^{-2}, *ACS Nano*, 2023, **17**(13), 12884–12894.
205 Y.-F. Shi, *et al.*, Methanol Synthesis from CO_2/CO Mixture on Cu–Zn Catalysts from Microkinetics-Guided Machine Learning Pathway Search, *J. Am. Chem. Soc.*, 2022, **144**(29), 13401–13414.
206 H. Li, *et al.*, C_{2+} Selectivity for CO_2 Electroreduction on Oxidized Cu-Based Catalysts, *J. Am. Chem. Soc.*, 2023, **145**(26), 14335–14344.
207 J. Zhang, *et al.*, Surface promotion of copper nanoparticles with alumina clusters derived from layered double hydroxide accelerates CO_2 reduction to ethylene in membrane electrode assemblies, *Nano Res.*, 2023, **16**(4), 4685–4690.
208 F. Scholten, *et al.*, Plasma-Modified Dendritic Cu Catalyst for CO_2 Electroreduction, *ACS Catal.*, 2019, **9**(6), 5496–5502.
209 H. Deng, *et al.*, Amino Assisted Protonation for Carbon−Carbon Coupling During Electroreduction of Carbon Dioxide to Ethylene on Copper(I) Oxide, *ChemCatChem*, 2021, **13**(20), 4325–4333.
210 X. Xu, *et al.*, Density functional theory study of CO_2 reduction to CH_3OH on the surfaces of metal (Cu, Ni, and Mn)-doped carbon nanotubes, *J. Phys. Chem. Solids*, 2022, **162**, 110537.
211 J. Shan, *et al.*, Effective CO_2 electroreduction toward C_2H_4 boosted by Ce-doped Cu nanoparticles, *Chem. Eng. J.*, 2022, **433**, 133769.
212 D. Mao, *et al.*, The influence of the compositions and structures of Cu-ZrO_2 catalysts on the catalytic performance of CO_2 hydrogenation to CH_3OH, *Chem. Eng. J.*, 2023, **471**, 144605.
213 K. Eid, *et al.*, Precise fabrication of porous one-dimensional gC_3N_4 nanotubes doped with Pd and Cu atoms for efficient CO oxidation and CO_2 reduction, *Inorg. Chem. Commun.*, 2019, **107**, 107460.
214 F. Gao, *et al.*, Efficient CO_2 reduction to formate using a Cu-doped $BiVO_4$ electrocathode in a WO3 photoanode-assisted photoelectrocatalytic system, *J. Electroanal. Chem.*, 2023, **930**, 117146.
215 M. Fang, *et al.*, Aluminum-Doped Mesoporous Copper Oxide Nanofibers Enabling High-Efficiency CO_2 Electroreduction to Multicarbon Products, *Chem. Mater.*, 2022, **34**(20), 9023–9030.
216 S. Yang, *et al.*, Near-Unity Electrochemical CO_2 to CO Conversion over Sn-Doped Copper Oxide Nanoparticles, *ACS Catal.*, 2022, **12**(24), 15146–15156.
217 Y. Zhang, X.-Y. Zhang and W.-Y. Sun, *In Situ* Carbon-Encapsulated Copper-Doped Cerium Oxide Derived from

MOFs for Boosting CO_2-to-CH_4 Electro-Conversion, *ACS Catal.*, 2023, **13**(2), 1545–1553.

218 B. Kim, *et al.*, Trace-Level Cobalt Dopants Enhance CO_2 Electroreduction and Ethylene Formation on Copper, *ACS Energy Lett.*, 2023, **8**(8), 3356–3364.

219 X. Zhong, *et al.*, Sn Dopants with Synergistic Oxygen Vacancies Boost CO_2 Electroreduction on CuO Nanosheets to CO at Low Overpotential, *ACS Nano*, 2022, **16**(11), 19210–19219.

220 H. Shen, *et al.*, *In Situ* Constructuring of Copper-Doped Bismuth Catalyst for Highly Efficient CO_2 Electrolysis to Formate in Ampere-Level, *Adv. Energy Mater.*, 2023, **13**(1), 2202818.

221 W. Ju, *et al.*, Sn-Decorated Cu for Selective Electrochemical CO_2 to CO Conversion: Precision Architecture beyond Composition Design, *ACS Appl. Energy Mater.*, 2019, **2**(1), 867–872.

222 C. S. Chen, J. H. Wan and B. S. Yeo, Electrochemical Reduction of Carbon Dioxide to Ethane Using Nanostructured Cu_2O-Derived Copper Catalyst and Palladium(II) Chloride, *J. Phys. Chem. C*, 2015, **119**(48), 26875–26882.

223 C. Hu, *et al.*, Porosity-Induced High Selectivity for CO_2 Electroreduction to CO on Fe-Doped ZIF-Derived Carbon Catalysts, *ACS Catal.*, 2019, **9**(12), 11579–11588.

224 P. Li, *et al.*, p–d Orbital Hybridization Induced by p-Block Metal-Doped Cu Promotes the Formation of C_{2+} Products in Ampere-Level CO_2 Electroreduction, *J. Am. Chem. Soc.*, 2023, **145**(8), 4675–4682.

225 S. Nellaiappan, *et al.*, Electroreduction of Carbon Dioxide into Selective Hydrocarbons at Low Overpotential Using Isomorphic Atomic Substitution in Copper Oxide, *ACS Sustainable Chem. Eng.*, 2020, **8**(1), 179–189.

226 M. H. Ravari, A. Sarrafi and M. Tahmooresi, Synthesizing and characterizing the mixed Al,Cu-pillared and copper doped Al-pillared bentonite for electrocatalytic reduction of CO_2, *S. Afr. J. Chem. Eng.*, 2020, **31**, 1–6.

227 H. Yuan, *et al.*, Dynamic re-construction of sulfur tailored Cu_2O for efficient electrochemical CO_2 reduction to formate over a wide potential window, *Appl. Surf. Sci.*, 2023, **613**, 156130.

228 C. An, *et al.*, Cooperated catalytic mechanism of atomically dispersed binary Cu–N_4 and Zn–N_4 in N-doped carbon materials for promoting electrocatalytic CO_2 reduction to CH_4, *Chem. Eng. J.*, 2023, **471**, 144618.

229 Y. Zhang, *et al.*, CO_2 reduction performance of Cu/Er supported on N-doped graphene: a first principles study, *Mol. Catal.*, 2023, **547**, 113335.

230 D. Choukroun, *et al.*, Bifunctional Nickel–Nitrogen-Doped-Carbon-Supported Copper Electrocatalyst for CO_2 Reduction, *J. Phys. Chem. C*, 2020, **124**(2), 1369–1381.

231 K. K. Patra, *et al.*, Operando Spectroscopic Investigation of a Boron-Doped CuO Catalyst and Its Role in Selective Electrochemical C–C Coupling, *ACS Appl. Energy Mater.*, 2020, **3**(11), 11343–11349.

232 D. Yang, *et al.*, Selective electroreduction of carbon dioxide to methanol on copper selenide nanocatalysts, *Nat. Commun.*, 2019, **10**(1), 677.

233 W. Zhang, *et al.*, Br-Doped CuO Multilamellar Mesoporous Nanosheets with Oxygen Vacancies and Cetyltrimethyl Ammonium Cations Adsorption for Optimizing Intermediate Species and Their Adsorption Behaviors toward CO_2 Electroreduction to Ethanol with a High faradaic Efficiency, *Inorg. Chem.*, 2021, **60**(18), 14371–14381.

234 A. Saxena, *et al.*, Copper Cobalt Selenide as a Bifunctional Electrocatalyst for the Selective Reduction of CO_2 to Carbon-Rich Products and Alcohol Oxidation, *ACS Appl. Mater. Interfaces*, 2023, **15**(11), 14433–14446.

235 D. G. Park, *et al.*, Increasing CO Binding Energy and Defects by Preserving Cu Oxidation State *via* O_2-Plasma-Assisted N Doping on CuO Enables High C_{2+} Selectivity and Long-Term Stability in Electrochemical CO_2 Reduction, *ACS Catal.*, 2023, **13**(13), 9222–9233.

236 X. Ma, *et al.*, Facet Dopant Regulation of Cu_2O Boosts Electrocatalytic CO_2 Reduction to Formate, *Adv. Funct. Mater.*, 2023, **33**(16), 2213145.

237 D. Liu, Y. Liu and M. Li, Understanding How Atomic Sulfur Controls the Selectivity of the Electroreduction of CO_2 to Formic Acid on Metallic Cu Surfaces, *J. Phys. Chem. C*, 2020, **124**(11), 6145–6153.

238 K. R. Phillips, *et al.*, Sulfide-Derived Copper for Electrochemical Conversion of CO_2 to Formic Acid, *J. Phys. Chem. Lett.*, 2018, **9**(15), 4407–4412.

239 M. Zheng, *et al.*, Electrocatalytic CO_2-to-C_{2+} with Ampere-Level Current on Heteroatom-Engineered Copper *via* Tuning *CO Intermediate Coverage, *J. Am. Chem. Soc.*, 2022, **144**(32), 14936–14944.

240 L. Gao, *et al.*, Fabrication of Cu(1 0 0) facet-enhanced ionic liquid/copper hybrid catalysis *via* one-step electrocodeposition for CO_2ER toward C_2, *Fuel*, 2022, **322**, 124103.

241 J. Yu, *et al.*, Enhancing the electrochemical reduction of carbon dioxide to multi-carbon products on copper nanosheet arrays *via* cation-catalyst interaction, *Cell Rep. Phys. Sci.*, 2023, **4**(4), 101366.

242 Z. Lyu, Y. Shang and Y. Xia, Shape-Controlled Synthesis of Copper Nanocrystals for Plasmonic, Biomedical, and Electrocatalytic Applications, *Acc. Mater. Res.*, 2022, **3**(11), 1137–1148.

243 G. Mangione, *et al.*, Dual-facet mechanism in copper nanocubes for electrochemical CO_2 reduction into ethylene, *J. Phys. Chem. Lett.*, 2019, **10**(15), 4259–4265.

244 S. C. Mandal, *et al.*, Hexagonal Cu(111) Monolayers for Selective CO_2 Hydrogenation to CH_3OH: Insights from Density Functional Theory, *ACS Appl. Nano Mater.*, 2019, **2**(12), 7686–7695.

245 G. L. De Gregorio, *et al.*, Facet-dependent selectivity of Cu catalysts in electrochemical CO_2 reduction at commercially viable current densities, *ACS Catal.*, 2020, **10**(9), 4854–4862.

246 J. Y. Kim, *et al.*, High Facets on Nanowrinkled Cu *via* Chemical Vapor Deposition Graphene Growth for Efficient CO_2 Reduction into Ethanol, *ACS Catal.*, 2021, **11**(9), 5658–5665.

247 P. Iyengar, *et al.*, Elucidating the facet-dependent selectivity for CO_2 electroreduction to ethanol of Cu–Ag tandem catalysts, *ACS Catal.*, 2021, **11**(8), 4456–4463.

248 W. Luo, *et al.*, Facet dependence of CO_2 reduction paths on Cu electrodes, *ACS Catal.*, 2016, **6**(1), 219–229.
249 W. Fu, *et al.*, Promoting C_{2+} Production from Electrochemical CO_2 Reduction on Shape-Controlled Cuprous Oxide Nanocrystals with High-Index Facets, *ACS Sustainable Chem. Eng.*, 2020, **8**(40), 15223–15229.
250 Y. Ma, *et al.*, Confined growth of silver–copper janus nanostructures with {100} facets for highly selective tandem electrocatalytic carbon dioxide reduction, *Adv. Mater.*, 2022, **34**(19), 2110607.
251 A. Rahmani and H. Farsi, Nanostructured copper molybdates as promising bifunctional electrocatalysts for overall water splitting and CO_2 reduction, *RSC Adv.*, 2020, **10**(64), 39037–39048.
252 M. Zheng, *et al.*, The Facet Dependence of CO_2 Electroreduction Selectivity on a Pd_3Au Bimetallic Catalyst: A DFT Study, *Molecules*, 2023, **28**(7), 3169.
253 G. Zhang, *et al.*, Efficient CO_2 electroreduction on facet-selective copper films with high conversion rate, *Nat. Commun.*, 2021, **12**(1), 5745.
254 L. Han, *et al.*, Copper nanowire with enriched high-index facets for highly selective CO_2 reduction, *SmartMat*, 2022, **3**(1), 142–150.
255 L. Gao, *et al.*, Fabrication of Cu(100) facet-enhanced ionic liquid/copper hybrid catalysis *via* one-step electrocodeposition for CO_2ER toward C_2, *Fuel*, 2022, **322**, 124103.
256 J. Yu, *et al.*, Enhancing the electrochemical reduction of carbon dioxide to multi-carbon products on copper nanosheet arrays *via* cation-catalyst interaction, *Cell Rep. Phys. Sci.*, 2023, **4**(4), 101366.
257 Y. Ma, *et al.*, Confined Growth of Silver–Copper Janus Nanostructures with {100} Facets for Highly Selective Tandem Electrocatalytic Carbon Dioxide Reduction, *Adv. Mater.*, 2022, **34**(19), 2110607.
258 L. Han, *et al.*, Copper nanowire with enriched high-index facets for highly selective CO_2 reduction, *SmartMat*, 2022, **3**(1), 142–150.
259 A. Ahmad, *et al.*, Cu-doped zeolite imidazole framework (ZIF-8) for effective electrocatalytic CO_2 reduction, *J. CO_2 Util.*, 2021, **48**, 101523.
260 L. Garcia, *et al.*, Methanol electrosynthesis from CO_2 reduction reaction in polymer electrolyte reactors–fuel cell type using [6,6′-(2,2′-bipyridine-6,6′-diyl)bis(1,3,5-triazine-2,4-diamine)](dinitrate-O) copper(II) complex, *Mater. Today Sustainability*, 2022, **19**, 100177.
261 Y. Zhou, *et al.*, Spatial confinement in copper-porphyrin frameworks enhances carbon dioxide reduction to hydrocarbons, *Cell Rep. Phys. Sci.*, 2020, **1**(9), 100182.
262 Z. Zhao, *et al.*, Generalized surface coordination number as an activity descriptor for CO_2 reduction on Cu surfaces, *J. Phys. Chem. C*, 2016, **120**(49), 28125–28130.
263 H. Zhou, *et al.*, Coordination Engineering in Cobalt–Nitrogen-Functionalized Materials for CO_2 Reduction, *J. Phys. Chem. Lett.*, 2019, **10**(21), 6551–6557.
264 J. Liu, *et al.*, Controlled Synthesis of EDTA-Modified Porous Hollow Copper Microspheres for High-Efficiency Conversion of CO_2 to Multicarbon Products, *Nano Lett.*, 2020, **20**(7), 4823–4828.
265 X. Tan, *et al.*, Restructuring of Cu_2O to Cu_2O@ Cu–metal–organic frameworks for selective electrochemical reduction of CO_2, *ACS Appl. Mater. Interfaces*, 2019, **11**(10), 9904–9910.
266 Y. Wu, *et al.*, Sn Atoms on Cu Nanoparticles for Suppressing Competitive H_2 Evolution in CO_2 Electrolysis, *ACS Appl. Nano Mater.*, 2021, **4**(5), 4994–5003.
267 S. Kusama, *et al.*, Crystalline copper(II) phthalocyanine catalysts for electrochemical reduction of carbon dioxide in aqueous media, *ACS Catal.*, 2017, **7**(12), 8382–8385.
268 R. Wang, *et al.*, Partial Coordination-Perturbed Bi-Copper Sites for Selective Electroreduction of CO_2 to Hydrocarbons, *Angew. Chem., Int. Ed.*, 2021, **60**(36), 19829–19835.
269 Y. Y. Liu, *et al.*, A Stable Metal-azolate Framework with Cyclic Tetracopper(I) Clusters for Highly Selective Electroreduction of CO_2 to C_2 Products, *Chem. – Asian J.*, 2022, **17**(21), e202200764.
270 Y. Zhang, *et al.*, Hydroxy-Group-Functionalized Single Crystal of Copper(II)-Porphyrin Complex for Electroreduction CO_2 to CH_4, *ChemSusChem*, 2022, **15**(4), e202102528.
271 Q. Tang, *et al.*, Lattice-hydride mechanism in electrocatalytic CO_2 reduction by structurally precise copper-hydride nanoclusters, *J. Am. Chem. Soc.*, 2017, **139**(28), 9728–9736.
272 L. Xue, *et al.*, Hydrophobic 1-octadecanethiol functionalized copper catalyst promotes robust high-current CO_2 gas-diffusion electrolysis, *Nano Res.*, 2022, **15**, 1393–1398.
273 Y.-H. Xiao, *et al.*, Helical copper-porphyrinic framework nanoarrays for highly efficient CO_2 electroreduction, *Sci. China: Mater.*, 2022, **65**(5), 1269–1275.
274 B. Yang, *et al.*, Electrocatalytic CO_2 reduction to alcohols by modulating the molecular geometry and Cu coordination in bicentric copper complexes, *Nat. Commun.*, 2022, **13**(1), 5122.
275 M. Fang, *et al.*, Hydrophobic, Ultrastable Cuδ+ for Robust CO_2 Electroreduction to C_2 Products at Ampere-Current Levels, *J. Am. Chem. Soc.*, 2023, **145**(20), 11323–11332.
276 A. K. Singh, *et al.*, Exploring Ligand-Controlled C_2 Product Selectivity in Carbon Dioxide Reduction with Copper Metal–Organic Framework Nanosheets, *Inorg. Chem.*, 2023, **62**(23), 8803–8811.
277 X. Han, *et al.*, Atomic Layer Infiltration Enabled Cu Coordination Environment Construction for Enhanced Electrochemical CO_2 Reduction Selectivity: Case Study of a Cu Metal–Organic Framework, *Chem. Mater.*, 2022, **34**(15), 6713–6722.
278 K. Yao, *et al.*, Mechanistic Insights into OC–COH Coupling in CO_2 Electroreduction on Fragmented Copper, *J. Am. Chem. Soc.*, 2022, **144**(31), 14005–14011.
279 Y. Liu, *et al.*, Ligand-Controlled Electroreduction of CO_2 to Formate over Facet-Defined Bimetallic Sulfide Nanoplates, *Nano Lett.*, 2023, **23**(13), 5911–5918.
280 Y.-Y. Liu, *et al.*, Insight into the Effect of the d-Orbital Energy of Copper Ions in Metal–Organic Frameworks on the Selectivity of Electroreduction of CO_2 to CH_4, *ACS Catal.*, 2022, **12**(5), 2749–2755.
281 X. K. Lu, *et al.*, Stabilization of Undercoordinated Cu Sites in Strontium Copper Oxides for Enhanced Formation of

C_{2+} Products in Electrochemical CO_2 Reduction, *ACS Catal.*, 2022, **12**(11), 6663–6671.

282 L. M. S. Garcia, *et al.*, Methanol electrosynthesis from CO_2 reduction reaction in polymer electrolyte reactors – fuel cell type using [6,6′-(2,2′-bipyridine-6,6′-diyl)bis(1,3,5-triazine-2,4-diamine)] (dinitrate-O) copper(II) complex, *Mater. Today Sustainability*, 2022, **19**, 100177.

283 Y. Zhou, *et al.*, Spatial Confinement in Copper-Porphyrin Frameworks Enhances Carbon Dioxide Reduction to Hydrocarbons, *Cell Rep. Phys. Sci.*, 2020, **1**(9), 100182.

284 X. Tan, *et al.*, Restructuring of Cu_2O to Cu_2O@Cu-Metal–Organic Frameworks for Selective Electrochemical Reduction of CO_2, *ACS Appl. Mater. Interfaces*, 2019, **11**(10), 9904–9910.

285 S. Kusama, *et al.*, Crystalline Copper(II) Phthalocyanine Catalysts for Electrochemical Reduction of Carbon Dioxide in Aqueous Media, *ACS Catal.*, 2017, **7**(12), 8382–8385.

286 R. Wang, *et al.*, Partial Coordination-Perturbed Bi-Copper Sites for Selective Electroreduction of CO_2 to Hydrocarbons, *Angew. Chem., Int. Ed.*, 2021, **60**(36), 19829–19835.

287 Y.-Y. Liu, *et al.*, A Stable Metal-azolate Framework with Cyclic Tetracopper(I) Clusters for Highly Selective Electroreduction of CO_2 to C_2 Products, *Chem. - Asian J.*, 2022, **17**(21), e202200764.

288 Y. Zhang, *et al.*, Hydroxy-Group-Functionalized Single Crystal of Copper(II)-Porphyrin Complex for Electroreduction CO_2 to CH_4, *ChemSusChem*, 2022, **15**(4), e202102528.

289 L. Xue, *et al.*, Hydrophobic 1-octadecanethiol functionalized copper catalyst promotes robust high-current CO_2 gas-diffusion electrolysis, *Nano Res.*, 2022, **15**(2), 1393–1398.

290 Z. Yang, *et al.*, Modulable Cu(0)/Cu(I)/Cu(II) sites of Cu/C catalysts derived from MOF for highly selective CO_2 electroreduction to hydrocarbons, *Vacuum*, 2023, 112231.

291 W. Liu, *et al.*, Edge-located Fe–N_4 sites on porous Graphene-like nanosheets for boosting CO_2 electroreduction, *Chem. Eng. J.*, 2022, **431**, 134269.

292 C. Zhu, *et al.*, Product-specific active site motifs of Cu for electrochemical CO_2 reduction, *Chem*, 2021, **7**(2), 406–420.

293 S. Chen, *et al.*, MOF encapsulating N-heterocyclic carbene-ligated copper single-atom site catalyst towards efficient methane electrosynthesis, *Angew. Chem.*, 2022, **134**(4), e202114450.

294 D. Cheng, *et al.*, The nature of active sites for carbon dioxide electroreduction over oxide-derived copper catalysts, *Nat. Commun.*, 2021, **12**(1), 395.

295 X. Yuan, *et al.*, Controllable Cu^0–Cu^+ sites for electrocatalytic reduction of carbon dioxide, *Angew. Chem.*, 2021, **133**(28), 15472–15475.

296 A. Guan, *et al.*, Boosting CO_2 Electroreduction to CH_4 *via* Tuning Neighboring Single-Copper Sites, *ACS Energy Lett.*, 2020, **5**(4), 1044–1053.

297 C. Hahn, *et al.*, Engineering Cu surfaces for the electrocatalytic conversion of CO_2: controlling selectivity toward oxygenates and hydrocarbons, *Proc. Natl. Acad. Sci. U. S. A.*, 2017, **114**(23), 5918–5923.

298 J.-M. Heng, *et al.*, A Conductive Dinuclear Cuprous Complex Mimicking the Active Edge Site of the Copper(100)/(111) Plane for Selective Electroreduction of CO_2 to C_2H_4 at Industrial Current Density, *Research*, 2022, **2022**, 0008.

299 Y. Liang, *et al.*, Stabilizing copper sites in coordination polymers toward efficient electrochemical CC coupling, *Nat. Commun.*, 2023, **14**(1), 474.

300 C. Shan, *et al.*, Site-selective growth of AgPd nanodendrite-modified Au nanoprisms: high electrocatalytic performance for CO_2 reduction, *Chem. Mater.*, 2017, **29**(14), 6030–6043.

301 K. Zhang, *et al.*, Status and perspectives of key materials for PEM electrolyzer, *Nano Res. Energy*, 2022, **1**, e9120032.

302 S. B. Varandili, *et al.*, Synthesis of Cu/CeO_{2-x} Nanocrystalline Heterodimers with Interfacial Active Sites To Promote CO_2 Electroreduction, *ACS Catal.*, 2019, **9**(6), 5035–5046.

303 H. Han, *et al.*, Lattice-disorder layer generation from liquid processing at room temperature with boosted nanointerface exposure toward water splitting, *Sustainable Energy Fuels*, 2022, **6**(12), 3008–3013.

304 H.-L. Zhu, *et al.*, Highly Efficient Electroconversion of CO_2 into CH_4 by a Metal–Organic Framework with Trigonal Pyramidal Cu(I)N_3 Active Sites, *ACS Catal.*, 2021, **11**(18), 11786–11792.

305 T. Yan, *et al.*, Copper(II) Frameworks with Varied Active Site Distribution for Modulating Selectivity of Carbon Dioxide Electroreduction, *ACS Appl. Mater. Interfaces*, 2022, **14**(11), 13645–13652.

306 Z. Yang, *et al.*, Modulable Cu(0)/Cu(I)/Cu(II) sites of Cu/C catalysts derived from MOF for highly selective CO_2 electroreduction to hydrocarbons, *Vacuum*, 2023, **215**, 112231.

307 T. Dou, *et al.*, Sulfurization-derived Cu^0–Cu^+ sites for electrochemical CO_2 reduction to ethanol, *J. Power Sources*, 2022, **533**, 231393.

308 C. Ma, *et al.*, Bimetallic atomic Fe–Mn metal–nitrogen active sites for synergistic enhancement of CO_2 electroreduction efficiency, *Environ. Funct. Mater.*, 2022, **1**(3), 284–297.

309 X. Yuan, *et al.*, Controllable Cu^0–Cu^+ Sites for Electrocatalytic Reduction of Carbon Dioxide, *Angew. Chem., Int. Ed.*, 2021, **60**(28), 15344–15347.

310 J.-M. Heng, *et al.*, A Conductive Dinuclear Cuprous Complex Mimicking the Active Edge Site of the Copper(100)/(111) Plane for Selective Electroreduction of CO_2 to C_2H_4 at Industrial Current Density, *Research*, 2022, **2022**, 0008.

311 Y. Liang, *et al.*, Stabilizing copper sites in coordination polymers toward efficient electrochemical C–C coupling, *Nat. Commun.*, 2023, **14**(1), 474.

312 Z. Li, *et al.*, Coupling Atomically Dispersed Fe–N_5 Sites with Defective N-Doped Carbon Boosts CO_2 Electroreduction, *Small*, 2022, **18**(38), 2203495.

313 X. Wang, *et al.*, Microenvironment and Nanoreactor Engineering of Single-Site Metal Catalysts for Electrochemical CO_2 Reduction, *Energy Fuels*, 2021, **35**(12), 9795–9808.

314 T. Kim, *et al.*, How Strain Alters CO_2 Electroreduction on Model Cu(001) Surfaces, *ACS Catal.*, 2021, **11**(11), 6662–6671.

315 W.-J. Kang, *et al.*, Strain-Activated Copper Catalyst for pH-Universal Hydrogen Evolution Reaction, *Adv. Funct. Mater.*, 2022, **32**(18), 2112367.

316 Y. Du and W. An, Effects of Uniaxial Lattice Strain and Explicit Water Solvation on CO_2 Electroreduction over a Cu Electrode: A Density Functional Theory Perspective, *J. Phys. Chem. C*, 2021, **125**(17), 9138–9149.

317 T. Adit Maark and B. R. K. Nanda, Enhancing CO_2 Electroreduction by Tailoring Strain and Ligand Effects in Bimetallic Copper–Rhodium and Copper–Nickel Heterostructures, *J. Phys. Chem. C*, 2017, **121**(8), 4496–4504.
318 F. Liu, C. Wu and S. Yang, Strain and Ligand Effects on CO_2 Reduction Reactions over Cu–Metal Heterostructure Catalysts, *J. Phys. Chem. C*, 2017, **121**(40), 22139–22146.
319 D. Yu, *et al.*, Strain-Stabilized Metastable Face-Centered Tetragonal Gold Overlayer for Efficient CO_2 Electroreduction, *Nano Lett.*, 2021, **21**(2), 1003–1010.
320 Z. Wei, *et al.*, Enhancing Selective Electrochemical CO_2 Reduction by *In Situ* Constructing Tensile-Strained Cu Catalysts, *ACS Catal.*, 2023, **13**(7), 4711–4718.
321 H. Wang, *et al.*, Strain in Copper/Ceria Heterostructure Promotes Electrosynthesis of Multicarbon Products, *ACS Nano*, 2023, **17**(1), 346–354.
322 J. Feng, *et al.*, Improving CO_2-to-C_{2+} Product Electroreduction Efficiency *via* Atomic Lanthanide Dopant-Induced Tensile-Strained CuO_x Catalysts, *J. Am. Chem. Soc.*, 2023, **145**(17), 9857–9866.
323 J. Hao, *et al.*, Strain Relaxation in Metal Alloy Catalysts Steers the Product Selectivity of Electrocatalytic CO_2 Reduction, *ACS Nano*, 2022, **16**(2), 3251–3263.
324 H. Li, *et al.*, Strain-Regulated Pd/Cu Core/Shell Icosahedra for Tunable Syngas Electrosynthesis from CO_2, *Chem. Mater.*, 2022, **34**(17), 7995–8003.
325 H. Guzmán, *et al.*, Ultrasound-assisted synthesis of copper-based catalysts for the electrocatalytic CO_2 reduction: effect of ultrasound irradiation, precursor concentration and calcination temperature, *Sustainable Mater. Technol.*, 2023, **35**, e00557.
326 C. A. Downes, *et al.*, Electrocatalytic CO_2 Reduction over Cu_3P Nanoparticles Generated *via* a Molecular Precursor Route, *ACS Appl. Energy Mater.*, 2020, **3**(11), 10435–10446.
327 Y. Zhang, *et al.*, Cu/Cu_2O Nanoparticles Supported on Vertically ZIF-L-Coated Nitrogen-Doped Graphene Nanosheets for Electroreduction of CO_2 to Ethanol, *ACS Appl. Nano Mater.*, 2020, **3**(1), 257–263.
328 T. Dou, *et al.*, CuS Nanosheet Arrays for Electrochemical CO_2 Reduction with Surface Reconstruction and the Effect on Selective Formation of Formate, *ACS Appl. Energy Mater.*, 2021, **4**(5), 4376–4384.
329 S. Chen, *et al.*, Anisotropic Seeded Growth of Cu–M (M = Au, Pt, or Pd) Bimetallic Nanorods with Tunable Optical and Catalytic Properties, *J. Phys. Chem. C*, 2013, **117**(17), 8924–8932.
330 Y. Zheng, *et al.*, Seeded Growth of Gold–Copper Janus Nanostructures as a Tandem Catalyst for Efficient Electroreduction of CO_2 to C_{2+} Products, *Small*, 2022, **18**(19), 2201695.
331 Y. Wang, *et al.*, Tunable Syngas Formation from Electrochemical CO_2 Reduction on Copper Nanowire Arrays, *ACS Appl. Energy Mater.*, 2020, **3**(10), 9841–9847.
332 H. Wang, *et al.*, Scalable Edge-Oriented Metallic Two-Dimensional Layered Cu_2Te Arrays for Electrocatalytic CO_2 Methanation, *ACS Nano*, 2023, **17**(5), 4790–4799.
333 S. Sirisomboonchai, *et al.*, Efficient CO_2 Electrochemical Reduction by a Robust Electrocatalyst Fabricated by Electrodeposition of Indium and Zinc over Copper Foam, *ACS Appl. Energy Mater.*, 2022, **5**(8), 9846–9857.
334 Y. Gao, *et al.*, Hydrothermal Synthesis of CuS Catalysts for Electrochemical CO_2 Reduction: Unraveling the Effect of the Sulfur Precursor, *ACS Appl. Energy Mater.*, 2023, **6**(3), 1340–1354.
335 X. Pan, *et al.*, Poly(ionic liquid) nanovesicles *via* polymerization induced self-assembly and their stabilization of Cu nanoparticles for tailored CO_2 electroreduction, *J. Colloid Interface Sci.*, 2023, **637**, 408–420.
336 C. Ye, *et al.*, Enhanced Electrochemical CO_2 Reduction to Formate on Poly(4-vinylpyridine)-Modified Copper and Gold Electrodes, *ACS Appl. Mater. Interfaces*, 2022, **14**(40), 45263–45271.
337 M. Jun, *et al.*, Polymer-Covered Copper Catalysts Alter the Reaction Pathway of the Electrochemical CO_2 Reduction Reaction, *ACS Omega*, 2022, **7**(47), 42655–42663.
338 M. Chang, *et al.*, Ionomers Modify the Selectivity of Cu-Catalyzed Electrochemical CO_2 Reduction, *ChemSusChem*, 2023, **16**(5), e202201687.
339 Q. Chang, *et al.*, Electrochemical CO_2 Reduction Reaction over Cu Nanoparticles with Tunable Activity and Selectivity Mediated by Functional Groups in Polymeric Binder, *JACS Au*, 2022, **2**(1), 214–222.
340 J. Wang, *et al.*, Selective CO_2 Electrochemical Reduction Enabled by a Tricomponent Copolymer Modifier on a Copper Surface, *J. Am. Chem. Soc.*, 2021, **143**(7), 2857–2865.
341 X. Wei, *et al.*, Highly Selective Reduction of CO_2 to C_{2+} Hydrocarbons at Copper/Polyaniline Interfaces, *ACS Catal.*, 2020, **10**(7), 4103–4111.
342 L. Zhang, *et al.*, Enhanced Cuprophilic Interactions in Crystalline Catalysts Facilitate the Highly Selective Electroreduction of CO_2 to CH_4, *J. Am. Chem. Soc.*, 2021, **143**(10), 3808–3816.
343 J. Li, *et al.*, Polyquinone Modification Promotes CO_2 Activation and Conversion to C_{2+} Products over Copper Electrode, *ACS Energy Lett.*, 2022, **7**(11), 4045–4051.
344 H. Zhang, *et al.*, Creating Polycrystalline Cu Catalysts *via* Capping Agents and Electrochemical Treatment for CO_2 Reduction to C_2H_4, *Energy Fuels*, 2023, **37**(1), 529–538.
345 Y. Hao, *et al.*, Self-supported copper selenide nanosheets for electrochemical carbon dioxide conversion to syngas with a broad H_2-to-CO ratio, *Electrochim. Acta*, 2023, **449**, 142213.
346 S. Dongare, N. Singh and H. Bhunia, Oxide-derived Cu–Zn nanoparticles supported on N-doped graphene for electrochemical reduction of CO_2 to ethanol, *Appl. Surf. Sci.*, 2021, **556**, 149790.
347 J. Han, *et al.*, Insight into the effect of surface coverage of carbon support on selective CO_2 electroreduction to C_2H_4 over copper-based catalyst, *Appl. Surf. Sci.*, 2023, **609**, 155394.
348 L. Gu, J. Ftouni and A. D. Chowdhury, Evaluating carbon dioxide reduction over copper supported on precipitated calcium carbonate *via* electrochemical route, *Mater. Today Chem.*, 2023, **30**, 101539.
349 J. W. Lim, *et al.*, Spontaneously Formed CuS_x Catalysts for Selective and Stable Electrochemical Reduction of

Industrial CO_2 Gas to Formate, *ACS Appl. Mater. Interfaces*, 2020, **12**(20), 22891–22900.

350 C. Kim, L.-C. Weng and A. T. Bell, Impact of pulsed electrochemical reduction of CO_2 on the formation of C_{2+} products over Cu, *ACS Catal.*, 2020, **10**(21), 12403–12413.

351 S. Ahn, *et al.*, Poly-amide modified copper foam electrodes for enhanced electrochemical reduction of carbon dioxide, *ACS Catal.*, 2018, **8**(5), 4132–4142.

352 X. An, *et al.*, Bi-Doped SnO Nanosheets Supported on Cu Foam for Electrochemical Reduction of CO_2 to HCOOH, *ACS Appl. Mater. Interfaces*, 2019, **11**(45), 42114–42122.

353 O. A. Baturina, *et al.*, CO_2 electroreduction to hydrocarbons on carbon-supported Cu nanoparticles, *ACS Catal.*, 2014, **4**(10), 3682–3695.

354 A. Vijayakumar, *et al.*, A Nitrogen-Doped Porous Carbon Supported Copper Catalyst from a Scalable One-Step Method for Efficient Carbon Dioxide Electroreduction, *ChemElectroChem*, 2023, **10**(2), e202200817.

355 Y. Huo, *et al.*, High Selectivity Toward C_2H_4 Production over Cu Particles Supported by Butterfly-Wing-Derived Carbon Frameworks, *ACS Appl. Mater. Interfaces*, 2018, **10**(15), 12618–12625.

356 D. Kordus, *et al.*, Shape-Dependent CO_2 Hydrogenation to Methanol over Cu_2O Nanocubes Supported on ZnO, *J. Am. Chem. Soc.*, 2023, **145**(5), 3016–3030.

357 Y. Mi, *et al.*, Selective formation of C_2 products from electrochemical CO_2 reduction over $Cu_{1.8}Se$ nanowires, *ACS Appl. Energy Mater.*, 2018, **1**(10), 5119–5123.

358 H. Wang, *et al.*, Size Control of Zn, N-doped Carbon Supported Copper Nanoparticles for Effective and Selective CO_2 Electroreduction, *Catal. Lett.*, 2023, **153**(7), 2115–2124.

359 W. Lou, *et al.*, CuBi electrocatalysts modulated to grow on derived copper foam for efficient CO_2-to-formate conversion, *J. Colloid Interface Sci.*, 2022, **606**, 994–1003.

360 Y. Zhang, *et al.*, Three-dimensional porous copper-decorated bismuth-based nanofoam for boosting the electrochemical reduction of CO_2 to formate, *Inorg. Chem. Front.*, 2021, **8**(10), 2461–2467.

361 Y. Wang, *et al.*, Effect of Charge on Carbon Support on the Catalytic Activity of Cu_2O toward CO_2 Reduction to C_2 Products, *ACS Appl. Mater. Interfaces*, 2023, **15**(19), 23306–23315.

362 M. Wang, *et al.*, Electrochemical Reduction of CO_2 on Copper-Based Electrocatalyst Supported on MWCNTs with Different Functional Groups, *Energy Fuels*, 2022, **36**(11), 5833–5842.

363 J. W. Lim, *et al.*, Spontaneously Formed CuSx Catalysts for Selective and Stable Electrochemical Reduction of Industrial CO_2 Gas to Formate, *ACS Appl. Mater. Interfaces*, 2020, **12**(20), 22891–22900.

364 O. A. Baturina, *et al.*, CO_2 Electroreduction to Hydrocarbons on Carbon-Supported Cu Nanoparticles, *ACS Catal.*, 2014, **4**(10), 3682–3695.

365 A. Vijayakumar, *et al.*, A Nitrogen-Doped Porous Carbon Supported Copper Catalyst from a Scalable One-Step Method for Efficient Carbon Dioxide Electroreduction, *ChemElectroChem*, 2023, **10**(2), e202200817.

366 E. S. Koh, *et al.*, Influence of Support Material on the Structural Evolution of Copper during Electrochemical CO_2 Reduction, *ChemElectroChem*, 2023, **10**(5), e202200924.

367 Y. Mi, *et al.*, Selective Formation of C_2 Products from Electrochemical CO_2 Reduction over $Cu_{1.8}Se$ Nanowires, *ACS Appl. Energy Mater.*, 2018, **1**(10), 5119–5123.

368 Y. Zhang, *et al.*, Three-dimensional porous copper-decorated bismuth-based nanofoam for boosting the electrochemical reduction of CO_2 to formate, *Inorg. Chem. Front.*, 2021, **8**(10), 2461–2467.

369 Q. Zhang, *et al.*, High-Performance of Electrocatalytic CO_2 Reduction on Defective Graphene-Supported Cu_4S_2 Cluster, *Catalysts*, 2022, **12**(5), 454.

370 Q. Tan, Z. Shi and D. Wu, CO_2 Hydrogenation to Methanol over a Highly Active Cu–Ni/CeO_2–Nanotube Catalyst, *Ind. Eng. Chem. Res.*, 2018, **57**(31), 10148–10158.

371 Y. Zhou, *et al.*, Tuning the content of S vacancies in MoS_2 by Cu doping for enhancing catalytic hydrogenation of CO_2 to methanol, *Mol. Catal.*, 2023, **547**, 113288.

372 S. Chen, *et al.*, Highly Selective Carbon Dioxide Electroreduction on Structure-Evolved Copper Perovskite Oxide toward Methane Production, *ACS Catal.*, 2020, **10**(8), 4640–4646.

373 Y. Deng, *et al.*, On the Role of Sulfur for the Selective Electrochemical Reduction of CO_2 to Formate on CuS_x Catalysts, *ACS Appl. Mater. Interfaces*, 2018, **10**(34), 28572–28581.

374 Y. Wang, *et al.*, Single-Atomic Cu with Multiple Oxygen Vacancies on Ceria for Electrocatalytic CO_2 Reduction to CH_4, *ACS Catal.*, 2018, **8**(8), 7113–7119.

375 H. Yang, *et al.*, Defect-engineering of tin oxide *via* (Cu, N) co-doping for electrocatalytic and photocatalytic CO_2 reduction into formate, *Chem. Eng. Sci.*, 2020, **227**, 115947.

376 Y. Zhang, *et al.*, Selective CO_2 Reduction to Ethylene Over a Wide Potential Window by Copper Nanowires with High Density of Defects, *Inorg. Chem.*, 2022, **61**(50), 20666–20673.

377 Q. Wu, *et al.*, Defect-Engineered Cu-Based Nanomaterials for Efficient CO_2 Reduction over Ultrawide Potential Window, *ACS Nano*, 2023, **17**(1), 402–410.

378 T. Le, T. Salavati-fard and B. Wang, Plasmonic Energetic Electrons Drive CO_2 Reduction on Defective Cu_2O, *ACS Catal.*, 2023, **13**(9), 6328–6337.

379 H. Wang, *et al.*, Cu/CuO_x In-Plane Heterostructured Nanosheet Arrays with Rich Oxygen Vacancies Enhance Nitrate Electroreduction to Ammonia, *ACS Appl. Mater. Interfaces*, 2022, **14**(30), 34761–34769.

380 H. Zhang, *et al.*, Selective CO_2-to-formic acid electrochemical conversion by modulating electronic environment of copper phthalocyanine with defective graphene, *Chin. J. Struct. Chem.*, 2023, 100089.

381 K. K. Patra, *et al.*, Boosting Electrochemical CO_2 Reduction to Methane *via* Tuning Oxygen Vacancy Concentration and Surface Termination on a Copper/Ceria Catalyst, *ACS Catal.*, 2022, **12**(17), 10973–10983.

382 J. Ye, M. Neurock and D. G. Truhlar, Effect of Missing-Linker Defects on CO_2 Hydrogenation to Methanol by Cu Nanoparticles in UiO-66, *J. Phys. Chem. C*, 2022, **126**(31), 13157–13167.

383 S. Pablo-García, *et al.*, Mechanistic routes toward C_3 products in copper-catalysed CO_2 electroreduction, *Catal. Sci. Technol.*, 2022, **12**(2), 409–417.
384 K. Zhao, *et al.*, CO_2 Electroreduction at Low Overpotential on Oxide-Derived Cu/Carbons Fabricated from Metal Organic Framework, *ACS Appl. Mater. Interfaces*, 2017, **9**(6), 5302–5311.
385 Y.-L. Qiu, *et al.*, Selective Electrochemical Reduction of Carbon Dioxide Using Cu Based Metal Organic Framework for CO_2 Capture, *ACS Appl. Mater. Interfaces*, 2018, **10**(3), 2480–2489.
386 L. Ma, *et al.*, Covalent triazine framework confined copper catalysts for selective electrochemical CO_2 reduction: operando diagnosis of active sites, *ACS Catal.*, 2020, **10**(8), 4534–4542.
387 S. Kim, *et al.*, Grain Boundary-Rich Copper Nanocatalysts Generated from Metal–Organic Framework Nanoparticles for CO_2-to-C_{2+} Electroconversion, *Adv. Sci.*, 2023, **10**(9), 2207187.
388 W. Nie, *et al.*, Organic Additive-derived Films on Cu Electrodes Promote Electrochemical CO_2 Reduction to C_{2+} Products Under Strongly Acidic Conditions, *Angew. Chem.*, 2023, **135**(12), e202216102.
389 S.-M. Hwang, *et al.*, Investigation on electroreduction of CO_2 to formic acid using $Cu_3(BTC)_2$ metal–organic framework (cu-mof) and graphene oxide, *ACS Omega*, 2020, **5**(37), 23919–23930.
390 D. Li, *et al.*, MOF-Derived Cu_2O/Cu Nanospheres Anchored in Nitrogen-Doped Hollow Porous Carbon Framework for Increasing the Selectivity and Activity of Electrochemical CO_2-to-Formate Conversion, *ACS Appl. Mater. Interfaces*, 2020, **12**(6), 7030–7037.
391 L. Li, *et al.*, Control of evolution of porous copper-based metal–organic materials for electroreduction of CO_2 to multi-carbon products, *Mater. Adv.*, 2023, **4**(8), 1941–1948.
392 Y.-S. Cheng, *et al.*, An MOF-derived copper@ nitrogen-doped carbon composite: the synergistic effects of N-types and copper on selective CO_2 electroreduction, *Catal. Sci. Technol.*, 2019, **9**(20), 5668–5675.
393 S. Wei, *et al.*, Construction of single-atom copper sites with low coordination number for efficient CO_2 electroreduction to CH_4, *J. Mater. Chem. A*, 2022, **10**(11), 6187–6192.
394 B. Xu, *et al.*, Anion-regulation engineering toward Cu/In/MOF bimetallic electrocatalysts for selective electrochemical reduction of CO_2 to CO/formate, *Mater. Rep.: Energy*, 2022, **2**(3), 100139.
395 W. Guo, *et al.*, Metal–organic framework-derived indium–copper bimetallic oxide catalysts for selective aqueous electroreduction of CO_2, *Green Chem.*, 2019, **21**(3), 503–508.
396 Y.-H. Zou, *et al.*, Implanting MWCNTs in BiCu-MOFs to enhance electrocatalytic CO_2 reduction to formate, *Sep. Purif. Technol.*, 2023, **317**, 123806.
397 X. Han, *et al.*, Hollow structured Cu@ ZrO_2 derived from Zr-MOF for selective hydrogenation of CO_2 to methanol, *J. Energy Chem.*, 2022, **71**, 277–287.
398 N. Rashid, *et al.*, Tailoring Motif and Channel Terminating Groups of Conventional Copper MOFs for Their Enhanced Activity, Selectivity, and Stability toward the Electroreduction of CO_2 to Hydrocarbons, *ACS Appl. Energy Mater.*, 2023, **6**(3), 1378–1388.
399 C. Liu, *et al.*, *In Situ* Reconstruction of Cu–N Coordinated MOFs to Generate Dispersive Cu/Cu_2O Nanoclusters for Selective Electroreduction of CO_2 to C_2H_4, *ACS Catal.*, 2022, **12**(24), 15230–15240.
400 J. B. Parambath, *et al.*, Copper-Based Metal-Organic Frameworks (MOFs) for Electroreduction of CO_2, *Catal. Sci. Technol.*, 2023, **13**, 3740–3761.
401 L.-Z. Dong, *et al.*, Porous copper cluster-based MOF with strong cuprophilic interactions for highly selective electrocatalytic reduction of CO_2 to CH_4, *Nano Res.*, 2022, **15**(12), 10185–10193.
402 S. Kim, *et al.*, Grain Boundary-Rich Copper Nanocatalysts Generated from Metal-Organic Framework Nanoparticles for CO_2-to-C_{2+} Electroconversion, *Adv. Sci.*, 2023, **10**(9), 2207187.
403 W. Nie, *et al.*, Organic Additive-derived Films on Cu Electrodes Promote Electrochemical CO_2 Reduction to C_{2+} Products Under Strongly Acidic Conditions, *Angew. Chem., Int. Ed.*, 2023, **62**(12), e202216102.
404 L. Li, *et al.*, Control of evolution of porous copper-based metal–organic materials for electroreduction of CO_2 to multi-carbon products, *Mater. Adv.*, 2023, **4**(8), 1941–1948.
405 S. Wei, *et al.*, Construction of single-atom copper sites with low coordination number for efficient CO_2 electroreduction to CH_4, *J. Mater. Chem. A*, 2022, **10**(11), 6187–6192.
406 B. Xu, *et al.*, Anion-regulation engineering toward Cu/In/MOF bimetallic electrocatalysts for selective electrochemical reduction of CO_2 to CO/formate, *Mater. Rep.: Energy*, 2022, **2**(3), 100139.
407 W. Guo, *et al.*, Metal–organic framework-derived indium–copper bimetallic oxide catalysts for selective aqueous electroreduction of CO_2, *Green Chem.*, 2019, **21**(3), 503–508.
408 L. D. Chen, Cations play an essential role in CO_2 reduction, *Nat. Catal.*, 2021, **4**(8), 641–642.
409 J. Fernández-Vidal, *et al.*, Effect of alkali-metal cation on oxygen adsorption at Pt single-crystal electrodes in non-aqueous electrolytes, *Faraday Discuss.*, 2024, **248**(0), 102–118.
410 B. Pan, Y. Wang and Y. Li, Understanding and leveraging the effect of cations in the electrical double layer for electrochemical CO_2 reduction, *Chem. Catal.*, 2022, **2**(6), 1267–1276.
411 J. J. Masana, *et al.*, Influence of halide ions on the electrochemical reduction of carbon dioxide over a copper surface, *J. Mater. Chem. A*, 2022, **10**(3), 1086–1104.
412 T. Yuan, *et al.*, The effect of specific adsorption of halide ions on electrochemical CO(2) reduction, *Chem. Sci.*, 2022, **13**(27), 8117–8123.
413 Q. Zhang, *et al.*, An experimental study of electroreduction of CO_2 to HCOOH on SnO_2/C in presence of alkali metal cations (Li^+, Na^+, K^+, Rb^+ and Cs^+) and anions (HCO_3^-, Cl^-, Br^- and I^-), *Chin. J. Chem. Eng.*, 2020, **28**(10), 2549–2554.